

# **Seawater as a Hydraulic Fluid; Corrosion Mechanisms and Rates of Engineering Materials**

Azzura Ismail

Submitted in accordance with the requirements for the degree of  
Doctor of Philosophy

The University of Leeds  
School of Mechanical Engineering

January, 2014

The candidate confirms that the work submitted is her own and that appropriate credit has been given where reference has been made to the work of others.

This copy has been supplied on the understanding that it is copyright material and that no quotation from the thesis may be published without proper acknowledgement.

## **Acknowledgements**

I would like to express my deep and sincere gratitude to my supervisor, Professor Anne Neville, Director of the Institute of Engineering Thermofluids, Surfaces and Interfaces (iETSI). Her wide knowledge, logical way of thinking and friendly supervision has been of great value for me. Her understanding, encouragement and personal guidance have provided a good foundation for the present thesis.

I would like to express my gratitude to the Ministry of Higher Education (MOHE), Malaysia, my employer, University Tun Hussein Onn Malaysia (UTHM) and Aker Solutions for their financial support. Many thanks to Dr Andrew Gledhill, David Johnston and Walter Oswald at Aker Solutions for their expertise, technical support and supply of the hydraulic fluids and materials tested.

My warm thanks to Mr. Graham Jakeman, Ron Cellier and all the technical staff for their technical assistance. My most sincere gratitude to Dr Chun for her academic suggestions and endless support during my PhD. Many thanks also to Dr Simon, Lei, Ardian, Tomasz, Rock, Rupesh, Eleftheria, Wendy, Abinesh and Kuldeep for their academic support.

My gratitude to my colleagues, Jonathan, Abu Bakar, Isma, Khaleed, Benissa, Shahriar, Jane, Hui, Mike, Rick, Laura, Naseer, Violette, Juan, Penny, John, Thibaut, Aike, Louise, Inga, Andrew, Feth-Allah, Mohd Ligreid, Akbar and the Malaysian society in the UK.

Special thanks to the School of Mechanical Engineering staff, especially Jackie, Debra, Fiona, Jane and Cath for their help and encouraging talks.

I owe my loving thanks to my family, especially my late dad, Allahyarham Mr Ismail and my mom, Mdm. Salasiah for their support and prayers. My most and sincere appreciation for the exceptional understanding of my husband, Ady, along with my children Humaira, Ammar and Aqeef, who sometimes did not get the attention they deserved.

## **Abstract**

With the increasing demand for environmentally friendly hydraulic fluids in the oil and gas sector, recent advances in hydraulic technology have sparked renewed interest in the application of water instead of oil. For industry, using seawater as a hydraulic fluid would bring many benefits as it can be discharged to the sea. The main corrosion challenges associated with the use of seawater are addressed in this study, particularly on how to extend the material life when corrosion attack is likely to be very severe. On the other hand, the material's degradation which is common in subsea applications is studied in detail which includes how corrosion mechanisms occur. The materials chosen in this research are those which are used extensively in subsea applications especially in Directional Control Valves (DCV) and piping operating with hydraulic fluids namely: (1) carbon steel, (2) stainless steel, and (3) cermet alloys (WC-Ni and WC-Co).

As an active material, carbon steel corrodes in a general way whereas passive materials such as stainless steel are more prone to localised corrosion which is often more catastrophic and difficult to predict and detect. However, cermet alloys (WC-Ni and WC-Co) which consist of metals and ceramics may exhibit both active and passive trends. Electrochemistry methods which are used in this study provide quantitative data which demonstrates different major corrosion parameters. Generally, temperature, oxygen, anions and pH are the main parameters that affect corrosion attack. In this research the effects of temperature, sulphate to chloride ratio and oxygen were studied on corrosion performance of DCV materials and compared the performance in seawater with a typical commercial hydraulic fluid HW443. From the analysis, it shows that temperature has a severe impact on corrosion rate, but alteration of sulphate to chloride ratio could decrease the corrosion rate close to HW443. Therefore, it is clear that by changing the sulphate/chloride ratio in seawater and adding green corrosion inhibitor similar performance to that compared to the use of commercial hydraulic fluids yet reduce the environmental harm on discharge could be attained. The thesis also presents information of generic interest in corrosion of carbon steel and other materials of interest in subsea environments. Corrosion trends of carbon steel, stainless steel and WC-cermet and their prevalent corrosion mechanisms (from electrochemical analysis) are discussed.

## Contents

ACKNOWLEDGEMENTS	ii
ABSTRACT	iii
CONTENTS	iv
LIST OF FIGURES	ix
LIST OF TABLES	xv
NOMENCLATURE	xvii
<b>Chapter 1</b>	<b>1</b>
<b>INTRODUCTION</b>	
1.1 Economic Impact of Corrosion	1
1.2 The Industrial Problem/Challenge	5
1.3 Background of This Study	8
1.4 Objectives	10
1.5 Thesis Outline	11
<b>Chapter 2</b>	<b>13</b>
<b>REVIEW OF RELEVANT THEORY</b>	
2.1 Basic Aqueous Corrosion	13
2.2 Solution Characteristics	13
2.2.1 Conductivity	13
2.2.2 Acidity of alkalinity of a solution	14
2.2.3 Oxidizing solution	15
2.3 Corrosion Mechanisms	15
2.3.1 Anodic reaction	17
2.3.2 Cathodic reaction	17
2.3.3 Cell potential and exchange current density	18
2.4 Determination of Corrosion Rates by Electrochemical Measurements	19
2.5 Corrosion Thermodynamics	20
2.5.1 Free energy	20

2.6 Electrochemical Kinetics of Corrosion	22
2.6.1 The three electrode cell	22
2.6.2 Activation polarisation	24
2.6.3 Concentration polarisation	26
2.6.4 Resistance polarisation	28
2.7 Forms of Corrosion	29
2.7.1 General corrosion	29
2.7.2 Pitting corrosion	30
2.8 Crevice Corrosion	33
2.9 Prevention of Corrosion Damage	35
2.10 Corrosion Parameters	36
2.10.1 Chlorides	36
2.10.2 Temperature	37
2.10.2.1 Arrhenius equation	37
2.10.3 Oxygen	38
2.11 Determination of Corrosion Rates in the Laboratory	39
2.11.1 Linear polarization resistance (LPR)	39
2.11.2 Potentiodynamic polarisation	41
<b>Chapter 3</b>	<b>45</b>
<b>LITERATURE REVIEW</b>	
3.1 Introduction	45
3.2 Seawater	45
3.2.1 Freezing point of seawater, $T_f$ and chemical additions	46
3.2.2 Role of anions on corrosion attack	47
3.2.3 Saturation	51
3.3 Seawater as a Corrosive Medium	51
3.4 Hydraulic Fluids	52
3.4.1 History of hydraulic fluids	52
3.4.2 Types of hydraulic fluid	53
3.4.3 Purposes of hydraulic fluids	54
3.4.4 Hydraulic fluid criteria	55
3.4.5 Corrosion in hydraulic fluid	55
3.5 Impact of Oil and Gas Activities on The Environment	56
3.5.1 Oil and gas Exploration and Production (E&P) wastes	56

3.5.2 Evaluation of the hazard and risk of chemicals used by the UK offshore oil and gas industry	57
3.6 Inhibitors	57
3.6.1 Green Inhibitors	62
3.6.2 Norwegian Legislation	64
3.6.3 UK Legislation	65
3.6.4 Environmental test methods	65
3.7 Oceanic HW Fluids	66
3.8 Carbon Steels	66
3.8.1 Composition of carbon steel	67
3.8.2 Corrosion of carbon steel in seawater	67
3.9 Stainless Steels	69
3.9.1 Stainless steel 316L	69
3.9.2 The 25Cr Duplex stainless steel	70
3.9.3 The passive film	71
3.10 Nickel Alloys	72
3.10.1 Corrosion of Inconel 625	73
3.10.2 The passive film of nickel alloys	74
3.11 Cermets Alloys	75
3.11.1 Tungsten carbide cermets	75
3.11.2 Structure and microstructure	76
3.11.3 Corrosion of cemented tungsten carbides	77
3.12 Materials Selection for Offshore	79
3.13 Summarising the Literature Review	81
<b>Chapter 4</b>	<b>82</b>
<b>MATERIALS AND EXPERIMENTAL PROCEDURES</b>	
4.1 Materials Under Study	82
4.2 Solution Analysis	83
4.3 Electrochemical Tests	87
4.4 Experimental Procedure	89
4.4.1 Anodic and cathodic polarization curves	90
4.5 Surface Analysis	92
4.5.1 Light microscopy	92
4.5.2 ESEM and EDAX	93

<b>Chapter 5</b>	94
<b>SETTING THE SCENE FOR CARBON STEELS</b>	
5.1 Introduction	94
5.2 Determination of the Corrosion Rate	95
5.3 Benchmarking	97
5.4 Corrosion Rate in 3.5% NaCl and Other Solutions	98
5.5 Immersion Tests	99
5.6 Carbon Steels in Different Sulphate to Chloride Ratios	99
5.7 The Critical Chloride Concentration	102
5.8 Critical Oxygen	105
5.9 Carbon Steel with Inhibitor	107
5.10 Summary	113
<b>Chapter 6</b>	115
<b>PASSIVE MATERIALS</b>	
6.1 Introduction	115
6.2 Bench Marking – Materials in HW443	116
6.3 Materials in 3.5% NaCl at Different Temperatures	119
6.4 Materials in Seawater	122
6.5 Materials in Different Sulphate-Chloride Ratio	126
6.6 Materials with Inhibitor	136
6.7 Materials in a Reduced Oxygen Environment	137
6.8 Summary	151
<b>Chapter 7</b>	154
<b>CERMETS ALLOYS</b>	
7.1 Introduction	154
7.2 Cermet Alloys in HW443	156
7.3 WC-Co in Seawater and Different $\text{SO}_4^{2-}/\text{Cl}^-$ Ratios	158
7.4 WC-Ni in Seawater and Different $\text{SO}_4^{2-}/\text{Cl}^-$ Ratios	162
7.5 Summary	166

<b>Chapter 8</b>	168
<b>DISCUSSION</b>	
8.1 Introduction	168
8.2 The Demand for Green Hydraulic Fluid	169
8.3 The Corrosion Mechanism on Carbon Steel	170
8.3.1 Protective film on passive alloys	175
8.4 The Role of Metastable Pitting.	176
8.5 Pitting Corrosion on Passive Alloys	179
8.6 Passivation	180
8.7 Role of Anion on Corrosion Attack	182
8.8 Passive Potential Range	186
8.9 Effect of Temperature on Pitting Corrosion	189
8.10 Effect of Oxygen on Corrosion Attack	190
8.11 The Role of Inhibitor to Corrosion Protection	191
8.12 25Cr Duplex Stainless Steel	192
8.13 CermetsAlloy	192
8.13.1 Introduction	192
8.14 Pseudo-passivation	194
8.15 Active Corrosion of Cermet Alloys	195
8.16 Effect of Binder	195
8.17 The Effect of pH to Corrosion Attack	197
<b>Chapter 9</b>	202
<b>CONCLUSIONS AND FUTURE WORK</b>	
9.1 Conclusions	202
9.2 Suggestions for future work	203
<b>References</b>	204



## List of Figures

Figure 1.1 Diagram showing a typical subsea manifold and subsea field equipment arrangement	2
Figure 1.2 Nine slot template being lifted from a work boat and being deployed from a drilling rig	3
Figure 1.3 Hydraulic fracturing in a vertical well	4
Figure 1.4 Typical oil and gas production flow diagram	6
Figure 1.5 The pressure difference between water-base hydraulic fluid and hydraulic fluid oil in increasing seawater depth	7
Figure 1.6 The oil hydraulic fluid increase in viscosity as the pressure increases	7
Figure 1.7 Directional Control Valve	10
Figure 1.8 A schematic diagram of the Directional Control Valve (DCV)	10
Figure 2.1 Oxygen solubility in seawater	15
Figure 2.2 Corrosion mechanism of iron	16
Figure 2.3 Mechanical analogy of free-energy change	21
Figure 2.4 Reaction potential energy profile	22
Figure 2.5 The schematic of three-electrode test cell	23
Figure 2.6 Combined diagram of an anodic and cathodic reaction with activation polarisation	25
Figure 2.7 Schematic diagrams of the three forms of activation polarization	26
Figure 2.8 Onset of concentration polarization at more reducing potentials for a cathodic reduction reaction	27
Figure 2.9 Effect of resistance polarization on the current in a corrosion cell	28
Figure 2.10 Uniform corrosion attack	30
Figure 2.11 Pitting corrosion mechanisms	31
Figure 2.12 Variation in cross sectional shape of pits	32
Figure 2.13 Pitting corrosion of stainless steel 316L in seawater	33
Figure 2.14 A schematic of the crevice corrosion propagation mechanism	34
Figure 2.15 Stages of crevice corrosion	35

Figure 2.16 LPR measurement from Tafel plot	41
Figure 2.17 A cathodic and anodic polarization plots cyclic potentiodynamic analysis	43
Figure 2.18 A cyclic polarization curve of negative and positive hysteresis	44
Figure 3.1 Composition of seawater	46
Figure 3.2 Variation of the logarithm of pitting corrosion current density with time for steel electrode immersed in solutions of $1 \times 10^{-3}$ M $\text{Ca}(\text{OH})_2$ containing increasing concentrations of NaCl at 25°C	48
Figure 3.3 Dependence of $E_{\text{pitting}}$ of carbon steel on the $\text{Cl}^-$ ions concentration	49
Figure 3.4 Effects of $\text{Na}_2\text{SO}_4$ concentration on the anodic behaviour of carbon steel in deaerated 0.5 M $\text{NaHCO}_3$ solutions at scan rate of 25 mV/s	50
Figure 3.5 Past applications of water and oil hydraulics	53
Figure 3.6 Types of hydraulic fluid	54
Figure 3.7 Adsorption type inhibitor	58
Figure 3.8 Polarisation diagram of an active-passive metal showing the dependence of the current on concentration of passivation-type inhibitor	59
Figure 3.9 Schematic representation of the benzimidazole molecule	60
Figure 3.10 Schematic of double layer in a liquid	61
Figure 3.11 Structure of inhibitor molecules	63
Figure 3.12 Norwegian Legislation	64
Figure 3.13 Pits with lace-like cover over the top and flat-walled opening	69
Figure 3.14 WC-Co microstructure (white is WC and black is Co)	76
Figure 3.15 Hexagonal structure of $\alpha$ -WC	77
Figure 3.16 Cermets and cemented carbides are formed of a main ceramic phase bond by a metal binder. Both metal and ceramic phase form continuous interpenetrated skeletons	77
Figure 4.1 Experimental set up for static corrosion test	88
Figure 4.2 Cyclic polarization curve	89
Figure 4.3 Tafel polarization for carbon steels	90

Figure 4.4 Schematic anodic and cathodic polarisation curve	91
Figure 4.5 Light microscope	92
Figure 4.6 Philips XL30 ESEM	93
Figure 5.1 Corrosion rate of AISI 1040 in different ‘seawaters’ (electrolytes) at 20°C	95
Figure 5.2 Linear polarisation for carbon steel	96
Figure 5.3 Comparison of AISI 1040 on corrosion rate in HW443 hydraulic fluid and distilled water	97
Figure 5.4 Corrosion rate of (a) AISI 1040 in 3.5% NaCl as a function of temperature and (b) comparison AISI 8620, AISI 1040 and AISI 4140 in 3.5% NaCl as a function of temperature	98
Figure 5.5 Carbon steel in immersion test at 20°C	99
Figure 5.6 AISI 1040 in HW443 and solution 1 for all temperatures	100
Figure 5.7 AISI 1040 in 3.5% NaCl and different sulphate to chloride ratios	102
Figure 5.8 Carbon steel in increasing chloride concentration	103
Figure 5.9 To determine the critical chloride concentration in 3.5% NaCl at 20°C	105
Figure 5.10 The corrosion rates of AISI 1040 (a) as a function of oxygen concentration at 4°C, 20°C and 50°C (b) eliminating 50°C data and the critical oxygen concentration was identified	106
Figure 5.11 Comparison of corrosion rate of AISI 1040 in solution 1 with CRW 85155 inhibitor added and hydraulic fluid HW443 at 20°C	107
Figure 5.12 The corrosion rate of AISI 1040 (a) at different temperatures with increasing concentrations of CRW 85155 (b) The “acceptable” corrosion rate	108
Figure 5.13 Percentage protection efficiency of CRW 85155 on AISI 1040 at different temperatures.	110
Figure 5.14 Effect of corrosion rate to chemisorption of inhibitor	111
Figure 5.15 Carbon steel in CRW 89000 inhibitor	111
Figure 5.16 Corrosion rate for carbon steel in HW443, CRW 85155 and CRW 89000 at 20°C	112
Figure 5.17 Corrosion rate for carbon steel in S1 added with 50ppm, 100ppm, 200ppm and 400ppm CRW 89000, solution 1, 3.5% NaCl and HW443	113

Figure 6.1 Schematic of anodic polarisation curve for passive materials at 20°C	116
Figure 6.2 Anodic polarisation curve of 316L in HW443 at 20°C (a) E-log i plot (b) E-I plot	117
Figure 6.3 Anodic polarisation curve of 316L, 25Cr duplex and Inconel 625 in HW443 at 20°C (a) E-log i plot (b) E-I plot	119
Figure 6.4 The anodic polarisation of 316L as a function of temperature in 3.5% NaCl	120
Figure 6.5 Anodic polarisation of materials in 3.5% at 20°C	121
Figure 6.6 Stainless steel 316L in solution 1( $\text{SO}_4^{2-}/\text{Cl}^-=0.14$ ) at different temperatures	123
Figure 6.7 25Cr duplex in solution 1( $\text{SO}_4^{2-}/\text{Cl}^-=0.14$ ) at different temperatures	123
Figure 6.8 Inconel 625 in solution 1 ( $\text{SO}_4^{2-}/\text{Cl}^-=0.14$ ) (a) at different temperatures (b) having metastable pitting at 80°C	124
Figure 6.9 The breakdown potential in S1 as a function of temperature with compared to $E_b$ in HW443	125
Figure 6.10 Stainless steel 316L in S2 ( $\text{SO}_4^{2-}/\text{Cl}^-=19.15$ ) at different temperatures.	127
Figure 6.11 Stainless steel 316L in S3 ( $\text{SO}_4^{2-}/\text{Cl}^-=0.75$ ) at different temperatures	128
Figure 6.12 Stainless steel 316L in S4 ( $\text{SO}_4^{2-}/\text{Cl}^-=0.99$ ) at different temperatures	128
Figure 6.13 25Cr duplex in S2 ( $\text{SO}_4^{2-}/\text{Cl}^-=19.15$ ) at different temperatures	129
Figure 6.14 25Cr duplex in S3 ( $\text{SO}_4^{2-}/\text{Cl}^-=0.75$ ) at different temperatures	129
Figure 6.15 25Cr duplex in S4 ( $\text{SO}_4^{2-}/\text{Cl}^-=0.99$ ) at different temperatures	130
Figure 6.16 Inconel 625 in S2( $\text{SO}_4^{2-}/\text{Cl}^-=19.15$ ) at different temperature	130
Figure 6.17 Inconel 625 in S3 ( $\text{SO}_4^{2-}/\text{Cl}^-=0.75$ ) at different temperatures	131
Figure 6.18 Inconel 625 in S4 ( $\text{SO}_4^{2-}/\text{Cl}^-=0.99$ ) at different temperatures	133
Figure 6.19 The breakdown potential in S2 as a function of temperature	133
Figure 6.20 The breakdown potential in S3 as a function of temperature	134
Figure 6.21 The breakdown potential in S4 as a function of temperature	134
Figure 6.22 The breakdown potential value of every material in different $\text{SO}_4^{2-}$	134

/Cl<sup>-</sup> solutions as compared to HW443 at 20°C

Figure 6.23 Microscopic image shows pitting of (a) 316L in solution 3 at 80°C, (b) 316L in solution 2 at 50°C and (c) 316L in solution 2 at 80°C	135
Figure 6.24 Microscopic image shows pitting (a) 25Cr duplex in solution 3 at 80°C, (b) 316L in solution 2 at 80°C, (c) 25Cr duplex in solution 1 at 20°C, (d) 25Cr duplex in solution 1 at 50°C, (e) Inconel 625 in solution 3 at 80°C (f) 316L solution 3 at 20°C (g) Inconel 625 in solution 4 at 4°C (h) Inconel 625 in solution 3 at 4°C	136
Figure 6.25 $E_b$ of materials in S1 with and without CRW 89000 (100ppm) at 20°C	137
Figure 6.26 316L in S1 with and without oxygen at 4°C	138
Figure 6.27 316L in S1 with and without oxygen at 20°C	138
Figure 6.28 316L in S2 with and without oxygen at 4°C	139
Figure 6.29 316L in S2 with and without oxygen at 20°C	139
Figure 6.30 316L in S3 with and without oxygen at 4°C	140
Figure 6.31 316L in S3 with and without oxygen at 20°C	140
Figure 6.32 316L in S4 with and without oxygen at 4°C	141
Figure 6.33 316L in S4 with and without oxygen at 20°C	141
Figure 6. 3425Cr duplex in S1 with and without oxygen at 4°C	142
Figure 6. 3525Cr duplex in S1 with and without oxygen at 20°C	142
Figure 6. 3625Cr duplex in S2 with and without oxygen at 4°C	143
Figure 6. 3725Cr duplex in S2 with and without oxygen at 20°C	143
Figure 6. 3825Cr duplex in S3 with and without oxygen at 4°C	144
Figure 6. 3925Cr duplex in S3 with and without oxygen at 20°C	144
Figure 6. 4025Cr duplex in S4 with and without oxygen at 4°C	145
Figure 6. 4125Cr duplex in S4 with and without oxygen at 20°C	145
Figure 6. 42Inconel 625 in S1 with and without oxygen at 4°C	146
Figure 6. 43Inconel 625 in S1 with and without oxygen at 20°C	147
Figure 6. 44Inconel 625 in S2 with and without oxygen at 4°C	147

Figure 6. 45Inconel 625 in S2 with and without oxygen at 20°C	148
Figure 6. 46Inconel 625 in S3 with and without oxygen at 4°C	148
Figure 6. 47Inconel 625 in S3 with and without oxygen at 20°C	149
Figure 6. 48Inconel 625 in S4 with and without oxygen at 4°C	149
Figure 6. 49Inconel 625 in S4 with and without oxygen at 20°C	150
Figure 6.50 Comparison of breakdown potential for passive alloys in every solution at 4 °C	150
Figure 6.51 Comparison of breakdown potential for passive alloys in every solution at 20 °C	151
Figure 6.52 Comparison of materials in different media as compared to HW443	153
Figure 7.1 SEM/EDX analysis of received cobalt tungsten carbide sample	155
Figure 7.2 SEM/EDX analysis of received nickel tungsten carbide sample	155
Figure 7.3 Potential versus current density for WC-Co and WC-Ni in HW443 at 20°C	157
Figure 7.4 Anodic polarisation of WC-Co in S1 at different temperatures	158
Figure 7.5 Reverse potential of WC-Co as a function of temperature in every solution	161
Figure 7.6 Corrosion rate, $C_R$ (mpy) of WC-Co in different sulphate/chloride ratios as a function of temperature	161
Figure 7.7 WC-Ni in solution 1 at 4°C	162
Figure 7.8 Reverse potential of WC-Ni as a function of temperature in every solution	165
Figure 7.9 Corrosion rate of WC-Ni in all solutions at increasing temperature	165
Figure 7.10 Cermets alloy under microscopic observation (a) WC-Ni in solution 4 at 4°C, (b) WC-Ni in solution 4 at 50°C, (c) WC-Ni in solution 2 at 50°C and (d) WC-Co in solution 1 at 80°C	167
Figure 8.1 Arrhenius relations in 3.5% NaCl	171
Figure 8.2 Schematic of the activation energy peaks for nucleation	171
Figure 8.3 Microscopy view of AISI 1040 in 3.5% after corrosion attack at	172

20°C

Figure 8.3 Oxygen concentration profiles through seawater and corrosion product (rust) layer	177
Figure 8.4 Oxygen concentration profiles through seawater and corrosion product (rust) layer	175
Figure 8.5 Current (oxygen) transfer through water and rust layer	176
Figure 8.6 Changes of number of metastable pits with time on different paper finished surfaces	177
Figure 8.7 Schematic model of metastable pits	179
Figure 8.8 Schematic drawing showing an adsorption of two kinds of anions at different concentration	186
Figure 8.9 Passive range for 316L, 25Cr duplex and Incoenl 625 in all solutions as a function of temperature	187
Figure 8.10 The difference in passive range from 4°C to 80°C for passive alloys in different sulphate-chloride ratio solutions	188
Figure 8.11 Schematic presentation of the reactions taking place on the WC-Co surface	194
Figure 8.12 WC-Ni in S1 at 20°C	196
Figure 8.13 Current density appear as independent applied potential	197
Figure 8.14 Corrosion rate for cermets alloy in different sulphate/chloride ratio at increasing temperature. (a: Solution 1( $\text{SO}_4^{2-}/\text{Cl}^- = 0.14$ g/L), b: Solution 2( $\text{SO}_4^{2-}/\text{Cl}^- = 19.15$ g/L), c: Solution 3( $\text{SO}_4^{2-}/\text{Cl}^- = 0.75$ g/L) and d: Solution 3( $\text{SO}_4^{2-}/\text{Cl}^- = 0.99$ ))	201

## List of Tables

Table 2.1 Standard oxidation-reduction potentials, 25°C, Volts (V) versus normal hydrogen electrode	19
Table 3.1 Composition of seawater and pure water properties.	52
Table 3.2 Toxicity classification parameters for the HOCNF Scheme	66
Table 3.3 Material selection for retarding corrosion	80
Table 4.1 Carbon steel composition of samples (wt%)	82
Table 4.2 Alloy composition of samples (wt%)	83
Table 4.3 Mechanical properties of materials	83
Table 4.4 Standard seawater composition	84
Table 4.5 The six major elements in seawater being used	85
Table 4.6 Ionic contents of the solutions used	86
Table 4.7 Composition of solutions	87
Table 5.1 Sulphate and chloride for all solutions	101
Table 5.2 Corrosion rates and % Protection efficiency of AISI 1040	109
Table 6.1 Electrochemical data of materials in HW443 at 20°C	119
Table 6.2 Electrochemical data of 316L in 3.5% NaCl	121
Table 6.3 Electrochemical data of materials in 3.5% NaCl at 20°C	122
Table 6.4 The performance of breakdown potential, $E_b$ for passive alloys in different composition of sulphate/chloride ratio at increasing temperature	152
Table 6.5 The rank of performance for passive alloys in different sulphate/chloride ratio (1-5 is Best to Worst)	152
Table 7.1 Element value	157
Table 7.2 Electrochemical parameters of materials in HW443 at 20°C	158



Table 7.3 Electrochemical parameter for WC-Co in all solutions	160
Table 7.4 Electrochemical parameter for WC-Ni in all solutions	164
Table 7.5 Ranking of cermets alloy in different solutions	166

## Nomenclature

$G$	Energy (J)
$\Delta G$	Free energy (J)
$\Delta G^{\#}$	Activation-energy barrier (J)
$M$	Metal
$G$	Activation-energy barrier (J)
$M$	Metal
$M^{n+}$	Metal charged ions
$ne^{-}$	Transferred electrons
$E$	Actual potential in volts which is measured against a reference electrode
$E_0$	Equilibrium electrode potential (V)
$E_0^{\circ}$	Standard metal equilibrium electrode potential at 25°C
$R$	Ideal gas constant 1.986 calories/mole ° K (8.3143J/mol·K),
$T$	Temperature (° K)
$n$	Number of electrons in the anodic half reaction
$F$	Faraday's constant of 96,494 Coulombs/mole
$a$	Chemical activity of the species involved in the reaction
$a_{product}$	The activities of product species
$a_{reactant}$	The activities of reactant species
$r_{oxid}$	The equilibrium oxidation rate
$r_{red}$	The equilibrium reduction rate
$I$	Current (A)
$i$	Current density (A/cm <sup>2</sup> )
$\eta$	Overpotential (V)
$\beta$	Tafel constant (mV/decade)
$\beta_a$	Tafel constants for the anodic reaction (mV/decade)
$\beta_c$	Tafel constants for the cathodic reactions (mV/decade)
$D$	Diffusion coefficient
$C_B$	The concentration of the reacting molecules or ions
$x$	Thickness of the diffusion layer
$E_{corr}$	Free corrosion potential (V)
$E_{0,anod}$	Equilibrium electrode potential for the anodic reaction (V)
$E_{0,cath}$	Equilibrium electrode potential for the cathodic reaction (V)

$E_H$	Hydrogen evolution potential (V)
$E_{rep}$	Potential of repassivation (V)
$i_{0,anod}$	The exchange current density for the anodic reaction ( $A/cm^2$ )
$i_{0,cath}$	The exchange current density for the cathodic reaction ( $A/cm^2$ )
$i_{corr}$	Corrosion current density ( $A/cm^2$ )
$i_L$	Limiting current density ( $A/cm^2$ )
$i_{rev}$	Reversed current density ( $A/cm^2$ )
$i_{max}$	Maximum current density ( $A/cm^2$ )
$i_s$	Stabilised current density ( $A/cm^2$ )
$i_a$	Amplitude of current density ( $A/cm^2$ )
$C_{dl}$	Capacitor (V)
$R_p$	Resistance polarisation ( $\Omega$ )
$R_s$	Resistance of the bulk solution
$H_V$	Vickers hardness value
$PRE(n)$	Pitting Resistance Equivalent number
$R_r$	Reaction rate
$CPT$	Critical Pitting Temperature
$SE$	Secondary Electron
$BSE$	Back Scattered Electron
$Ag/AgCl$	Silver/Silver chloride
$\rho$	Particle density ( $g/cm^3$ )
$t$	Time (sec)
$E_b$	Breakdown potential (mV)
$\sigma$	Standard deviation
$Q$	Total charge transfer (Coulombs/ $cm^2$ )

## Chapter 1

### INTRODUCTION

#### 1.1 Economic Impact of Corrosion

Corrosion is a complex electrochemical process involving the interaction between metallic materials and their environment, which produces corrosion products and leads to the degradation of the materials [1]. Various factors affect the corrosion process, such as the type of material, design, water vapour, anions in the environment, such as sulphate, chloride and carbonate. Although it is often impossible to completely stop corrosion in metals, it can be controlled.

Downhole tubing, surface pipelines, pressure vessels and storage tanks in oil and gas production are subjected to internal corrosion by water, which is enhanced by the presence of carbon dioxide (CO<sub>2</sub>) and hydrogen sulphide (H<sub>2</sub>S) in the gas phase. The major cost item is for internal corrosion control. The total annual cost of corrosion in the oil and gas production in the US industry is almost \$300 billion [2], which includes the additional costs for new constructions, maintenance costs for aging or corroding equipment, the cost of inspections and structural integrity evaluations as well as the costs associated with corrosion-related failures and outages. This analysis shows that the "cost of corrosion" is a major economic consequence to society, which is reflected in the increased losses that it causes to various industrial sectors of the economy. The engineers responsible for specifying materials are continually searching for ways to reduce costs and increase performance in industry without sacrificing reliability. Generally, the successful and economical exploration and exploitation is heavily dependent on material performance and the need for protection against the corrosion of equipment. Most importantly, the principles of corrosion must be understood in order to effectively select materials and to design, fabricate and utilize metal structures for the optimum economic life of facilities and safety in operation.

The oil and gas industry comprises two parts: upstream (the exploration and production sector of the industry) and downstream (the sector which deals with refining and processing of crude oil and gas products, their distribution and marketing. Subsea

production systems comprise a wellhead, valve tree (Xmas tree) equipment, pipelines, structures and a piping system. A number of wellheads have to be controlled from a single location. The operations from a subsea control system are part of the subsea production system performance whereas the reliability of the control system is a critical factor in ensuring safe operation. The control system governs the operation of the valves and chokes on subsea completion, templates, manifolds and pipelines (Figure 1.1 and 1.2). In addition to satisfactory operational function, the design of a control system must also provide the means for a safe shutdown on failure of the equipment or on the loss of hydraulic or electrical control from the surface (a platform or floating facility) and other safety features that automatically prevent dangerous occurrences. Other than design, material degradation of the valve is another factor that causes the failure of the equipment.

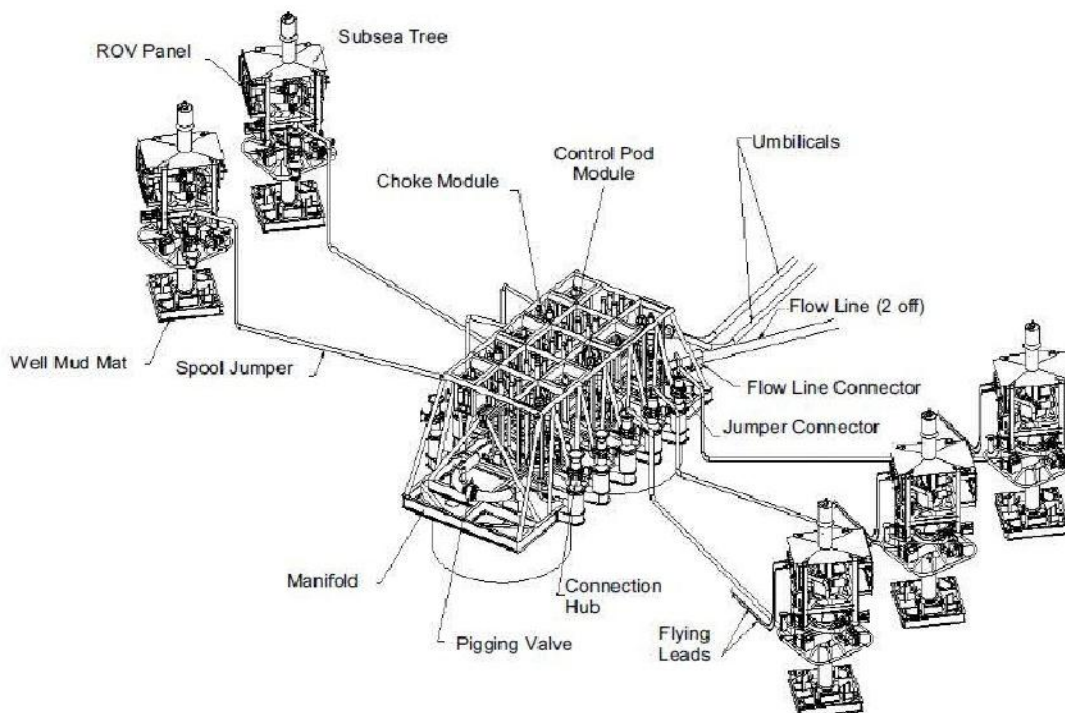


**Figure 1.1 Diagram showing a typical subsea manifold and subsea field equipment arrangement [3].**



**Figure 1.2 Nine slot template being lifted from a work boat (left) and being deployed from a drilling rig (right)[4].**

Materials degrade due to corrosion caused by the aggressiveness of seawater. However, technological advances on many fronts are increasing the productivity and efficiency of oil and gas production. Research shows that by using certain chemicals (inhibitors), corrosion can be controlled on conventional carbon steels. With the concern over environmental issues, the main topic concerning the usage of chemical is how they are discharged into the sea.

Extracting oil and gas from shale sometimes requires horizontal drilling and hydraulic fracturing. Hydraulic fracturing is a process involves using water, sand and a small amount of chemicals to fracture the hydrocarbon-bearing rock formation to allow flow of hydrocarbons into the wellbore of oil and natural gas locked inside dense, impermeable shale. A multiple barrier comprised of layers of protective steel casing and cement around the casing are installed in the wells to ensure that neither the fluid that will eventually be pumped through the well nor the oil or gas that will eventually be collected enter the water supply as shown in Figure 1.3. After that, at sufficient pressure, high volumes of fracturing fluids are pumped deep into the well to create or restore the small fractures in the reservoir rock. According to industry estimates,

hydraulic fracturing has been applied to more than 1 million wells nationwide, and often multiple times per well [5].

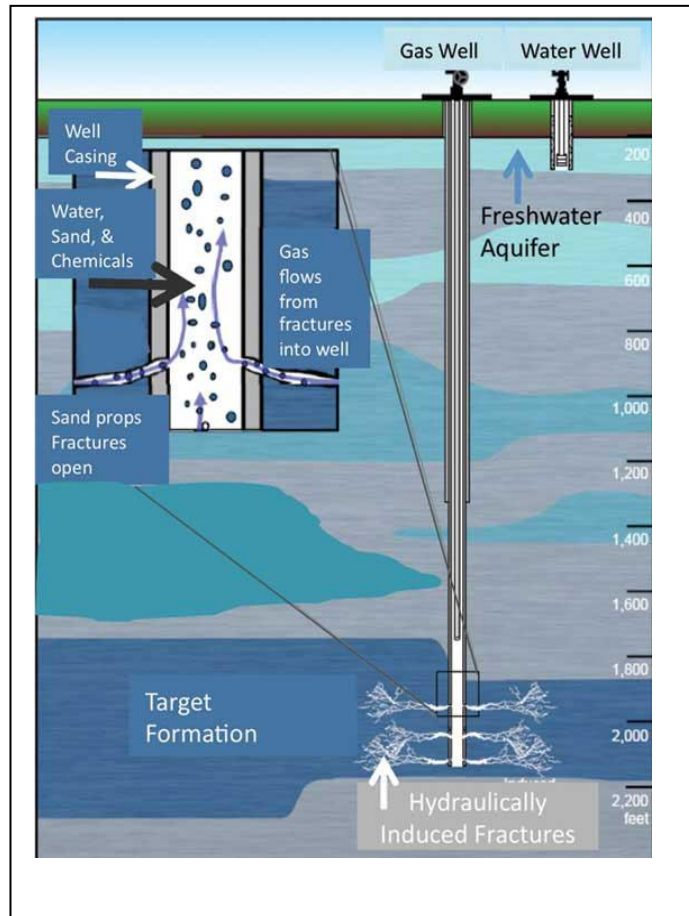


**Figure 1.3 Hydraulic fracturing in a vertical well [6].**

Apart of that, some types of hydraulic fluids also use to flush through umbilical to remove any seawater that may be caught between the umbilical connectors and their manifold docking points during installations. These flush fluids will be discharged to the sea by operating the hydraulic circuitry to flush each relevant part. The discharge volume has to be small (typically <10 litres) and the fluid should be low toxicity. Currently, they are using Oceanic HW443 hydraulic fluid which has a very low toxicity [7].

The subsea control module which is located at each well tree in subsea field equipment will hydraulically operate the tree valves. This operation will cause small loss of hydraulic fluid from the valve to the sea and therefore needs intermittently the hydraulic fluids to be topped up. This can be done by supplying the hydraulic fluid through an umbilical from the host platform. From this activity it was estimated that approximately 2,500 litres per annum of hydraulic fluids were discharged directly to the

sea. For that reason, hydraulic fluids should be low toxicity and water-based hydraulic fluid are the best choice to replace oil-based hydraulic fluids [7].

Generally, the progress of the oil and gas business stems from practices and values that respond to the nation's ongoing commitment to a clean environment. The report by the National Energy Policy Development Group, in the US stated that energy companies are focusing on 'the three pillars' of sustainable development – economic, environment and social considerations[8]. With the growing number of companies, the annually reported progress is based on these three pillars. In reflecting on this matter, the oil and natural gas industry makes major investments in environmental protection, both in complying with regulations, implementation, learning and safety. The results have reduced the environmental problem every year. Other efforts targeting environmental issues concern protecting surface and groundwater, and preserving plant and animal life.

It can be concluded that applying new technologies at every stage of oil and gas production will simultaneously increase productivity. In addition, manufacturers keep identifying solutions that balance the benefits of production with the ongoing drive for environmental protection. Where companies once focused solely on complying with regulations, many now view environmental performance more broadly as a core business value. This research is part of finding an alternative or environment choice for discharging the waste from oil and gas production to the environment. It would be easier if seawater is treated with inhibitors or deionised in some way that could be used as a hydraulic fluid; however, this presents many challenges associated with the corrosion of the materials of construction, the environment and the material's lifetime.

## **1.2 The Industrial Problem Challenge**

It is proven that pitting corrosion can be avoided by using oil-based hydraulic fluids [9]. However, oil and gas operations insist that oil needs to be cleaned before being discharged into the sea. Such cleaning under marine conditions is complicated and the oil-water mixtures are needed to be transported along the pipelines to onshore separation units. This task could be minimised by using seawater as a hydraulic fluid. In addition to the potential cost benefits, seawater could also be easily discharged into the sea. Figure 1.4 shows a typical oil and gas production flow diagram. It includes the process of extraction of oil, water and mixed gases from the rock formation.



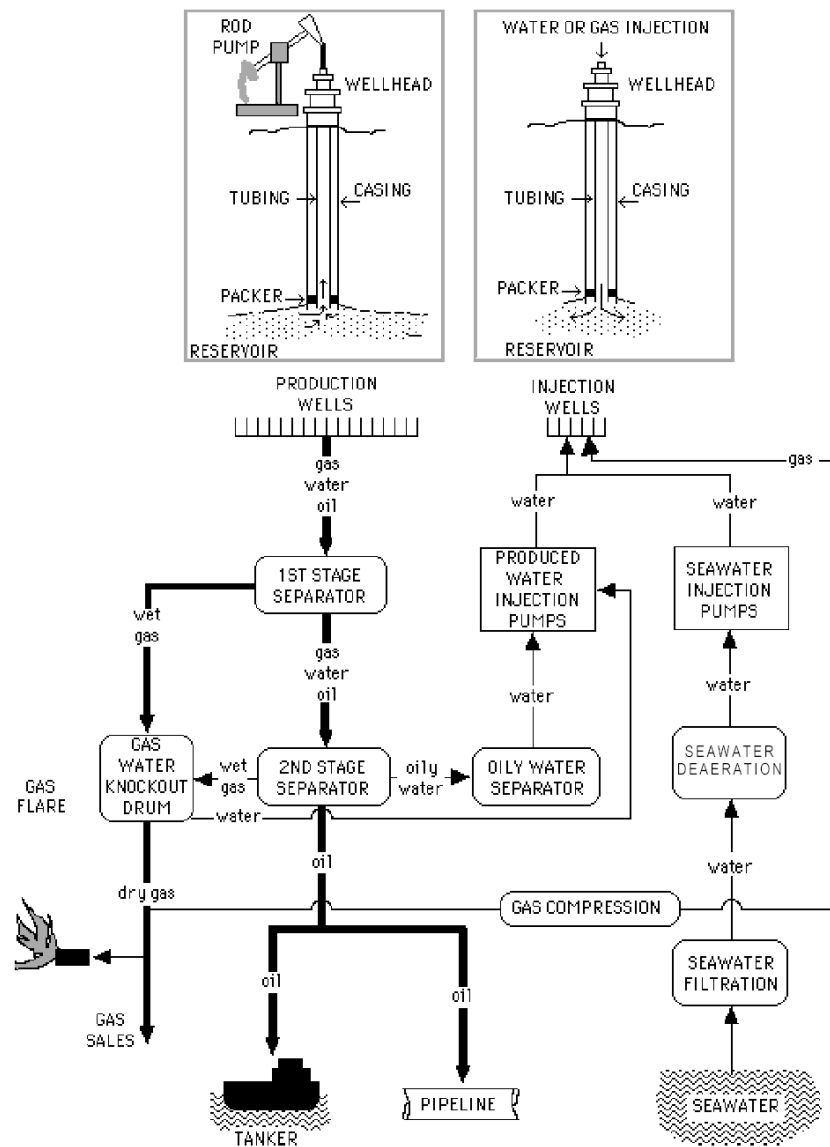


**Figure 1.4 Typical oil and gas production flow diagram [10]**

According to Simon McManus [11], the using of hydraulic fluids in the extreme water depth, will affectreliability due to work-over cost, stability and compatibility of the fluid, and pressure to the static system in the subsea. There is a large pressure difference for oil-based hydraulic fluids as compared to the pressure needed for seawater at increasing depths of seawater. In contrast to water-based hydraulic fluids, the pressure difference between water-based hydraulic fluids and seawater needed is not more than 2 baras the depth increased as shown in Figure 1.5. He also added that, due to drastic changes in pressure, the viscosity of hydraulic oil increases compared to water-based hydraulic fluids as shown in Figure 1.6. In long umbilicals, increasing the

viscosity will give effect to hydraulic fluid especially when the diameter of the umbilical is changed. This is more crucial in narrow umbilicals which need more time to pressurise oil-based hydraulic fluids due to compressibility and viscosity. The system afterwards will clog due to redundant hydraulic line and leaves the fluids end up in the ocean. This might be harmful for marine life, whereas, water-based hydraulic fluid without any chemical addition considered to be less toxic to marine life. Overall, this would be safe if the operations used seawater as hydraulic fluid. Water-based hydraulic fluids bring many benefits compared to oil hydraulic fluid due to low viscosity, low compressibility and high specific gravity. Also there is an associated reduced cost of operating in the oil and gas operations.

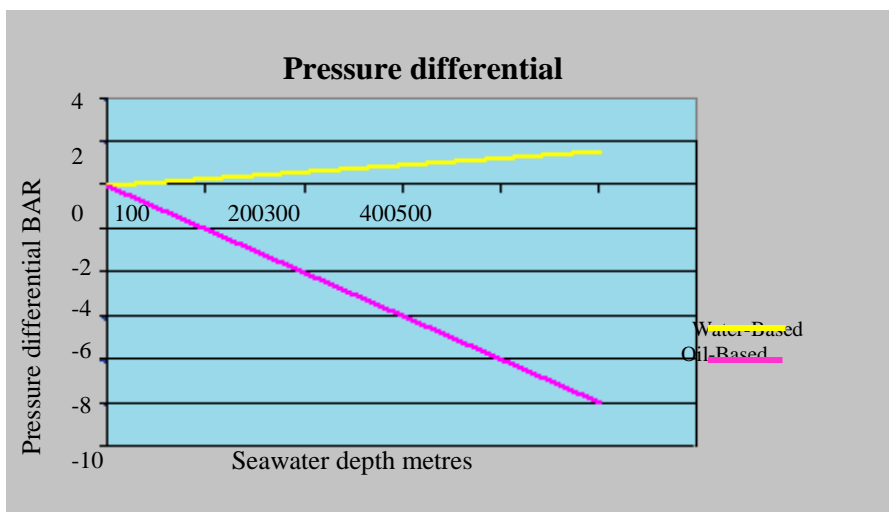


Figure 1.5 The pressure difference between water-based hydraulic fluids and hydraulic oil in increasing seawater depth [11].

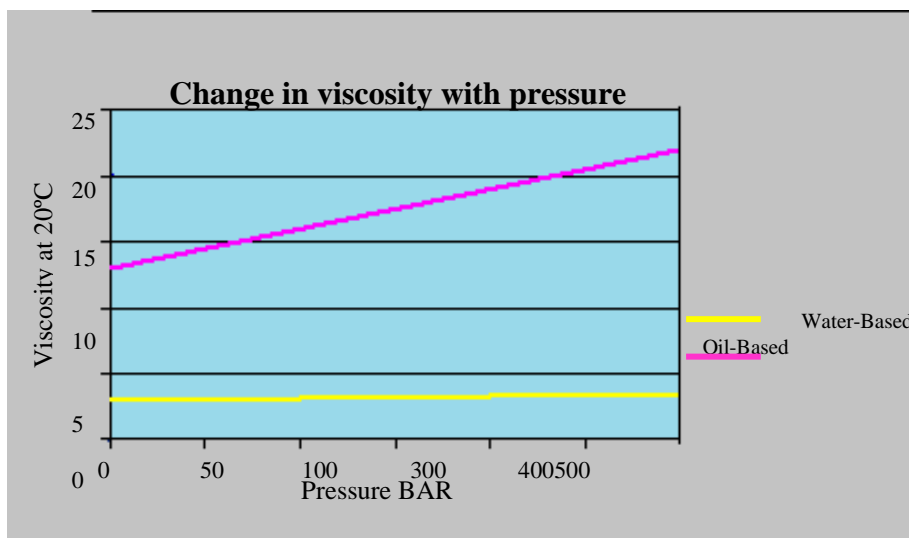


Figure 1.6 The oil hydraulic fluid increase in viscosity as the pressure increases [11].

With concerning the environmental issue and cost of oil and gas operations, therefore the usage of seawater as a hydraulic fluid would bring many benefits to replace oil-based hydraulic fluids. The most crucial issue is how to control the corrosion attack and ensure the water-based hydraulic fluids perform and comparable way to oil-based hydraulic fluids. Corrosion in oil and gas production varies from location to location. Corrosion can be classified into one of three general categories; internal corrosion caused by the produced fluids and gases, external corrosion caused by exposure to groundwater or seawater and atmospheric corrosion caused by salt spray and weathering offshore. Of these, internal corrosion is the most costly since internal mitigation methods cannot be easily maintained and inspected.

### **1.3 Background of This Study**

Generally, oil and gas plant controls the oil or gas well through a wellhead control panel. Each well is equipped with a downhole valve, which consists of a master valve (MV). This on-off valve is controlled from the control system by sending a signal through umbilicals to about 1,300 metres below. These umbilicals also distribute electrical power, communication and a supply of hydraulic fluid to the subsea. When the signal arrives, the valve acts on spring pressure allowing hydraulic fluid to flow through a directional control valve (DCV as in Figure 1.7) to open the master valve. The whole system, including the DCV, are made from different types of material ranging from carbon steel to high strength and corrosion resistant materials.

The health and safety practices for subsea activities, means the hydraulic fluid is no longer suitable for use in oil and gas operations. The process of discharging the waste hydraulic fluid is very costly, which has led to the suggestion to use seawater as the hydraulic fluid. Not only is seawater available subsea, but by using the seawater as a hydraulic fluid, no more treatment is needed when discharging the waste, which could reduce the cost of the operation. The principal problem in using seawater as a hydraulic fluid is the risk of corrosion.

The main objective of this research is to investigate, from a corrosion point of view, the feasibility of using seawater as a hydraulic fluid. The best hydraulic fluid is the benchmark to determine an acceptable corrosion rate and the hydraulic fluid chosen is HW443 which is described in detail later. Compared to other commercial hydraulic fluids used by oil and gas companies, HW443 shows the best corrosion resistance at elevated temperature [12]. The selection of materials in this study includes those mostly

used in subsea systems including DCV materials.

Most industries use inhibitors as their corrosion control. However, when the environment is of prime concern, whenever anything is discharged overboard into the water in offshore operations it should meet the relevant regulatory requirements. With the environmental requirement and the necessity to obtain an acceptable corrosion rate that is comparable to commercial hydraulic fluids, this project was undertaken by way of contributing to the present practices of the oil and gas industry. Corrosion could be controlled by alteration of the corrosion factors or by adding an inhibitor as previously practiced by most companies. However, most of the effective inhibitors have an issue concerning biocompatibility, biodegradability, bioaccumulation and toxicity composition that is harmful to the sea habitat. Most issues arise when discharging the waste direct to the sea through bioaccumulation, which can be described as a chemical's tendency to be taken up and stored by living organisms through their environment and diet[13].

This is the first study, undertaken in conjunction with Aker Solutions, to assess the feasibility of using seawater as a hydraulic fluid and the associated corrosion challenges. The deterioration of the Directional Control Valve (DCV as shown in Figure 1.7) materials in seawater was studied and compared with the degradation rates and mechanisms in a commercial hydraulic fluid. This DCV functions as shown schematically in Figure 1.8. To achieve better results than a commercial hydraulic fluid, some alterations were made by either changing the sulphate-chloride ratio of seawater or the addition of an inhibitor. Although changing the sulphate-chloride ratio in seawater would be difficult in practice (perhaps, treatment water to appropriate sulphate/chlorite ratio to get acceptable corrosion rate), previous research has elucidated that aggressive anions can increase corrosion attack whereas non aggressive anions penetrate the corrosion attack. Thus, by changing the ratio in this research, the critical ratio of aggressive and non aggressive anions can be assessed on corrosion attack.

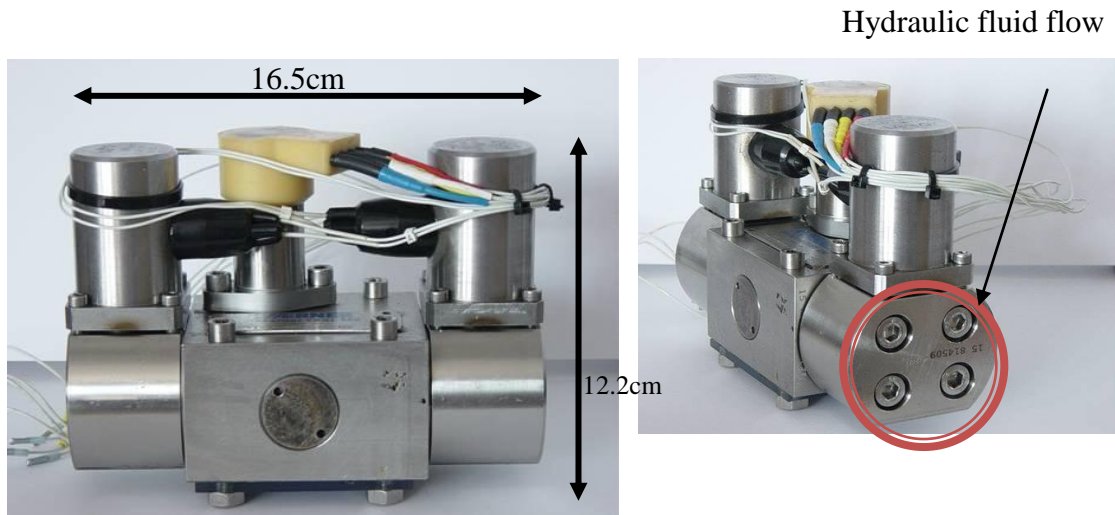


**Figure 1.7 Directional Control Valve**

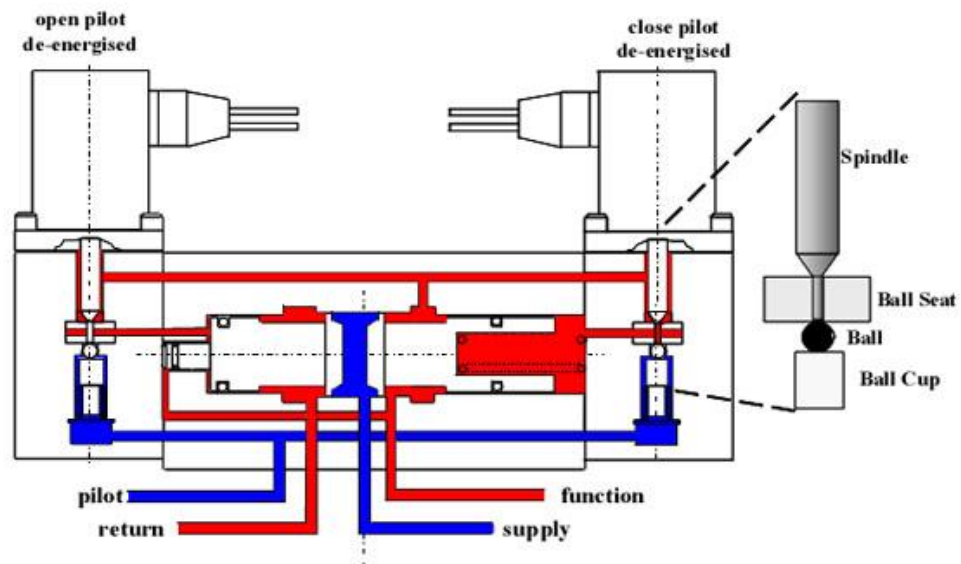


**Figure 1.8 A schematic diagram of the Directional Control Valve (DCV) [12].**

## 1.4 Objectives

The objectives of this study are

1. To evaluate the corrosion performance of Directional Control Valve (DCV) materials of construction (carbon steels, stainless steel 316L, 25Cr duplex, Inconel 625, nickel carbide, cobalt tungsten carbide) as a function of seawater parameters such as temperature, oxygen, sulphate-chloride ratio and with green inhibitors in static conditions.

2. To evaluate the corrosion attack on materials in seawater in comparison to commercial hydraulic fluid HW443.

3.To focus on key areas relating to the performance and durability of the materials and assess the corrosivity of materials and critical parameters that decrease corrosion resistance.

4.To prepare critical parameters and suitable corrosion control strategies for the management of corrosion in seawater systems that are comparable to commercial hydraulic fluids.

## **1.5 Thesis Outline**

The layout of this thesis is as follows:

Chapter 1 provides the introduction and background to the project.

Chapter 2 presents some basic corrosion theory relating to this study involving thermodynamics and electrochemistry.

Chapter 3 presents the literature review relating to static corrosion, hydraulic fluids and repassivation-depassivation of passive materials. Some models and techniques developed are also reviewed.

Chapter 4 describes the composition and properties of the materials, as well as the experimental procedures and calculations for possible solutions.

Chapter 5 presents the results of a detailed study of the corrosion of carbon steel in seawater and in the benchmark HW443 Hydraulic fluid.

Chapter 6 presents the results of 316L, 25Cr Duplex and Inconel 625.

Chapter 7 presents the results of WC-Co and WC-Ni.

The results chapters contain the electrochemical data for different corrosion parameters including sulphate to chloride ratio, temperature, oxygen, identification of acceptable corrosion rates that are comparable to commercial hydraulic fluid.

Chapter 8 discusses the numerous important aspects relating to corrosion and the areas that this study makes a contribution to the current understanding.

Chapter 9 summarises the conclusions of the present project and outlines some suggestions for future work. Finally, the references cited in the thesis are listed.

## Chapter 2

### **REVIEW OF RELEVANT THEORY**

#### **2.1 Basic Aqueous Corrosion**

Corrosion is defined as the deterioration of a material through a chemical or electrochemical reaction with its environment [13-14]. Materials often have a natural tendency to combine with other chemical elements to return to their lowest energy state. In order to return to lower energy states, materials frequently combine with oxygen and water, both of which are present in most natural environments, to form hydrated oxides and in the case of iron the iron oxide refers to “rust”. Depending on the environment, corrosion can be classified as “wet” or “dry” corrosion. Wet corrosion occurs when a liquid is present and usually involves an aqueous solution or electrolytes. It accounts for the greatest proportion of corrosion incidences in the various industries[15]. A common example is corrosion of steel by water. Dry corrosion occurs in the absence of a liquid phase or above the dew point of the environment. Vapours and gases are usually the corrodents. Dry corrosion is most often associated with high temperatures. In this chapter, attention is given to corrosion in aqueous solutions, and dry corrosion, or as commonly known, high temperature oxidation, is not considered. The basic aqueous corrosion theory will aid the understanding of the corrosion behaviour of materials under the specific conditions addressed in this study.

#### **2.2 Solution Characteristics**

##### **2.2.1 Conductivity**

One of the important characteristics of aqueous solutions with respect to corrosion is the conductivity of the solution. It is a measure of its ability to transport current. Seawater has conductivity of around 54000  $\mu\text{S}/\text{cm}$  while fresh drinking water will have conductivity less than 100  $\mu\text{S}/\text{cm}$ . In a good conductor such as seawater, the distant parts of the structure which are cathodic to some other area can play an effective part in the cathodic reaction but if the liquid is of poor conductivity, the flow of current will be limited to the immediate areas of contact between the two areas [14]. Current is transported easily in high-conductivity solutions but much less effectively in low-conductivity solutions. Various solutions exhibit a wide range of conductivities.



Seawater is a highly conductive solution and has a very low resistance to transporting current. Distilled water, however, is a very low conductivity solution and has a high resistance to the transport of current. In general, as the concentration of dissolved species in the solution increases, the conductivity increases, and, in general, as the conductivity of the solution increases, the corrosion of metals in that solution increases.

### 2.2.2 Acidity of alkalinity of a solution

Alkalinity can be defined as measurement of the ability of a solution to neutralize acids or a parameter to characterize the capacity of a solution to accept acid inputs without becoming 'too acidic'. Alkaline compounds in the water such as bicarbonates, carbonates, and hydroxides remove  $H^+$  ions and lower the acidity of the water which is increasing the pH value. The pH and alkalinity provide information about the acid-base properties of a solution and although the two parameters are related, they are independent. pH is defined as a negative decimal logarithm of the hydrogen ion activity in a solution [16]. Specifically pH is characterized as the activity of  $H^+$  in solution whereas alkalinity characterizes the stability of the system to stay at or near the original pH when the other substances are added.

$$pH = -\log [a_{H^+}] \quad 2.1$$

where  $a_{H^+}$  is the activity of hydrogen ions (molar concentration). Activity has a sense of concentration, however activity is always less than the concentration and is defined as a concentration (mol/L) of an ion multiplied by activity coefficient. The activity coefficient for diluted solutions is a real number between 0 and 1. The pH has a great effect on corrosion for particular metals. Solutions can be described as acidic, neutral or alkaline, based on the relative ratio of hydrogen ions to hydroxyl ions. When the hydrogen ions predominate over hydroxyl ions, the solution is acidic, whereas when the hydroxyl ions predominate over the hydrogen ions, the solution is alkaline and the solution is neutral when both are in balance. Strongly acidic solutions have a greater number of hydrogen ions, and strongly alkaline solutions have a greater concentration of hydroxyl ions. A value of pH 7 defines a neutral solution, and low values of pH identify the solutions as being acidic and higher values from 7-14 identify as alkaline. Tap water and seawater typically have neutral pH values.

### 2.2.3 Oxidizing solution

Oxidizing is a measurement of the tendency of a metal to corrode or oxidize. A solution of low oxidizing tendency corrodes only those metals at the lower (more active) end of the electromotive force series. A solution of strong oxidizing tendency corrodes all metals on the series except those with the most positive (most noble) values of the emf series. With the oxygen dissolved in a solution the oxidising tendency increases.

The oxygen dissolved in seawater is typically around 6-8 ppm [17]. The solubility of oxygen generally decreases with increasing temperature and salinity, and increases with increasing pressure.

Oxygen solubility is strongly temperature dependent and decreases at higher temperatures. Consequently, oxygen solubility in freshwater exceeds that in seawater by 1-3 mg/L, depending on temperature. It means that oxygen solubility increases as the pH increases from acidic to alkaline. Thus, the oxygen concentrations in rivers or lakes in mountainous areas is usually lower than in lowlands, because it is pressure dependent. Figure 2.1 shows the oxygen solubility in seawater at different temperature.

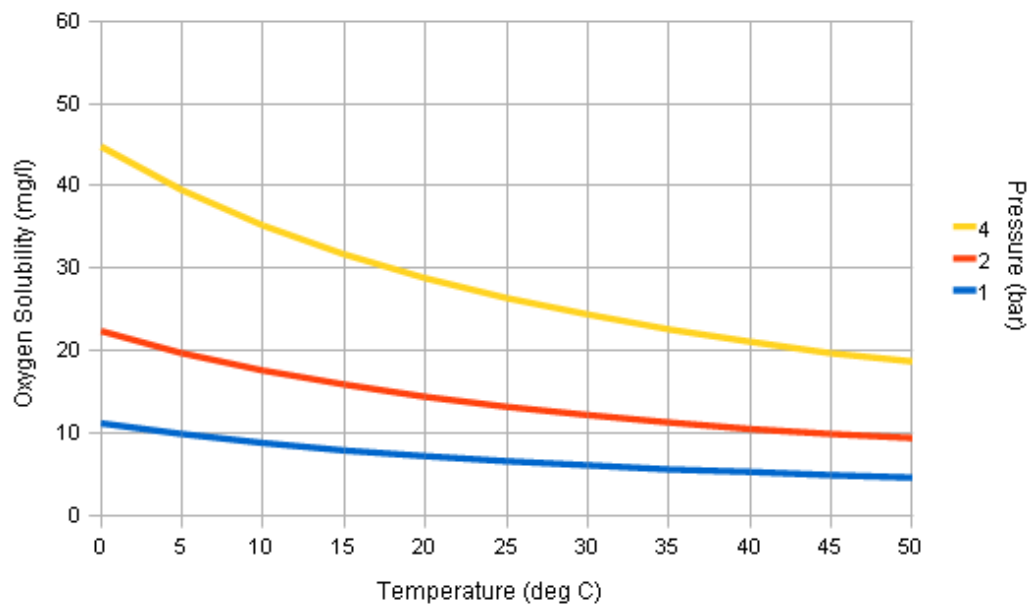


Figure 2.1 Oxygen solubility in seawater[17].

### 2.3 Corrosion Mechanisms

The mechanism of corrosion is the actual atomic, molecular or ionic transport process that takes place at the interface of a material [18]. Because the corrosion rate

cannot be observed directly on an atomic scale, it is necessary to infer possible mechanisms from indirect measurements and observations. Examples are the rate of change in weight or dimensions, the rate of build up of corrosion products in the environment, changes in surface appearance examined by microscope, or changes in the mechanical or physical properties. When electrochemical corrosion occurs, the mechanism may be inferred from the measurement of electrical potential and current. Figure 2.2 shows how a material degrades by the corrosion process.

The corrosion of metals in an aqueous environment is electrochemical in nature involving two or more electrochemical reactions taking place on the surface of the metal. As a result, some of the elements of the metal or alloy change from a metallic state into a non-metallic state. The energy of the system is lowered as the metal converts to a lower-energy form (explained in section 2.2). The change in the energy of the system is the driving force for the corrosion process, which behaves according to the laws of thermodynamics.

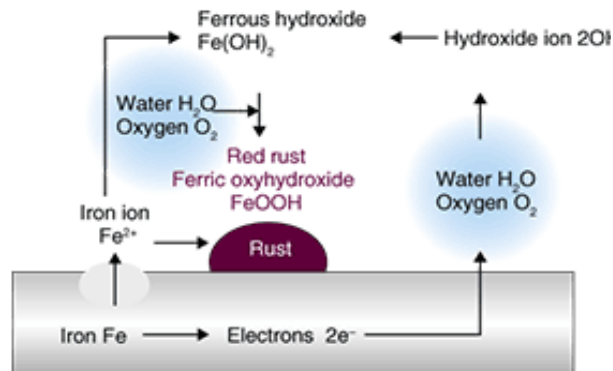
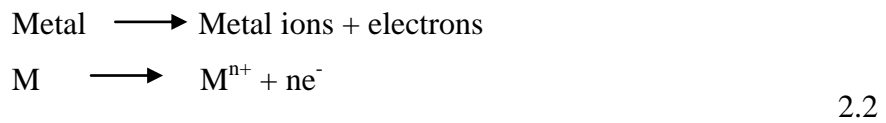


**Figure 2.2 Corrosion mechanism of iron [19]**

For corrosion to occur, three essential elements must be present: electrolyte, anode, and cathode. An electrolyte is a solution that can conduct an electric current. An electrolytic liquid refers to any liquid that contains ions. Electrodes can be of different metals or the same metal with different sizes or areas. Corrosion occurs because there is a difference in the electrical potential between the two electrodes/areas such that electricity flows in the electrolyte between them. This circuit must be completed by a metallic path between the two electrodes.

### 2.3.1 Anodic reaction

The anode is the site at which metal is corroded, i.e. at which metal dissolution takes place. Metal is dissolved and transferred to the solution as metal ions. Positively charged atoms of metal detach themselves from the surface and enter into the solution or electrolyte as ions. The electrons flow, as electrical current, to the cathode where they are consumed. This process is known as oxidation. The detached positive ions bear one or more charge. For example in the corrosion of zinc, each Zn atom releases two electrons and the Zn ions will carry two positive charges. The electrons travel through the metal to the cathode area.

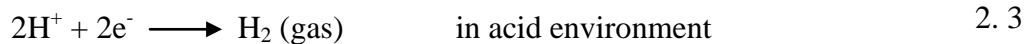


The reactions above take place at the anode and must be balanced by other reduction processes that occur at the cathode.

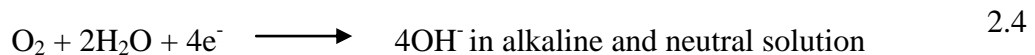
### 2.3.2 Cathodic reaction

Electrons reach the cathode by passing through the metal. At a cathode they may discharge, for example,  $\text{H}^{+}$  ions are present in acid electrolytes and form hydrogen gas. This process is known as reduction. In reduction, electrons are consumed. Thus, a cathodic reaction is a reaction that consumes electrons. When proton reduction occurs, the concentration of hydrogen ions in the electrolyte decreases and, thus, this increases the alkalinity of the electrolyte in the area of the cathode. The main reactions that occur at the cathode are:

- Hydrogen evolution



- If oxygen ions are present, oxygen reduction takes place



Several environmental factors can influence the corrosion rate:

- i. If  $\text{H}^{+}$  ions increase in concentration (pH drops), the corrosion rate will increase because there are more  $\text{H}^{+}$  ions to receive electrons at the cathode (i.e. the amount of oxidant increases).

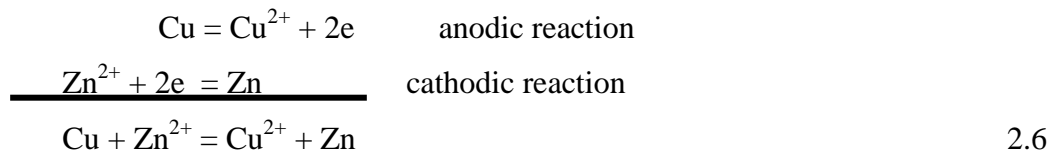
- ii. If the solution is made more alkaline, the corrosion rate may be reduced (i.e. by passivation).
- iii. If the concentration of the dissolved material is lowered, the conductivity of the electrolyte will decrease. Therefore, the resistance is increased, and impedes the flow of current. As a result, the overall corrosion rate is reduced.

### 2.3.3 Cell potential and exchange current density

As explained in section 2.3, corrosion occurs because there is a difference in the potential between the two electrodes. This potential results from the reaction between the anodic and cathodic areas on the surface of the metal. By understanding the cell potential of the reaction accompanying an electrochemical or corrosion reaction, the change in free energy (explained in section 2.5) can be calculated. This can be illustrated by the reaction between copper and zinc occurring at equilibrium:



This reaction can be divided into two half-cell reactions:



To determine the potential of a system in which the reactants are not at unit activity, the Nernst equation can be employed, which is:

$$E = E_0 + 2.3 \frac{RT}{nF} \log \frac{a_{\text{product}}}{a_{\text{reactant}}} \quad 2.7$$

Where  $E$  is the half-cell potential,  $E_0$  is the standard half-cell potential,  $R$  is the gas constant,  $T$  is the absolute temperature,  $n$  is the number of electrons transferred,  $F$  is Faraday's constant,  $a_{\text{product}}$  and  $a_{\text{reactant}}$  are the activities of product and reactant species. The activity is measurement for effective concentration of a species in a mixture. As indicated in the above equation, the half-cell potential becomes more positive as the amount of oxidised species increases. Table 2.1 shows the list of standard half-cell

potentials ( $E_0$ ) for some electrochemical reactions at 25°C versus the normal hydrogen electrode.

**Table 2.1 Standard oxidation-reduction potentials, 25°C, Volts (V) versus normal hydrogen electrode[20]**

Half cell reaction	Potential	Half cell reaction	Potential
$\text{Au} = \text{Au}^{3+} + 3\text{e}$	1.498	$\text{Pb} = \text{Pb}^{2+} + 2\text{e}$	-0.126
$\text{O}_2 + 4\text{H}^+ + 4\text{e} = 2\text{H}_2\text{O}$	1.229	$\text{Sn} = \text{Sn}^{2+} + 2\text{e}$	-0.136
$\text{Pt} = \text{Pt}^{2+} + 2\text{e}$	1.220	$\text{Ni} = \text{Ni}^{2+} + 2\text{e}$	-0.250
$\text{Pd} = \text{Pd}^{2+} + 2\text{e}$	0.987	$\text{Co} = \text{Co}^{2+} + 2\text{e}$	-0.277
$\text{Ag} = \text{Ag}^+ + \text{e}$	0.799	$\text{Cd} = \text{Cd}^{2+} + 2\text{e}$	-0.403
$\text{Hg} = \text{Hg}^{2+} + 2\text{e}$	0.788	$\text{Fe} = \text{Fe}^{2+} + 2\text{e}$	-0.440
$\text{Fe}^{3+} + \text{e} = \text{Fe}^{2+}$	0.771	$\text{Cr} = \text{Cr}^{3+} + 3\text{e}$	-0.744
$\text{O}_2 + 2\text{H}_2\text{O} + 4\text{e} = 4\text{OH}^-$	0.401	$\text{Zn} = \text{Zn}^{2+} + 2\text{e}$	-0.763
$\text{Cu} = \text{Cu}^{2+} + 2\text{e}$	0.337	$\text{Al} = \text{Al}^{3+} + 3\text{e}$	-1.662
$\text{Sn}^{4+} + 2\text{e} = \text{Sn}^{2+}$	0.150	$\text{Na} = \text{Na}^+ + \text{e}$	-2.714
$2\text{H}^+ + 2\text{e} = \text{H}_2$	0.000	$\text{K} = \text{K}^+ + \text{e}$	-2.925

Exchange current density  $i_0$  is a fundamental characteristic of electrode behaviour that can be defined as the rate of oxidation and reduction reactions at an equilibrium potential expressed in terms of current density. Exchange current density is a misnomer since there is no net current. The relationship between the exchange reaction rate and current density can be derived from Faraday's law [13].

$$r_{oxid} = r_{red} = \frac{i_0}{nF} \quad 2.8$$

Where  $r_{oxid}$  and  $r_{red}$  are the equilibrium oxidation and reduction rates and  $i_0$  is the exchange current density;  $n$  is the number of electrons transferred and  $F$  is Faraday's constant.

## 2.4 Determination of Corrosion Rates by Electrochemical Measurements

Electrochemical reactions are caused by an external voltage (voltage caused by a chemical reaction) as in an electrochemical cell. In general, electrochemistry deals with

oxidation and reduction reactions. To determine the potential of active polarisation, the Ohm's Law are widely used:

$$I = \frac{E}{R} \quad 2.9$$

Where  $E$  is the electric potential, defined as the capacity of an electric field to do work, and is measured in Volts (1 Volt = 1 Joule/Coulomb); Coulomb is the quantity of electricity measured in Amperes (1A = 1Coulomb/sec);  $I$  is the electric current, which is the movement of electrically charged particles and measured in amperes.  $R$  is the resistance, a term that describes the forces that oppose the flow of electron current and which are measured in Ohms (Volt/Ampere).

There are various ways of measuring the rate of corrosion, including AC impedance and electrochemical noise [21]. The modern techniques for the measurement of corrosion rates are based on the classical work of Stern and Geary [22]. The theoretical relationship between a metal freely corroding potential ( $E$ ), current density ( $i$ ) and the rate of corrosion was developed by Stern.

## 2.5 Corrosion Thermodynamics

Thermodynamics is the science of energy conversion and has been broadly applied to corrosion studies. It describes equilibria as a function of the elements and compounds present and the environmental conditions, such as pressure, temperature, and chemical composition. It includes the studies and calculations that indicate the spontaneous direction of a reaction, which are used to determine whether or not corrosion can occur, and to predict the stable corrosion products that may form.

### 2.5.1 Free energy

A law of nature is that the most stable state for a set of reactants is the state that has the lowest free energy,  $\Delta G$ . Accordingly, a metal in contact with a solution moves towards the lowest free-energy state. When the system arrives at this state, there is no further change. This final lowest-energy state is called equilibrium. At this stage, the system is stable, and there is no driving force for any change from that state. These principles are illustrated in Figure 2.3 by a mechanical analogy. If the ball moves from position 1 to position 2, this represents a decrease in free energy. The transition from position 1 to position 2 is a spontaneous direction for this particular system. Chemical

and corrosion reactions behave in the same way. The free-energy change accompanying an electrochemical reaction can be calculated by the following equation:

$$\Delta G = -nFE \quad 2.10$$

where  $\Delta G$  is the free-energy change,  $n$  is the number of electrons involved in the reaction,  $F$  is the Faraday constant, and  $E$  equals the cell potential.

Large negative free-energy changes give rise to large positive potential differences, and large positive free-energy changes give rise to large negative potential differences. If the change in free energy accompanying the transition of a system from one state to another is negative, this indicates that spontaneous reaction of the system is possible. If no external forces act on the system, the system will tend to transform to its lowest energy state. If the change in free energy is positive, this indicates that the transition represents an increase in energy, and this requires that additional energy be added to the system.

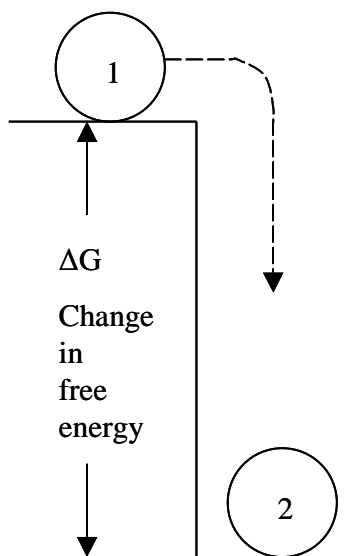


**Figure 2.3 Mechanical analogy of free-energy change [1]**

Figure 2.4 shows how a reactant forms a new product along the progress of reactions. For a chemical reaction to begin, there must be contact (collision) between the reactants. As the reaction proceeds, the potential energy rises to a maximum and the reactants form a cluster of atoms, called the activated complex. The highest point on the diagram is the activation energy,  $\Delta G$ , the energy that must be overcome for a reaction to occur. After the maximum, the potential energy starts falling as the atoms rearrange in the cluster, until it reaches a certain state of energy. Finally, colliding reactant molecules form products. There is the possibility that a collision between reactant



molecules may not form products. The outcome depends on the factors mentioned in the Transition State Theory. If the activated complex can pass the barriers, the product forms. Otherwise, the complex falls apart and reverts to the reactants[1].

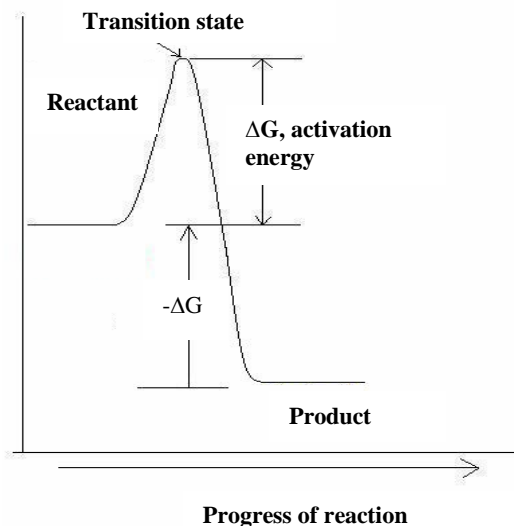


**Figure 2.4 Reaction potential energy profile**

## **2.6 Electrochemical Kinetics of Corrosion**

As explained in section 2.3.3, an electrochemical reaction involves Faraday's law. Michael Faraday discovered that current is generated by anodic reaction to an equivalent mass loss or corrosion penetration rate. Faraday's empirical laws of electrolysis relate the current of an electrochemical reaction to the number of moles of the element being reacted and the number of moles of electrons involved [20]. According to this, the reaction of 1 mol requires 1 mol of electron or 1 Avogadro's number of electrons ( $6.023 \times 10^{23}$ ). The charge carried by 1 mol of electrons is known as 1 faraday (F). The Faraday is related to another electrical unit through the electronic charge,  $1.6 \times 10^{-19}$  Coulombs (C).

### **2.6.1 The three electrode cell**

Most electrochemical accelerated tests make use of a three-electrode system, as shown in Figure 2.5. A potentiostat is used to control the potential of the working electrode versus a stable reference electrode submerged in an electrolyte, and together with an electrometer, an ammeter, logarithmic converter, and data acquisition device is

an automated instrument that provides variability of continuous sweep over a desired potential range. External current only flows between the working electrode and the counter electrode (also called auxiliary electrode).

The sample to be tested works as working electrode and it was carefully prepared with identified surface area. During running the experimental, the immersion time must be constant in order to stabilize the electrode in the electrolyte prior to start the test. The reference electrode has a stable and well-known potential. The high stability of the electrode potential is usually reached by employing a redox system with constant (buffered or saturated) concentrations of each participants of the redox reaction. The counter electrode exists to ensure that current does not run through the reference electrode, and often has a surface area much larger than that of the working electrode to ensure that the reactions occurring on the working electrode are not surface area limited by the counter electrode. Each electrode represents a half cell reaction.

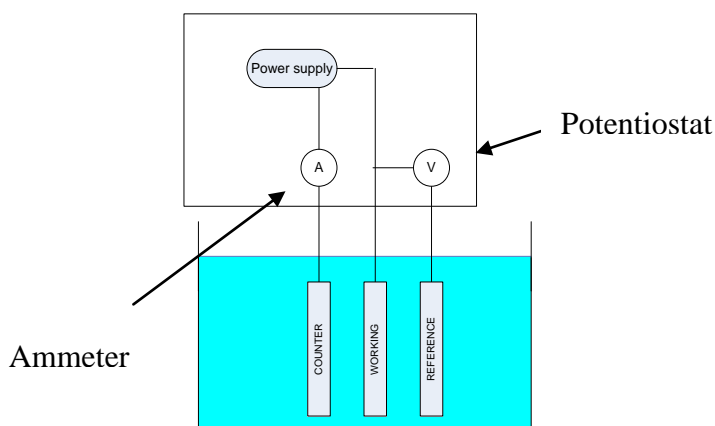


**Figure 2.5 The schematic of three-electrode test cell**

The basis of electrochemical accelerated test techniques is to change the potential of the working electrode and monitoring the current which is produced as a function of time or potential through the three-electrode system. As mentioned previously, changing an electrode potential from its OCP is referred to as polarization. Generally, polarization methods include linear polarization, Tafel plot measurement, wide range anodic polarization and cyclic polarization according to the scan range and direction.

### 2.6.2 Activation polarisation

Electric current from a potentiostat changes a test electrode potential from its open circuit potential (OCP), to a potential value that is determined by the magnitude of potentiostat current.

Electrochemical polarisation is divided into three main types – activation polarisation, concentration polarisation and resistance polarisation. Activation polarisation refers to the situation in which an electrochemical reaction is controlled by a slow step in the reaction sequence. Figure 2.6 graphically illustrates an activation polarisation for the anodic and cathodic reactions. This plot could be considered as a combination of anodic and cathodic reactions or mixed-potential. The requirements of mixed-potential theory are met at only a single point, that is, the point where the anodic and cathodic reaction curves cross. This is the only location at which the anodic reaction rate equals the cathodic reaction rate. The potential of this intersection is defined as  $E_{corr}$ , and the current at this intersection is defined as the corrosion current density,  $i_{corr}$ . The  $E_{corr}$  is referred to by several terms, including the corrosion potential, the free corrosion potential and the open-circuit potential. At potentials that are more positive or more oxidizing than the current potential, the anodic current is greater than the cathodic current, and more electrons are generated than are consumed. At potentials more negative or more reducing than the corrosion potential, the cathodic current is greater than the anodic current, and more electrons are consumed than are generated. A steady state of no net consumption or generation of electrons is only achieved at the corrosion potential ( $E_{corr}$ ) but not at more oxidizing and more reducing than the corrosion potential. In order to maintain a system away from the  $E_{corr}$ , an external current or other reactions must be supplied.

The slopes of the  $E$ - $\log i$  plots in the anodic regime and cathodic regime are referred to  $\beta_a$ ,  $\beta_b$  and give the Tafel slopes. The slopes are determined by the properties of both the surface of the metal and the electrolyte. Many researchers are assuming the Tafel values are 120 mV/decade for both anodic and cathodic for corrosion of steel. Their basis for assumption comes from related published work.

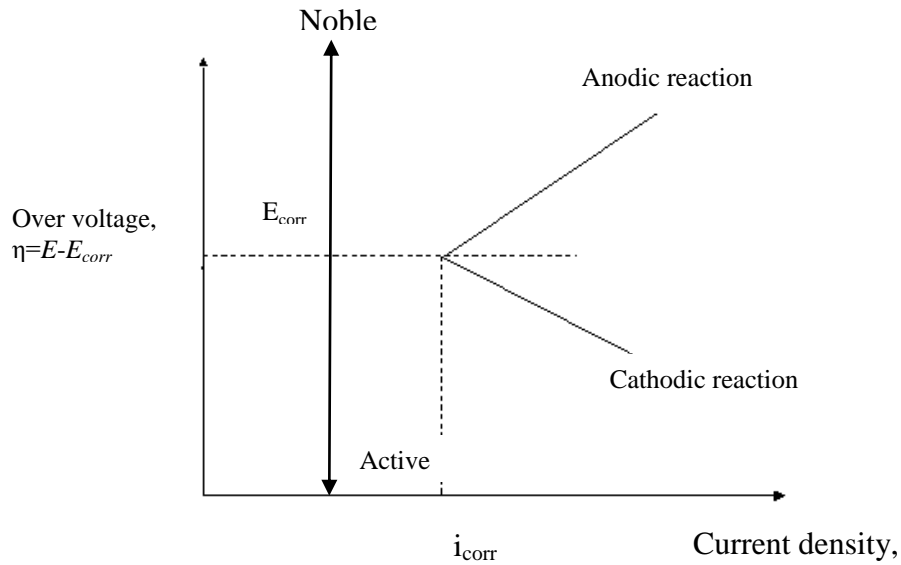


**Figure 2.6 Combined diagram of an anodic and cathodic reaction with activation polarisation [22].**

There are three forms of activation polarization control: mixed control, cathodic control and anodic control (Figure 2.7). The type of control basically results from the slope values of the anodic and cathodic curves. Under mixed control, the corrosion rate is equally sensitive to shifts in the anodic or oxidation reaction and the cathodic or reduction reaction. Under cathodic control, the slope of the reduction curve is greater than the slope of the oxidation curve. This results in the corrosion reaction being more sensitive to changes in the reduction reaction kinetics than to changes in the oxidation reaction kinetics. Under anodic control, the slope of oxidation reaction is greater than the slope of the reduction reaction curve. This results in the corrosion rate being more sensitive to changes in the anodic reaction kinetics than to changes in the cathodic reaction kinetics. With this knowledge it is possible to focus on the best method for corrosion control.

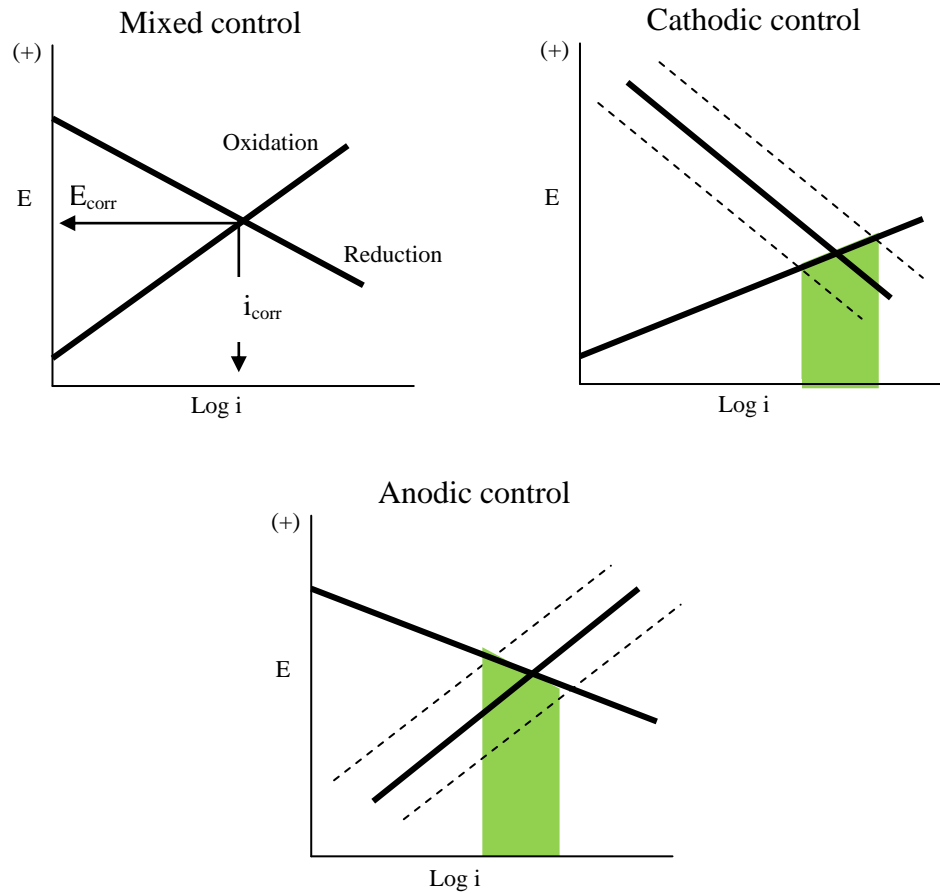


**Figure 2.7 Schematic diagrams of the three forms of activation polarization**

### 2.6.3 Concentration polarisation

Concentration polarisation refers to the situation in which a reaction is controlled by the supply of the reactant or the removal of products from a surface. The effect of concentration polarization on the shape of the cathodic polarization curve for a reduction reaction is shown in Figure 2.8. A frequent case of concentration polarization occurs when the cathodic processes depend on the reduction of dissolved oxygen since it is usually in low concentration. At low oxygen-reduction rates, the distribution of oxygen molecules in the solution adjacent to the electrode surface is relatively uniform. At very high reduction rates the region adjacent to the electrode surface will become depleted of oxygen molecules. Concentration polarization only becomes important when the dissolution current density approaches its limit,  $i_L$ , and causes an extended polarization curve. This represents the maximum rate of possible reduction in a system; the equation expressing this parameter is:

$$i_L = DnFC_B / x \quad 2.11$$

Where  $i_L$  is the limiting current density,  $D$  is the diffusion coefficient,  $C_B$  is the concentration of the reacting molecules or ions in the bulk solution, and  $x$  is the thickness of the diffusion layer. The equation shows that the limiting current density is a function of  $D$ ,  $C_B$  and  $x$ . Changes in these parameters will result in the change of limiting current density. The smaller the initial exchange current density, the larger will be the current density range over which the Tafel equation is likely to apply. The diffusion layer thickness is influenced by the shape of the particular electrode, the geometry of the system and by agitation. Agitation tends to decrease the diffusion layer thickness because of the convection current and, consequently, increases the limiting diffusion current density.

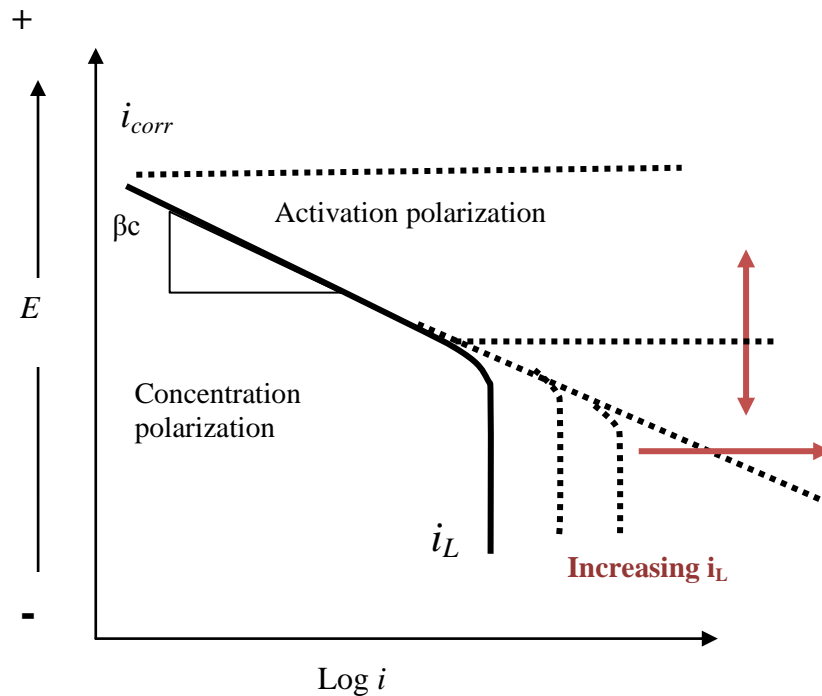


**Figure 2.8 Onset of concentration polarization at more reducing potentials for a cathodic reduction reaction.**

The effect of increasing the magnitude of the limiting current is shown by the dashed lines. As increasing the  $i_L$  moves the vertical segment of the line further to the right to higher current values, more of the linear portion controlled by activation control is observed.

### 2.6.4 Resistance polarisation

The third form of polarization in an electrochemical cell is resistance polarization, also known as ohmic polarization, which results from pure resistance elements along the current path in the cell. Ohmic resistance is also referred to as  $iR$  effects. Ohmic polarization is observed either in the region of ionic conductivity, where the current is transported by the movement of ions through the electrolyte from the anode to the cathode, or in the electronic conductivity region, where the current is transported through the metallic path from the cathode to the anode.

The effect of resistance polarization on the corrosion current in an electrochemical cell is shown in Figure 2.9 as potential versus current density. Three cases are shown, with the resistance of the solution increasing from the value of  $R_1$  (where resistance is essentially 0) to  $R_3$  (a high resistance value). The resulting current through the corrosion cell for each of these resistances is indicated by  $i_1, i_2$ , and  $i_3$ . When the conductivity of the solution is quite high, corresponding to essentially no resistance in the electrolyte, the cathodic reduction curve and the anodic oxidation curve intersect at  $i_L$ . In this case, the potentials of the anode and cathode are polarized to the same value. As the resistance of the solution increases, the potentials of the anode ( $E_a$ ) and the cathode ( $E_c$ ) are no longer equal. A potential drop ( $iR$ ) in the solution results from the passage of current ( $i$ ) through to the resistive solution ( $R$ ).

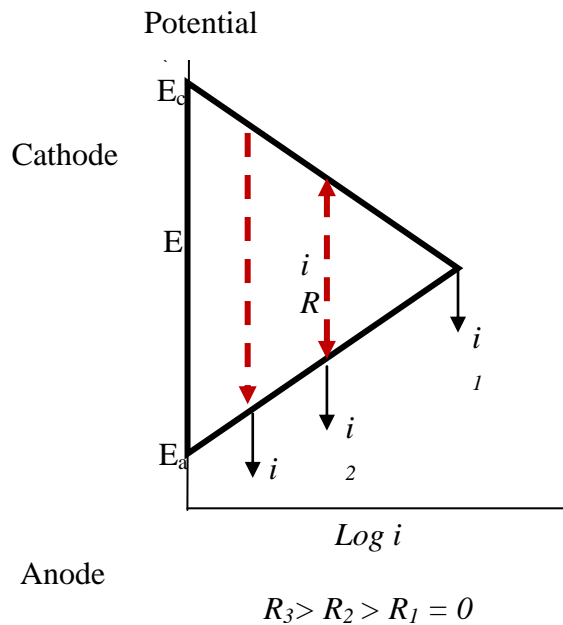


**Figure 2.9 Effect of resistance polarization on the current in a corrosion cell [20].**

The resulting effect is that some of the potential difference between the anode and cathode is taken up by the potential drop through the solution and is, as a consequence, unavailable to drive the activation controlled reactions. As the resistance of the solution increases from  $R_1$  to  $R_2$  to  $R_3$ , the magnitude of the potential drop of resistance polarization in the cell increases, with a resulting decrease in the corrosion current of the cell from  $i_1$  to  $i_2$  to  $i_3$ .

In seawater, which has high conductivity, there is very little resistance for a current to flow and, consequently, it has a high corrosion rate ( $i_1$ ), whereas tap water and distilled water have less conductivity, respectively, and, therefore, a low corrosion rate. Hence, an effective way to reduce the corrosion current in a corrosion cell is to increase the resistance to the ionic current flow through the cell.

## **2.7 Forms of Corrosion**

Corrosion problems can be divided into eight categories based on the appearance of the corrosion damage or the mechanism of attack: uniform, pitting, crevice, galvanic, erosion-corrosion, intergranular, dealloying and stress-corrosion-cracking (SCC) corrosion. Although these forms are present in aqueous corrosion, many of them are also operative at high temperature.

### **2.7.1 General corrosion**

General or uniform corrosion occurs uniformly over the entire metal surface causing a general thinning to take place until failure, as shown schematically in Figure 2.10. This form of corrosion is the most common sight where steel structures are abandoned to rust. The simplest method for dealing with uniform attack is based on the possible loss of material thickness in designing the system. However in some circumstances high general corrosion rates make it necessary to replace components, however, because the corrosion is uniform and measurable the management of corrosion is relatively simple. It is practically to control the corrosion by cathodic protection, coatings or paints or simply by specifying a corrosion allowance as it occurs uniformly over the entire surface of the metal component. In other cases, uniform corrosion adds colour and appeal to the surface.



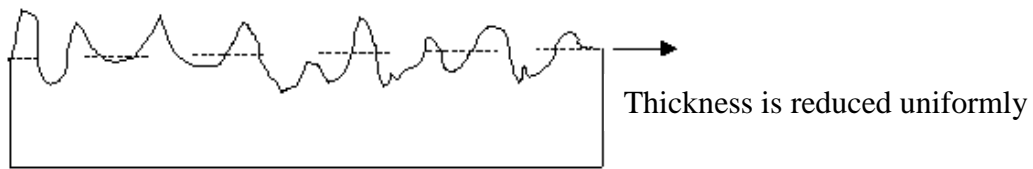


**Figure 2.10 Uniform corrosion attack**

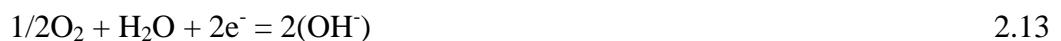
### **2.7.2 Pitting corrosion**

Pitting and crevice are two modes of localized corrosion. A major characteristic of these modes of corrosion is a large ratio of cathode area to anode area. Consequently, the current density and, hence, the corrosion rate over the occluded area is very large. Other than crevice, pitting corrosion is one of the most insidious forms of attack that can severely damage engineering alloys with undesirable consequences. It could be the most common type of localized corrosion in which small volumes of metal are removed by corrosion from certain areas on the surface to produce craters or pits that may culminate in complete perforation of a pipe or vessel wall. It occurs on a metal surface in a stagnant or slow-moving liquid.

Pitting corrosion is usually associated with active-passive-type alloys and occurs under conditions specific to each alloy and environment. Generally, it occurs on alloys when they are in the passive state. This mode of localized attack may create stress concentrations and, thus, reduce the fatigue life of a component. Pitting corrosion is characterized by two stages of pit initiation and growth. Generally, pits are initiated at pre-existing conditions on a passive surface or as a consequence of local events such as physical or chemical damage to the passive surface (Figure 2.11). Pit propagation will not occur if conditions lead to immediate repassivation of the local region. Pitting is usually preceded by an induction time to activate the local region following which the pit propagates as an occluded cell. Pit propagation presence of chloride ions growing by autocatalytic mechanism. Pitting corrosion of a stainless steel is illustrated in the Figure 2.11. The anodic reaction inside the pit begins with dissolution of iron;



The electrons given up by the anode flow to the cathode (passivated surface) where they are discharged in the cathodic reaction:



As a result of these reactions the electrolyte enclosed in the pit gains positive electrical charge in contrast to the electrolyte surrounding the pit, which becomes negatively charged. The positively charged pit attracts negative ions of chlorine  $\text{Cl}^-$  increasing acidity of the electrolyte according to the reaction:



pH of the electrolyte inside the pit decreases (acidity increases) from 6 to 2-3, which causes further acceleration of corrosion process[20]. Large ratio between the anode and cathode areas favors increase of the corrosion rate. Corrosion products ( $\text{Fe}(\text{OH})_3$ ) form around the pit resulting in further separation of its electrolyte.

Pitting cavities may fill with corrosion products and form caps over the pit cavities sometimes creating nodules or tubercles. Although the shapes of pits vary widely, as shown in Figure 2.12, they are usually roughly saucer-shaped, conical, or hemispherical for steel and many associated alloys. The image clearly illustrates that weight-loss methods are inadequate for pitting evaluations because even a very small weight loss can be concentrated in a few pits, with those of maximum depth penetrating the wall thickness to produce failure by leakage. However, pit depth increases not only with time, as would be expected, but also with surface area. Thus, to predict plant life from the small laboratory size test coupon results would be unwise. However, the pitting resistance of various alloys can be compared reasonably well from the maximum pit depth measurements in the laboratory.

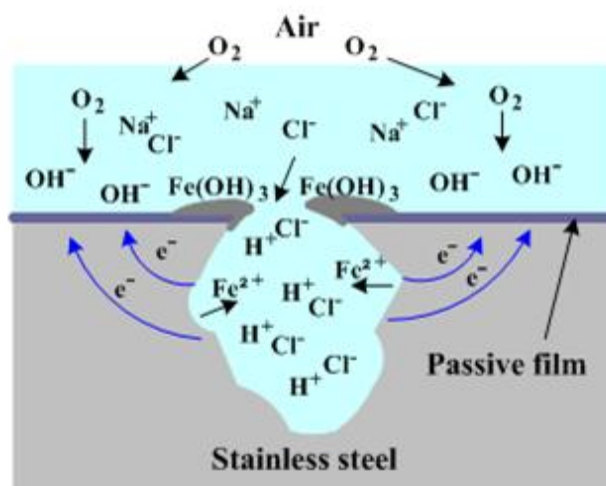
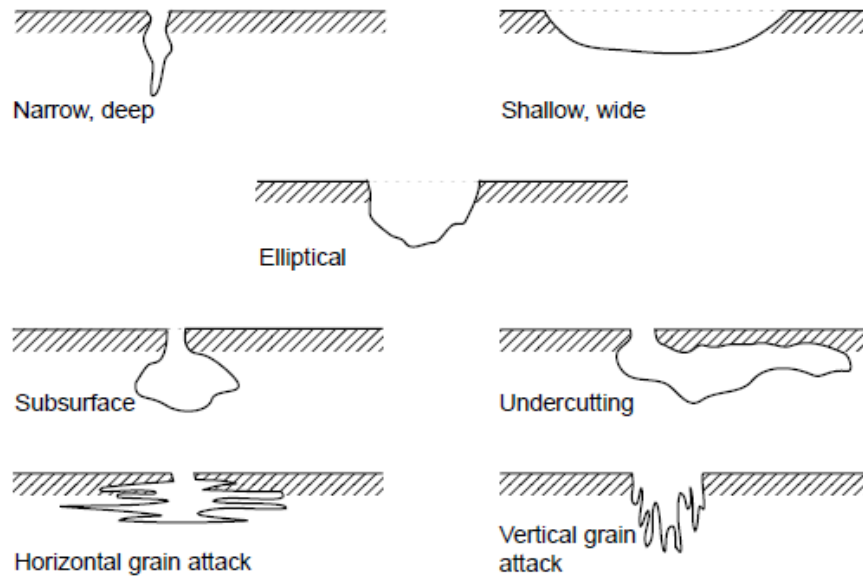


Figure 2.11 Pitting corrosion mechanisms [20].



**Figure 2.12 Variation in cross sectional shape of pits [24]**

It is generally accepted that temperature is one of the most important factors in pitting corrosion. When pitting occurs on the surface of stainless steels, the temperature dependence of pitting reactions is determined conventionally by measuring current densities under constant temperature conditions and controlled varying potentials over a number of different temperatures. Based on this point of view, the concept of Critical Pitting Temperature (CPT) was first introduced by Brigham and Tozer in 1973[25] and has been widely used as a criterion for ranking the pitting susceptibility in stainless steels.

Other than temperature, there are other factors that contribute to the initiation and propagation of pitting corrosion;

- Localized chemical or mechanical damage to a protective oxide film.
- Chemistry factors that can cause the breakdown of a passive film such as acidity; low dissolved oxygen concentrations, which tend to render a protective oxide film less stable; and high chloride concentrations
- Localized damage to or poor application of a protective coating
- The presence of nonuniformities in the metal structure of the component, for example, non-metallic inclusions

Growth of pitting or propagation will typically lead to the initiation of a pit due to the presence of an abnormal anodic site surrounded by normal surface, which acts as a cathode, or by the presence of an abnormal cathodic site surrounded by a normal surface in which a pit will have disappeared due to corrosion at the local cell, as shown in Figure 2.13 below.

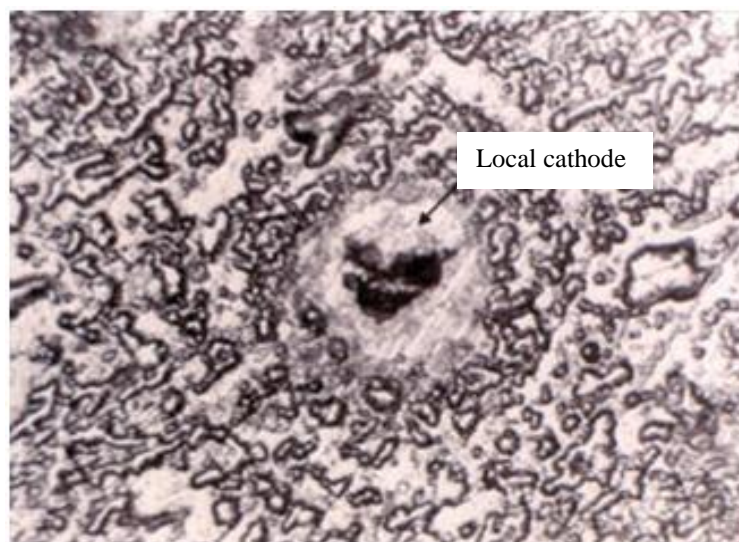


**Figure 2.13: Pitting corrosion of stainless steel 316L in seawater [26].**

The chromium (Cr), molybdenum (Mo) and nitrogen (N) contents of passive alloys, such as duplex stainless steels, are greatly influenced by their pitting and crevice corrosion behaviour. A usual way to rank the pitting resistance in stainless steels is by the use of the Pitting Resistance Equivalent Number (PREN). This is represented by the following equation:

$$\text{PREN} = \% \text{Cr} + 3.2\% \text{ Mo} + 16\% \text{ N} \quad 2.15$$

The higher the PREN, the better the pitting resistance[25]. This parameter is strongly dependent on the content of three most important elements Cr, Mo and N. Since there are two phases in the duplex stainless steel, with the three elements unevenly partitioned between them, the PREN for each phase should be calculated. The actual pitting resistance is governed by whichever phase gives the lower value[25]. A PREN above 38 is supposed to provide resistance to marine corrosion [27].

## 2.8 Crevice Corrosion

Although much of the previous discussion is applicable to pitting and crevice-type corrosion in that both involve occluded cells, crevice corrosion exhibits several

distinguishing features. A significant difference is that a crevice has the geometry of a pre-existing site for the occluded cell. Therefore, the initiation stages for the two modes differ. Crevice geometries are conducive to crevice corrosion in overlapping metal or non-metal surfaces, bolts, nuts, washers, joints, irregular surfaces associated with scratches and welds, poor adhering surface coatings and inert surface deposits.

The crevice corrosion propagation process is illustrated in Figure 2.14 for stainless steel corroding in a neutral aerated sodium chloride solution. The anodic metal dissolution reaction within the crevice is balanced by the cathodic reaction on the adjacent surface. The increased concentration of  $M^+$  within the crevice results in the influx of chloride ions ( $Cl^-$ ) to maintain neutrality. When the metal chloride formed, it is hydrolysed by water to the hydroxide and free acid. The acid produced by the hydrolysis reaction keeps the pH value low, while the pH of the solution outside the crevice remains neutral (pH 7).

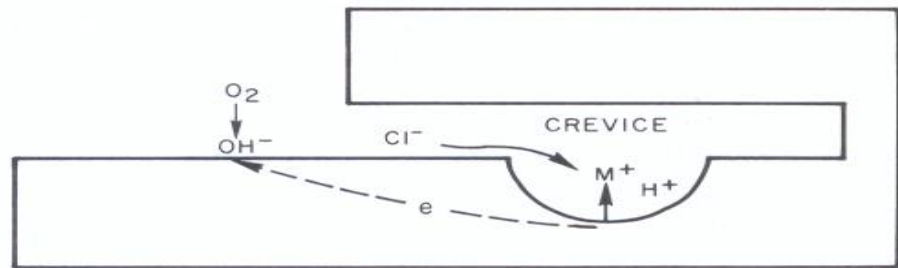


**Figure 2.14 A schematic of the crevice corrosion propagation mechanism**

The formation of crevice corrosion can be divided into three stages, as shown in Figure 2.15. At time zero, the oxygen content in the water occupying a crevice is equal to the level of soluble oxygen and is the same everywhere. In stage two, because of the difficult access caused by the crevice geometry, oxygen consumed by maintaining the passive film is very soon depleted in the crevice. The corrosion reactions now concentrate in the crevice (anodic) and on the open surface (cathodic). The large ratio of cathodic area compared to the anodic area that forms in these conditions is an aggravating factor that accelerates the anodic reaction. In stage three of the crevice development a few more accelerating factors fully develop:

- The metal ions produced by the anodic corrosion reaction readily hydrolyse giving off protons (acid) and forming corrosion products.
- The corrosion products seal the crevice environment even further.

- The accumulation of a positive charge in the crevice becomes a strong attractor to negative ions in the environment that can be corrosive in their own right.
- The pH in a crevice can reach very acidic values.

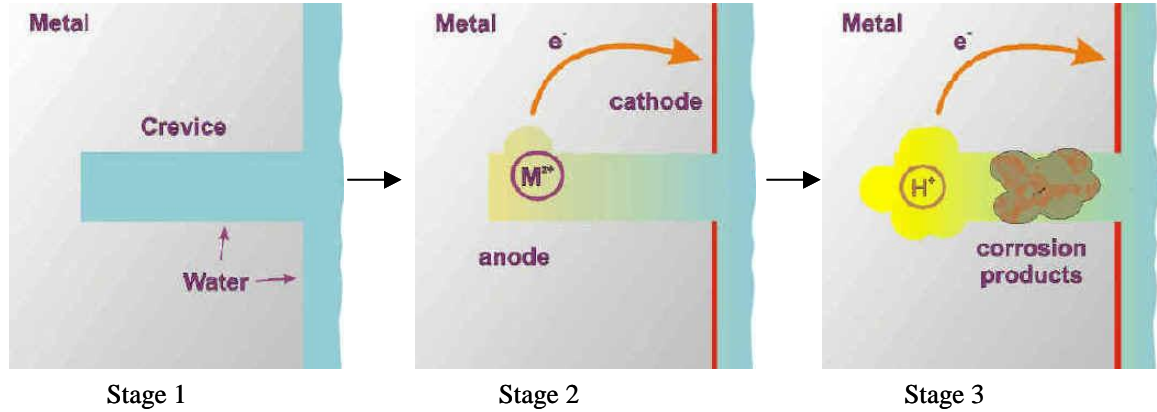


**Figure 2.15 Stages of crevice corrosion [28]**

## 2.9 Prevention of Corrosion Damage

Recognizing the symptoms and mechanism of a corrosion problem is an important preliminary step to find a convenient solution. There are basically five methods of corrosion control:

- i. Change to a more suitable material
- ii. Modifications to the environment
- iii. Use of protective coatings
- iv. The application of cathodic or anodic protection
- v. Design modifications to the system or component

Some preventive measures are generic to most forms of corrosion. These are most applicable at the design stage, probably the most important phase in corrosion control. It cannot be overemphasized that corrosion control must start at the “drawing board” and that design details are critical for ensuring adequate long-term corrosion protection. It is generally good practice to provide adequate ventilation and drainage to minimize the accumulation of condensation.

## 2.10 Corrosion Parameters

Environment is the one of the important key factors in any corrosion situation as environment is a variable that can change with time and conditions. This variable is a complex one, since all the environment factors actually affects a metal corresponds to the local environment at the surface of the metal. The corrosion parameters that affect aggressiveness of corrosion are anions such as chlorides and sulphates, pH, temperature and oxygen.

### 2.10.1 Chlorides

Salinity distinctly increases the corrosion rates. Apart from the enhanced surface electrolyte formation by hygroscopic salts such as NaCl and MgCl<sub>2</sub>, direct participation of chloride ions in the electrochemical corrosion reactions is also likely. In ferrous metals, chloride anions are known to compete with hydroxyl ions for combining with ferrous cations produced in the anodic reaction. In the case of hydroxyl ions, stable species tend to be produced. In contrast, iron chloride complexes tend to be unstable (soluble), resulting in further stimulation of corrosive attack. On this basis, metals such as zinc and copper, whose chloride salts tend to be less soluble than those of iron, should be less prone to chloride induced corrosion damage, consistent with practical experience.

According to Frankel [29], pitting corrosion will only occur in the presence of aggressive anionic species, and chloride ions are usually, although not always the cause. The severity of pitting tends to vary with the logarithm of the bulk chloride concentration [30]. The reason for the aggressiveness of chloride has been pondered for some time and a number of notions have been put forth. Chloride is an anion of a strong acid and many metal cations exhibit considerable solubility in chloride solutions [31]. It also relatively small anion with a high diffusivity and can interfere with passivation and it is ubiquitous as a contaminant.

In the study by Leckie and Uhlig (1966) on the effect of anions on the critical potential for pitting corrosion of stainless steel, they found that increasing the chloride concentrations shift the critical potential to more active values and the potential shifted to more noble values by the presence of other anions such as ClO<sub>4</sub><sup>-</sup>, SO<sub>4</sub><sup>2-</sup>, NO<sub>3</sub><sup>-</sup> and OH<sup>-</sup> in sufficient concentrations to act as pitting inhibitors [30]. But according to Schwenk, he found that the potential of stainless steel in 0.1N NaCl moves to more noble values with increasing Na<sub>2</sub>SO<sub>4</sub> concentration. But, above 0.15M Na<sub>2</sub>SO<sub>4</sub>, no

pitting observed and it means that sufficient  $\text{SO}_4^{2-}$  added to  $\text{Cl}^-$  solution inhibits pitting. [32]. Other anions also act as inhibitors and the amount necessary for complete inhibition varying with the anion. Thus, the sulphate/chloride ratio will study in this research to find the critical ratio that accelerates corrosion attack.

### 2.10.2 Temperature

The effect of temperature on atmospheric corrosion rates is complex in nature. An increase in temperature will tend to stimulate a corrosive attack by increasing the rate of electrochemical reactions and diffusion processes. For a constant humidity, an increase in temperature would lead to a higher corrosion rate. Raising the temperature will, however, generally lead to a decrease in relative humidity and more rapid evaporation of surface electrolyte. By reducing the time of wetness in this manner, the overall corrosion rate would tend to diminish.

For closed-air spaces, such as indoor atmospheres, the increase in corrosion rate is affected by the relative humidity, which is associated with a drop in temperature. At temperatures below freezing, where the electrolyte film solidifies, the electrochemical corrosion activity will drop to negligible levels in the absence of chloride contamination. The very low atmospheric corrosion rates reported in extremely cold climates are consistent with this effect.

#### 2.10.2.1 Arrhenius equation

After observing that many chemical reaction rates depended on the temperature, Svante Arrhenius, a chemist from Sweden developed Arrhenius equation to characterize the temperature-dependent reactions. The resulting negatively sloped line of logarithm of the rate constant,  $K$ , versus the inverse temperature,  $1/T$ , is useful for finding the missing components of the Arrhenius equation.

$$k = Ae^{-\frac{E_a}{RT}} \quad \text{or} \quad \ln k = -\frac{E_a}{RT} + \ln A$$

Where,  $k$  = chemical reaction rate,  $A$  = Pre-exponential factor

$E_a$  = Activation energy,  $R$  = Gas constant

$T$  = Temperature (K)



The activation energy,  $E_a$ , is the minimum energy molecules must possess in order to form a product. The pre-exponential is related to the amount of times molecules will hit in the orientation necessary to cause a reaction. It is important to note that the Arrhenius equation is based on the collision theory which particles must collide with proper orientation and with enough energy. The denominator of the exponential function contains the gas constant,  $R$  (J/mol\*k), and the temperature,  $T$ . It should be noted that Arrhenius plot shows that reaction rates are inversely proportional to temperature changes. Therefore, the negative slope from the Arrhenius plot gives the activation energy.

### 2.10.3 Oxygen

Pure water, without dissolved gases (e.g.: oxygen, carbon dioxide and sulphur dioxide) does not cause undue corrosion attack on most metals and alloys at temperatures up to the boiling point of water [33]. Even at temperatures of about 450°C, almost all of the common structural metals (except magnesium and aluminium) offer adequate corrosion resistance to high-purity water and steam [11]. Although electrochemical corrosion is intensified markedly in strong electrolytes, such as oil-field brines, the principal basic corrosive agents in injection waters are the common dissolved gases: oxygen, free carbon dioxide and hydrogen sulphide. According to Watkins and Kincheloe [34] (1958), corrosion of steel in water increased as the concentration of dissolved oxygen increased.

From the standpoint of corrosion, a significant water component is dissolved oxygen (DO) from ambient air. Oxygen acts both as a cathodic depolarizer and as an oxidizer. As a cathodic depolarizer, DO can remove hydrogen from the cathode during electrochemical corrosion and accelerate the corrosion attack. As an oxidizer, DO can be reduced on the metallic surface but participate directly in the electrochemical processes. According to Sridhar *et al.* [35], reduction in oxygen less than 0.06 ppm is required for stainless steel 316L to prevent localised corrosion. However, in this thesis the oxygen set for passive alloys are 0.04ppb and below (for without oxygen condition solutions).

A study by Uhlig *et al.* stated the effects of dissolved oxygen on the effectiveness of corrosion inhibitor absorption onto mild steel. Uhlig demonstrated that high concentrations of corrosion inhibitor increased corrosive attack of the metal substrate. He concluded that, small amounts of corrosion inhibitor, which is below a critical

dissolved oxygen concentration, could decrease the corrosion rate of carbon steels in oxygen containing environments. Furthermore, his findings demonstrate that the effectiveness of inhibitors rely on a critical dissolved oxygen content of the solution [36]. Caceres *et al.* [37] also agree that kinetic parameters of carbon steel has a significant dependence from dissolved oxygen (DO) and NaCl concentration when they study about the variation patterns for corrosion kinetics as a function of DO and NaCl concentration.

As increasing the temperature accelerates the corrosion rate of the steel due to faster reaction kinetics. The solubility of oxygen increases with increasing temperature, hence, increasing the corrosion rate of metal. For all above reasons, effect of dissolved oxygen will be study as a function to different sulphate-chloride ratio and temperature for every material.

## **2.11 Determination of corrosion rates in the laboratory**

Laboratory test methods include a number of direct current measurement techniques that are commonly used in electrochemical testing. Specific methods include linear polarisation, potentiodynamic polarisation, potentiostatic polarisation, galvanostatic polarisation, Tafel polarisation and polarisation resistance determinations. This electrochemical test as shown in Figure 2.5 provides the means for predicting long-term corrosion behaviour and service lifetime of metallic structures and also a tool for the monitoring of equipment to prevent catastrophic failure. The application of an electrochemistry test in the laboratory, can provide useful information for a variety of tasks and can also contribute to the selection and development of materials. The electrochemical corrosion measurements utilize the electrochemical nature of metallic corrosion. An external power source is used to apply a voltage or range of voltages to a metal specimen surface submerged in an electrolyte. The applied voltage or the voltage range pushes the metal-electrolyte interface beyond its steady state conditions, causing a measurable electric current to flow. Voltage and its corresponding current are independent and their relationship is used to determine metallic corrosion behaviour or estimate corrosion resistance or impedance.

### **2.11.1 Linear polarization resistance (LPR)**

The polarization resistance ( $R_p$ ) of a corroding metal is defined using Ohm's Law as the slope of the potential ( $E$ ) versus the current ( $I$ ) plot at the corrosion potential

( $E_{corr}$ ). By measuring this slope, the rate of corrosion can be measured. The correlation between  $i_{corr}$  and slope is given by:

$$\frac{\Delta E}{\Delta I} = \frac{\beta_a \beta_c}{2.303 i_{corr} (\beta_a + \beta_c)} \quad 2.16$$

where  $\beta_a$  and  $\beta_c$  are the anodic and cathodic for Tafel slopes (mV/decade), respectively (as described in 2.6).

The linear polarization resistance (Figure 2.16) method is capable of measuring the corrosion rate of a system. It is achieved by shifting the corrosion potential typically 10 to 20mV in the noble and active direction from  $E_{corr}$ . Both the potential and the current required to achieve this potential are recorded. The potential is stepped in increments (called over-potentials, typically 1mV scanning at 0.25 mV/sec) from one extreme to the other and each of these steps is recorded. The plotting of these data yield a polarization curve. When this is done, it is observed that the applied current density is a linear function of the electrode potential. The polarization resistance,  $R_p$ , is equal to the slope of this curve ( $\Delta E / \Delta i_{app}$ ), as shown in Figure 2.16. The corrosion rate can then be determined using the Stern-Geary equation:

$$R_p = \frac{\Delta E}{\Delta i_{app}} i_{corr} = \frac{\beta_a \beta_c}{2.3(\beta_a + \beta_c)} \quad 2.17$$

The quantity  $\beta_a$  and  $\beta_b$  are referred to as the Tafel constant, which can be measured experimentally or estimated. Corrosion rate can be obtained from Faraday's Law;

$$\text{Corrosion rate} \Rightarrow \frac{i_{corr}}{nF} = \text{moles} / \text{cm}^2 / \text{sec} \quad 2.18$$

Where F= Faraday constant = 96500 Coulombs/mole

Michael Faraday discovered that current is generated by the anodic reaction to an equivalent mass loss or corrosion penetration rate. Faraday's empirical laws of electrolysis relate the current of an electrochemical reaction to the number of moles of the element being reacted and the number of moles of electrons involved [13].

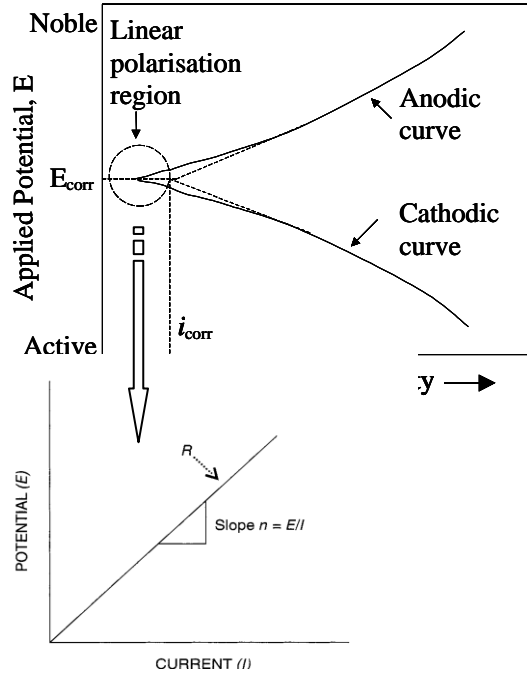


**Figure 2.16 LPR measurement from Tafel plot [22]**

According to this, the reaction of 1 mol requires 1 mol of electron or 1 Avogadro's number of electrons ( $6.023 \times 10^{23}$ ). The charge carried by 1 mol of electrons is known as 1 faraday (F). The Faraday is related to another electrical unit through the electronic charge,  $1.6 \times 10^{-19}$  Coulomb (C). The corrosion rate in mm per year (mm/year) can be obtained by multiplying the steel molecular weight (55.65 g/mol for carbon steel and 52 g/mol for stainless steel) as per density ( $7.8 \text{ g/cm}^3$  for carbon steel and  $8.0 \text{ g/cm}^3$  for stainless steel).

### 2.11.2 Potentiodynamic polarisation

Polarisation diagrams of corroding metals, sometimes called Evans diagrams are graphs of potential versus log current or log current density. The design of electrochemical cell used in many corrosion laboratories (as shown in figure 2.5) consist of electrode being studied (working electrode), reference electrode and the inert counter (or auxiliary) electrode that is usually made of platinum. All the electrodes are submerged in electrolyte such as seawater which is a medium for electron transfer.

In seawater, passive film forming alloys like aluminium or stainless steel require an induction time for pitting to occur. Thus, the scan rate in a potentiodynamic test can significantly influence the results obtained. The dynamic nature of these test methods

may preclude the natural formation of films on a metal or alloy surface, which can cause the distorted results. Cyclic polarisation methods are often applied in studying localised corrosion. Electrochemical methods to measure the susceptibility of alloys to pitting corrosion are reviewed elsewhere. The disadvantages associated with selecting the proper scan rate in the potentiodynamic method do not apply to the cyclic methods.

The Tafel extrapolation test is capable of determining very low metal corrosion rates. When conditions are ideal, its accuracy is equivalent to or better than weight loss measurements. However, to maintain accuracy, the Tafel regions must encompass at least one order of magnitude of current. Also, this method can only be applied to systems that have one reduction process or the Tafel region may be distorted and corrosion rate determinations will be inaccurate. Finally, the Tafel method only yields an average uniform corrosion rate and is not sensitive to localised corrosion. Therefore, the use of this technique in seawater is considered to be limited primarily to obtaining an indication of the corrosion rate within an order of magnitude [38].

Potentiodynamic scanning (PDS) (Figure 2.17) and cyclic polarisation (CP) (Figure 2.18(a) and (b)) have cathodic branch curves similar to the Tafel plot. The PDS and CP curves also have anodic branches. However, they extend over a wider potential range and are often much more complex than the Tafel plot anodic branches. Figure 2.17 shows additional information obtained when the anodic branch is polarised more than 700 to 800 mV beyond the Tafel range. For all the polarisation, the scan starts from point 1 and progresses in the positive potential direction. There are a number of notable features concerning the curve. The Open Circuit Potential (OCP) is the electrical potential difference between two metals submerged in an electrolyte when no electrical current flows between them (in this laboratory test is the potential between working electrode and the reference electrode). At this potential, the sum of the anodic and cathodic reaction rates on the electrode surface is zero. As a result, the measured current will be close to zero. This is due to the fact that the potential only measures the current, which it must apply to achieve the desired level of polarization.

As the potential increases in the active region, metal oxidation takes place until it is beyond the Tafel plot. When the current and potential increase to a certain limit, the current decreases or is essentially constant over a finite range, the primary passivation potential,  $E_{pp}$  can be obtained. The log value for current at this point is identified as the critical current density  $i_{cc}$ . As the applied potential increases above this value, the current density is seen to decrease with increasing potential until a low passive region is

achieved. Once the potential reaches a sufficiently positive value, the breakdown potential ( $E_b$ ) is obtained. This is the most point localized corrosion susceptibility was evaluated and also known as pitting potential. This is considered a potential, which could be univocally determined according to any given combination of material/ambient/testing methods.

After this point, the applied current rapidly increases due to various phenomena, depending on the alloy or environment combination. For some systems, this sudden increase in current may be the breakdown of the passive film while for others it may be transpassive dissolution. For some alloys, typically those with a very protective oxide such as cobalt, the sudden increase in current is due to oxygen evolution[39]. For some materials, second passivity happens while for others it does not. It should be noted that the schematic diagram illustrates some of the possible regions present on an anodic polarization scan. Depending on the nature of a particular system, some or all of these features may be present.

Cyclic polarisation (CP) curves can be considered as extensions of potential dynamic curves. The test electrode potential is increased in the anodic direction until the test electrode polarization either reaches approximately +1000mV from OCP, or the current density reaches a given magnitude (area x 0.005 A/cm<sup>2</sup>), then the potential decreases towards the OCP. Figure 2.18 (a) and (b) show examples of CP curves. The arrows indicate the potential scan directions.

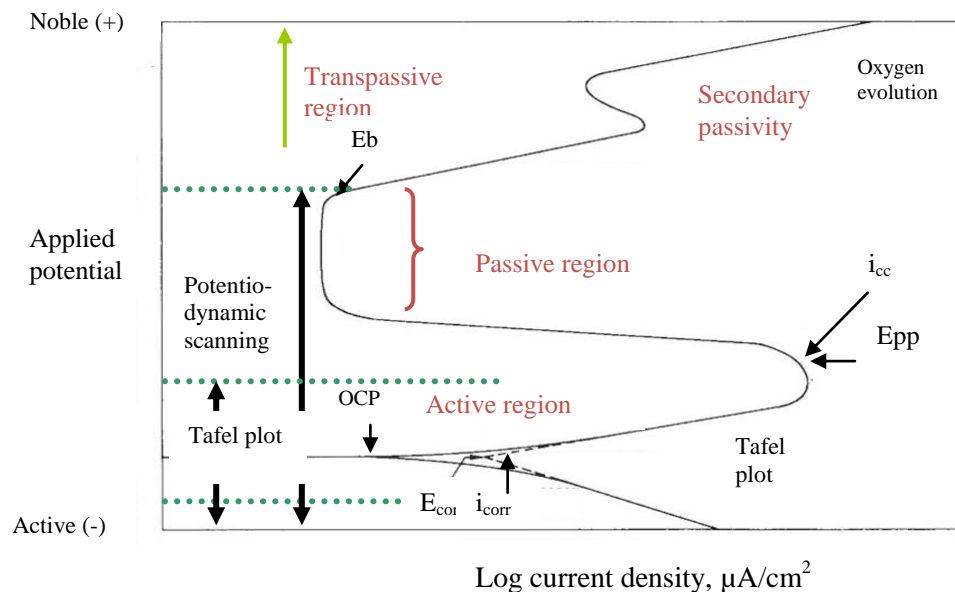


**Figure 2.17** A cathodic and anodic polarization plots cyclic potentiodynamic analysis [24].

Negative hysteresis in figure (a) occurs when the reverse scan current density is less than that for the forward scan, whereas positive hysteresis in figure (b) occurs when the reverse scan current density is greater than that for the forward scan.

As mentioned before, the passive film is destroyed when the potential is increased into the transpassive region of a PDS or CP curve. Pitting can occur and initiate at discrete locations on metal surfaces when the surface film is demolished. It is generally believed that pits will continue to grow when OCP is greater than the repassivation potential ( $E_p$ ), and pits will not grow when OCP is less than  $E_p$ [23]. Otherwise, passive film damage is not repaired and will contribute to pits initiated in positive hysteresis but not when negative hysteresis occurs. Damaged passive film repairs itself and pits do not initiate in negative hysteresis.

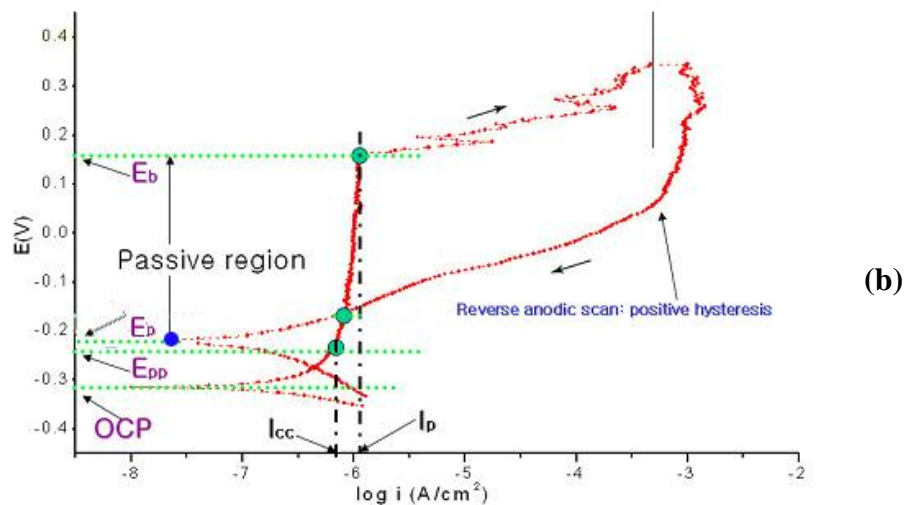
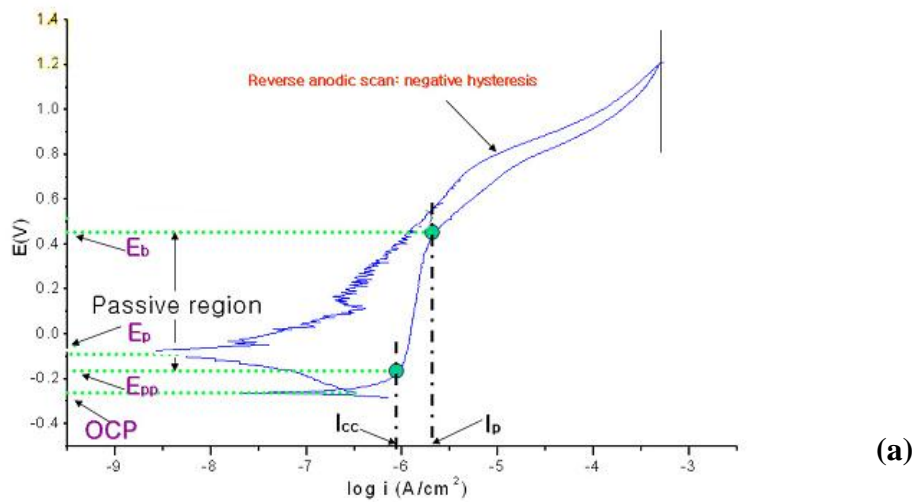


**Figure 2.18** A cyclic polarization curve. (a) negative hysteresis and (b) positive hysteresis [23].

## Chapter 3

### LITERATURE REVIEW

#### 3.1 Introduction

This chapter will elaborate upon the properties of seawater that accelerate corrosion, as well as the requirements of the oil and gas industry and the history of hydraulic fluids pertaining to the industry. This includes how the trend changed from using water as a hydraulic fluid to oil-based hydraulic fluids. Then, with the improvement in research and development, the usage of inhibitors has ensured that in the oil and gas sector productivity has been maintained by managing corrosion attack. However, with increasing environmental concerns, the chemicals added as inhibitors are controlled by environmental legislation to ensure that all discharges are safe for marine life. The waste is characterised in four different categories – biocompatibility, bioaccumulation, biodegradability and toxicity. The last paragraph explains about the materials used in this research, which can be categorised as active and passive materials.

#### 3.2 Seawater

Seawater is an extremely complex ionic aqueous solution containing at least 70 elements in widely-varying concentrations[40]. It has a very good electrical conductivity approximately  $0.04 \text{ m}\Omega \text{ cm}^{-1}$ , which is at least 4,000 times better than most freshwater[16]. Salinity, pH, oxygen level, and temperature are parameters that have a strong influence on corrosion reactions. These factors vary in vertical distribution from the seabed to the surface. The salinity and pH of seawater are relatively stable measurements whereas temperature and dissolved oxygen may vary. The salinity increased as the depth increased and thus decreased pH to more acidic. Temperature may varies with the amount of sun and oxygen content depends on life forms in the seawater.

Theoretically, salinity is the mass of dissolved salt ions present in 1 Kg of seawater. Normal salinity is 35 grams/kg of water (3.5%). Figure 3.1 provides a simple illustration of the constituents comprising the 3.5% salt content of seawater. Salinity is



also used to express the salt content of seawater. Almost 99% of all seawaters have a salinity ranging between 33 ppt and 37 ppt.

The pH of seawater is usually 7.7-8.3 at the surface, but will decrease and become more acidic (3-4) in deep water as the density increases. The pH is also affected by bacterial action. Organic compounds produce carbon dioxide, which can lower the pH to  $\approx 5-6$ . [16].

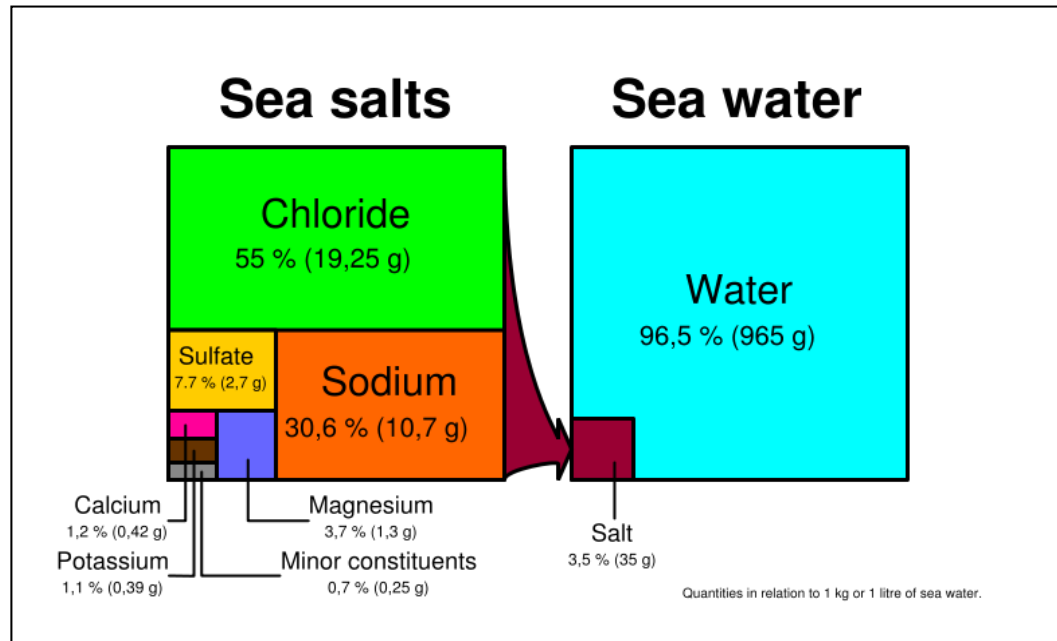


**Figure 3.1 Composition of seawater [41]**

### 3.2.1 Freezing point of seawater, $T_f$ and chemical additions

The freezing point of seawater is the temperature at which pure ice and seawater are in thermodynamic equilibrium[42]. This temperature decreases with increasing salinity and increasing water pressure. Examples of antifreeze include ethylene glycol, which is toxic and not biodegradable and propylene glycol, which is non toxic and biodegradable but not so effective and very expensive.

Other than antifreeze, chlorine in the form of typical biocides is also added to seawater to prevent marine growth, which would cause tube blockage resulting in the loss of heat transfer or impingement attack. Extra care must be taken in adding chlorine as excess chlorination can produce corrosion effects on steel and copper base alloys. Research by the Copper Development Association found that the best way is to measure

the residual chlorine at the plant outlet and adjust and maintain the chlorine dose at a low level, e.g. 0.1-0.2 ppm [43].

Temperature, pH, salinity and biological activity are the other factors that should be considered when dealing with seawater. The temperature and salinity controls seawater density, which is the major factor governing the vertical movement of ocean water [44]. The density of seawater normally increases with depth.

### **3.2.2 Role of anions on corrosion attack**

Corrosion is the physicochemical interaction between a metal and its environment that results in changes in the properties of the metal, and which may lead to significant impairment of the function of the metal, the environment, or the technical system, of which these form a part. It is known that every substance interacts differently with the environment in which it is used. Furthermore, each ionic species present in the environment behaves uniquely. While no general theory has been established, so far, that accounts with certainty for the corrosion interaction between metals and the environment, it is realised that there is more than one factor that influences the corrosion of metals in aqueous solutions. This makes it necessary to study the effects of the ions in the solution on the corrosion phenomenon, with due consideration to such factors as the type of the metal, temperature, pH, oxygen and ions.

In contrast to general corrosion, attack by pitting sometimes occurs in some particular environmental conditions. These problems result from the presence of specific aggressive species such as chloride, sulphate or nitrate[45]. Each of these species alone can produce pitting corrosion in alloy but with different levels of aggressiveness. For some corrosive resistance alloy such as copper, sulphate ions appear more aggressive than chloride ions and nitrate ions are more aggressive than sulphate ions[46].

El Wanees *et al.*[47]., in his study about pitting corrosion in the presence of  $\text{Cl}^-$  as aggressive ions and  $\text{CrO}_4^{2-}$ ,  $\text{HPO}_4^{2-}$ ,  $\text{NO}_2^-$ ,  $\text{WO}_4^{2-}$  and  $\text{MoO}_4^{2-}$  as inhibiting anions, found that the limiting corrosion currents increase with an increase in the  $\text{Cl}^-$  ion concentration and decrease with an increase in the pH and inhibiting ions concentration for reinforcing steel (carbon steel) in concrete. The injection of the inhibiting anions in solution causes repassivation of pre-formed pits through competition with  $\text{Cl}^-$  ions for adsorption sites on metal oxide surface. Figure 3.2 shows that concentrations of  $\text{Cl}^-$  ions are not enough to influence the passive character of the steel surface when  $\text{Cl}^-$  ions present with concentrations below  $5 \times 10^{-5}$  M. With slight increase in the concentration

of the aggressive  $\text{Cl}^-$  ions, corrosion current starts to flow compared to presence of  $\text{Cl}^-$  ions with concentrations below  $5 \times 10^{-5} \text{ M}$  and the flowing currents reach limiting values in the higher concentration of  $\text{Cl}^-$  ions. Currents start to decrease once again either to reach zero value in presence of  $5 \times 10^{-5} \text{ M}$   $\text{Cl}^-$  ions, or to reach slightly higher values that depend also on the  $\text{Cl}^-$  ions concentration.

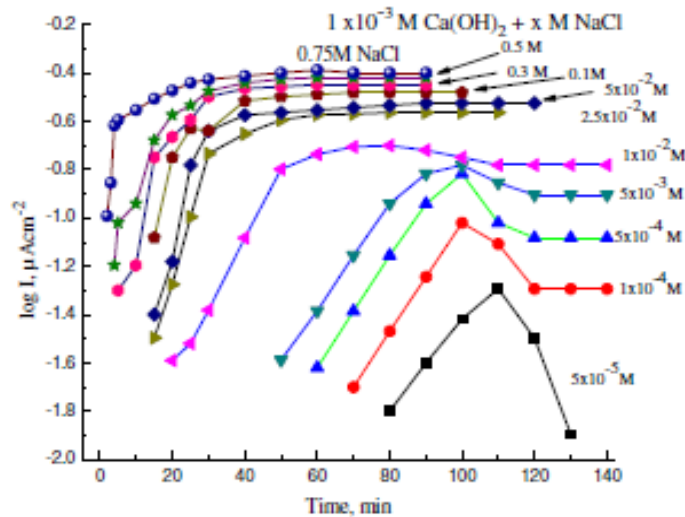


**Figure 3.2 Variation of the logarithm of pitting corrosion current density with time for steel electrode immersed in solutions of  $1 \times 10^{-3} \text{ M}$   $\text{Ca(OH)}_2$  containing increasing concentrations of  $\text{NaCl}$ , at  $25^\circ\text{C}$  for medium carbon steel [47].**

In a study by Takasaki and Yamada [45] about the effects of temperature and aggressive anions on the corrosion of carbon steel in potable water it was concluded that the corrosion rate increased in proportion to the concentration of aggressive anions and with increasing temperature. A study by Strehblow and Titze [48] on iron and nickel in  $\text{Cl}^-$ ,  $\text{Br}^-$  and  $\text{I}^-$ , as aggressive anions and  $\text{NO}_3^-$  and  $\text{ClO}_4^-$  as the inhibiting anion, found that the pitting region within the passive potential range became greater when the concentration of the aggressive anions was increased and smaller when the inhibitor concentration was increased.

El-Naggar[49], who studied the aggressive anions  $\text{Cl}^-$ ,  $\text{NO}_3^-$  and  $\text{SO}_4^{2-}$  on the corrosion and passivation behaviour of carbon steel in 0.50 M sodium bicarbonate solutions found that the presence of these aggressive anions stimulates the anodic dissolution rate in both the active and pre-passive potential regions. Pitting corrosion was only observed in the presence of  $\text{Cl}^-$  anions, while the presence of  $\text{NO}_3^-$  and  $\text{SO}_4^{2-}$  anions was only facilitated by the oxygen in the water without themselves participating in the cathodic process. The effect of  $\text{SO}_4^{2-}$  anion exerts an indirect effect on increasing

the cathodic reaction and influence the anodic reaction [49]. He found that increasing the concentration of  $\text{Cl}^-$  ion in the range from 0.002 to 0.100 M in 0.50 M  $\text{NaHCO}_3$  solutions shows a very low anodic passivating current followed by pitting potential ( $E_{\text{pitting}}$ ). Increasing the  $\text{Cl}^-$  ion concentrations from 0.003 to 0.040 M reduce the oxygen evolution on passive electrode and cause the current density increase abruptly and developing pitting corrosion at  $E_{\text{pitting}}$ . Increasing the concentrations of  $\text{Cl}^-$  ion to 0.04 M,  $E_{\text{break}}$  coincide with  $E_{\text{pitting}}$  thus,  $\text{Cl}^-$  ions concentration is considered as the limiting concentration. The dependence of  $E_{\text{pitting}}$  on the concentration of  $\text{Cl}^-$  ion is shown in Figure 3.3. The figure shows that the presence of lower concentrations of the  $\text{Cl}^-$  ions has a slight effect on the value of  $E_{\text{pitting}}$ . The latter is slowly shifted in the active direction as the concentration of the aggressive anions in increased. This suggests that lower concentrations of  $\text{Cl}^-$  ions are not sufficient to form an active pit. The pits formed under these conditions are passivable in nature. The pits formed in the presence of high concentrations of  $\text{Cl}^-$  ions (more than 0.0025 M) are active and cannot undergo repassivation and the attainment of nearly constant  $E_{\text{pitting}}$  at higher  $\text{Cl}^-$  ions concentrations can be attributed to the formation pitting propagation.

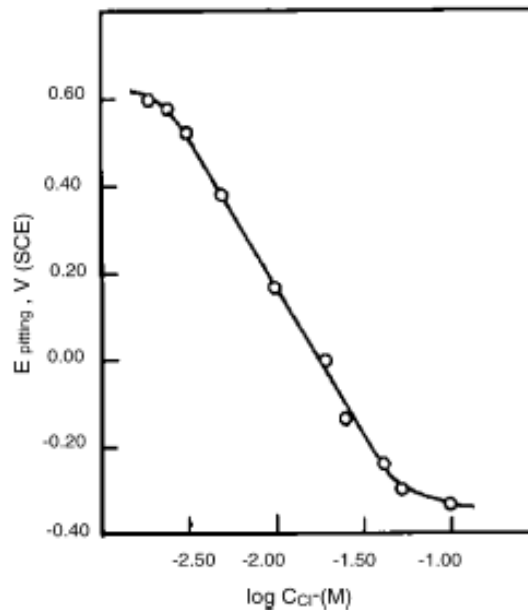


**Figure 3.3 Dependence of  $E_{\text{pitting}}$  of carbon steel on the  $\text{Cl}^-$  ions concentration [49]**

Naggar [49] also found that increasing the concentration of  $\text{SO}_4^{2-}$  ions in the range from 0.0 to 0.2 M in deaerated 0.5 M  $\text{NaHCO}_3$  solutions shows no pitting and he elucidated that the role of  $\text{SO}_4^{2-}$  ions is to facilitate repassivation depending on the potentials and passivation currents on the nature of  $\text{SO}_4^{2-}$  ions. From his study obviously shows that

the rate of anodic dissolution increase continuously in the passive region until the concentrations of  $\text{SO}_4^{2-}$  ions reach 0.20 M, the corrosion rate increase and it decreases with further increase in potential as shown in Figure 3.4. Thus, he considered that 0.20 M of  $\text{SO}_4^{2-}$  ions is the limiting concentration concentrations and he grouped 0.02 M to 0.18 M  $\text{SO}_4^{2-}$  ions is low concentration ranges whereas 0.2 M  $\text{SO}_4^{2-}$  ions is high concentration range as indicative to the changes in the mechanisms of the passivation process. With the evidence of anions effect in increasing and retarding the corrosion rate, therefore, some of these anions in seawater were studied in this research. The effects were studied by varying the ratio of  $\text{Cl}^-$  and  $\text{SO}_4^{2-}$  in seawater in terms of corrosion rate and breakdown potential in DCV materials.

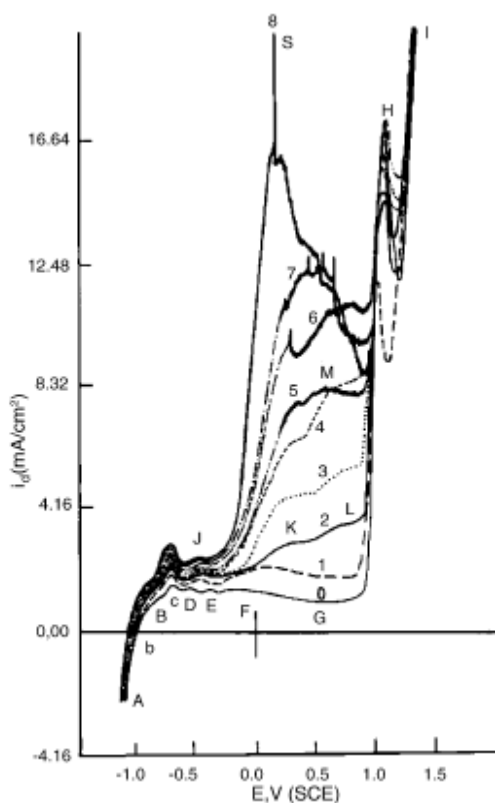


**Figure 3.4 Effects of  $\text{Na}_2\text{SO}_4$  concentration on the anodic behaviour of carbon steel in deaerated 0.5 M  $\text{NaHCO}_3$  solutions at scan rate of 25 mV/s; (0) blank; (1) 0.020 M; (3) 0.055 M; (4) 0.070 M; (5) 0.100 M; (6) 0.150 M (7) 0.180 M; (8) 0.200 M [49].**

### **3.2.3 Saturation**

Deep ocean water is usually under saturated with respect to carbonates, whereas surface water is usually saturated due to wave action exposure to CO<sub>2</sub> in the atmosphere. Saturation will affect the deposition of calcium and magnesium salts in cathodic reaction during corrosion. Saturation is also caused by Dissolved Oxygen (DO). The amount of dissolved gas in seawater is also affected by the water temperature and salinity. Increasing the temperature or salinity would reduce the amount of gas that could be dissolved. Nominal DO in seawater  $\approx$  6-8 ppm at 25-30° C [50]. The DO may be higher depending upon wave action, slurry and life activities.

Supersaturation of oxygen may occur due to photosynthesis by phytoplankton bloom. When the DO is low, bacteria or biological action and chemical oxygen demand will decrease as well. Localised variations might also change the DO and temperature as well. As depth increases, the temperature will decrease. The surface of the ocean is about 13°C and decreases to 5°C at 3,000 feet while the DO decreases to 6ppm[16].

### **3.3 Seawater as a Corrosive Medium**

Water has the highest heat capacity of all solids and liquids except liquid NH<sub>3</sub> because it takes a lot of energy to break the hydrogen bonds and change the structure of water[15]. Thus, water has a large thermal buffer capacity and acts as a climate buffer. The partial charge of the water molecules allows them to pull apart and dissolve ionic compounds like salt very easily. The salts have the effect of making the water molecules cluster and become more ordered, and, thus, harder to pull apart and evaporate.

In addition to pure water, seawater systems are used by many industries, such as shipping, offshore oil and gas production and power plants. The main use of seawater is for cooling purposes. However, it is also used for fire fighting, oilfield water injection and desalination plants. Although corrosion problems in these systems have been well studied over many decades, and despite the published information concerning the behaviour of materials in seawater, failures still occur. Seawater is normally more corrosive than freshwater because of the higher conductivity and the penetrating power of the chloride ion through surface films on a metal. The rate of corrosion is controlled by the chloride content, oxygen availability and temperature[14]. In Table 3.1, the physical properties of seawater and freshwater are compared.

**Table 3.1 Comparison of seawater and pure water properties**

Property	Seawater (35 ‰)	Pure Water
Density, g/cm <sup>3</sup> , 25°C	1.024	1.003
Specific conductivity, ohm <sup>-1</sup> cm <sup>-1</sup> , 25°C	0.0532	-
Viscosity, milipoise, 25°C	9.02	8.90
Vapour pressure, mm Hg, 20°C	17.40	17.34
Isothermal compressibility, vol/atm, 0°C	46.4 x 10 <sup>-6</sup>	50.3 x 10 <sup>-6</sup>
Temperature of maximum density, °C	-3.25	3.98
Freezing point °C	-1.91	0
Surface tension, dyne cm <sup>-1</sup> , 25°C	72.74	71.97
Velocity of sound, m s <sup>-1</sup> , 0°C	1450	1407
Specific heat, J g <sup>-1</sup> °C <sup>-1</sup> , 17.5°C	3.898	4.182
Refractive index	1.33940	1.33300
Osmotic Pressure, bar, 25°C	25.9	-
pH	8.2 ± 0.1	7 ± 0.1

### 3.4 Hydraulic Fluids

#### 3.4.1 History of hydraulic fluids

Oil hydraulics overtook water hydraulics in the early part of the last century for both research effort and industrial applications even though water hydraulics were pioneered by the ancient Greeks[51]. The growing concern about environmental issues has led to renewed interest in water hydraulics because water is non-toxic, environmentally friendly and readily available. In many industries, people are steadily turning to water-hydraulic systems to replace their oil-hydraulic counterparts, especially in the oil and gas industries because water can be easily discharged into the sea. Thus, the use of water as a hydraulic fluid would not only reduce the environmental issues,

but also reduce the cost of operation in the oil and gas operations. Figure 3.2 shows the past applications of hydraulic fluids.

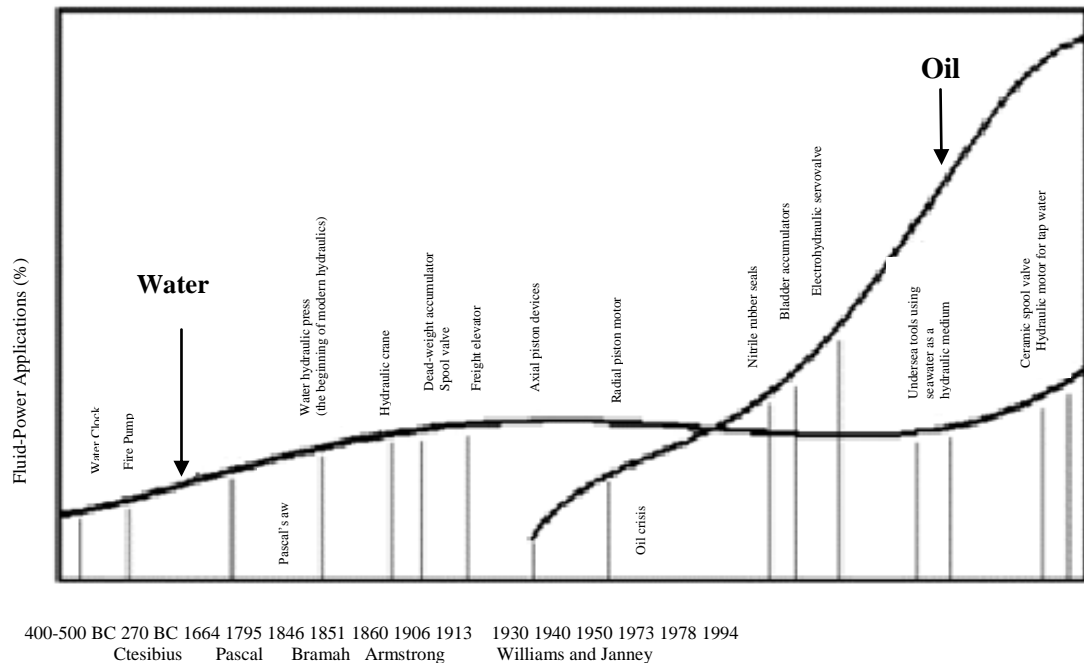


**Figure 3.5 Past applications of water and oil hydraulics [51].**

### 3.4.2 Types of hydraulic fluid

The hydraulic fluid is the connecting element in any hydraulic unit. It is important to select with care the hydraulic fluid for the hydrostatic circuit. Quality and cleanliness of the hydraulic fluid are decisive factors for the operational reliability, efficiency and life cycle of the system. Hydraulic fluids must conform with, and be selected and used in accordance with, the safety provisions as well as the generally acknowledged rules of technology.

Hydraulic fluids are a large group of liquids comprising many kinds of chemicals that are used in machines and equipment to transfer pressure from one point to another. Figure 3.6 shows the types of hydraulic fluid from oil and water-bases [52].



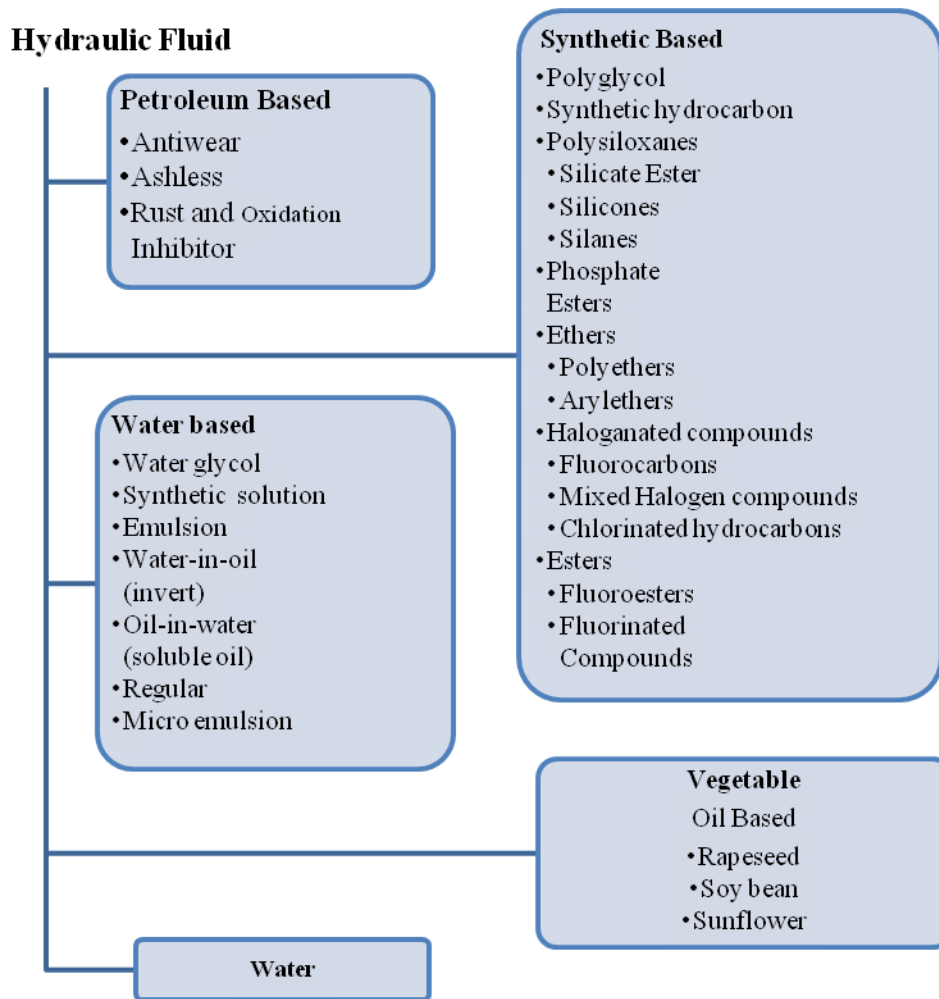


**Figure 3.6 Types of hydraulic fluid [52]**

### **3.4.3 Purposes of hydraulic fluids**

Generally, there are four main purposes of hydraulic fluid – power transmission, lubrication, sealing and cooling. The primary purpose of any hydraulic fluid is to transmit power mechanically throughout a hydraulic power system. As power transmission hydraulic fluid flows easily, power losses can be reduced and make the circuit respond quickly.

Hydraulic fluids must provide the lubricating characteristics and qualities necessary to protect all hydraulic system components against friction and wear, rust, oxidation, corrosion and demulsibility. These protective qualities are usually provided through the use of additives. Some fluids may need special consideration in component design to overcome their lack of lubricity.

Many hydraulic system components, such as control valves, are operating with tight clearances where seals are not provided. In this application, the hydraulic fluid must provide the seal between the low-pressure and high-pressure side of the valve ports. The amount of leakage will depend on the closeness or the tolerances between the adjacent surfaces and the fluid viscosity. For cooling purposes, the circulating hydraulic fluid must be capable of removing the heat generated throughout the system. To change the hydraulic fluid from oil to water, the melting point is the important criterion to consider.

#### **3.4.4 Hydraulic fluid criteria**

To make the hydraulic fluid successfully fulfil all the requirements, it must be chemically inert, have good oxidation and thermal stability and be resistant to degradation. The other criterion is that it should exhibit minimal change of viscosity with temperature and remain stable and non-volatile at high temperature. As some applications are for valves, hydraulic fluids will have high pressure in high temperature, thus, it is preferable to be non-inflammable and in some instances resistant to nuclear radiation. By using water hydraulics, engineers can be sure that the hydraulic fluids are clean and readily available.

#### **3.4.5 Corrosion in hydraulic fluids**

The most common hydraulic fluids used in sub sea applications systems are the petroleum-based oils. These fluids contain additives to protect the fluid from oxidation, corrosion, reduce the fluid to foam and improve viscosity. To protect from corrosion attack, the hydraulic fluid were added with certain amount of inhibitor to provide deposit of protective film on metal surfaces. These additives (inhibitor) must exhibit excellent hydrolytic stability in the presence of water to prevent fluid breakdown and the acid formation that causes corrosion. In some applications, hydraulic fluid needs fire-resistance fluids like mineral-oil-based hydraulic fluid. But, even that development work has established a successful technology, but they are all some degree of toxicological or combustion risk and lead to certain engineering difficulties [53].

The development of water-based hydraulic systems is further motivated by the diminishing resources and increasing cost of mineral oils. The problems of loss of viscosity, porting, shear losses in bearing represent a significant proportion of the efficiency losses in hydrostatic transmission. This clearly shows that there are advantages in developing hydraulic equipment to operate on a low viscosity, high bulk

modulus fluid such as water. However, the use of water alone as a hydraulic fluid presents problems because of the high freezing point, low boiling point and corrosion problems, particularly with ferrous metals. Because of that, the use of hydraulic fluids added with inhibitor could control the corrosion attack, however the major change will influence the formulations and will be demanding on environmental legislation and the desire for the offshore industry to show its commitment to preserving the sea and marine ecosystems.

Many thousands of pounds and man hours have already been spent in producing new fluids and these fluids are about 100 times less toxic than already 'environmentally acceptable' hydraulic fluids [54]. With the increased awareness in environmental issues, the concern and pressure not only towards industrial activities but also in oil and gas industry due to its past record of spillage and discharges and the damage that these have caused the environment. The legislation limits the quantities of fluids that can be discharge into the sea depending upon the chemical content of these fluids and the manner in which they are used. The consequence of such legislation require subsea control and drilling mud operators to identify chemicals disposed during routine operation and evaluate the possible effects that may cause to the environment. As a consequence, the design of control systems and hydraulic fluids use in these systems is consider in great detail. The producers are looking for a system that is not only capable of functioning at high temperature but also can be direct discharge to the sea which is accepted by regulatory bodies.

### **3.5 Impact of Oil and Gas Activities on the Environment**

#### **3.5.1 Oil and gas Exploration and Production (E&P) wastes**

The American Petroleum Institute (API) estimated that 149 million barrels of drilling waste, 17.9 billion barrels of produced water and 20.6 million barrels of other associated wastes were generated in 1995 from exploration and production (E&P) operations [55]. Once generated, managing these wastes in a manner that protects human health and the environment is essential to ensure the waste is subject to hazardous waste regulations. Prudent waste management decisions, even for non-hazardous wastes, should be based on the inherent nature of the waste and obviously not all waste management options are appropriate for every waste.

With respect to crude oil, the primary field operations include activities occurring at or near the wellhead including exploration, development, and the primary, secondary and tertiary production of oil or gas, such as water separation. In 1988, the Environmental Protection Agency (EPA) published a list of wastes that were determined to be either exempt or non-exempt, although it should not be considered to be comprehensive. The exempt wastes include produced water, rig wash, drilling fluids and cutting and accumulated materials such as hydrocarbons, solids, sand and emulsion from the production separator. Whilst non-exempt wastes include cleaning and painting wastes, solvents, acids, refinery, used equipment lubricating oils, boiler cleaning wastes and used hydraulic fluids. However, with the increasing concern for environmental issues pertaining to the discharge of waste direct to seawater including wastewater has caused the environmental board to strengthen the policy. Accordingly, the use of seawater with water treatment to reduce the corrosion attack will reduce the environmental issues.

### **3.5.2 Evaluation of the hazard and risk of chemicals used by the UK offshore oil and gas industry**

As mentioned before, in every stage of oil and gas operations, a wide range of chemicals are required to enhance drilling performance, to promote production and separation of oil or gas, to protect equipment from corrosion and to maintain safety. Since the start of oil and gas production in the North Sea in the early 1970's, the regulation of chemicals used by the offshore industry on the UK continental shelf (UKCS) has evolved from a basic consideration of chemical toxicity into a more comprehensive assessment and management of the risks posed [56]. In the UK, following the introduction of the offshore chemicals regulations, OCR operators of offshore oil and gas installations are required to only use chemicals present on the list of notified chemicals. Test data describing the persistence, bioaccumulation and toxicity (PBT) of chemicals with the exception of some natural materials, salts and similarly benign substances considered to pose little or no risk (PLONOR), is required before they can be added to the list.

### **3.6 Inhibitors**

A corrosion inhibitor is a substance, solid or liquid, which when added in only moderate quantities to a corrosive fluid should significantly reduce the corrosivity of that fluid towards a particular metal [55]. Corrosion inhibitor reduces the corrosion attack in two ways. In some situations, the added inhibitors can alter the corrosive

environment into a noncorrosive or less corrosive environment through its interaction with the corrosive species. In other cases, the corrosion inhibitor interacts with the metal surface and therefore inhibits the corrosion of the metal. The inhibitors interact with the metal surface and form a passive film or an adsorbed layer acting as a barrier film. Therefore, based on the mode of interaction, inhibitor can be divided into two broad classes which are environment modifiers and adsorption. Environment modifiers act by simple interaction with the aggressive species in the environment and reduce the attack of the metal by the aggressive species. Adsorption type act by adsorb on the metal surface and inhibit the corrosion (Figure 3.7). Regardless of their type, most of the inhibitors currently used are either organic or inorganic chemicals for the retardation of the corrosion progress under different environments. Inorganic compounds must be able to oxidize the metal and form a passive layer on its surface. Its molecules may have a large structure, double bonds, an active centre or group, thus, giving the molecule an ability to cover a large area of metal surface with a firmly attached film.

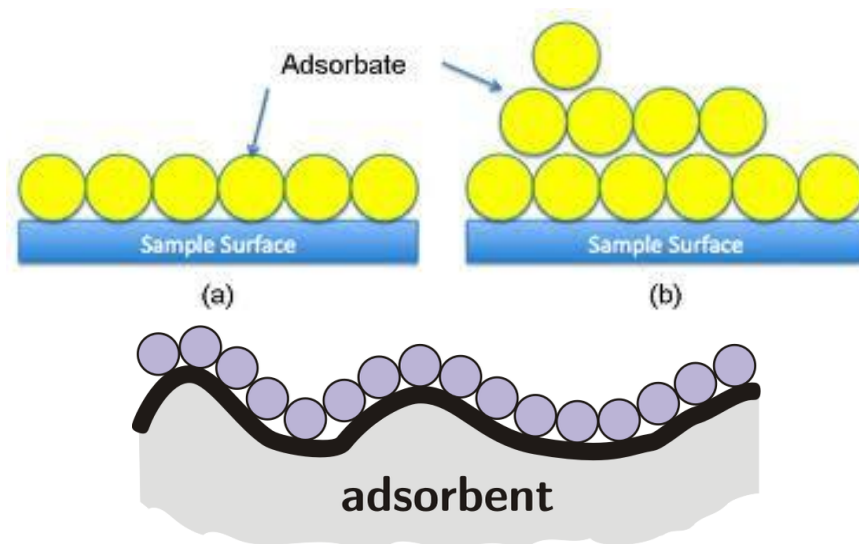


**Figure 3.7 Adsorption type inhibitor [57]**

Inhibitor can be designed to act as anodic or cathodic inhibitors depending upon reaction. They are also mixed inhibitors that inhibit both anodic and the cathodic reactions and this type are generally represent by organic compounds[55]. Cathodic inhibitors inhibit the hydrogen evolution in acidic solutions or the reduction of oxygen in neutral or alkaline solutions. Substances with high overpotential for hydrogen in acidic solutions and those that form insoluble products in alkaline solutions are generally effective cathodic inhibitors [59]. Anodic inhibitors are generally effective in

pH range of 6.5 – 10.5 (near neutral to basic) [189]. Nevertheless, the concentration of inhibitor is the main factor which affects the effectiveness of inhibitor. The mechanism of anodic inhibition can be explained using the polarization diagram of an active-passive metal (Figure 3.8) [159]. In the absence of inhibitors, the metal corrodes in the active state at a rate corresponding to point A. As the concentration of inhibitor is increased, the corrosion rate also increases until a critical concentration and a critical corrosion rate (point B) are reached. At the critical concentration, there is a rapid transition of the metal to the passive state, and the corrosion rate is decreased (point C).

This diagram clearly illustrates the critical aspects of inhibitors concentrations. It shows that the protection is rendered when sufficient amount of inhibitor is used. Otherwise, corrosion is increased if the inhibitor is insufficient.

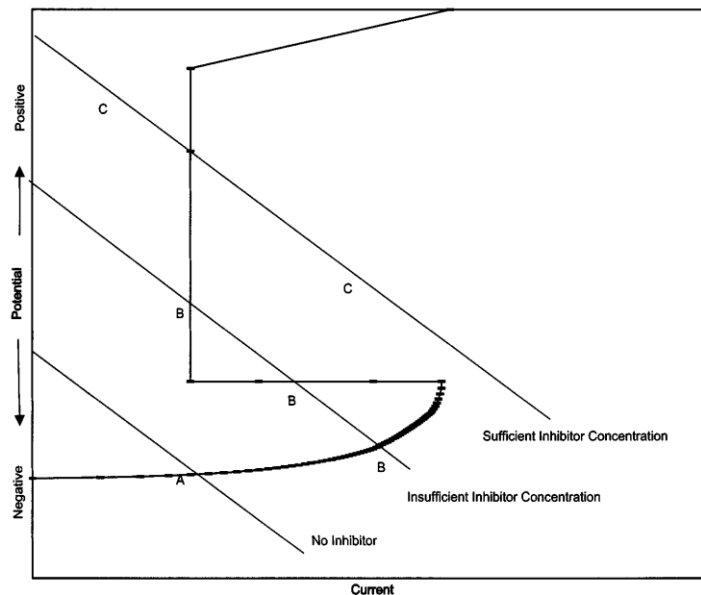


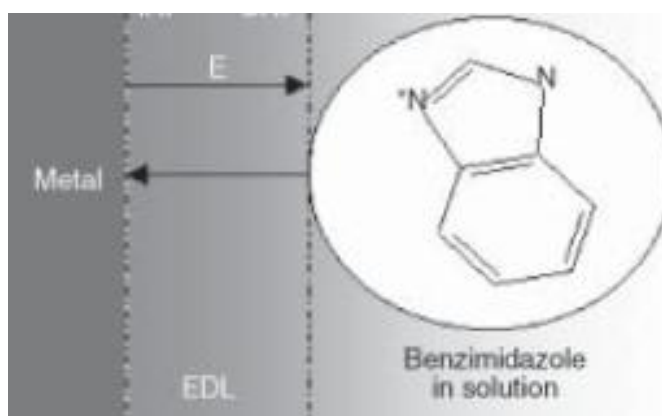
**Figure 3.8** Polarisation diagram of an active-passive metal showing the dependence of the current on concentration of passivation-type inhibitor [60].

Apart of two broad classes of inhibitor mentioned before, inhibitor also can be classified into (a) passivators, (b) barrier inhibitors, (c) poisons, (d) scavengers and (e) neutralizers. Whichever it is, the most important thing is that it must be a non-toxic and environmentally friendly chemical. Passivators act as depolarisers in contact with a metal surface initiating high current densities at residual anodic areas exceeding the critical current density of passivation. Passivator ions are those thermodynamically have either an oxidizing capacity (noble in oxidation-reduction potential) or that are readily reduced (shallow cathodic polarization curve) as shown in Figure 3.8. Barrier inhibitor

forms a layer on a metal or metal oxide surface and frequently, these barriers are as thin as one or two layers on inhibitor molecules. Contrary to green inhibitor, poisons or toxic inhibitor may harm the habitat and cause side effect in future. A scavenger is used to purge out gas that contribute to corrosion attack such as oxygen. Tannin is normally used in steam boiler to reduce corrosion attack while neutraliser is used to reduce corrosion attack by neutralising the water in water treatment process.

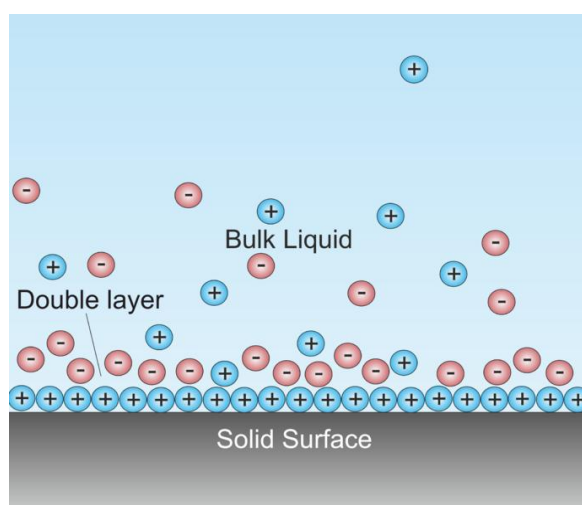
The use of corrosion inhibitors in all petrochemical facilities in the world is currently, because they are cost effective and flexible. The total consumption of corrosion inhibitors in the United States has doubled from approximately \$600 million in 1982 to nearly \$1.1 billion in 1998 and the demands for chemical inhibitors is expected to increase 3.9% annually [61]. Therefore, an organic inhibitor would bring many benefits as it would be non-toxic, environmentally favourable and not contain heavy metals. However, there is also the possibility that some organics can serve as food sources for bacteria in closed-loop systems, thus, crevice corrosion might occur. The tendency to form a stronger coordination bond and, consequently, inhibition efficiency is expected to increase in the following order Oxygen < Nitrogen < Sulphur < Phosphorus [62]. Nitride is always used as an inhibitor for localised corrosion caused by chlorides. Their limitation is because they are toxic to the environment and that high levels of inorganic phosphates are also restricted by law.

Figure 3.9 shows the schematic of a corrosion inhibitor, benzimidazole molecule as it enters into electric double layer (EDL). The inhibitor action generally consist of two processes: diffusion of the inhibitor molecule to metal/solution interphase (EDL), and its adsorption on the metal surface.



**Figure 3.9 Schematic representation of the benzimidazole molecule [63].**

An electrical double layer, EDL is a structure that appears on the surface of an object when it is placed into a liquid. The object might be a solid particle, a gas bubble, a liquid droplet, or a porous body. The EDL refers to two parallel layers of charge surrounding the object as shown in Figure 3.10. The first layer, the surface charge (either positive or negative), comprises ions adsorbed directly onto the object due to a host of chemical interactions. The second layer is composed of ions attracted to the surface charge via the Coulomb force. This second layer is loosely associated with the object, because it is made of free ions which move in the fluid under the influence of electric attraction and thermal motion rather than being firmly anchored. It is thus called the diffuse layer.



**Figure 3.10 Schematic of double layer in a liquid [64].**

There are several inhibitors available such as volatile, passivating (anodic), precipitation, cathodic, organic, inorganic and mixed. Volatile inhibitors are also known as vapour phase inhibitors. These are suitable for vapour environments when inhibitor molecules in the vapour get in contact with the surface of metal. Examples of this inhibitor include amines and nitrides for ferrous metal inhibition [65].

Passivating inhibitors are anodic inhibitors. There are two categories of passivating inhibitors, namely, oxidizing anions and non-oxidizing anions. Oxidizing anions have the ability to passivate metal in the absence of oxygen such as chromate, nitrite and nitrate. Non-oxidising anions such as phosphate, tungstate and molybdate, require oxygen to perform passivation.



Precipitation and organic inhibitors are often film forming in nature. They inhibit by blocking anodic and cathodic sites and precipitating on metal surfaces as a protective barrier. Organic inhibitors form a hydrophobic layer on the surface of the metal to prevent dissolution of the metal. They are classified into organic anions and cations, for instance sulphonates and phosphonates. For precipitation, film forming can be found in two types, either by slowing down the corrosion without stopping it completely or by preventing the attack completely. However, the efficiency depends on the pH and saturation index, which is determined by the water composition and temperature, for instance, silicates and phosphates [66].

The effectiveness of organic inhibitors is related to the extent to which they adsorb and cover the metal oxide surface on the structure and the chemical properties of the layer formed on the metal surface under particular experimental conditions. The adsorption depends on the structure of the compounds, the surface charge on the metal and on the type of electrolyte. Molybdate and tungstate were proposed as corrosion inhibitors for carbon steel in 1951, but until now no clear and deep insight into the mechanism of action is available [56]. Its effectiveness varies with its concentration, pH of solution, immersion time, corrosive medium and surface properties of the alloy.

For inorganic inhibitors, only the active groups of compounds carrying negative anions would reduce the corrosion rate. The common inorganic inhibitors are crystalline salts such as sodium chromate and molybdate. Overall, corrosion inhibitor should not only mitigate the corrosion, but also be compatible with the environment in the sense that it should not cause any complications.

### **3.6.1 Green Inhibitors**

In the past two decades, the research in the field of “green” corrosion inhibitors has been directed toward the goal of using cheap, effective molecules of low or zero negative environmental impact. Therefore, the use of non-toxic inhibitors has also become one of the major selection requirements [67]. Omanovic and Ghareba [68]. In introduce 12-aminododecanoic acid (AA) as a green corrosion inhibitor to carbon steel in CO<sub>2</sub>-saturated acidic medium also known as sweet corrosion. They identified AA as non-toxic, biocompatible and easily biodegradable molecule and be considered as green corrosion inhibitor. It also can be considered as high efficiency as it inhibits carbon steel from corrosion attack within one hour of application by spontaneous adsorption.

Sethuraman and Kamal [69] found *Spirulina platensis* as green inhibitor for mild steel in HCl and H<sub>2</sub>SO<sub>4</sub> media. They found that inhibition efficiency increased with increasing the inhibitor concentrations. *Spirulina platensis* inhibits the corrosion of mild steel through adsorption following Temkin isotherm,  $\Delta G$ . Temkin isotherm,  $\Delta G$  was calculated by using;

$$\Delta G = -RT \ln (55.5 K) \quad 3.1$$

relationship where  $R$  is universal gas constant (kJ/mol), 5535 is a concentration of water (mol/L) and  $T$  is the temperature and  $K$  is equilibrium constant value.

The use of inhibitors is one of the most practical methods of protection against corrosion, especially in acidic media [70]. Inhibitors are commonly used in these processes to control the metal dissolution as well as acid consumption [71]. The most acid corrosion inhibitors are nitrogen-sulfur and oxygen-containing organic compounds [72]. Saracoglu *et al.* [73] used Benzamide (BA) and 4-aminobenzenesulfonamide (ABSA) to replace Amides Benzotriazole (BTA) which is known toxic and not biodegradable to corrosion of copper in 1.0 M HCl. Figure 3.11 below shows the structure of BA and ABSA. Saracoglu *et al.* found that ABSA more effective than BA and the adsorption of inhibitor are followed Langmuir isotherm model.

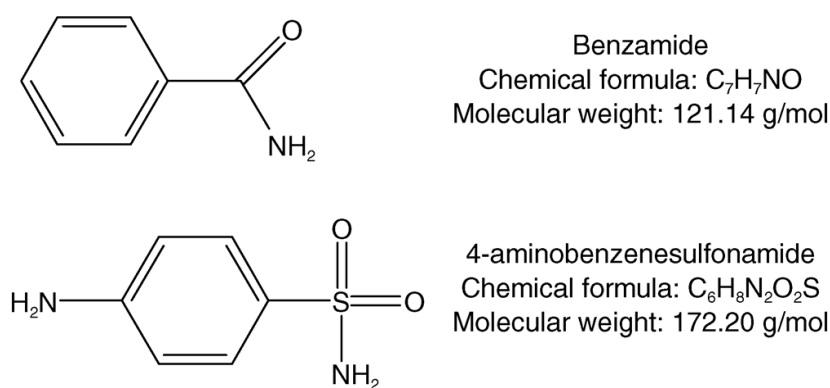


**Figure 3.11 Structure of inhibitor molecules [73].**

To claim the inhibitor are “green” for subsea applications, the inhibitor should meet the Norwegian and UK regulatory requirements, such that they can be classed as environmentally acceptable. Regarding the discharge of water overboard in offshore operations, the Norwegian legislation bodies have drawn up a set of guidelines out of concern for the environment. These guidelines differ from those of the UK sector that

require chemicals for field applications to have specific properties in terms of biodegradation, toxicity and bioaccumulation, and, which initially resulted in many of the ‘classic’ water discharges being discounted. They classified the hazardous into four categories black, red, yellow and green, as shown in Figure 3.12.

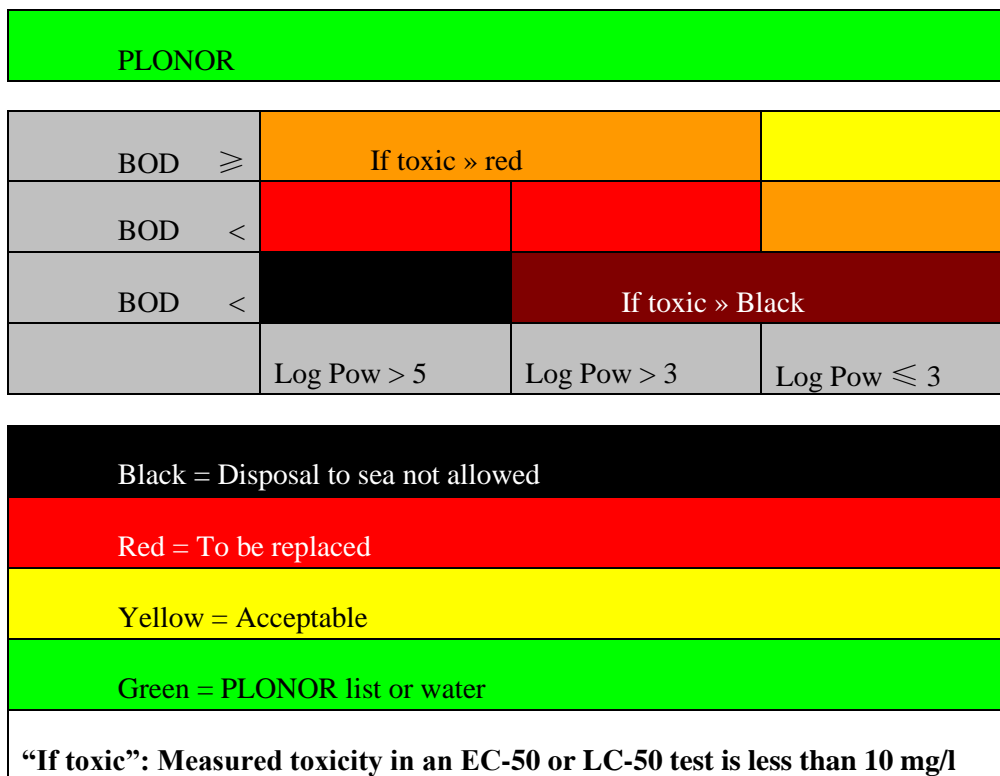


**Figure 3.12 Norwegian Legislation [74]**

### 3.6.2 Norwegian legislation

Green inhibitors refer to inhibitors that are less toxic, efficient in their manufacturing process and can deliver into the system when needed with the correct amount. Norwegian authorities divide offshore chemicals into one of four colour categories. These categories are based on biodegradation, bioaccumulation and (worst case) toxicity tests run according to OSPAR (Convention for protection of the marine environment of the North-East Atlantic Ocean) guidelines by GLP (Good Laboratory Practice) approved laboratories.

The worst case chemicals, categorised as Black, are not permitted to be discharged unless in exceptional circumstances. Red category chemicals are to be phased out and banned (after 2017 according to OSPAR). Yellow category chemicals are permitted and Green chemicals are those on the Pose Little or No Risk to the Environment (PLONOR) list. For the chemical to meet the Yellow category, the requirements it must meet are:

- Biodegradation > 20%
- Log Pow < 3
- Toxicity > 10 mg/l

Or it must not be a chemical that is either Red or Black or on the PLANOR list.

### **3.6.3 UK legislation**

As for Norway test data biodegradation, bioaccumulation and toxicity is required to conform with the OSPAR guidelines. The UK accepts extended marine biodegradation data beyond 28 days and also freshwater biodegradation data. Typically if the biodegradation of a chemical is > 20% in 28 days; it will be judged according to criteria as follows:

- Biodegradation < 70%
- Bioaccumulation log Pow  $\geq 3$  or Bioconcentration Factor (BCF) > 100
- Toxicity < 10 mg/l

These characterisations are clarified in Organisation for Economic Co-operation and Development (OECD) in detail.

### **3.6.4 Environmental test methods**

OSPAR publish guidelines for completion of the Harmonised Offshore Chemical Notifications Format (HOCNF). The objective of this HOCNF scheme is to prevent unacceptable damage to the marine environment by offshore oil and gas industry activities. It also standardises the requirements for the testing and reporting of all chemicals used by the offshore oil and gas industries operating within the North Sea and northeast Atlantic.

The classification systems places chemicals into one of five categories, A to E, as shown in Table 3.2. Chemicals in category A have the potential to cause the greatest damage to the environment, and category E chemicals have the potential to cause the least damage to the environment.

**Table 3.2: Toxicity classification parameters for the HOCNF Scheme [75]**

Initial grouping	A	B	C	D	E
Result for aquatic toxicity	1	> 1 to 10	> 10 to 100	> 100 to 1,000	> 1,000
Results for sediment	10	> 10 to 100	> 100 to 1,000	> 1,000 to 10,000	> 10,000

Recently the Registration, Evaluation, Authorisation and Restriction of Chemicals (REACH) legislation has come into force within the EU. The scope of the REACH extends to all chemicals manufactured in, imported to and exported from the EU.

### 3.7 Oceanic HW Fluids

Oceanic HW Fluids are all water-based formulation and therefore it needs to be use with products compatible with water glycol systems. The usage also depends on temperature where high glycol content in needed for low temperature condition. Oceanic HW600 were designed for use in subsea hydraulic control circuits. It can be use in topside controls if the equipment is suitable for use with low viscosity. In Oceanic HW600 series technical manual report, it was reported that Oceanic HW600 have extremely low toxicity, a high degree of biodegradability and do not bio-accumulate [76]. To ensure this is accepted by regulation scheme, the hydraulic fluid need to tested in accordance with the OSPARCOM Harmonised Offshore Chemical Notification Format (HOCNF). The testing includes data which is used to determine the potential

### 3.8 Carbon Steels

Carbon steel is widely used in engineering applications and comprises about 85% of the annual steel production worldwide. Generally, metallic materials are classified as ferrous and nonferrous. Ferrous materials consist of steels and cast irons, while nonferrous materials consist of the rest of the metals and alloys. Ferrous metals and alloys are basically irons with carbon added to them. As the carbon content rises, the metal becomes harder and stronger but less ductile and more difficult to weld. Alloys with less than 2%C are classified as steels, while those with more than 2% C are called

cast iron[77]. As the name implies, cast iron is predominantly produced by casting whereas steels are predominantly produced as wrought products, which needs to be deformed and shaped after casting.

### **3.8.1 Composition of carbon steel**

Steels are classified or grouped according to some common characteristics. The most common classification is by their composition and then by their yield or tensile strength. According to their composition, the classification is made regarding to their carbon content and the alloy content, which can be classified as low carbon, medium carbon and high carbon. Low carbon consists of less than 0.25% carbon content, while medium carbon consists of 0.25-0.55% carbon content and high carbon consistsof greater than 0.55% carbon content.

Alloys such as manganese, nickel and molybdenum are added to increase the strength. If the alloying elements are less than 5%, they are called low-alloy steels while more than 5% alloy content are classified as high-alloy steels. The plain carbon (without alloy content) and low-alloy steels are coded according to the AISI-SAE (American Iron and Steel Institute and Society for Automotive Engineering) system of designation, and, due to economic factors, this class of steel are the materials mostly used in the construction industry for oil and gas including pipelines even though they corrode easily in the environment.

### **3.8.2 Corrosion of carbon steel in seawater**

With considering the cost of product, carbon steel has been widely employed as a construction material in oil and gas production. However, one of the major problems related to its use is its low corrosion resistance in this environment. Rusting is an important phenomenon accompanied with the corrosion of carbon steel and the formation of corrosion products such as iron oxides is an biotic process of chemical reactions. It was generally agreed by most of the researches that carbon steels are generally attacked by uniform corrosion or general corrosion (Figure 2.10). The term 'uniform' or 'general' corrosion is used to describe the corrosion damage that proceeds in a relatively uniform manner over the entire surface of an alloy. It is an even rate of metal loss over the exposed surface. It also characterised by a chemical or electrochemical reaction or metal loss due to chemical attack or dissolution that proceeds uniformly over the entire exposed surface or over a large area. During this

process, the material becomes thinner as it corrodes until its thickness is reduced to the point at which failure occurs. In a study by Ueda (2006) it was explained that carbon steel not only may be attacked by uniform corrosion, but also may suffer severe localised corrosion which is commonly known as 'ringworm corrosion' or 'mesa corrosion' at temperature around 100°C in CO<sub>2</sub> environments [78]. Yang *et al.* in their study about the effect of carbon content in carbon steel found that a homogeneous microstructure has better corrosion resistance and proper amounts of carbon content and fine carbon-rich phases are beneficial to the corrosion resistance of carbon steel [79].

Besides of metallurgical composition, lattice structure also plays important roles in corrosion behaviours. Xu *et al.* in their study of corrosion behaviour of carbon steel in molten zinc bath found that face-centered-cubic (fcc) structure is more corrosion resistance than body-centered-cubic (bcc) possibly due to the compactness of the atomic structure [80]. Andijani and Turgoose elucidate that corrosion rates for carbon steel are very low at 25°C and neutral pH when they comparing the corrosion rates of carbon steel in deaerated 1 M NaCl solution and artificial seawater. However, a long-run measurements at 50°C and pH 8.5 shows low corrosion rates compared to short-run measurements at the same conditions. This is because of the formation of a protective hydroxide film on the metal surface which restricted the access of water to the surface [81].

Oxygen is known to be one of the main parameters for corrosion to happen. Lee *et al.* in their study of carbon steel corrosion under stagnant seawater conditions found that the surface are covered with intact, tenacious iron oxide when carbon steel were exposed to aerobic seawater for 396 days whereas non tenacious sulphides were developed when carbon steel were exposed in anaerobic conditions over the same period. They concluded that anaerobic conditions is not inhibit corrosion and oxygen are not required for aggressive localised corrosion, but once oxygen is introduced to carbon steel which previously maintained under strictly anaerobic conditions, the corrosion is extremely aggressive [82]. Apart of this study, Caceres *et al.* in their study for corrosion kinetics of carbon steel as a function of dissolved oxygen and NaCl concentration elucidate that all kinetic parameters exhibit a significant dependence from both the dissolved oxygen and NaCl concentration [37]. The dissolved oxygen in aqueous media can behave as a cathodic depolariser and able to support iron dissolution at the anode. Nesmeyanova in her study of carbon steel of pearlite structure in deaerated and oxygenated media found that at 280°C, corrosion rate decreased when constant

supply of oxygen to the sample. This is due to the formation of protective layer on the sample surface [83].

### 3.9 Stainless Steels

#### 3.9.1 Stainless steel 316L

Stainless steels (SS) have been widely used in industrial components for decades. The selection of stainless steels results from their well-documented resistance to corrosion but yet, stainless steel still suffers for corrosion attack especially in corrosive media such as seawater. Corrosion of stainless steel in seawater is dependent mainly on the salt content (which increase the electrical conductivity) and its oxygen content. A number of variables can influence and complicate the course of corrosion in different ways such as chloride, sulphate and temperature.

In the context of corrosion, stainless steels are characterized by their passivity. Under certain conditions, steel is passive, where the corrosion rate for the metal is relatively low. Iron is considered an active-passive metal and, therefore, steel behaves similarly. Passivity can be defined as the loss of chemical reactivity under certain conditions [1]. Steel achieves this by having a passive film form along its surface. Figure 3.13 (a) below shows the formation of pitting corrosion on SS covered with a lace-like layer [84]. This is indicating that the passive film is scarcely soluble, both in the bulk electrolyte and that within the pit. The flat-walled pit in Figure 3.13 (b) indicated that there is no ohmic layer within the pit which can maintain equal current density at all points of the pit surface. The hemispherical (or partly spherical) pits suggest that there probably occur processes similar to those accompanying electropolishing within the pit [84].

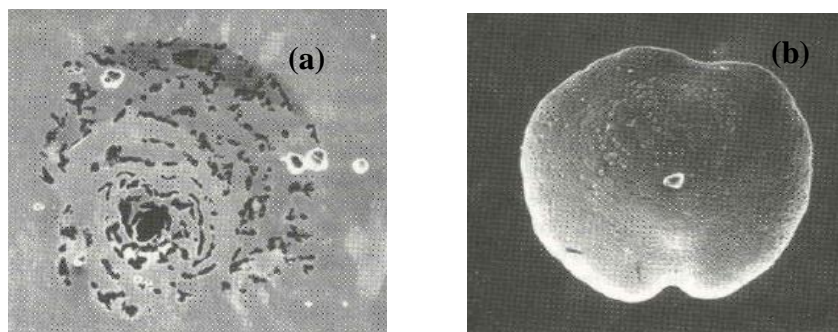


**Figure 3.13 Pits with (a) lace-like cover over the top and (b) flat-walled opening [84].**



The characterisation of SS is according to the minimum 10.5% wt% Cr (Chromium) addition to iron [85]. For most SS, the maximum chromium content is about 30% and the minimum iron content is 50%. The stainless characteristic arises from the formation of an invisible and very adherent chromium-rich oxide surface film. This puts the steel in a passive state and when the film is breached, it immediately heals when oxygen is present. It is highly corrosion resistant and shows little or no corrosion if the passive film remains intact. According to Strafford *etal.*, corrosion resistance obtained when chromium content increased from 1% to 12% by plasma-nitriding process [86].

Modifications of lower grade stainless steel produce the other classes, according to their metallurgy structure, to achieve higher specific strength stainless steels: austenitic (face-centred cubic), ferritic (body-centred cubic), martensitic (transformed from the austenite face-centred cubic structure at high temperatures to the body-centred tetragonal, which is martensite structure at low temperatures when the austenite is rapidly cooled in air or in a liquid) and duplex stainless steel (ferritic plus austenitic). The choice of austenitic stainless steels is steadily increasing with the introduction of newer alloys and by the modification of traditional ones to improve one or more of their properties.

The American Iron and Steel Institute (AISI) designate the wrought standard grades of stainless steels by three digit numbers. The austenitic grades are designated by numbers in the 200 and 300 series, while the 400 grades are either ferritic or martensitic [77]. A study by the Society for Automotive Engineers (SAE) and the American Society for Testing Materials (ASTM) resulted in the Unified Numbering System (UNS). The letters identify stainless steels, however, some stainless alloys use the letter N because of their higher nickel content.

The austenitic stainless steels generally contain from 16% to 26% chromium, up to 35% nickel, and up to 20% manganese. The corrosion resistance in a chloride environment can be enhanced by balancing the ferrite stabilizer, such as chromium and molybdenum.

### **3.9.2 The 25Cr Duplex stainless steel**

Duplex stainless steels exhibit excellent properties over either austenitic or ferritic stainless steels because of the presence of about equal amounts of the austenite and ferrite phases in microstructure. They first became available in the 1930s

[85]. Commercial grades of duplex stainless steels contain 22-26%Cr, 4-7% Ni, up to 4.5%Mo, 0.7%Cu and tungsten and 0.08-0.35% nitrogen. These are divided into four generic types: Fe-23Cr-4Ni-0.1N, Fe-22Cr-5.5Ni-3Mo-0.15N, Fe-25Cr-5Ni-2.5Mo-0.17N-Cu and Fe-25Cr-7Ni-3.5Mo-0.25N-W-Cu, which are referred to as super duplex stainless steels [77]. The modification of the composition enhances the corrosion resistance and the adding of nitrogen improves the pitting corrosion resistance.

Critical Pitting Temperature (CPT) is one of the important parameters for duplex and super duplex stainless steel. Its determination can be made by electrochemical methods or immersion test [87]. The ASTM G-48 Standard describes the CPT determination by immersion tests in 10% FeCl<sub>3</sub> solution. The samples are immersed at different peak temperatures, starting from a temperature estimated from the equation below. It was found that the higher the CPT value, the higher the pitting resistance of duplex stainless steels.

$$T (^{\circ}\text{C}) = (2.5 \times \% \text{Cr}) + (7.6 \times \% \text{Mo}) + (3.19 \times \% \text{N}) - 41 \quad [87]$$

Because of the attractive combination of mechanical properties and corrosion resistance duplex stainless steels are used in a wide range of industries, especially oil and gas. They are commonly used in aqueous chloride containing environments as a replacement for austenitic stainless steels that have suffered pitting during service.

### 3.9.3 The passive film

In appropriate conditions, some base metals can develop a surface condition that inhibits interactions with aqueous media. The condition is described as passivity and its development is called passivation. The effect is valuable in conferring corrosion resistance on bare metal surfaces even in aggressive environments. The corrosion resistance of austenitic stainless steels and hardenable stainless steels such as duplex stainless steel are depends on the formation of natural occurring transparent oxide films. These films may be impaired by surface contaminations such as organic compounds or metallic or inorganic materials [13].

Marcus *et al.* pointed out that passive layer is a simple uniform and homogeneous oxide (or hydroxide) films that blocks the transfer of cations from the metal surface to the electrolyte [88]. They also added that almost all passive films have multilayer structures, usually with inner oxide and outer hydroxide parts. Belo elucidate that the composition of the passive film depends on the environment to which it is exposed. In

neutral, non-aggressive solutions, it consists of two layers which are one with chromium (Cr) rich oxides and the external layer is essentially composed of ferum (Fe) oxides [89]. The Cr oxide layer is assumed to be responsible for the effectiveness of the passivation, whereas the Fe oxide layer displays some reactivity and is therefore significantly affected by the electrolyte. In mild solutions, the outer layer is reasonably well defined and thick relatively to the dimensions of the whole film. Immersing in artificial sea water, the films also show an internal layer mainly composed by chromium oxide and the external layer is a mixture of chromium and iron oxides with a small concentration of nickel [89].

Qvarfort and Olsson explained that the corrosion product formed on stainless steels under moderate low pH may form a protective layer, such as semi-passive layer which may prevent further attack. However, this protective layer only efficient in a limited potential range. They also added that such semi-passive oxides were only observed on the stainless steel, but not on the nickel based alloys [90].

Fredriksson *et al.* elucidate that the thickness of passive layer of 316L is estimated to 2.6 nm for a sample that was polarized at 0.6V in their research of observation full depth profile of passive films based on high resolution using non-destructive hard X-ray photoelectron spectroscopy (HAXPES) technique in combination with the angular resolved X-ray photoelectron spectroscopy (ARXPS). As they expected, the main component in the passive film is chromium. They also suggested that in high resolution of HAXPES spectra, chromium present in three different oxidation states present as well as iron three oxides [91].

Souza *et al.* mentioned that the corrosion resistance properties of a superduplex stainless steel containing approximately 50% of ferrite demonstrated good pitting resistance at room temperature at several NaCl concentrations. However, above 60 °C there is an increase in the average size and numbers of pits with a strong effect on the corrosion performance of this material. They concluded that, from the image analysis of the microstructure, number and size of pitting vary in function of the temperature [92].

### **3.10 Nickel alloys**

Nickel is predominantly used as an alloying element in stainless and low-alloy steels. About 13% of the total nickel is used in nickel-based alloys for corrosion resistance and heat-resistant properties. Nickel-Chromium (N06XXX) containing at least 15% chromium provides both oxidation and carburization resistance at temperatures

exceeding 760°C (1400°F) [93]. The chromium provides the formation of a protective surface oxide, and the nickels exhibit good retention of the protective coating, especially during on-off service exposure at high temperatures. Addition of niobium which acts with the molybdenum is to stiffen the alloy's matrix thereby providing high strength without the need of a strengthening by heat treatment [77].

Inconel 625 (UNS N06625) is a type of nickel-chromium-molybdenum alloy with excellent corrosion resistance in a wide range of corrosive media, being especially resistant to pitting and crevice corrosion. Apart from having nonmagnetic properties, alloy 625 also has excellent fatigue strength and stress-corrosion cracking resistance to chloride ions. Most typical applications of Inconel 625 are in chemical processing, aerospace and marine engineering, pollution-control equipment, and nuclear reactors.

### **3.10.1 Corrosion of Inconel 625**

It is generally recognized that chromium oxide plays an important role in both austenitic and duplex stainless steels materials. However, in the case of nickel-base alloys the role of the nickel and iron is not well established. According to Belo *et al.*, the critical chromium concentration necessary to develop a protective chromium oxide barrier at the film-metal interface is approximately the same (about 15%) for both Fe-Cr and Ni-Cr alloys. However, the films formed on nickel-base alloys are thinner than those formed on stainless steels [94].

Despite most of Ni-base alloys having almost the same elements, the various element contents are designed to provide exceptional resistance to a variety of corrosive environments [77]. For instance, the nickel content is sufficient for resistance to chloride-ion stress corrosion cracking. The nickel, in conjunction with molybdenum and copper, also gives outstanding resistance to reducing environments such as those containing sulphuric and phosphoric acids. The minor molybdenum also aids resistance to pitting and crevice corrosion and chromium also improves resistance to high-temperature oxidation and to attack by hot sulphur-bearing gases. Small quantities of both titanium and niobium are originally added as stabilising elements to tie up carbon against sensitisation to intergranular corrosion. Silicon is typically present only in small amount in most nickel-base alloys as a residual element from deoxidation practices or as an intentional addition to promote high-temperature oxidation resistance.

### 3.10.2 The passive film on nickel alloys

Similar to stainless steel, passive films form on nickel alloys when exposed to a corrosive environment. Wu *et al.*, studied the passive films formed on Alloy 690 in different pH solutions at high temperatures using potentiodynamic polarization, Auger electron spectroscopy, thermodynamic diagrams and the Mott–Schottky relation. They found that the chemical compositions and electronic structures of the passive films were to be strongly pH-dependent and the passive films were a mixture of  $\text{Cr}_2\text{O}_3$  and  $\text{FeCr}_2\text{O}_4$  [95].

The semiconducting properties of passive films formed on nickel–base alloys type Alloy 600 in borate buffer solution were studied by Belo *et al.* using capacitance measurements and photoelectrochemistry. They study the influence of the alloying elements (Fe, Ni, Cr) on the film properties using pure metals and pure alloys. The results obtained show that the presence of both chromium and mixed nickel–iron oxides in the films revealed by quantitative analysis develops a p-n heterojunction that controls their electronic structure, in a similar manner to the case of stainless steels. The nickel oxide present in the films acts as a barrier layer that confers improved protection [94].

According to Kawashima *et al.*, the surface films formed on nickel-based alloy at lower potentials in 1.5 M  $\text{H}_2\text{SO}_4$  solution contain  $\text{S}^{2-}$  ions other than  $\text{SO}_4^{2-}$  ions, whereas  $\text{S}^{2-}$  ions were not incorporated in the passive film. Passivation took place by the formation of hydrated chromium oxyhydroxide and pitting led to no substantial change in the average composition of the film [96] and Yin *et al.* reported that the passivation regions for nickel-based alloys are wider and stable [97]. Chen *et al.* proved that the passive films formed on nickel-based alloy consist of double layer structure where the outer layer composed of hydroxide as p-type semiconductor and inner layer composed of oxide as n-type semiconductor [98].

Marcus *et al.* studied of the growth and structure of passive films in high temperature water on a nickel-base alloy and found that in the early stages of oxidation of the alloy, an ultra-thin oxide layer (about 1 nm) is formed, which consists of chromium oxide ( $\text{Cr}_2\text{O}_3$ ) while  $\text{Cr}(\text{OH})_3$  at the outer layer with a very small amount of  $\text{Ni}(\text{OH})_2$ . This implies the transport of Cr and Ni through the oxide layer, and release of  $\text{Ni}^{2+}$  in the solution [99].

### 3.11 Cermet Alloys

Cermet alloys is the name given to a composite material composed of ceramic (cer) and metallic (met) materials. A cermet is ideally designed to have the optimal properties of both a ceramic, such as high temperature resistance and hardness, and those of a metal, such as the ability to undergo plastic deformation. The metal is used as a binder for an oxide, boride, or carbide. Generally, the metallic elements used are nickel, molybdenum, and cobalt. Depending on the physical structure of the material, cermets can also be metal matrix composites, however, cermets are usually less than 20% metal by volume [77].

#### 3.11.1 Tungsten carbide cermets

WC-based cemented carbides belong to a large family of hard metals that are widely used for cutting tools because they show an excellent combination of mechanical properties, such as high hardness, strength and wear resistance and, therefore, they are well established in several industrial applications[39]. However, their poor corrosion resistance in aqueous solutions reduces the spectrum of their applications. This heavy alloys were first produced by McLennan and Smithells in 1935 [100]. They are essentially three-component pseudoalloys consisting of large amounts of tungsten combined with either nickel or copper matrix. Cobalt-tungsten carbide (WC–Co) hardmetals are composed of hard WC particles into a tough metallic matrix produced during a liquid phase sintering process (Figure 3.14).

Cemented carbides are used for their outstanding resistance to wear and in many cases they also have a high resistance to corrosion. In the manufacturing of resistors (especially potentiometers), which may experience high temperature, cemented carbide also used as a capacitors and other electronic components. Instead of tungsten carbide, cermets are being used in saws and other brazed tools due to their superior wear and corrosion properties. Some types of cermets are also being considered for use as spacecraft shielding, as they resist the high velocity impact of micrometeoroids and orbital debris much more effectively than more traditional spacecraft materials such as aluminium and other metals.

The corrosion resistance of hardmetals, however, is far from outstanding. Several efforts have been made to reduce the corrosion susceptibility of WC–Co. It was found that using Ni instead of Co as the binder material or alloying  $\text{Cr}^3\text{C}^2$  into the binder

phase leads to higher corrosion resistance. However, as a disagreeable consequence, the mechanical properties are thereby diminished. Compared with pure nickel, hard metals with Ni and Co binders have very limited passivation range [101]. Nickel is more corrosion resistant than cobalt while chromium readily forms a protective film.

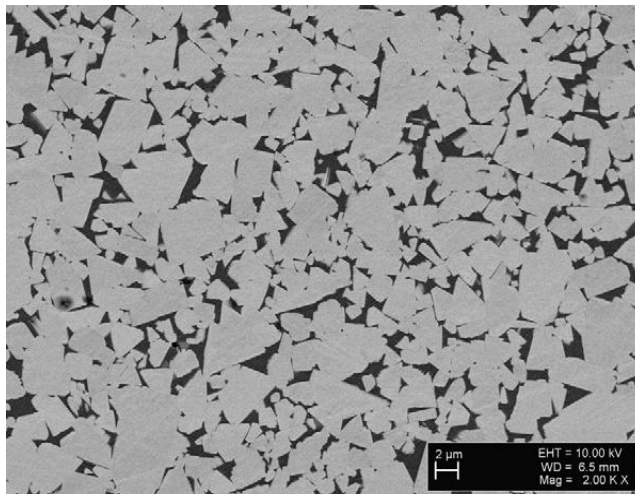


**Figure 3.14 WC-Co microstructure (white is WC and black is Co) [102].**

In neutral and acidic solutions, the corrosion process of WC-Co consists mainly of Co dissolution. This Co dissolution is the main corrosion process of WC-Co in neutral acidic solutions whereas WC dissolution becomes more significant at alkaline pH.

By anodic polarisation, the reaction behaviour of WC is influenced by the presence of adsorbing ions, which are the binders [39]. So far, no systematic investigation has been performed that considers the dissolution behaviour of WC in aqueous solutions or the influence of pH solutions.

### **3.11.2 Structure and microstructure**

Tungsten carbide (WC), tungsten dicarbide (WC<sub>2</sub>) or tungsten semicarbide (W<sub>2</sub>C) is a chemical compound containing tungsten and carbon with extreme hardness. It can be prepared by reaction of tungsten metal and carbon at 1400-2000°C. Other methods include a patented fluid bed process, which reacts either tungsten metal or blue WO<sub>3</sub> with CO/CO<sub>2</sub> mixture and H<sub>2</sub> between 900°C and 1200°C [103]. There are two forms of WC, a hexagonal form,  $\alpha$ -WC, and a cubic high temperature form,  $\beta$ -WC, which has the rock salt structure. The hexagonal form can be visualized as made up of hexagonally close packed layers of metal atoms with layers lying directly over one another, with carbon atoms filling half the interstices giving both tungsten and carbon a regular

trigonal prismatic, 6 coordination [104], as shown in Figure 3.15. It is high melting, extremely hard with relative low electrical resistivity. Compared with pure nickel, hard metals with Ni and Co binders have very limited passivation range [105]. Nickel is more corrosion resistant than cobalt while chromium readily forms a protective film. Presumably molybdenum is present to enhance the pitting resistance to chloride [106].

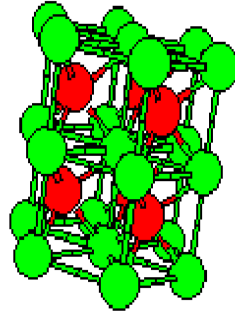


**Figure 3.15 Hexagonal structure of  $\alpha$ -WC [104]**

### 3.11.3 Corrosion of cemented tungsten carbides

The main properties affecting the corrosion performance of a cemented tungsten carbide in a service environment are the material structure and the binder material [107]. A binder with poor corrosion resistance can cause delamination between surface and substrate and serve as sources of corrosion attack. Potgieter *et al.* also pointed that tungsten carbide is chemically more stable than cobalt in acidic media and corrosion progresses by oxidation of the binder, leaving only a WC skeleton (Figure 3.16) which is easily broken down by mechanical action [108]. Scholl *et al.* study the corrosion resistance of 10vol.% Ni, Co and Fe cemented carbides in sulfuric acid solution and found that the corrosion resistance decrease in sequence of (WC, Ni) > (WC, Co) and (WC, Fe) [105].

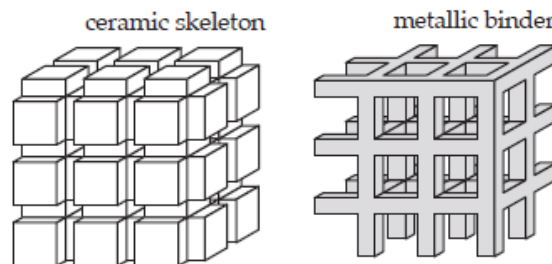


**Figure 3.16: Cermets and cemented carbides are formed of a main ceramic phase bond by a metal binder. Both metal and ceramic phase form continuous interpenetrated skeletons [109].**

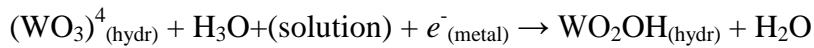


Tomlinson and Linzell [110] investigated the polarization of pure cobalt, nickel, tungsten and hard metals based on WC/Co and WC/Ni, in a solution of 0.01M sulfuric acid added with 0.99M sodium sulfate at the pH of 2.55. They found that passivation of the pure metals nickel, tungsten and cobalt is excellent, good and zero, respectively. The polarization of tungsten carbides reflects mainly the behaviour of the binder phase and their performance is less than that expected by comparison with pure nickel. Tungsten carbides with nickel binders have a superior performance compared with cobalt binders [105,110]. Tungsten carbide grain size and the presence of chloride ions in this acid environment have no noticeable effects. Also shown by Human *et al.*, the binder phase corrodes by a pitting mechanism and attack at the carbide/binder interfaces is exaggerated [111]. The binder regions adjacent to the corners of tungsten carbide grains are notably attacked and this is especially the case where the meeting of two tungsten carbide grains forms an acute angle in the binder phase.

The oxidation dissolution of tungsten carbide in acid has intermediate step which was suggested by Scholl [105]. As the potential increases, tungsten carbide is oxidized to  $WO_3$ , which, at potentials higher than +0.8V, is dissolved according to the following proposed reactions:

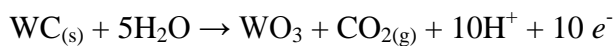


or

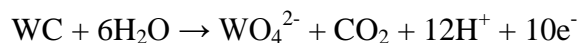


The grown films of  $WO_3$  undergo different types of breakdown in different electrolytes. The chemical dissolution of  $WO_3$  has also been reported by Burke *et al.* [112] and Fauconnier *et al.* [113].

Lekatou [114] reported that  $CO_2$  is one of the products of the electrochemical and chemical oxidation of tungsten carbide in a 2M  $H_2SO_4$  solution. In his work,  $CO_2$  was detected by mass spectroscopy and acid titration after absorption in NaOH according to the following reaction:

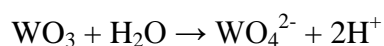


Ghandehari *et al.* (1976) investigated the anodic behaviour of cemented WC-6% Co alloy in phosphoric acid saturated with nitrogen by means of potentiostatic dissolution, polarization curves and micrographic studies [115]. On the basis of a mass balance, tungsten carbide is considered to be dissolved according to the following equation at potentials positive to the reversible potential.



The corrosion properties of cemented carbides with cobalt binder phase was examined in HCl and H<sub>2</sub>SO<sub>4</sub> solution at room temperature by Sutthiruangwong and Mori [116]. HCl was found to be more aggressive to cemented carbides with cobalt binders than H<sub>2</sub>SO<sub>4</sub>. Apart of that, dissolved oxygen has small influence on anodic behaviour of cobalt-based cemented carbides.

Warren *et al.* [117] have performed one of the few studies on the oxidation of tungsten carbide in aqueous media. They identified WO<sub>3</sub> as the oxidation product of hot pressed WC bars in dry and humid atmospheres. Another important aspect researched by Andersson and Bergtrom[118] is the dissolution of tungsten carbide in water. They found that WO<sub>3</sub> dissolves in water forming tungstate ions by the reaction:



The dissolution of tungsten carbide seems to be continuous after the reoxidation of the power, resulting in a decreasing pH with time.

In alkaline environments, the corrosion characteristics of cemented tungsten carbide with cobalt were investigated by Trueman *et al.* [119]. It was reported that the cathodic reactant would be dissolved oxygen and its reduction would be expected to promote metal dissolution followed by passivation. If there is sufficient oxygen present, the aggressive chloride ions will also promote spontaneous pitting corrosion. Trueman also stated that according to the Pourbaix diagram, the anodic polarization curves exhibit greater polarization in alkaline environment than in acidic environment and the polarization increases cobalt concentration [120]. This suggested metal dissolution followed by the formation of a partially protective film.

### **3.12 Materials Selection for Offshore**

Steels are the most extensively used structural material in industry. Mild steel is the most versatile general-purpose material; it has good mechanical strength, is easy to fabricate, has good formability and weldability, is abundant and is low cost. In corrosive environments, mild steel structures can be saved by coating and/or cathodic protection. However, mild steel may not be able to withstand more severe or aggressive environments, such as marine or seawater, and, consequently, austenitic stainless steels (UNS S31603 or 316L) have found applications as construction materials. The excellent corrosion resistance, good mechanical properties and reasonable cost are the

contributing factors for their application. It is a formidable material for the construction of evaporators, distiller pipes, pumps and valves. Stainless steel alloys are found to be one of the most dependable structural materials under dynamic flow conditions and show virtually no corrosion even after very long exposure. However, they are subjected to localised corrosion in the presence of chloride ions and under static or stagnant conditions.

Generally, the materials used for offshore structures should have a high ratio of strength to self-weight ratio. Other selection factors include degradation processes, ease of fabrication or construction, availability, anticipated life and relative cost. There are some preferred materials for offshore applications such as tungsten carbide-cobalt-chromium (WC–Co–Cr) and nickel-based alloys, which are in high demand due to their resistance to corrosion. The materials listed below are some of the preferred materials for offshore applications together with their best characteristics.

**Table 3.3 Material selection for retarding corrosion [77]**

Material	Characteristic
Duplex stainless steel	Preferred over carbon steel or other stainless steel. It combines the basic toughness of the more common austenitic stainless steel with the highest strength and improved corrosion resistance of ferritic steels. It can also be used in low temperatures and is able to resist stress corrosion cracking (SCC).
Aluminium	Despite its high corrosion resistance and low maintenance cost, it is not recommended because of low mechanical properties. Still new and requires additional research in material technology and design.
Composite	Fibreglass with polyester or epoxy.
Copper and its alloy	Good electrical and thermal conductivity. Thus, often used in heating and cooling systems.
Ceramic	Good corrosion resistance
Concrete	Depends on reinforcement
WC – Co - Cr	High demand due to resistance to corrosion.
Coating Ti-Al-N	Using Plasma Vapour Deposition (PVD) and is known as being the best coating material.
Brass	Widely used as tubing material for condensers and heat exchangers in various cooling water systems. It is susceptible to corrosion because of <i>dezincification</i> . Increased zinc content would increase the dezincification process.

### **3.13 Summarising the Literature Review**

From very cheap materials such as carbon steel to cermets alloys, it has been shown that improvements in research and development have produced not only high strength materials, but also improved corrosion resistance. However, due to cost constraints, the applications for high strength and corrosion resistant materials are limited in any construction including oil and gas operations. The reality is, every material shows a different degree of deterioration when corrosion is about to attack. Corrosion can be controlled if environmental factors that affect corrosion attack could be identified for different kind of materials types. The most environment factors that affect corrosion attack identified by research before are oxygen concentrations, temperature, pH, velocity and aggressive ions. Most of the results found that corrosion increased as the oxygen concentrations and temperature increased. In acidic media, the corrosion attack is more pronounced compared to alkaline medium. Even the velocity or flow of the medium does have effect for localised corrosion, but localised corrosion more pronounce in static corrosion compared materials in heavy flow. But, the velocity might contribute to erosion-corrosion of metals. Several researcher have found that aggressive ions such as chloride increased the corrosion attack while sulphate could retard corrosion attack [121-124]. The ratio of these aggressive ions is only studied by using the ratio of sulphuric acid to hydrochloric acid. There are no research studies using the ratio from actual compositions of natural seawater. Therefore, apart from using chemical (which need to comply with environmental procedure) to control the corrosion attack, some aggressive ions could be identified as a means of controlling corrosion attack in seawater. In this research, different level of materials grade, from mild steel to highly corrosion resistance materials will be use to study the corrosion attack. These materials are generally used in valve systems of oil and gas operations.

## Chapter 4

### MATERIALS AND EXPERIMENTAL PROCEDURES

#### 4.1 Materials Under Study

Three types of materials are used in this research: **carbon steels** AISI 1040 (UNS G10400), AISI 4140 (UNS G41400), AISI 8620 (UNS G86200); **stainless steels** 316L (UNS S31603), nitrogen alloyed stainless steel: 25Cr Duplex (UNS S32760) and Inconel 625 (UNS N06625); and **cermet materials** WC-Ni and WC-Co. 316L, 25Cr Duplex, Inconel 625 and WC-Co were cut from solid steel rod and WC-Ni was cut from coupon received from *Aker Solutions*. The composition given by the manufacturer of the materials is given in Tables 4.1 and 4.2. Also shown in Table 4.3 are the mechanical properties for each material.

25Cr Duplex is a type of stainless steel added with nitrogen whereas Inconel 625 is nickel alloy. The main reason for nitrogen alloying in Inconel 625 is to increase the mechanical strength of the steel and to replace some of the expensive nickel alloying element. In addition, increased nitrogen content can also increase the resistance to localised corrosion and retard the precipitation of the carbide and intermetallic phases [77].

The hard phase in cemented carbide (WC) of cermet alloys is known to be relatively unaffected by corrosive attack, as compared to the binder metallic phase (Co and Ni) [107]. Nickel binders in cemented carbides are more corrosion resistant than the corresponding cobalt containing grades. With some additional chromium in either cobalt or nickel containing cemented carbides the corrosion resistance can be improved, but it tends to cause reduction in strength [107]. In this research, the cermet alloys used are WC-6%Co and WC—9%Ni

**Table 4.1 Carbon steel composition of samples (wt%)**

<i>Composition</i>	<i>Cr</i>	<i>Ni</i>	<i>Mo</i>	<i>C</i>	<i>S</i>	<i>P</i>	<i>Mn</i>	<i>Si</i>
AISI 8620	0.4	0.4	0.15	0.18	0.04	0.035	0.70	0.15
AISI 4140	0.8	-	0.15	0.38	0.04	0.035	0.75	0.15
AISI 1040	-	-	-	0.37	0.05	0.04	0.60	-

**Table 4.2 Alloy composition of samples (wt%)**

<i>Composition</i>	<i>Other name</i>	<i>Cr</i>	<i>Ni</i>	<i>Mo</i>	<i>C</i>	<i>S</i>	<i>P</i>	<i>Mn</i>	<i>Si</i>	<i>Others</i>
UNS S31603	Austenitic SS	16.0	10.0	2.0	0.03	0.03	0.045	2.0	1.0	-
UNS S32760	25Cr Duplex	25.0	6.0	3.0	0.03	0.01	0.03	1.0	1.0	<i>Cu=0.,N=0.2,</i> <i>W=0.5</i>
UNS N06625	Inconel 625	22.0	58.0	9.0	0.05	0.003	0.01	0.03	0.25	<i>Fe=4.0,Nb=3.15,</i> <i>Ti=0.3,Al=0.3</i>

**Table 4.3 Mechanical properties of materials[79].**

Material	Mechanical Properties				
	Density, $\rho$ (kg/m <sup>3</sup> ) (X1000)	Elastic Modulus (GPa)	Tensile Strength (MPa)	Yield Strength (MPa)	Hardness
AISI 8620	7.7-8.03	190-210	536.4	385.4	149 (HB)
AISI 4140	7.7-8.03	190-210	655.0	417.1	197(HB)
AISI 1040	7.84	190-210	518.8	353.4	149(HB)
UNS S31603	8	79.3	276	152	42(HB)
UNS S32760	7.82	199	770	550	28(HC)
UNS N06625	8.44	205.8	940	430	88(HC)

## 4.2 Solution Analysis

The geographical variation in the corrosivity of natural seawaters results from the variations in the salinity, microbiological activity, dissolved oxygen concentration and temperature. Discounting the inland seas, such as the Dead Sea, the chloride (Cl<sup>-</sup>) concentration of seawater varies from about 5.8 g/kg to about 24 g/kg, the sulphate (SO<sub>4</sub><sup>2-</sup>) concentration varies from 0.8 g/kg to 3.4 g/kg, and the bicarbonate (HCO<sub>3</sub><sup>-</sup>) concentration varies from 0.01 g/kg to 0.2 g/kg [202].

Natural seawater is more aggressive than artificially made seawater (by mixing the appropriate compounds found in seawater) or seawater that has been sterilised [35]. The aggressiveness of seawater is due to salt content or composition in seawater which is not contain in fresh water. The major compositions in seawater are chloride (Cl<sup>-</sup>), sulphate (SO<sub>4</sub><sup>2-</sup>), calcium (Ca<sup>+</sup>), sodium (Na<sup>+</sup>), magnesium (Mg<sup>+</sup>) and potassium (K<sup>+</sup>), which together represent 99.8% of the mass of solutes dissolved in seawater. The density of seawater is determined by its salinity and temperature. Seawater from Wormly in southern England is used as the international standard for seawater composition [80]. The chlorinity is related to salinity, S% = 1.80655 Cl% [50]. Research has found that corrosion increases with water salinity up to about 5% of

sodium chloride [57]. Salinity can be measured by the refractive index and conductivity (charged ions increase with increasing conductivity). Table 4.4 shows the elements present in seawater. The conductivity of the solutions for this research are 54mS/cm and were prepared using distilled water.

**Table 4.4 Standard seawater composition [81]**

<b>Component</b>	<b>Concentration (mg/l)</b>	<b>% of total salt</b>
Chloride	18,980	55.04
Sulphate	2,649	7.68
Magnesium	1,272	3.69
Calcium	400	1.16
Potassium	380	1.1
Bicarbonate	140	0.41
Bromide	65	0.19
Fluoride	1	0
Boric Acid	26	0.07
Strontium	13	0.04
Sodium	10,556	30.61
<b>TOTAL</b>	<b>34,482</b>	<b>99.99</b>

For this research, materials were tested in 3.5% NaCl solutions and in seawater with different sulphate-chloride ratios (keeping the salinity close to 3.5%). The composition of fresh seawater is shown in Table 4.5. The four different solutions were prepared with different sulphate-chloride ratios to identify the effect of these ions on the corrosion attack while maintaining the other ion quantity and the same pH between 7.0-8.0. The solution with the same elements as real seawater was prepared and identified as solution 1. Other solutions are prepared based on the calculation shown and Table 4.6 was obtained.

**Table 4.5 The six major elements in seawater being used[16].**

Ion	Avg.g/kg Salinity $\approx$ 3.5%
Chloride (Cl <sup>-</sup> )	19.25
Sodium (Na <sup>+</sup> )	10.71
Sulphate (SO <sub>4</sub> <sup>2-</sup> )	2.71
Magnesium (Mg <sup>2+</sup> )	1.30
Calcium (Ca <sup>2+</sup> )	0.42
Potassium (K <sup>+</sup> )	0.39
<b>Total</b>	<b>34.78</b>

Based on the values in Table 4.5, the calculations of seawater in different sulphate-chloride ratios were made using the appropriate chemicals available. The chemicals are sodium chloride (NaCl), potassium chloride (KCl), calcium chloride hexahydrate (CaCl<sub>2</sub>.6H<sub>2</sub>O), magnesium sulphate heptahydrate (MgSO<sub>4</sub>.7H<sub>2</sub>O), magnesium chloride hexahydrate (MgCl<sub>2</sub>.6H<sub>2</sub>O), sodium bicarbonate (NaHCO<sub>3</sub>), hydrochloric acid (HCl) and sulphuric acid (H<sub>2</sub>SO<sub>4</sub>). The calculation starts with the least amount of ions used. The calculation below is for the amount of potassium chloride (KCl) in Solution 1 (Solution 1 (S1) has the same amount composition as natural seawater). The remaining calculations for sodium chloride (NaCl), calcium chloride hexahydrate (CaCl<sub>2</sub>.6H<sub>2</sub>O), magnesium sulphate heptahydrate (MgSO<sub>4</sub>.7H<sub>2</sub>O), magnesium chloride hexahydrate (MgCl<sub>2</sub>.6H<sub>2</sub>O), sodium bicarbonate (NaHCO<sub>3</sub>), hydrochloric acid (HCl) and sulphuric acid (H<sub>2</sub>SO<sub>4</sub>), S2, S3 and S4 can be found in Appendix. Considering the ratio of SO<sub>4</sub><sup>2-</sup> / Cl<sup>-</sup> for this S1 is 0.14, the calculation is as below;

- The reaction of *KCl*:  $KCl \longrightarrow K^+ + Cl^-$

As shown in Table 4.5, the amount of potassium (K<sup>+</sup>) needed is 0.39g. Thus, the amount of *KCl* needed is:

$$Mass\ of\ KCl = \frac{Mass\ of\ K^+}{Molecular\ weight\ of\ K^+} \times Molecular\ weight\ of\ KCl \quad 4.1$$



$$\text{Mass of } KCl = \frac{0.39}{39.098} \times (39.098 + 35.45) = 0.743g$$

$$\text{Mass of } Cl^- = \frac{0.39}{39.098} \times (35.45) = 0.3536g$$

From the calculations, the list in Table 4.6 is obtained. The solutions were prepared in 1000ml distilled water (considering the amount of water already existed in each chemical) and ensure the pH is between 7.0-8.0, and salinity is 3.5 wt%.

Table 4.6 shows the ratio of  $SO_4^{2-} / Cl^-$  used in this research. As mentioned before, solution 1 was based on  $SO_4^{2-} / Cl^-$  in real seawater. To find the effect of sulphate or chloride on corrosion attack, solution 2 was synthesised with a lower amount of chloride than sulphate whereas solutions 3 and 4 had a higher amount of chloride than sulphate. According to the above calculations, the chemical used to synthesise the artificial seawater was calculated. The composition of the solutions is shown in Table 4.7.

The sulphate-chloride ratio obtained in Table 4.7 is from the calculation shown. As shown in Table 4.6, other ions ( $Mg^{2+}$ ,  $Ca^{2+}$ ,  $Ca^{2+}$ ,  $K^+$  and  $Na^+$ ) except  $SO_4^{2-}$  and  $Cl^-$  are maintained as same as real seawater. To balance this ionic content and also the salinity (~35 g/L),  $SO_4^{2-} / Cl^-$  were varied according to Table 4.7 below by calculating the salts used using the calculation shown. This is a trial and error process in order to get not only 35 ppt salinity, but also pH of 7 to 8.

**Table 4.6 Ionic contents of the 4 solutions used**

Component	Seawater	$SO_4^{2-} / Cl^- = 0.14$	$SO_4^{2-} / Cl^- = 19.15$	$SO_4^{2-} / Cl^- = 0.75$	$SO_4^{2-} / Cl^- = 0.99$
	(Solution 1)	(Solution 2)	(Solution 3)	(Solution 4)	
	(g/kg)	(g/kg)	(g/kg)	(g/kg)	
Chloride ( $Cl^-$ )	19.25	1.09	12.54	11.0	
Sulphate ( $SO_4^{2-}$ )	2.71	20.87	9.41	10.95	
Magnesium ( $Mg^{2+}$ )	1.30	1.30	1.30	1.30	
Calcium ( $Ca^{2+}$ )	0.42	0.42	0.42	0.42	
Potassium ( $K^+$ )	0.39	0.39	0.39	0.39	
Sodium ( $Na^+$ )	10.71	10.71	10.71	10.71	
<b>Concentration (mg/l)</b>	<b>34.78</b>	<b>34.78</b>	<b>34.78</b>	<b>34.78</b>	

**Table 4.7 Composition of solutions**

Component	Solution 1	Solution 2	Solution 3	Solution 4
	SO <sub>4</sub> <sup>2-</sup> /Cl <sup>-</sup> =0.14	SO <sub>4</sub> <sup>2-</sup> /Cl <sup>-</sup> =19.15	SO <sub>4</sub> <sup>2-</sup> /Cl <sup>-</sup> =0.75	SO <sub>4</sub> <sup>2-</sup> /Cl <sup>-</sup> =0.99
NaCl (g)	24.70	-	5.08	15.29
HCl (ml)	1.40	-	4.70	0.65
CaCl <sub>2</sub> .6H <sub>2</sub> O (g)	1.14	2.29	1.16	1.16
MgSO <sub>4</sub> .7H <sub>2</sub> O (g)	6.89	12.87	-	13.21
MgCl <sub>2</sub> .6H <sub>2</sub> O (g)	5.18	-	10.87	-
H <sub>2</sub> SO <sub>4</sub> (ml)	-	15.57	9.61	5.93
NaHCO <sub>3</sub> (g)	3.58	38.35	31.77	17.16
KCl (g)	0.74	0.74	0.74	0.74

### 4.3 Electrochemical Tests

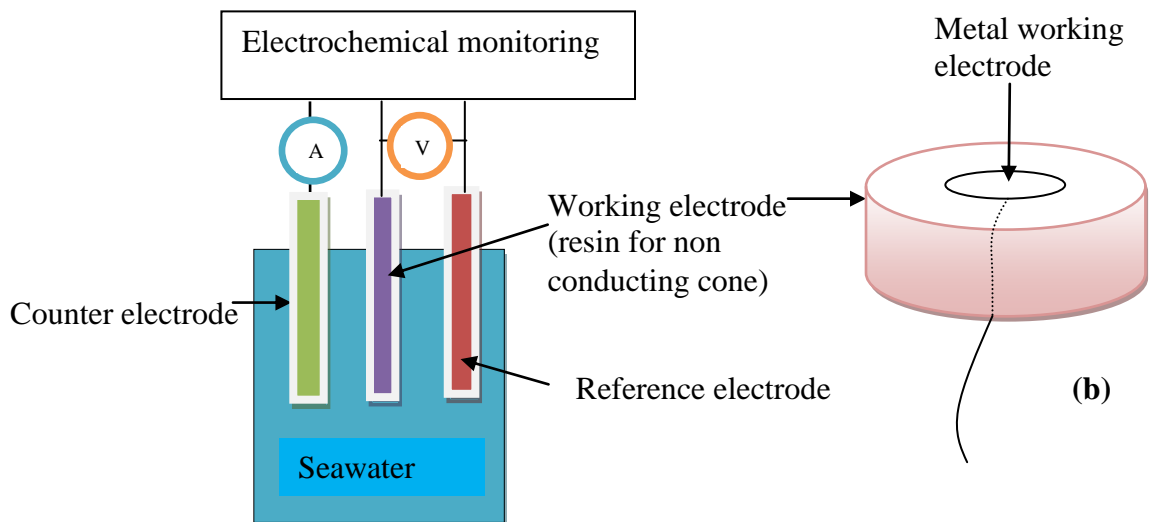
Linear polarisation tests were carried out for carbon steel, whereas cyclic potentiodynamic polarisation (CPP) tests were carried out for passive materials at four different temperatures (4°C, 20°C, 50°C and 80°C) in static conditions. Specimens with an electrical connecting wire were embedded in a non-conducting resin (Figure 4.1 (b)) and the exposed surface with known area was subsequently ground using SiC sandpaper and diamond polished to a 6-micron finish. The sample was held in each solution for 5min before starting the experiment to stabilize the surface.

This method makes use of a three-electrode electrochemical cell, as shown below. By using the cyclic polarisation test, the forward and reverse scan was plotted. The reference electrode used in all experiments is silver/saturated-silver-chloride (Ag/AgCl) half cell, the potential of which, versus normal hydrogen electrode (NHE), is +0.197 V. The working electrode is the sample and platinum is used as the counter electrode. This accelerated test method facilitates analysis of the kinetics of the corrosion reactions by controlling the potential between the reference and the working electrode and maintaining the current in the external cell between the counter and the working

electrode. The potential is controlled by a computer-controlled potentiostat (EG&G) and is shifted at a constant rate in the anodic direction from the open circuit potential (OCP), causing the working electrode to become the anode and causing electrons to be withdrawn from it. For linear polarisation, the measurement begins at approximately -20mV and scan in the positive direction to +20mV from OCP. The data are obtained from a linear plot of the potential versus current density graph. The slope of the graph was then calculated to obtain the corrosion rate by using the Stern and Geary equation.

For cyclic potentiodynamic polarisation (CPP) measurement, after the current density reaches a preset value of  $500\mu\text{A}/\text{cm}^2$ , the potential then gradually returns to the open circuit potential as shown in Figure 4.2. The breakdown potential,  $E_b$  (the least noble potential where corrosion will initiate and propagate) is then identified, which is the potential where the current increases with increasing potential.

The experiment was repeated in different solutions, with and without oxygen. To find the effect of oxygen, the solution was divided into oxygen saturated and non-oxygen saturated solutions. To get non-oxygen saturated, nitrogen was used to purge the oxygen in the solution until the solutions were almost at 0.04 ppb oxygen content. Then the electrochemical was run at  $4^\circ\text{C}$  and  $20^\circ\text{C}$ . At high temperature, it is difficult (could be say impossible) to control the oxygen content at 0.04 ppb. Therefore, the experimental was only focus at  $4^\circ\text{C}$  and  $20^\circ\text{C}$ . The oxygen level was measured by using portable dissolved oxygen meter.



(a) 3-Electrode electrochemical

**Figure 4.1 Experimental set up for static corrosion tests (a) 3-electrode electrochemical cell, (b) sample embedded in a non-conductive resin.**

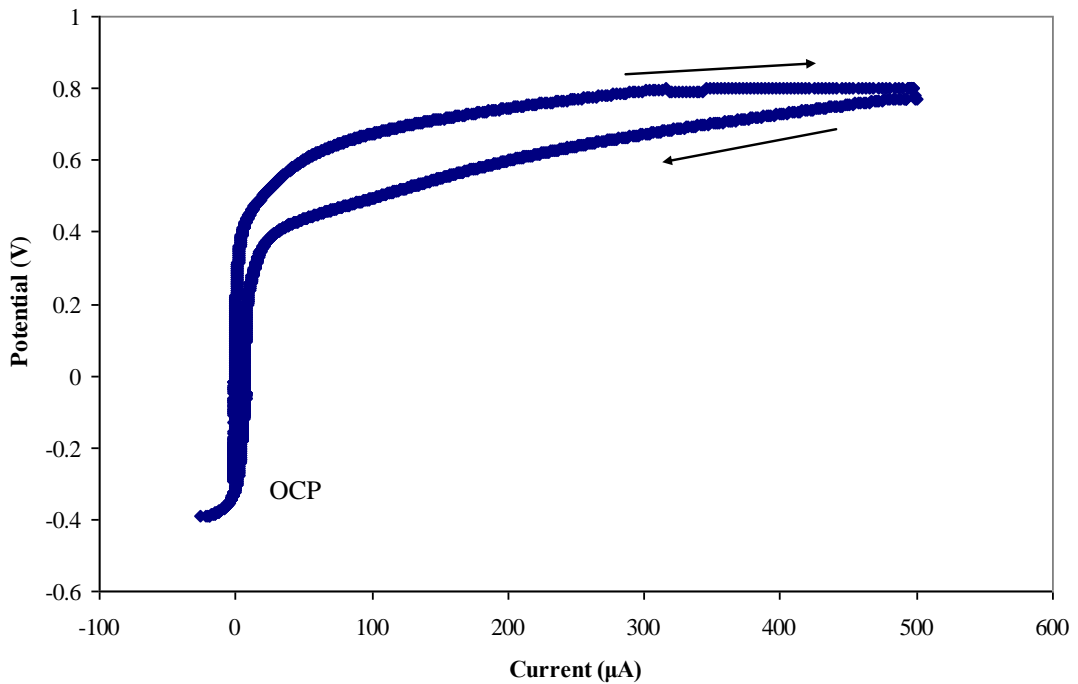


**Figure 4.2** Cyclic polarization curve

#### 4.4 Experimental Procedure

The computer-controlled potentiostat was used to conduct anodic and cathodic polarisation tests. These tests involved shifting the potential of the working electrode from the free corrosion potential,  $E_{corr}$  (also known as *OCP*) in the positive or negative potential direction. The potential-current ( $E-i$ ) relationship was then acquired from measuring the current between the working electrode and the counter electrode in the electrochemical cell.

For carbon steel, the linear polarization curve information was used in the formula to determine the corrosion rate. The Tafel constants,  $\beta_a$  and  $\beta_c$  generally used were 120 mV/decade. It is strongly agreed by Hinds that any values between 60 and 120 mV/decade, a maximum error of only 20% can be expected [126]. To be sure, this value was identified by the Tafel polarization run for carbon steels AISI 4140, AISI 1040 and AISI 8260. Figure 4.3 shows the values taken from the slope value of anodic and the value was assumed to be same for anodic curve as both polarisations are parallel. From the calculation, it is proved that the  $\beta_a$  is 120 mV/decade.

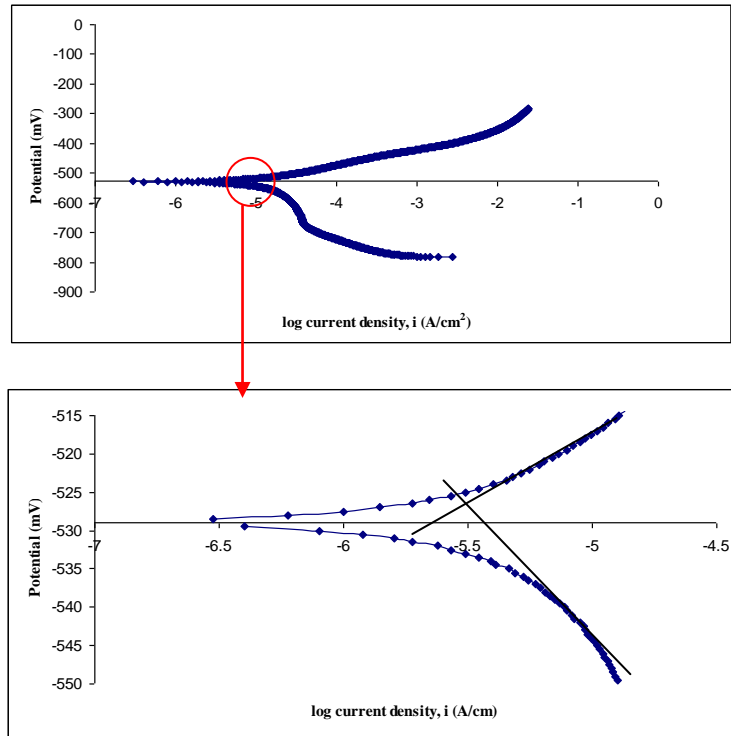


**Figure 4.3 Tafel polarization for carbon steels**

#### **4.4.1 Anodic and cathodic polarization curves**

For all materials, anodic polarisation is an accelerated technique to study the corrosion behaviour. This technique has been widely used to determine the resistance to passive breakdown due to pitting or crevice corrosion for passive materials and polarization resistance in the active region for carbon steels. A schematic anodic polarisation curve for a passive material is shown in Figure 4.4a. For passive materials, once the potential reaches the breakdown potential ( $E_b$ ) (at which the passive film breaks down), the current increases suddenly. With the absence of crevice corrosion, this potential is also referred to as the pitting potential. From an engineering point of view, the breakdown potential of the material provides information concerning the resistance of materials to passivity breakdown due to not only pitting corrosion but also crevice corrosion. Although the potential is reversed at  $i_{rev}$ , often the current does not reduce immediately and a maximum current density ( $i_{max}$ ) is attained, which gives an indication of the propensity for corrosion propagation to occur. An indication of the extent of propagation is, therefore, obtained by consideration of  $i_{max}$ .

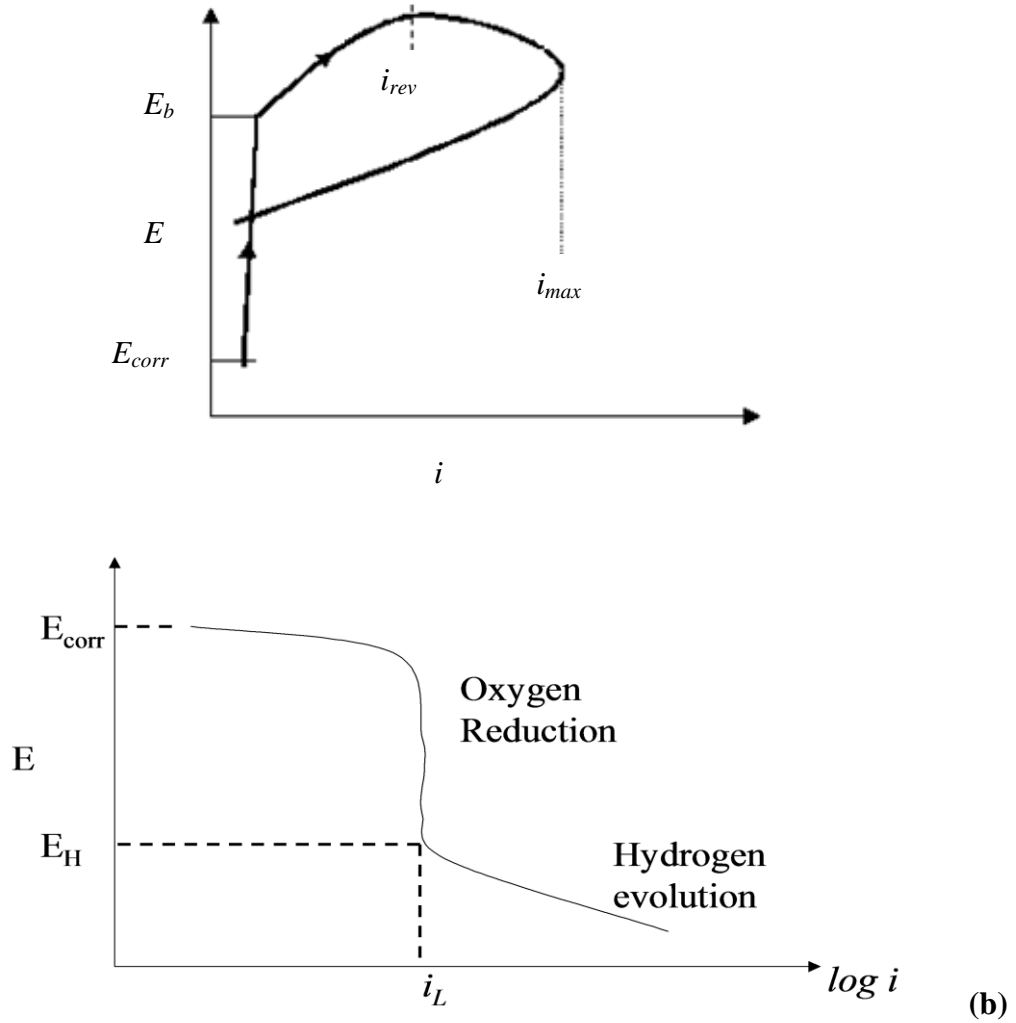


**Figure 4.4 Schematic (a) anodic polarisation curve (b) cathodic polarisation curve**

Figure 4.4b is schematically described the behaviour of cathodic polarisation. When the potential is scanned in the negative directive direction, the potential region from  $E_{corr}$  to  $E_H$ , represents the potential where the oxygen-reduction reaction dominates. The rate of reaction reaches a limiting current,  $i_L$ , which is diffusion controlled. In this regime the oxygen supply is depleted at the surface and the rate of reaction is controlled by the rate of arrival of oxygen at the surface. At a more negative potential than  $E_H$ , hydrogen-evolution becomes the dominating reaction. This will proceed according to a linear  $E$ - $\log i$  relationship.

## 4.5 Surface Analysis

The corrosion attack was viewed by an optical microscope. For a modern light microscope, the optical components are very complex and the whole optical path has to be very accurately set up and controlled. The probed region may be the extreme top layer of atoms, or it may extend up to several microns beneath the sample surface, depending on the technique used. From an engineering material's viewpoint, the impact of corrosion on a system is mostly a surface phenomenon, hence the scientists and engineers interested in fundamental corrosion processes have always been among the first to explore the utility of surface analysis techniques. In the following sections, the working principle of the surface analysis techniques used in this study are described.

### 4.5.1 Light microscopy

The light microscope used in this study was a NIKON standard binocular metallurgical microscope. The samples were cleaned and dried, placed in a holder and pressed to have a flat horizontal surface to use in the microscope. The objective lenses used were calibrated using a graticule and the individual magnification bar is shown in each photograph. A mounted camera on the microscope enabled the observations to be recorded.



**Figure 4.5 Light microscope**

#### 4.5.2 ESEM and EDAX

For electron microscopy, the Philips XL30 Environmental Scanning Electron Microscope (ESEM), as shown, was used to provide high-resolution secondary electron imaging and optimised X-ray analysis. In environmental mode the gaseous secondary electron detector can be used. In High Vacuum mode it offers superior performance for both imaging and X-ray analysis at all accelerating voltages on conventionally prepared specimens. The EDAX 'Phoenix' energy dispersive X-ray analysis system (EDX / EDS), with a UTW detector and LEAP+ technology was incorporated into the ESEM. All elements down to the atomic number of boron can be detected, including the light elements carbon, nitrogen and oxygen. Both qualitative and quantitative analysis is available, as well as the mapping of up to 15 elements at a time. EDX analysis is capable of producing high quality elemental data at a fast rate.

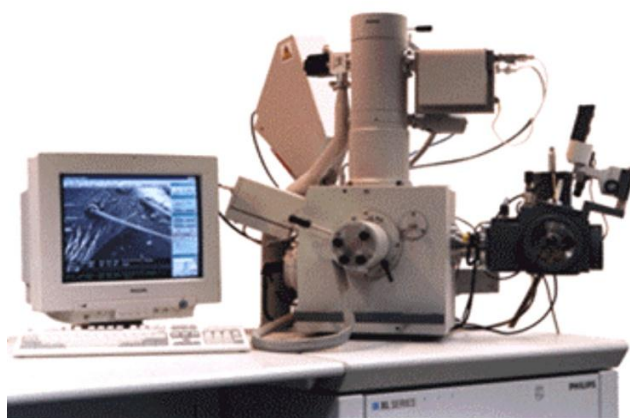


**Figure 4.6 Philips XL30 ESEM**



## Chapter 5

### SETTING THE SCENE FOR CARBONSTEELS

#### 5.1 Introduction

Carbon steels are characterised as actively corroding materials; they corrode at a relatively high rate in saline environments. Carbon steel can be divided into three groups which are **low** carbon steel, **medium** carbon steel and **high** carbon steel. Below 0.3% carbon content can be categorised as low carbon steel whereas between 0.3% to 0.6% are medium carbon steel and up to 0.95% are high carbon steel [77]. For this research, AISI 1040, AISI 8620 and AISI 4140 were chosen because they cover the different types of carbon steel and being used extensively in subsea applications. AISI 1040 is plain carbon steel without any alloying elements (except manganese, Mn not more than 1%) whereas AISI 4140 contains chromium (not more than 1%) and molybdenum (not more than 0.3%) as alloying elements. Both fall into the medium carbon steel category and it could be predicted that AISI 4140 is higher in strength compared to AISI 1040 because of alloying elements. AISI 8620 falls into the low category of carbon steel but contains nickel (0.55%), chromium (0.50%) and molybdenum (0.25%) as alloying elements [77]. Theoretically, AISI 8620 should have severe corrosion attack compared to AISI 1040 and AISI 4140 because it is low in chromium and carbon content (Figure 5.1). However, Melchers [127] in his research on the effect of carbon content of low alloy steels in marine immersion reveals that carbon content has a minimal effect on corrosion attack. For this current research and so no research was done on only one carbon steel; AISI 1040.

In this study, corrosion experiments were performed on metallographically prepared surfaces of carbon steel AISI 1040, AISI 4140 and AISI 8620 at four different temperatures: 4°C, 20°C, 50°C and 80°C. After several experiments, all carbon steels were shown to a similar trend. All of them show a lower corrosion rate in 3.5% NaCl and higher corrosion rate in seawater (solution 1). One carbon steel was then used for further experiments (in different sulphate-chloride ratio and the effect of oxygen on carbon steel), AISI 1040. The composition of solution 1 will be discussed later.

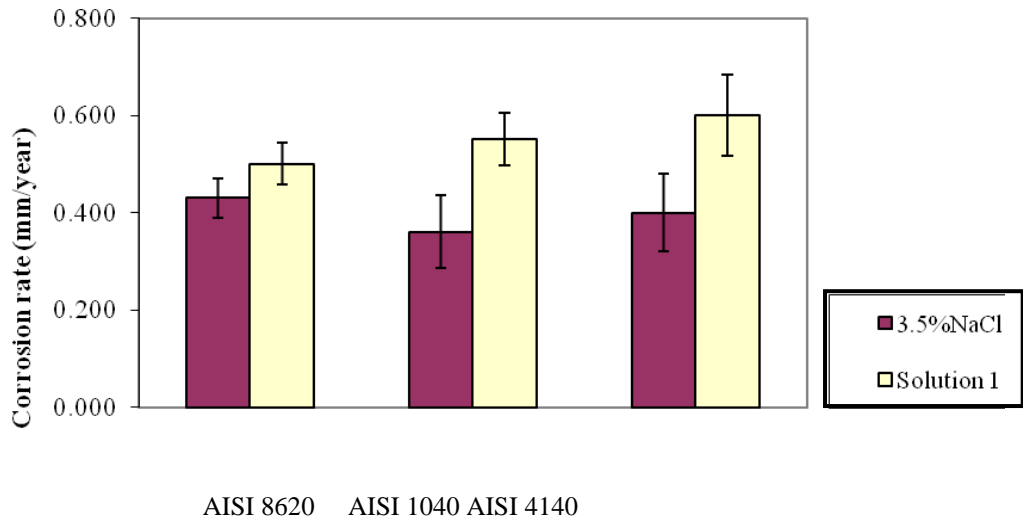


**Figure 5.1 Corrosion rate of AISI 1040 in different ‘seawaters’ (electrolytes) at 20°C**

For assessing the corrosion behaviour of carbon steels, linear polarization tests (Figure 5.2) were performed using four types of electrolyte to obtain the polarization resistance ( $R_p$ ) of carbon steel. The preparation of these electrolytes was described in Chapter 4 and they are labelled as solutions 1 ( $\text{SO}_4^{2-}/\text{Cl}^- = 0.14$ ), 2 ( $\text{SO}_4^{2-}/\text{Cl}^- = 19.15$ ), 3 ( $\text{SO}_4^{2-}/\text{Cl}^- = 0.75$ ) and 4 ( $\text{SO}_4^{2-}/\text{Cl}^- = 0.99$ ). Solution 1 (S1) consists of six major elements, similar to real seawater. Besides using these four solutions, the materials were also tested in 3.5% NaCl and commercial hydraulic fluid HW443. HW443 is the commercial hydraulic fluid and is the reference against which the materials in seawater will be compared. These preliminary experiments were run to find the sensitivity of corrosion to the electrolyte. The S1, S2, S3 and S4 solutions were also used for passive and cermets alloy materials for which the results are presented in Chapters 6 and 7.

## 5.2 Determination of the Corrosion Rate

For linear polarisation, the measurement scan range was -20mV to +20mV from OCP. The data were plotted on a linear scale as potential versus current density graphs. The slope was then calculated to obtain the Polarisation Resistance ( $R_p$ ) and the corrosion rate by using the Stern and Geary equation [22]. For example, Figure 5.2 represents Polarisation Resistance ( $R_p$ ) of carbon steel using a 0.25mV/sec scan rate. The linear slope obtained was  $837 \Omega \cdot \text{cm}^{-2}$ , which is referred to as the

polarisation resistance,  $R_p$ . This value was then substituted in the equation below to determine  $i_{corr}$ :

$$\begin{aligned}
 i_{corr} &= \frac{1}{2.303 R_p} \left[ \frac{\beta_a \times \beta_c}{\beta_a + \beta_c} \right] \\
 &= \frac{1}{2.303(837.37 \Omega cm^{-a})} \left[ \frac{0.12 \times 0.12}{0.12 + 0.12} \right] \\
 &= 3.105 \times 10^{-5} (A / cm^2)
 \end{aligned}
 \tag{5.1}$$

The value used for  $\beta_a$  and  $\beta_c$  is 120mV/decade. This is the value used by most researchers for carbon steel and the value was validated as shown in Figure 4.3. By using the  $i_{corr}$ , the corrosion rate in mm/year can be determined using the equation:

$$Corrosion\ rate = \left[ \left( \frac{i_{corr}}{nF} \right) \times \frac{molecular\ weight}{density} \right]
 \tag{5.2}$$

Where n= number of atoms

F= Faraday's constant = 96,500 coulombs/mole

$$\begin{aligned}
 Thus\ corrosion\ rate &= \frac{2.74 \frac{\mu A}{cm^2}}{2 \times 96500 \frac{C}{mole}} \times \frac{55.65 \frac{g}{mole}}{7.8 \frac{g}{cm^3}} \\
 &= 1.012 \times 10^{-10} cm/sec \\
 &= 0.32 mm/year
 \end{aligned}$$

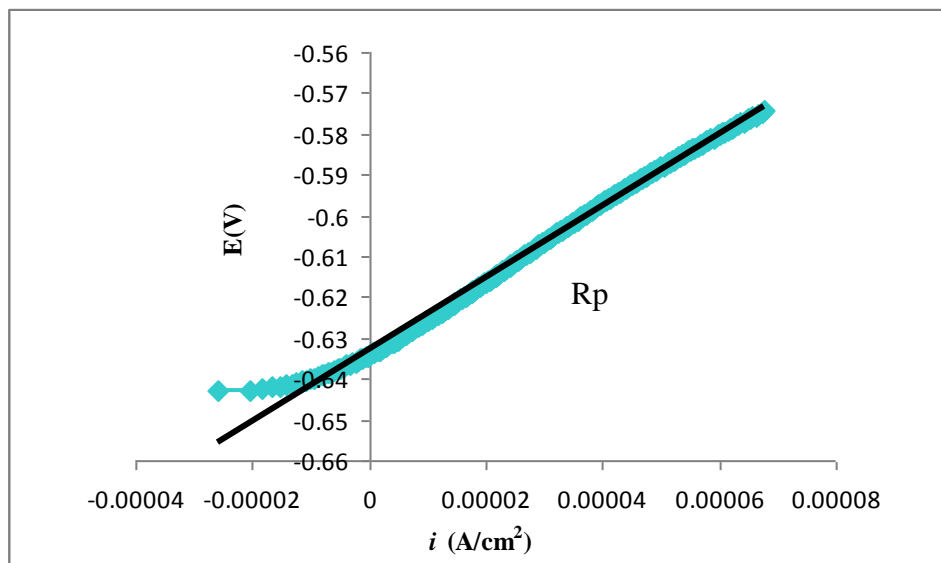


**Figure 5.2** Linear polarisation for carbon steel

### 5.3 Benchmarking

In order for any solution to be substituted as a hydraulic fluid, an acceptable corrosion rate needs to be established. In this study, HW443 is used as the benchmark. According to a previous study by Zheng [12], who studied the effectiveness of five different hydraulic fluids on corrosion attack to 316L and cermet alloys, it was found that some hydraulic fluids are better than others within certain parameters. However, HW443 shows better corrosion resistance for cermet alloys and 316L. The study also depicted that potential breakdown  $E_b$  decreased at elevated temperatures in HW443 while other hydraulic fluids showed no significant decrease in  $E_b$  at various temperatures. He also detected that HW443 contained about 20% by weight of water of 2-Dimethylamino-2-methyl-1-propanol (*DMAMP*), which is a vapour phase corrosion inhibitor. Another substance found was Tri-n-octyl phosphate (*TOP*), which can form stable hydrophobic complexes with some metals and is soluble in organic solvents as well as supercritical  $\text{CO}_2$ . *TOP* was detected in HW443 found to be the antifreezing component.

Since the corrosion rate for all carbon steels was similar, the tests reported from this point onwards in the thesis only concentrate on factors that affect the corrosion rate, not the corrosion rates of different types of carbon steel. Figure 5.3 shows the corrosion rate of carbon steel in hydraulic fluid HW443 and distilled water at different temperatures. The distilled water shows a lower corrosion rate compared to HW443 for every temperature as expected. The results are presented as an average of three tests. The “acceptable” corrosion rate will be determined according to the HW443 reference. Since that is the fluid currently used and for which control of corrosion is advised.

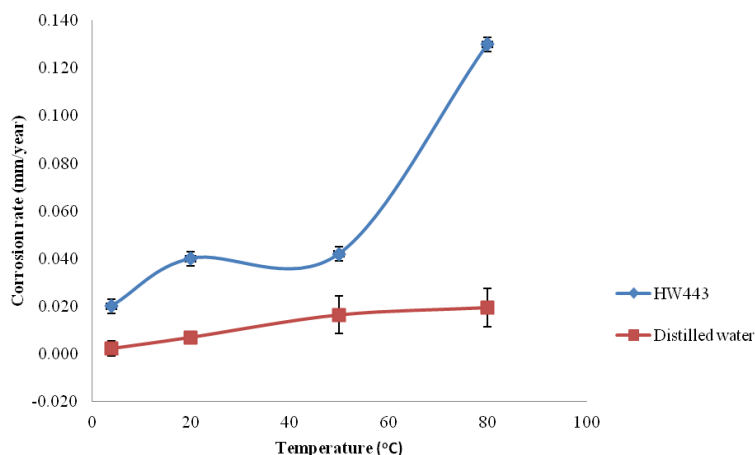


**Figure 5.3 Comparison of the corrosion rate of AISI 1040 in HW443 hydraulic fluid and distilled water as a function of temperature.**

## 5.4 Corrosion Rate in 3.5% NaCl and Other Solutions

Figure 5.4 (a) shows AISI 1040 in 3.5% NaCl at different temperatures. The curve obtained reveals that the corrosion rate increased with increasing temperature as expected. The effect of temperature on corrosion is discussed in Chapter 8. The corrosion rate increased by around 48% from 4°C to 20°C and significantly increased by 67% from 20°C to 50°C and 56% from 50°C to 80°C. The corrosion rates were also measured for other carbon steels and the trends are parallel (Figure 5.4 (b)).

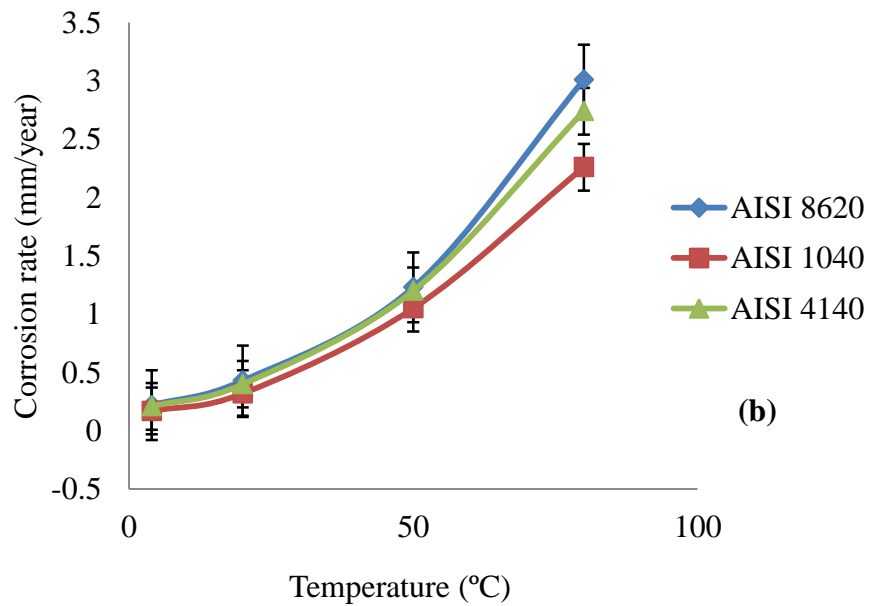
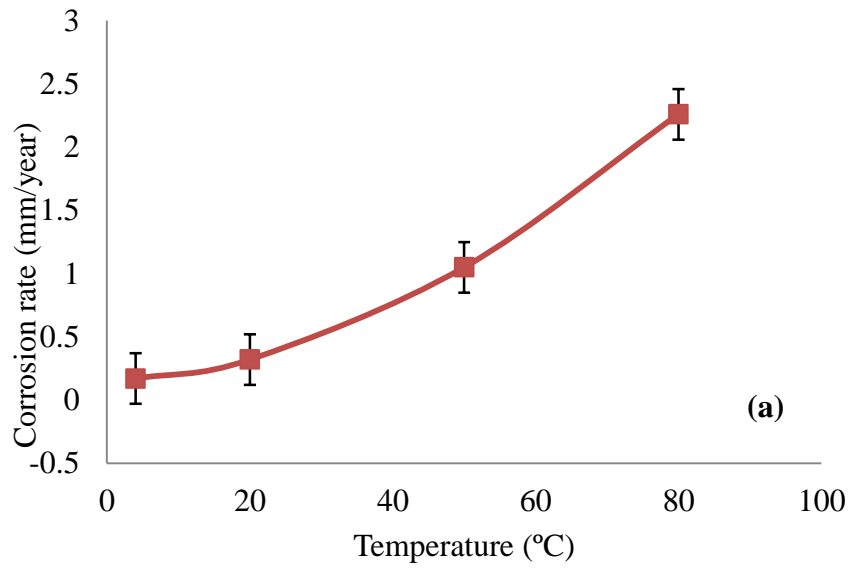


**Figure 5.4 Corrosion rate of (a) AISI 1040 in 3.5% NaCl as a function of temperature and (b) comparison AISI 8620, AISI 1040 and AISI 4140 in 3.5% NaCl as a function of temperature**

## 5.5 Immersion Tests

Figure 5.5 displays the immersion test for carbon steel in 3.5% NaCl for several hours at 20°C. This experiment was tested to three types of carbon steel to find out the effect of immersion to carbon steels. It can be concluded that the corrosion rate drastically decreased for all carbon steels once they were immersed in 3.5% NaCl for four hours. However, after four hours, the corrosion product seems stabilised on carbon steels and retards further corrosion attack. This result also shows that the corrosion rate was comparable to the measured corrosion rates from LPR as presented previously in Figure 5.1 and Figure 5.4(b).

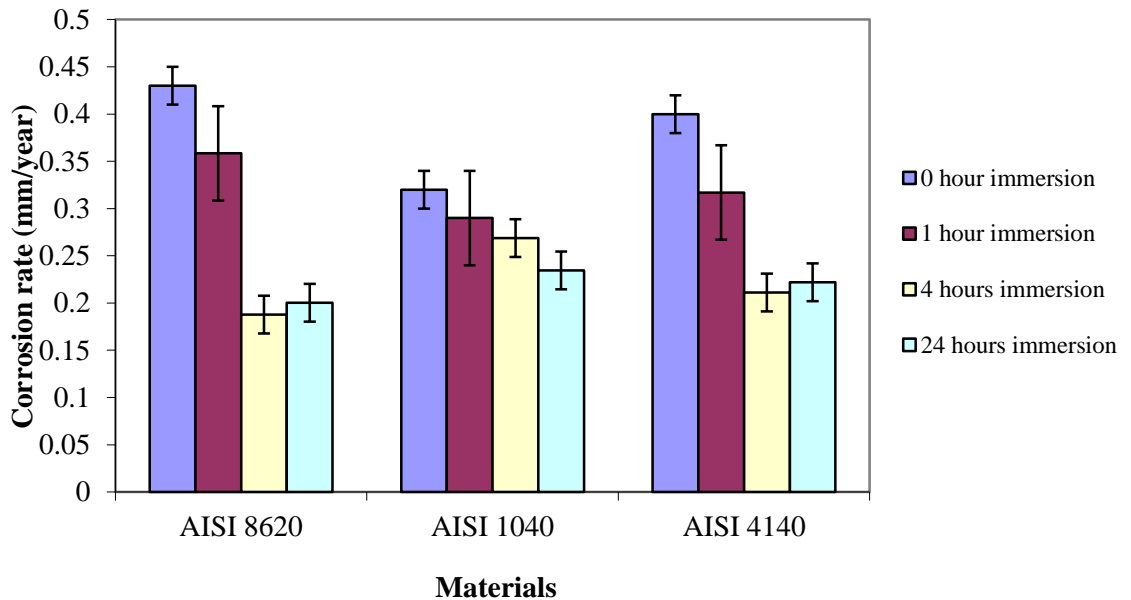
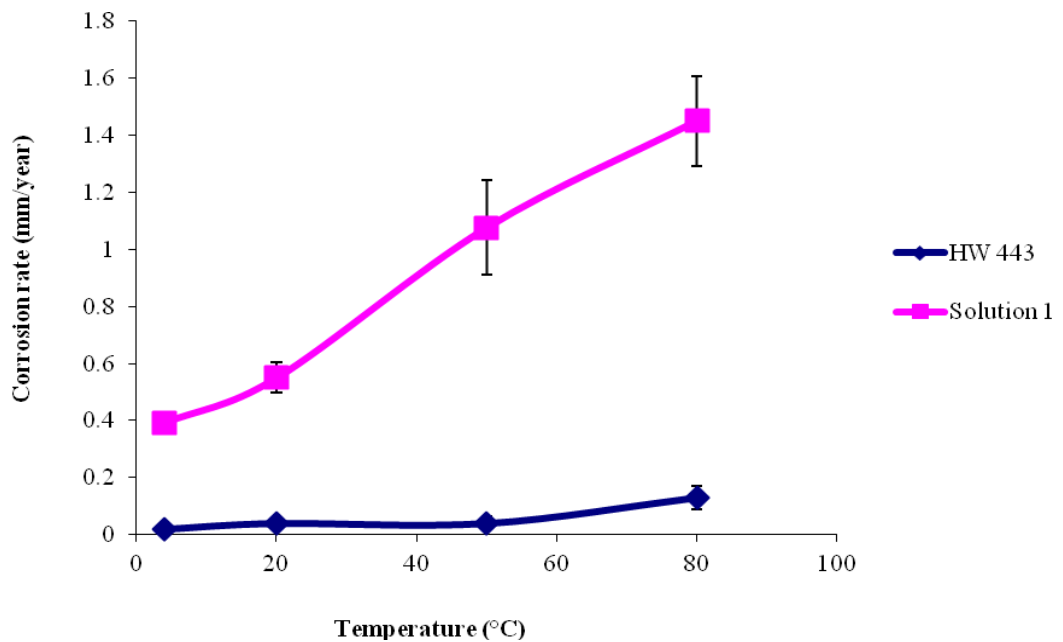


Figure 5.5 Carbon steel in immersion test at 20°C

## 5.6 Carbon Steels in Different Sulphate to Chloride Ratios

Chapter 3 explained that some aggressive anions in seawater could increase the corrosion rate and some could protect the metal and retard corrosion attack. But, none of the previous researchers have studied the effect of aggressive anions on corrosion based on the actual composition of seawater been studied. Szklarska-Smialowska [130], only added sulphuric acid ( $H_2SO_4$ ) with sodium chloride (NaCl) to obtain  $Cl^-/SO_4^{2-}$  ratio in his study about the kinetics of pit growth on nickel. For this research, the sulphate to chloride ratio was varied but other anions in seawater remain the same to maintain the

salinity as natural seawater and will concentrate on the corrosion rate for AISI 1040. Seawater with the same composition as natural seawater was synthesised and labelled as Solution 1 (S1). Figure 5.6 displays the corrosion rate of AISI 1040 in HW443 compared to solution 1 at 20°C. Similar to other media, the corrosion rate increased as the temperature increased. However, AISI 1040 shows a drastic increase after 20°C in solution 1 (artificial seawater) and it is a big challenge to reduce the corrosion rate to an “acceptable” corrosion rate (HW443). At 20°C, the corrosion rate for carbon steel in S1 (seawater) is fourteen times higher than corrosion rate in HW443 since there are no chemical additives to inhibit the corrosion attack. Furthermore, the difference in corrosion rates is increased at 50°C and is about 27 times higher compared to carbon steel in HW443. This shows that, using carbon steel in seawater without any corrosion control or water treatment is impossible as anticipated. As such the corrosion will have to be controlled by controlling the corrosion parameters (anions and oxygen concentrations in seawater) or addition of some appropriate inhibitor.



**Figure 5.6 AISI 1040 in HW443 and solution 1 for all temperatures**

From solution 1 or seawater composition, another three solutions were prepared with different ratios of sulphate and chloride. The amounts of sulphate and chloride are listed in Table 5.1 and all the pH values for the solutions are within the range 7.0 to 8.0. It is to be noted that solution 2 has the highest sulphate-chloride ratio that is permissible

to use. This is because the amount of chloride has to be reduced to obtain a salinity of 3.5%, which could affect the entire composition of all the other elements that chemically exist with chloride. For example, increasing the magnesium chloride will affect calcium chloride. However, we have to limit the usage of  $Mg^{2+}$  to 1.30 g/kg and  $Ca^{2+}$  to 0.42 g/kg only (refer to Table 4.6). The calculation for these solutions was presented in Chapter 4.

**Table 5.1 Sulphate and chloride for all solutions**

<b>Solution</b>	<b>1</b>	<b>2</b>	<b>3</b>	<b>4</b>
Sulphate (g/L)	2.71	20.87	9.41	10.95
Chloride (g/L)	19.25	1.09	12.54	11.0
<b>SO<sub>4</sub><sup>2-</sup>/Cl<sup>-</sup> ratio (g/L)</b>	<b>0.14</b>	<b>19.15</b>	<b>0.75</b>	<b>0.99</b>

Figure 5.7 shows the comparison of carbon steel AISI 1040 in 3.5% NaCl and seawater with different sulphate to chloride ( $SO_4^{2-}/Cl^-$ ) ratio, which are solutions 1 to 4 with the ratios indicated in Table 5.1. There is significant effect of corrosion rate as the temperature increased. Increasing the temperature increased the corrosion rate of AISI 1040 in all solutions. At 4°C and 20°C, there are all fairly similar in the corrosion rate. However, at 50°C and 80°C, the lowest corrosion rate occurs in solution 2, which is shown to be considerably lower than solution 1. Solution 2 has the highest  $SO_4^{2-}/Cl^-$  ratio compared to other solutions. This could be because sulphate improves the corrosion resistance when it exceeds the amount of chloride in the solution and indicates that by altering the  $SO_4^{2-}/Cl^-$  ratio, the corrosion rate could be reduced. However, it is still higher compared to the acceptable corrosion rate demonstrated by carbon steel in HW443 (Figure 5.3).



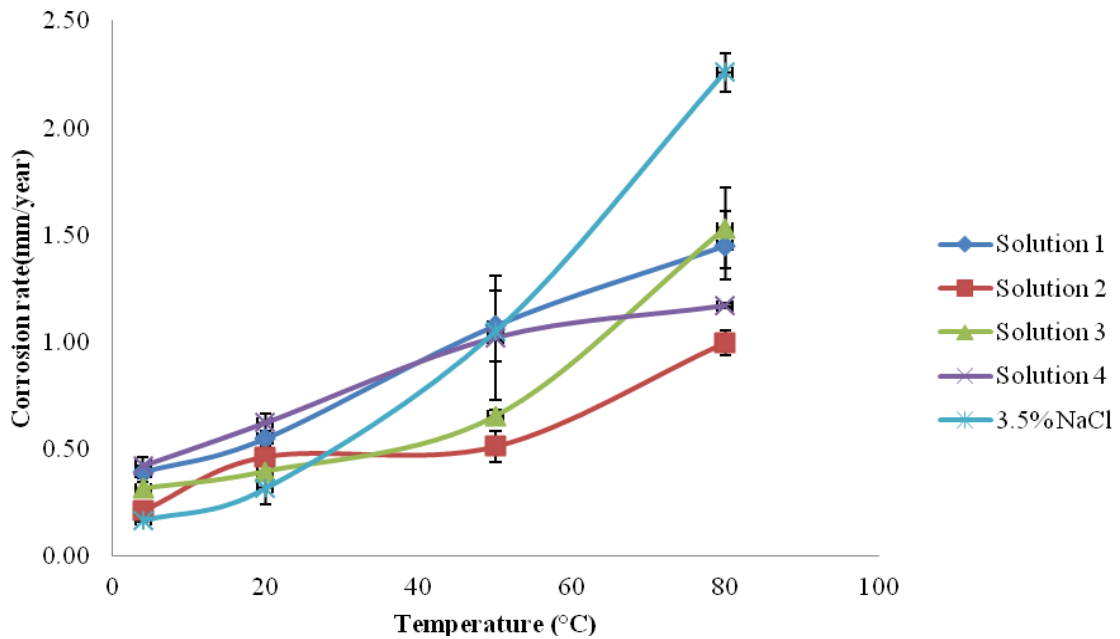
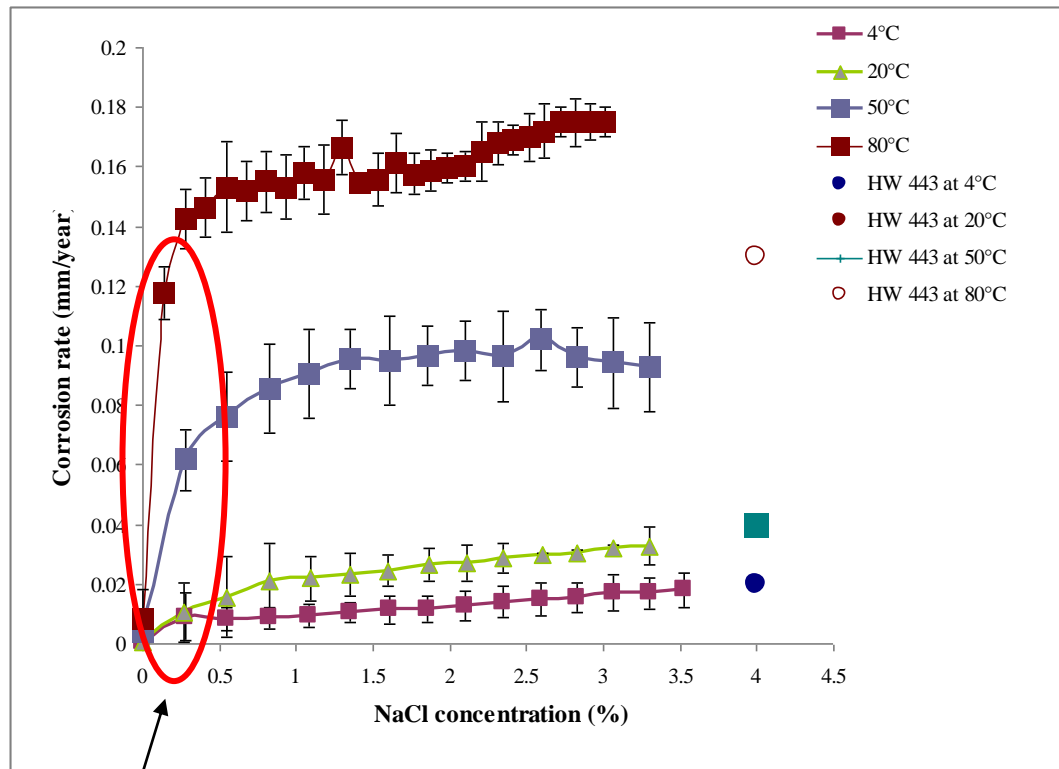


**Figure 5.7 AISI 1040 in 3.5% NaCl and different sulphate to chloride ratios**

### **5.7 The Critical Chloride Concentration**

Since chloride could accelerate the corrosion, the amount of chloride concentration was identified by testing the carbon steels in increasing chloride concentrations in oxygen saturated medium. This experiment was to identify the critical chloride concentration in the absence of other elements. Figure 5.8 clearly demonstrates that the corrosion rate increases as the temperature and chloride concentration increase (as shown in the red ellipse). This region identifies the critical chloride concentration because the corrosion rate increases drastically and remains stable after this region.

From Figure 5.8, the critical chloride concentration can be identified as suddenly increasing, which is shown by the red ellipse. The critical chloride concentration as identified regardless the value at 80°C. This is because the “acceptable” corrosion rate identified in HW443 at 20°C is 0.04 mm/year (Figure 5.6). Since the corrosion rate at 80°C is 0.12 mm/year, only the curve at 4°C, 20°C and 50°C will be considered.



The critical chloride area

**Figure 5.8 Carbon steel in increasing chloride concentration**

This critical area was then plotted and compared to the corrosion rate obtained in the hydraulic fluid HW443. The red marked area was enlarged and shown in Figure 5.9(a). From the value of “acceptable” corrosion rate, which is 0.04 mm/year, the critical chloride was identified from this identical line (Figure 5.9 (b)). Then, the critical chloride concentration identified is 0.05 g/L. The next step is to identify the critical oxygen concentration when chloride concentration is 0.05 g/L.

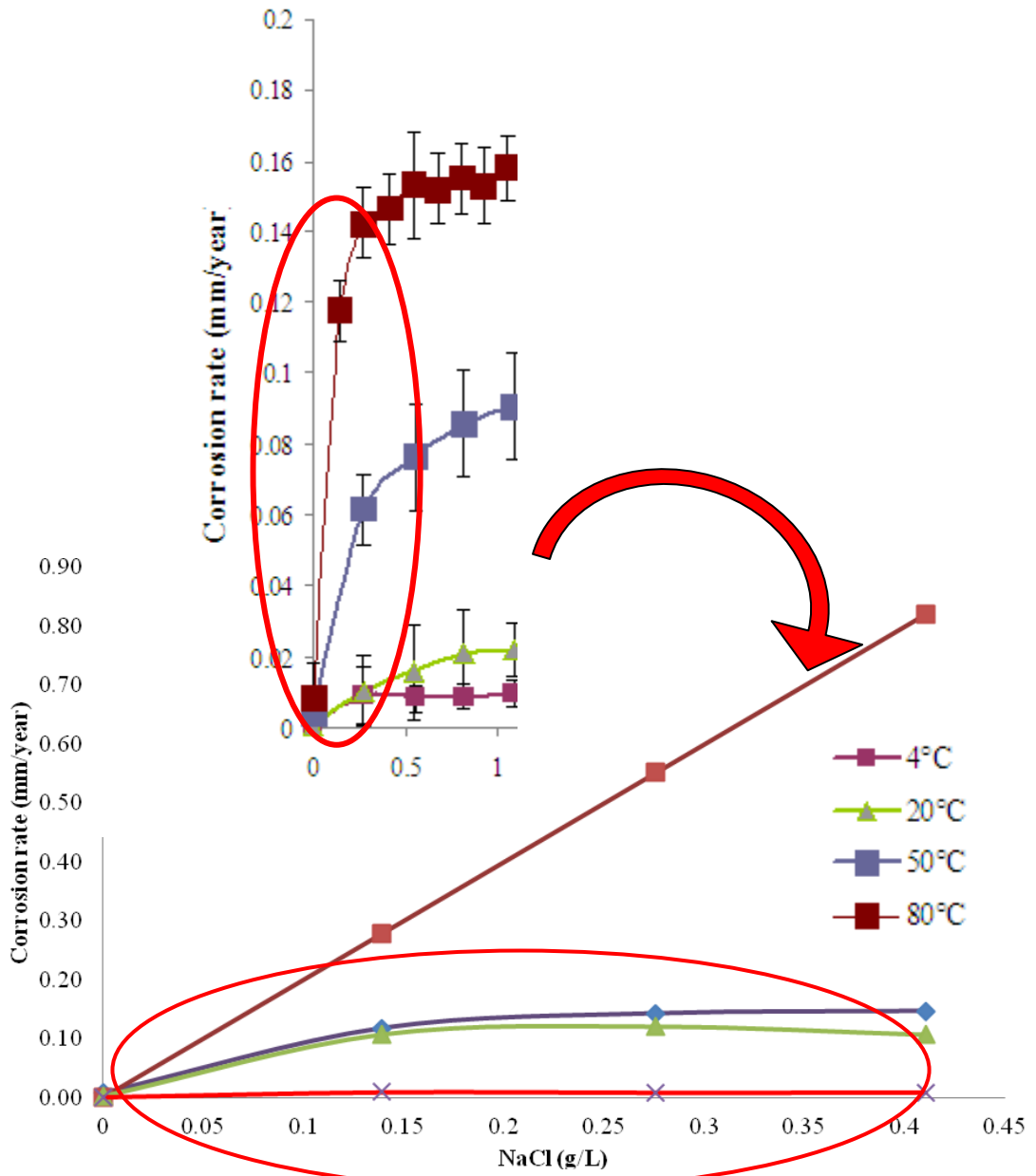
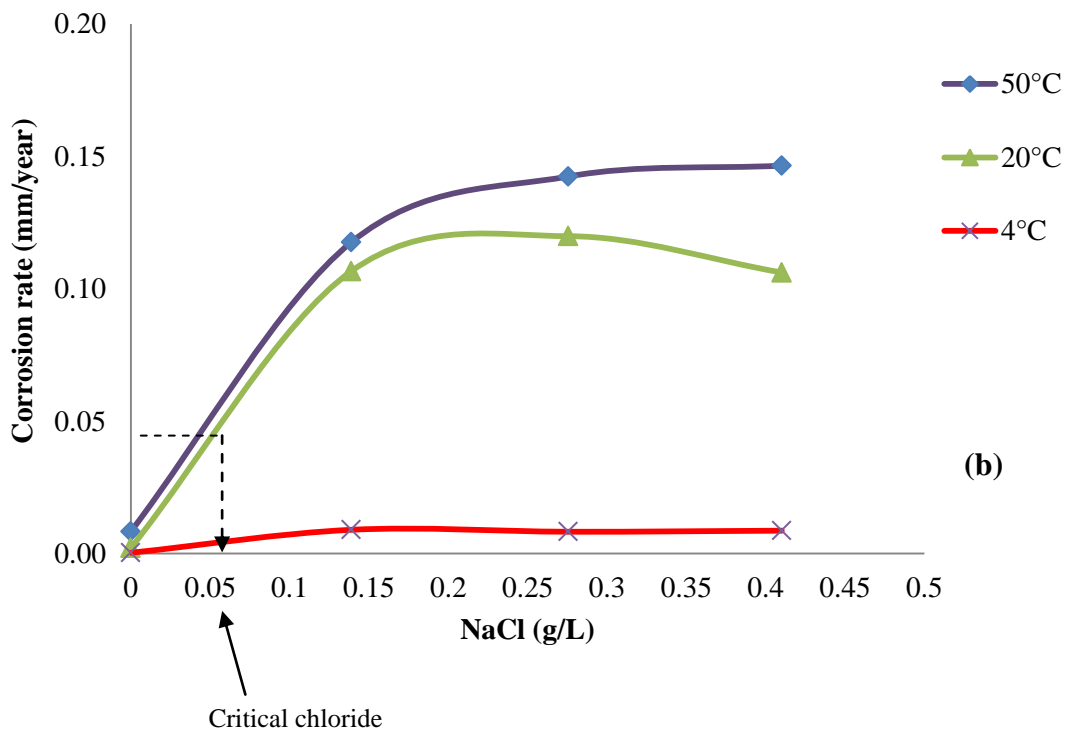


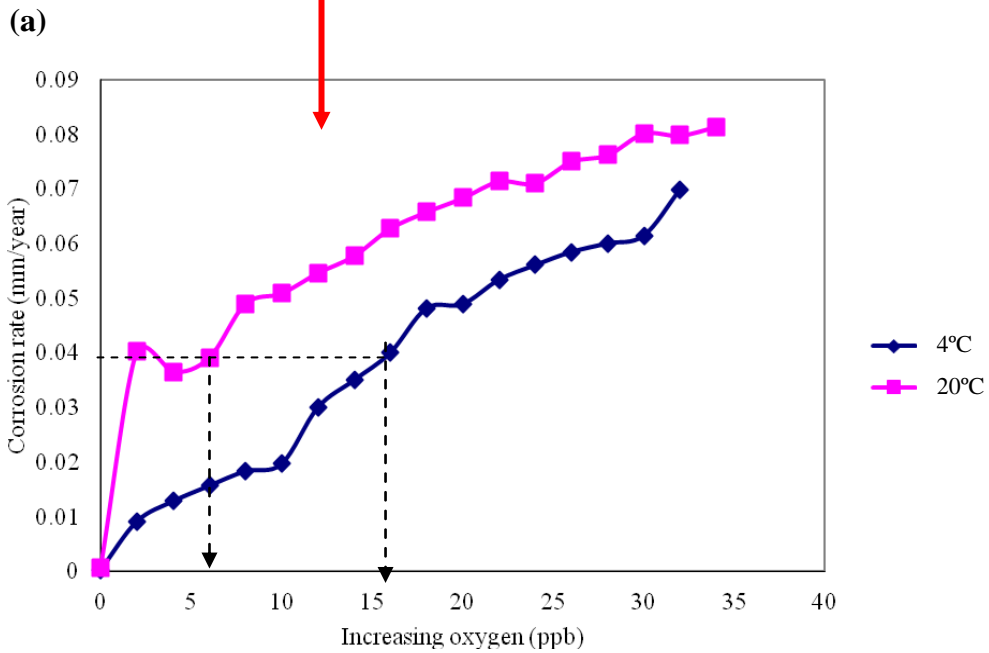
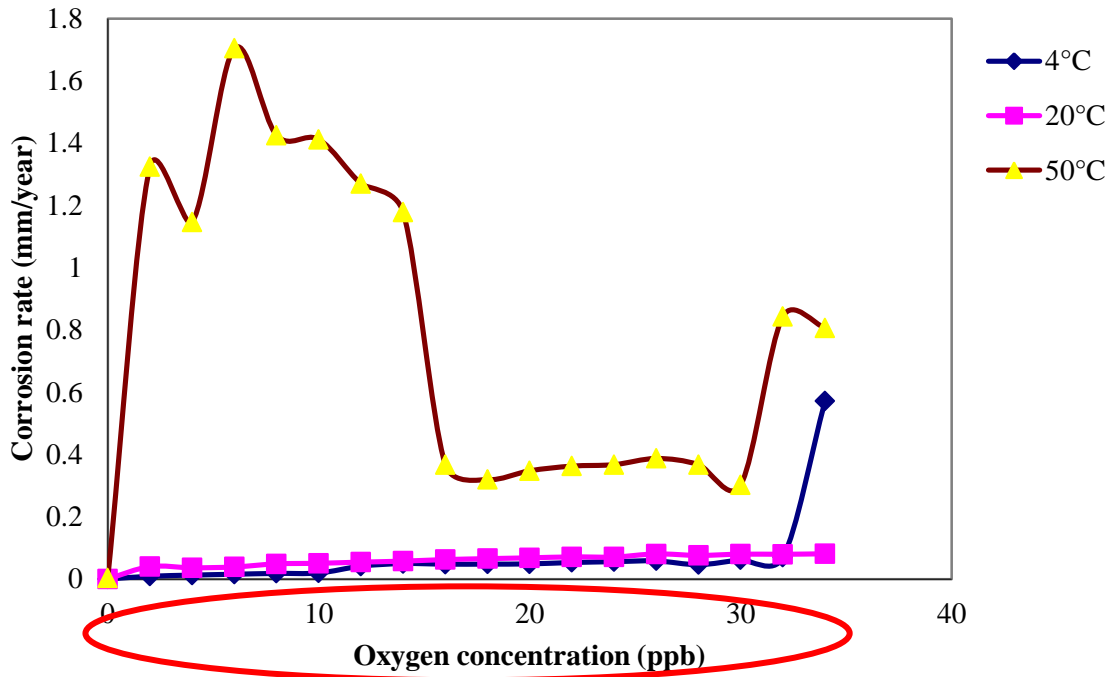
Figure 5.9 (a)



**Figure 5.9** To determine the critical chloride concentration in 3.5% NaCl at 20°C.(a) The graph was enlarge and eliminate the curve at 80°C (b) The “acceptable” corrosion rate (corrosion rate of AISI 1040 in HW443): 4°C=0.02mm/year, 20°C=0.04mm/year, 50°C=0.04mm/year and 80°C=0.13 mm/year

## 5.8 Critical Oxygen

The critical oxygen concentration was then identified by keeping the amount of NaCl at 0.05 g/L and increasing the oxygen content in the solution. In 0.05g/L of NaCl, oxygen was purged out by introducing nitrogen gas into the solution. This process was only run at 4°C, 20°C and 50°C because at 80°C, the oxygen content was very difficult to control. Figure 5.10 (a) presents the corrosion rate of AISI 1040 in 0.05 g/L NaCl as a function of oxygen concentration. However, it was detected that the corrosion rate is not significant at 50°C and several results show fluctuating values of corrosion rate. Therefore, the curve for 50°C was eliminated leaving the data at 4°C and 20°C. These two plots were enlarged and shown in Figure 5.10 (b).



**(a)** The corrosion rates of AISI 1040 as a function of oxygen concentration at 4°C, 20°C and 50°C **(b)** eliminating 50°C data and the critical oxygen concentration was identified

Since the corrosion rate in HW443 is 0.04 mm/year at 20°C, this value is plotted and the critical oxygen concentration identified (Figure 5.10 (b)). From the graph, the

value of critical oxygen concentration can be concluded to be approximately 6 ppb at 20°C and 16 ppb at 4°C. This is a useful information if the solution oxygen content can be managed, the corrosion attack can be controlled by treating the seawater. By using the target value, corrosion control can be managed by desalination and removal of oxygen in seawater.

## 5.9 Carbon Steel with Inhibitor

Apart from studying the effect of sulphate-chloride ratio and oxygen content to reduce the corrosion attack, the effect of the inhibitor was also studied. The AISI 1040 was studied in solution 1 with the addition of CRW 85155 (usually used in deaerated waters) and CRW 89000 (inhibitor for oxygen saturated conditions).

Figure 5.11 reveals the difference in the corrosion rate for carbon steel in solution 1 added with CRW 85155 inhibitor at increasing concentrations compared to HW443 at 20°C. The corrosion rate decreased by around 71% when CRW 85155 was added.

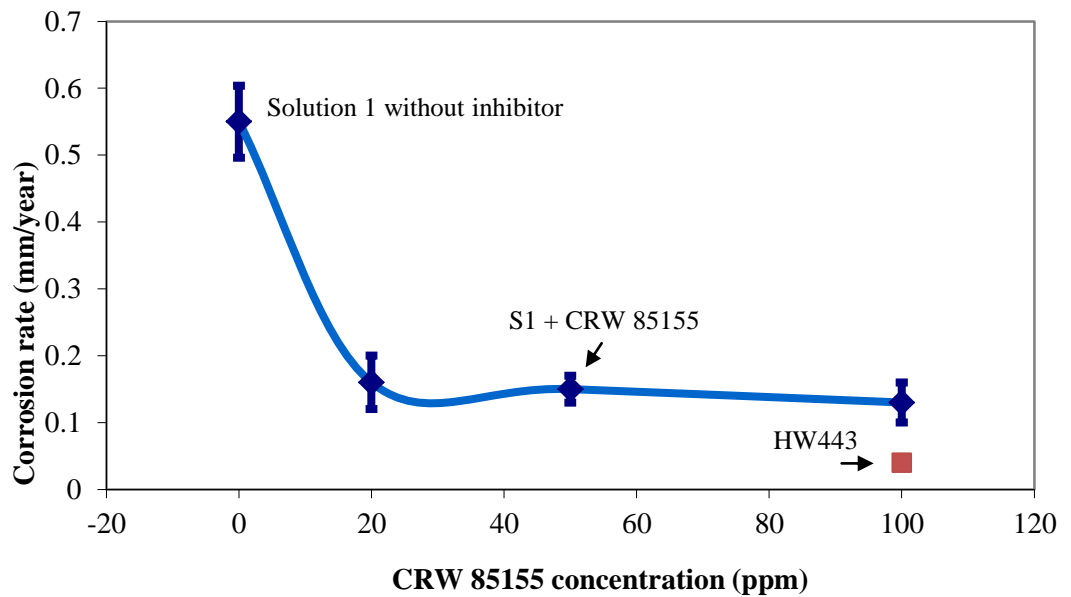


**Figure 5.11 Comparison of corrosion rate of AISI 1040 in solution 1 with CRW 85155 inhibitor added and hydraulic fluid HW443 at 20°C**

Therefore, it shows that there is a significant difference when inhibitor CRW 85155 is used. However, the efficiency of the inhibitor still low as compared to corrosion rate in HW443 when the concentrations of CRW 85155 used was 100ppm. This reveals that CRW 85155 is not the best choice for use. Furthermore, it can be seen

in Figure 5.11 that from 20ppm to 100ppm CRW 85155, the corrosion rate only decreased by around 18%.

The comparison foreach temperature is shown in Figure 5.12 (a) as compared to corrosion rate of AISI 1040 in hydraulic fluid HW443 (Figure 5.12(b)). From 20°C to 80°C, the corrosion rate does not decrease further even when the concentration of the inhibitor was increased. In addition, at 80°C the corrosion rate of AISI 1040 in HW443 is much lower than AISI 1040 in seawater added with 100 ppm CRW 85155.

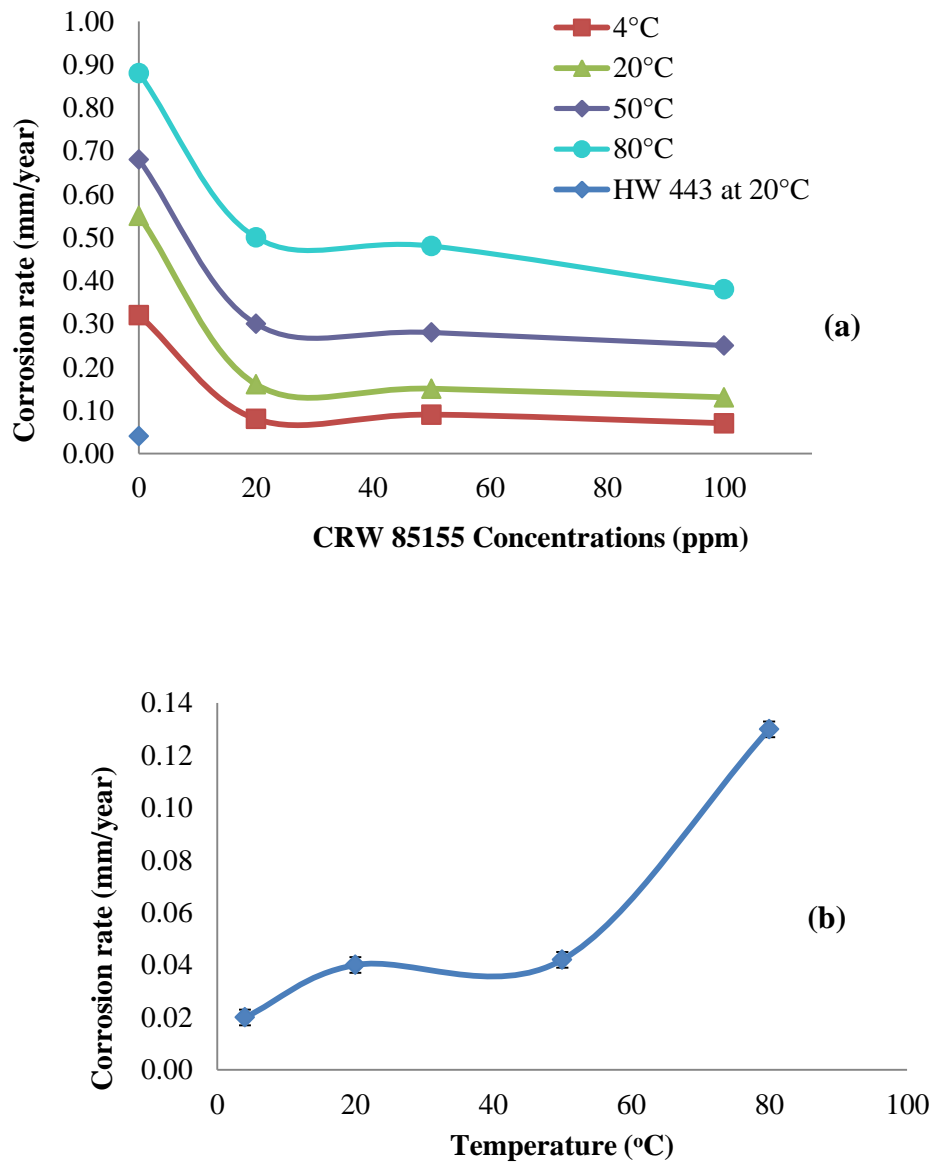


**Figure 5.12**The corrosion rate of AISI 1040 (a) at different temperatures with increasing concentrations of CRW 85155 (b) The “acceptable” corrosion rate

Surface adsorption to a solid can be categorized into two broad categories; physisorption and chemisorption. Physisorption is non-specific loose binding of the adsorbate to the solid via van der Waals type interaction which includes multilayered adsorption. However, chemisorption involves chemical reaction by monolayer. The inhibition effect of CRW 85155 on carbon steel property is attributed of molecular structure of the inhibitor's organic compounds to the carbon steel surface. This chemisorption is an important feature to determine the absorption of molecules on the metallic surface. They can absorb on the metal surface by blocking the active sites on the surface and thereby reducing the corrosion rate. From anodic polarization, the percentage protection efficiency (%P) is given by the equation below and the data is summarised in Table 5.2.;

$$\%P = \theta \times 100 \quad \text{where} \quad \theta = \frac{[i_{corr(uninhibited)} - i_{corr(inhibited)}]}{i_{corr(uninhibited)}} \quad [128] \quad 5.1$$

According to Christov and Popova [129], the mechanism of corrosion inhibitor is dependent on the metal, the medium and the structure of the inhibitor. This possible mechanism is the adsorption of the inhibitor by blocking the metal surface and this prevents the corrosion process from taking place. When this sole mechanism is considered, it is possible to develop adsorption isotherm data by using corrosion rate. The percentage of protection efficiency was plotted as a function of temperature in Figure 5.13. The curve depicted the protection efficiency decrease as the temperature increased and increased as the inhibitor concentration was increased.

**Table 5.2 Corrosion rates and % Protection efficiency of AISI 1040**

Medium	Temperature (°C)	Corrosion rate, mm/year (% Protection efficiency)			
		Inhibitor concentration			
		0 ppm	20 ppm (%)	50 ppm (%)	100 ppm (%)
S1	4	0.32	0.08 (61.5)	0.09 (72.2)	0.07 (83.1)
	20	0.55	0.16 (52.5)	0.15 (68.4)	0.13 (78.4)
	50	0.68	0.30 (34.2)	0.28 (52.6)	0.25 (64.5)
	80	0.88	0.50 (16.9)	0.48 (48.2)	0.38 (51.1)



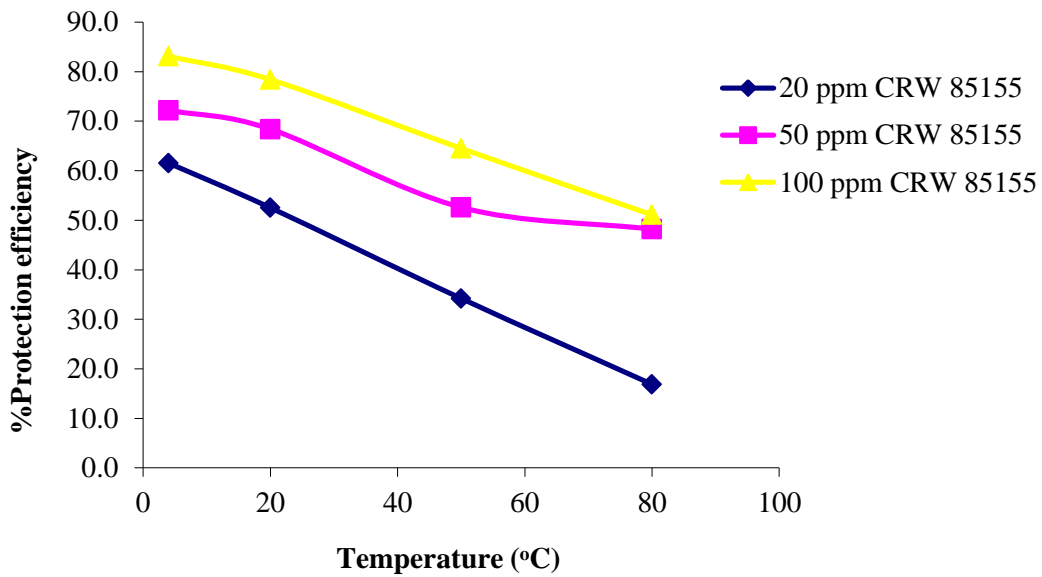


**Figure 5.13 Percentage protection efficiency of CRW 85155 on AISI 1040 at different temperatures**

The adsorption of organic inhibitors can be described by chemisorptions types of interaction. This involves charge-sharing or charge-transfer from the inhibitor molecules to the metal surface to form a coordinate type of a bond [194]. Adsorption of inhibitor molecules occur because the interaction energy between inhibitor molecules and the metal surface is higher than that between water molecules and the metal surface. Therefore, the inhibition effect by inhibitor molecules is attributed to the adsorption of inhibitors molecules through its functional groups onto the metal surface. Rapid adsorption rate protect and shielded the reactive metal from the aggressive environment. Figure 5.14 presents the corrosion rate of AISI 1040 when CRW 85155 was applied. The linear relationship elucidate that the Protection efficiency ( $\Theta$ ) is according to Langmuir adsorption isotherm.

While CRW85155 can be used in environments without oxygen, another alternative inhibitor that can be used in an oxygen environment is CRW89000, which consists of sodium hydroxide ( $2\text{mg/m}^3$ ) and sodium nitrate. Figure 5.15 depicts carbon steel AISI 1040 in solution 1 with four different concentrations of CRW89000 at elevated temperatures. By increasing the concentration, the corrosion rate decreased about 84%-90% from  $4^\circ\text{C}$  to  $80^\circ\text{C}$ .

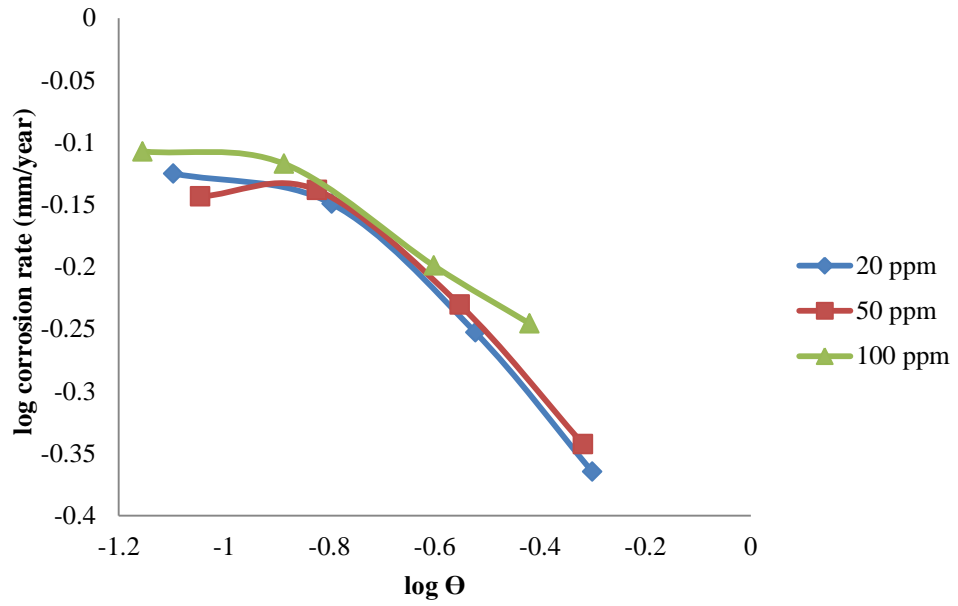


Figure 5.14 Effect of corrosion rate to chemisorption of inhibitor

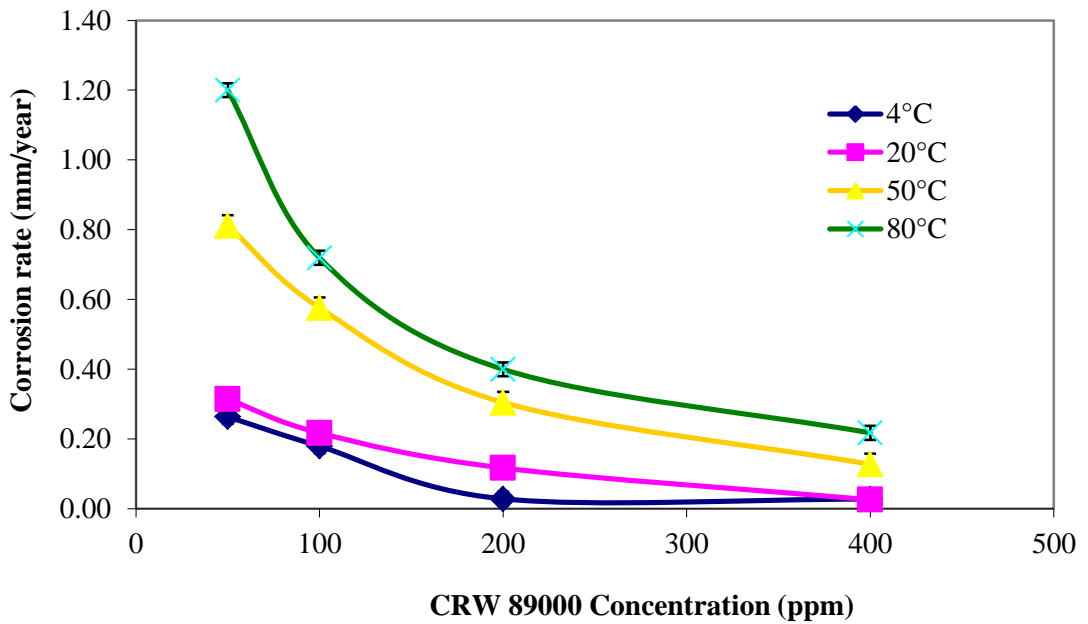


Figure 5.15 Carbon steel in CRW 89000 inhibitor

Figure 5.16 portrays the comparison of the corrosion rate for carbon steel AISI 1040 in different solutions, namely, HW443, solution 1 added with inhibitor CRW 85155 and solution 1 added with green inhibitor CRW 89000 at 20°C. The difference in corrosion rate of these three media can be seen at the point 100 ppm (considering HW443 is optimum at that point). However, these two inhibitors cannot reach the corrosion control provided by HW443 on AISI 1040. At 50 ppm and 100 ppm

concentrations, CRW 85155 shows better performance than CRW 89000. When the 100ppm concentration is added, the performance of CRW 89000 is 41% lower than CRW 85155 and 69% higher than HW443. Because of CRW 85155 does not shows much significant different as the concentration of inhibitor was added, CRW 8900 was added more (up to 400 ppm) to solution 1 (S1) to validate as it is comparable to HW443. The plot shows that when seawater (S1) added with 400 ppm CRW 89000, the corrosion rate of AISI 1040 is similar to corrosion rate in HW443.

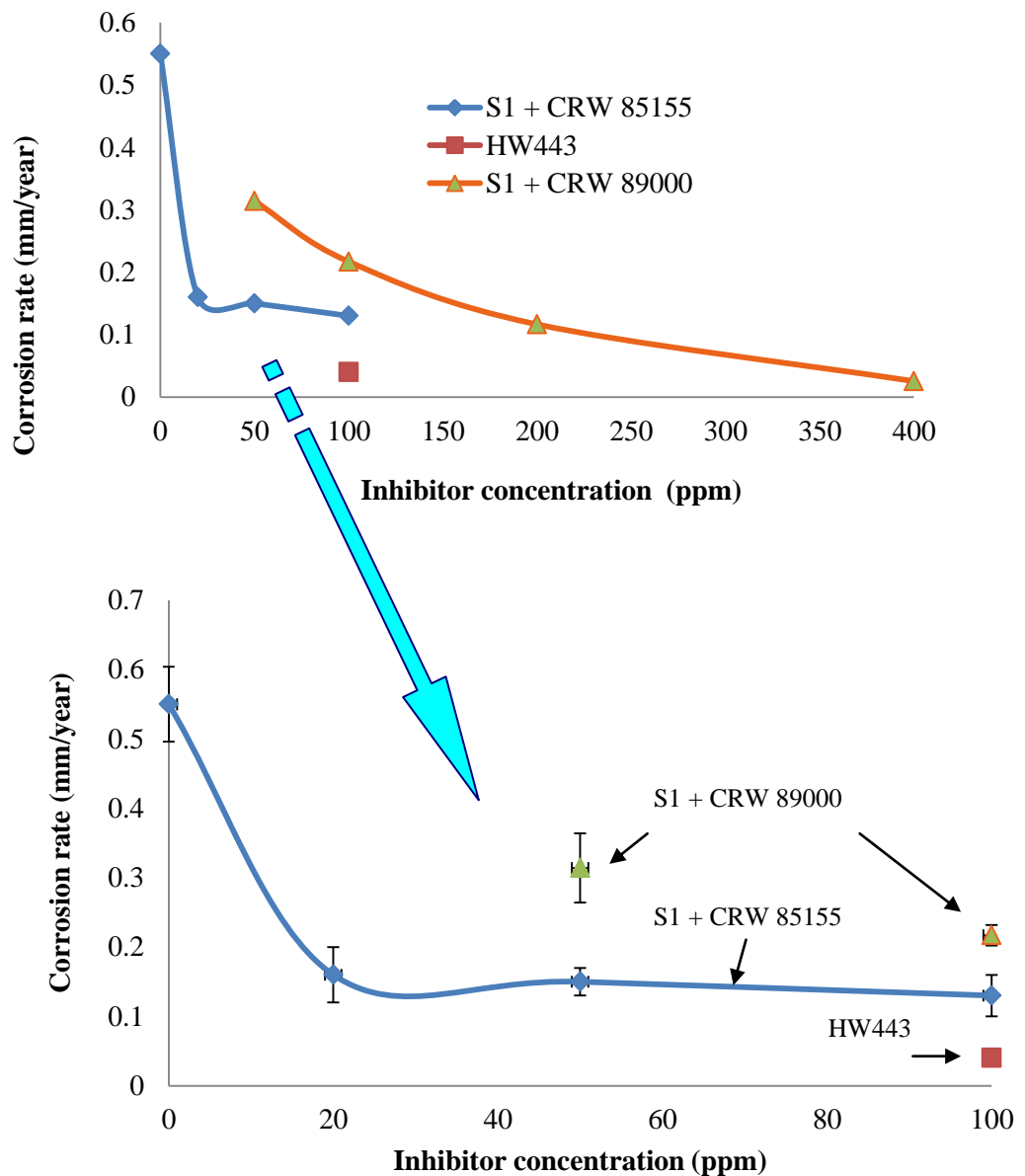
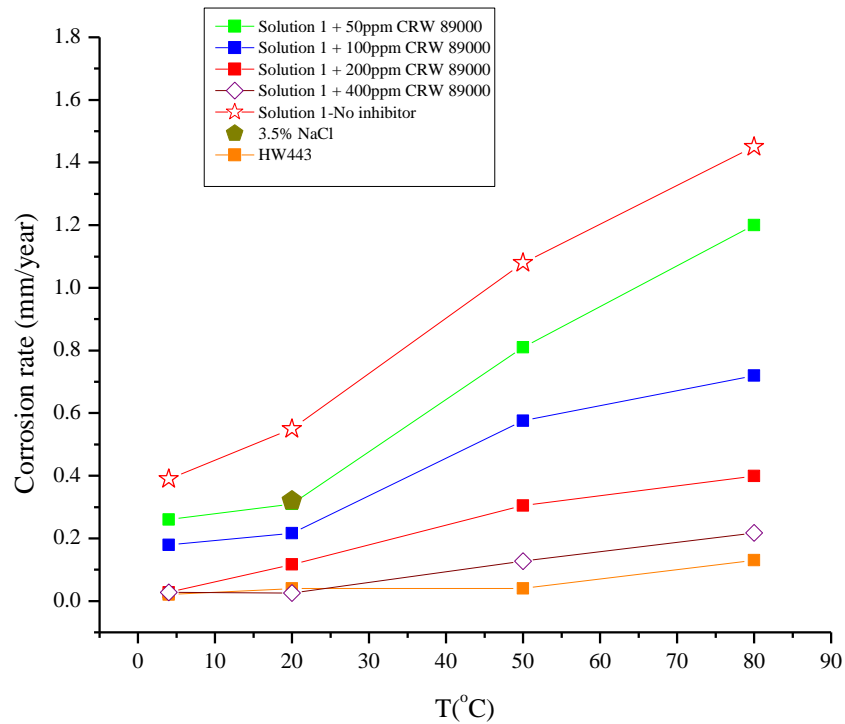


Figure 5.16 Corrosion rate for carbon steel in HW443, CRW 85155 and CRW 89000 at 20°C

The concentration of CRW 89000 was increased to 200ppm and 400ppm. Figure 5.17 indicates that at 20°C, when solution 1 had 400ppm CRW 89000 added, the corrosion rate obtained was close to the corrosion rate in HW443. This reveals that changing the sulphate-chloride ratio and also controlling the amount of oxygen, the corrosion rate can be manageable to acceptable corrosion rate. Furthermore, in oxygen environment, the corrosion attack of carbon steel can be managed by using green inhibitor. The corrosion rate can be reduced to acceptable corrosion rate by added 400ppm of CRW 890000 in seawater. Figure 5.17 compares the corrosion rate of AISI 1040 in different concentration of CRW 89000, artificial seawater (S1), 3.5% NaCl and commercial hydraulic fluid (HW443).



**Figure 5.17 Corrosion rate for carbon steel in S1 added with 50ppm, 100ppm, 200ppm and 400ppm CRW 89000, solution 1, 3.5% NaCl and HW443**

### 5.10 Summary

To conclude, the corrosion rate of carbon steel at 20°C can be reduced close to the acceptable corrosion rate obtained in HW443, by using the seawater with 400ppm CRW 89000 inhibitor. Altering the sulphate-chloride ratio is not an effective choice of reducing the corrosion attack of carbon steel. Apart of that, by controlling the chloride content at 0.05 g/L and oxygen concentration at 16 ppb, the corrosion rate can be reduced as much as corrosion rate of AISI 1040 in HW443 at 20°C. After these three

separate experimental methods, it shows that corrosion rate of carbon steel in seawater can be manageable by controlling the chloride content and oxygen dissolution or addition of a green inhibitor. In real situations, to use seawater as hydraulic can be realised by desalination or osmosis treatment to seawater. Temperature is a main key to corrosion susceptibility.

## Chapter 6

### PASSIVE MATERIALS

#### 6.1 Introduction

In the previous chapter, the strategy of treating the seawater to reach an acceptable corrosion rate was assessed. In this chapter the assessment of more advanced materials is presented. Still the same objective is addressed which is to assess the feasibility of using seawater as a replacement to hydraulic fluid.

In anodic polarisation tests, the electrode potential of the material is scanned from the free corrosion potential ( $E_{\text{corr}}$ ), also known as the Open Circuit Potential (OCP), in the more positive direction at a fixed rate. When passivity is exhibited, the current initially remains very small. Once the potential reaches the breakdown potential ( $E_b$ ) (at which the passive film breaks down due to the overpotential driving force), the current increases suddenly. The breakdown potential of the material provides information on the resistance of materials to passivity breakdown [131]. Each anodic polarisation scan was reversed once the current reached a set current ( $i_{\text{rev}}$ ) of  $500\mu\text{A}/\text{cm}^2$ . The degree of the increase in current beyond  $i_{\text{rev}}$  gives an indication of the propensity for corrosion propagation [132]. An indication of the extent of propagation is therefore obtained by consideration of  $i_{\text{max}}$ , which represents the maximum current attained should the current not begin to fall immediately after scan reversal. The comparison of corrosion behaviour among materials could be assessed based on their breakdown potential,  $E_b$ ,  $i_{\text{max}}$  and the passive potential range, which is the magnitude of  $|E_b - E_{\text{corr}}|$  in static conditions.

For this chapter, the results will only concentrate on the three types of alloy – **austenitic stainless steel** (UNS S31603 also known as 316L), **25Cr Duplex** and a high alloy, **nickel alloy** (UNS N06625 also known as Inconel 625), which exhibit passive behaviour in static 3.5% NaCl. The tests are done in different sulphate-chloride ratios. The inhibitor response at all temperatures from 4°C to 80°C and also in seawater (S1) with response to dissolved oxygen are assessed.

As shown in Figure 6.1, this curve reveals an electrochemical response during anodic polarisation when the potential is scanned in the positive direction from  $E_{\text{corr}}$  (also known as OCP); only very small currents (typically  $<10\mu\text{A}/\text{cm}^2$  [185]) are recorded until  $E_b$  is reached. At this point the current rises rapidly as a function of

potential indicating that corrosion attack has initiated. The current corresponding to the breakdown potential is denoted as breakdown current (current density,  $i_b$  ( $A/cm^2$ ))

As explained in the previous chapter, both stainless steels and other high alloy materials (including Ni and Co-based alloys) develop a thin passive film on their surface. Unlike active materials (carbon steel), passive materials depend on this thin passive film to protect themselves from corrosion. The nature of thin passive films, which preclude charge transfer and give the materials their superior corrosion resistance, has been the subject of many papers [25,33,133-135].

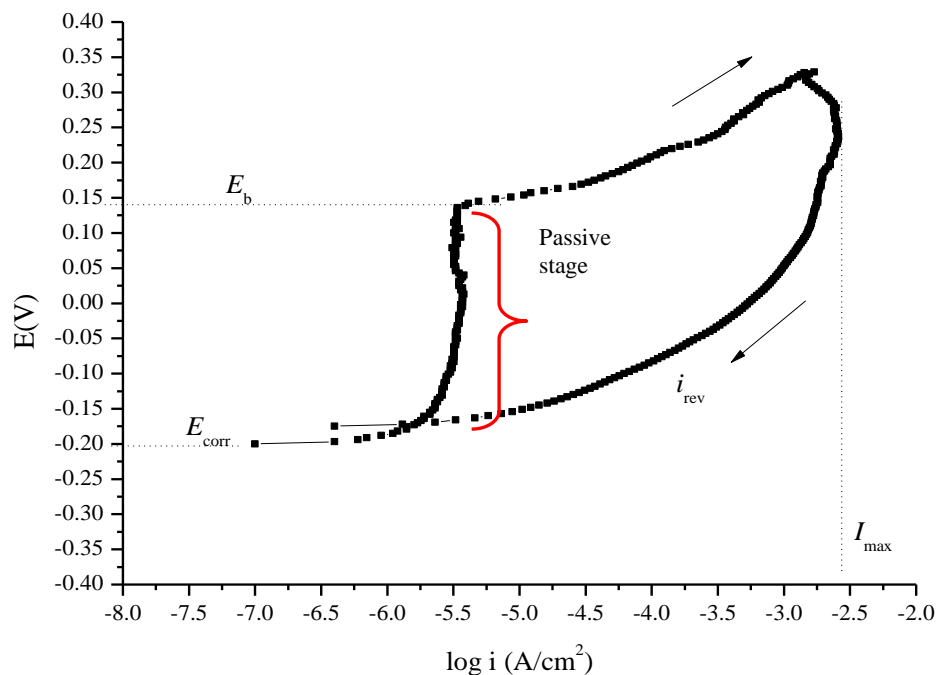


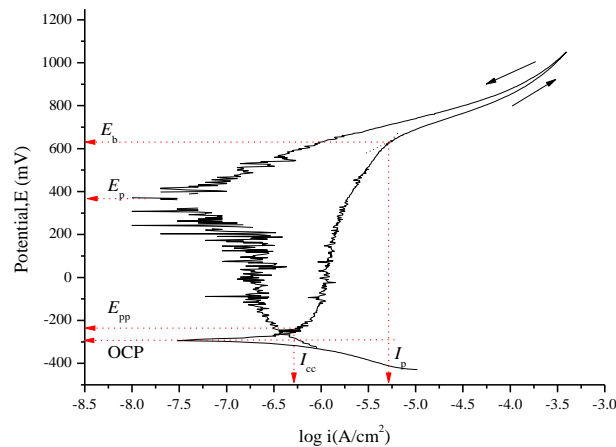
**Figure 6.1 Schematic of anodic polarisation curve for a passive material at 20°C.**

## **6.2 Bench Marking – Materials in HW443**

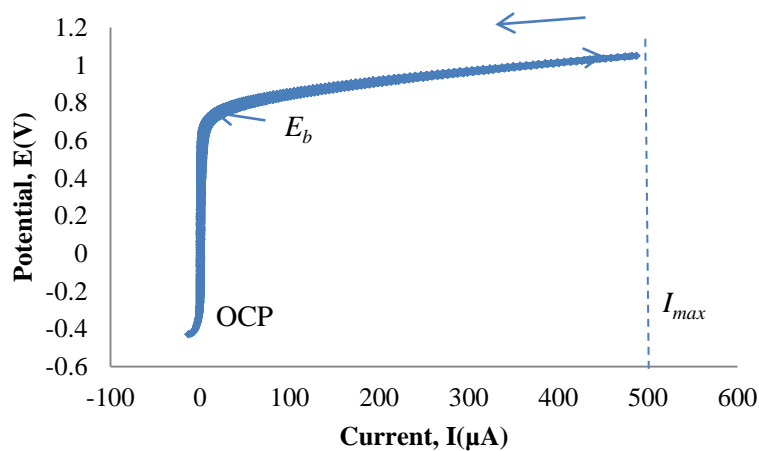
The first set of analyses examined the materials' performance in commercial hydraulic fluid HW443. Figure 6.2 presents the results obtained from the cyclic polarisation tests for 316L in HW443 at 20°C. The arrows indicate forward and reverse scans. As mentioned in Chapter 2, the cyclic polarisation curve hysteresis can provide information on pitting corrosion rates and how readily a passive film repairs itself. Positive hysteresis occurs when passive film damage is not repaired and pits will initiate

whereas negative hysteresis (Figure 6.2) occurs when a damaged passive film repairs itself and pits do not initiate.

The specific electrochemical parameters, previously described in section 2.11.2, are labelled on the graph, which include Open Circuit Potential (OCP), passivation potential ( $E_{pp}$ ), breakdown potential ( $E_b$ ), protection potential ( $E_p$ ), critical current density ( $i_{cc}$ ) and passive current density ( $i_p$ ). These three alloys all exhibited a passive region right from the corrosion potential,  $E_{corr}$ . When the potential was increased from the corrosion potential through the passive region, the potential corresponding to the abrupt rise in current was taken as the breakdown potential,  $E_b$  (some may refer to it as pitting potential). This was used as a criterion for evaluating the pitting corrosion resistance of the materials. It is directly influenced by the quantity of passivating elements present in the alloys.



(a)



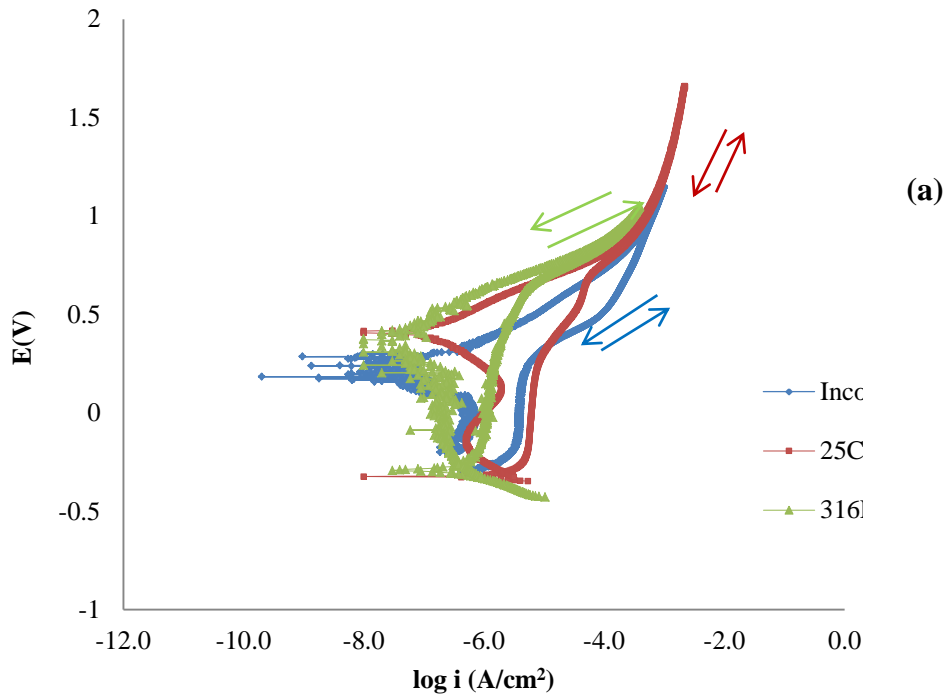
(b)

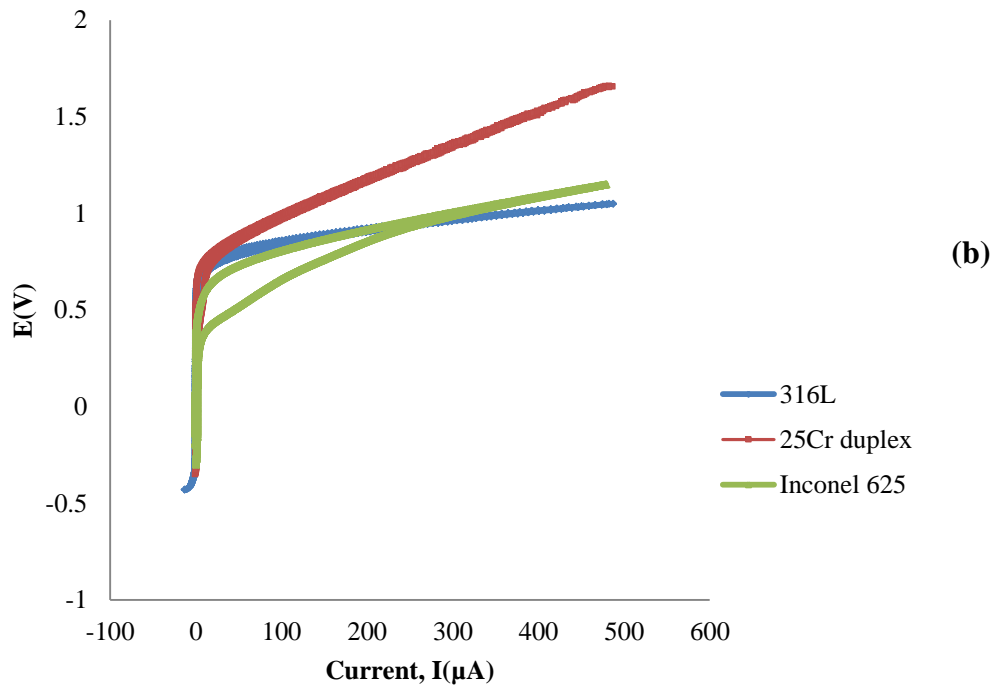
**Figure 6.2 Anodic polarisation curve of 316L in HW443 at 20°C (a) E-log i plot (b) E-I plot**



Figure 6.3 compares the anodic polarisation behaviour of 316L, 25Cr duplex and Inconel 625 in commercial hydraulic fluid, HW443 at 20°C. All the materials show negative hysteresis in their corrosion performance in HW443. The best performance is shown by 25Cr duplex, which has the highest  $E_b$ . The negative hysteresis is often thought to characterize an alloy in terms of localised corrosion. The interpretation include that the material would be expect to resist localised corrosion if the repassivation potential appear as negative hysteresis [26].

The electrochemistry parameters of 25Cr duplex, 316L and Inconel 625 in HW443 are listed in Table 6.1, which shows that in terms of passive film breakdown 25Cr duplex appears to be the most outstanding material compared to Inconel 625, which has almost the same chromium content. The passivating elements, such as chromium and nitrogen, hinder the development of pit growth, thereby increasing the extent of the potential passive region [106].





**Figure 6.3** Anodic polarisation curve of 316L, 25Cr duplex and Inconel 625 in HW443 at 20°C (a) E-log i plot (b) E-I plot

**Table 6.1** Electrochemical data of materials in HW443 at 20°C

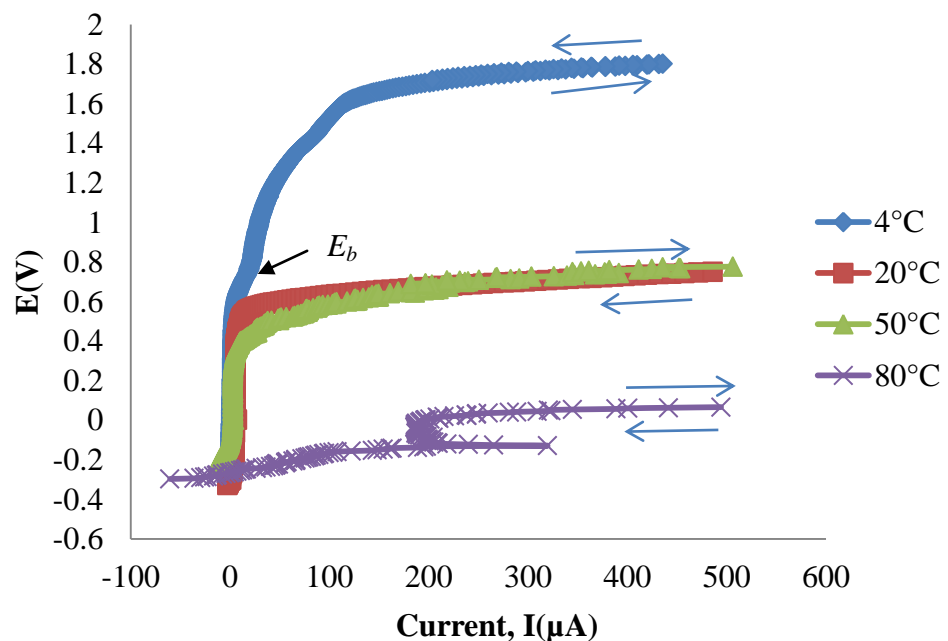
Material	OCP (mV)	$E_{pp}$ (mV)	Potential passive region	$E_b$ (mV)	$E_P$ (mV)	$i_p$ ( $\mu\text{A}/\text{cm}^2$ )	$i_{cc}$ ( $\mu\text{A}/\text{cm}^2$ )
316L	-311	-215	873	658	409	-5.17	-6.15
25Cr duplex	-324	-246	935	689	415	-4.21	-5.33
Inconel 625	-297	-196	619	423	284	-5.32	-5.51

### 6.3 Materials in 3.5% NaCl at Different Temperatures

Cyclic polarisation was also studied in 3.5% NaCl. Figure 6.4 compares the anodic curves for 316L in 3.5% NaCl at different temperatures. It is clear that the form of anodic polarisation curve on 316L is comparable at four temperatures. There is a significant reduction in  $E_b$  as the temperature increases. The drastic change in the nature and the properties of oxide films on passive alloys in water in increasing temperature is attributed to a breakdown of passivity [136, 137]. The curve shows a negative hysteresis

at 4°C and changed to positive hysteresis as the temperature increased from 20°C to 50°C. The positive hysteresis could indicate that the passive film damage is not repaired and that pits might initiate [23]. However, at 80°C, 316L was actively corroding as soon as potential and current increased. As a result, the anodic polarisation does not show any breakdown potential.

The cyclic polarisation properties of 316L for all temperatures are compiled in Table 6.2. The OCP values shifted towards more active values as the temperature increased, while the breakdown corrosion potential presented the opposite tendency. The breakdown potential,  $E_b$  decreased as the temperature increased. The difference in passivation potential value,  $E_{pp}$  and breakdown potential,  $E_b$  can be used to determine the existence of the potential passive region. The potential passive region reduced as the temperature increased. However, the  $E_b$  values of 316L at 20°C is higher than  $E_b$  values of 316L in HW443.



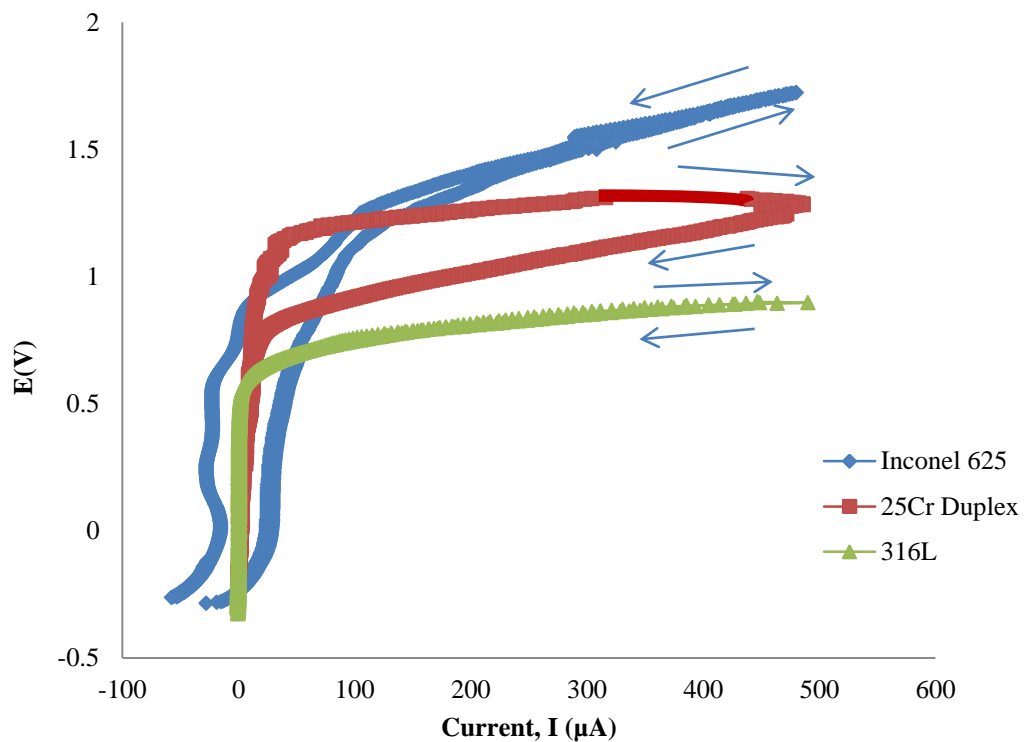
**Figure 6.4 The anodic polarisation of 316L as a function of temperature in 3.5% NaCl**

Figure 6.5 shows the anodic polarization curves in 3.5% NaCl at 20°C for 25Cr duplex, Inconel 625 and 316L. In the following results, the material degradation and susceptibility to localised corrosion will be discussed in terms of their breakdown of potential during anodic polarization. Table 6.3 shows the data for the cyclic polarization tests for 316L, 25Cr duplex and Inconel 625 in 3.5% NaCl at 20°C. The  $E_b$  values also shows a same trend as materials in HW443 which are 25Cr duplex > Inconel 625 >

316L. In addition, the potential passive region of 25Cr duplex performs a little bit higher than Inconel 625 which indicate that 25Cr duplex is more stable before the passive film destroy.

**Table 6.2 Electrochemical data of 316L in 3.5% NaCl**

Temperature	OCP (mV)	$E_{pp}$ (mV)	$E_b$ (mV)	$E_P$ (mV)	$i_p$ ( $\mu\text{A}/\text{cm}^2$ )	$i_{cc}$ ( $\mu\text{A}/\text{cm}^2$ )
4°C	-189	-93	561	509	-5.64	-6.51
20°C	-267	-110	594	310	-4.93	-5.36
50°C	-186	-70	257	79.97	-5.98	-6.24
80°C	-106	NA	NA	-164	-4.03	-4.74



**Figure 6.5 Anodic polarisation of materials in 3.5% NaCl at 20°C**

**Table 6.3 Electrochemical data of materials in 3.5% NaCl at 20°C**

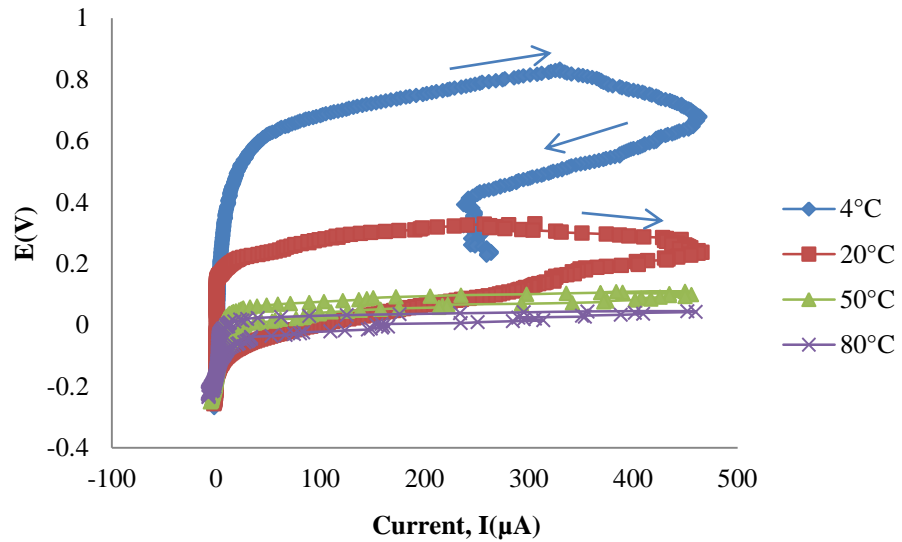
<b>Material</b>	<b>OCP (mV)</b>	<b><math>E_{pp}</math> (mV)</b>	<b><i>Potential passive region</i></b>	<b><math>E_b</math> (mV)</b>	<b><math>E_P</math> (mV)</b>	<b><math>i_p</math> (A/cm<sup>2</sup>)</b>	<b><math>i_{cc}</math> (A/c m<sup>2</sup>)</b>
316L	-267	-222	816	594	310	-4.93	-5.36
25Cr duplex	-161	105	988	1093	805	-0.272	-5.65
Inconel 625	-291	-123	964	1086	328	-5.17	-5.59

## 6.4 Materials in Seawater

It is possible that the variation in chemical composition of seawater may influence the corrosivity [138]. According to Takasaki and Yamada (2006) the corrosion rate increased in proportion to the concentration of aggressive anions and with increasing temperature [45]. Therefore, the effect of seawater (which contain aggressive anions) on corrosion attack was identified. In this study, seawater was synthesised according to the same major elements as natural seawater (Solution 1). The main reason we are not using the real seawater is because of the microbiological life in seawater will leads to an increased liability of local corrosion and an increased corrosion rate [139,140]. Therefore, it will affect the objective of assessing the feasibility of using seawater in subsea applications.

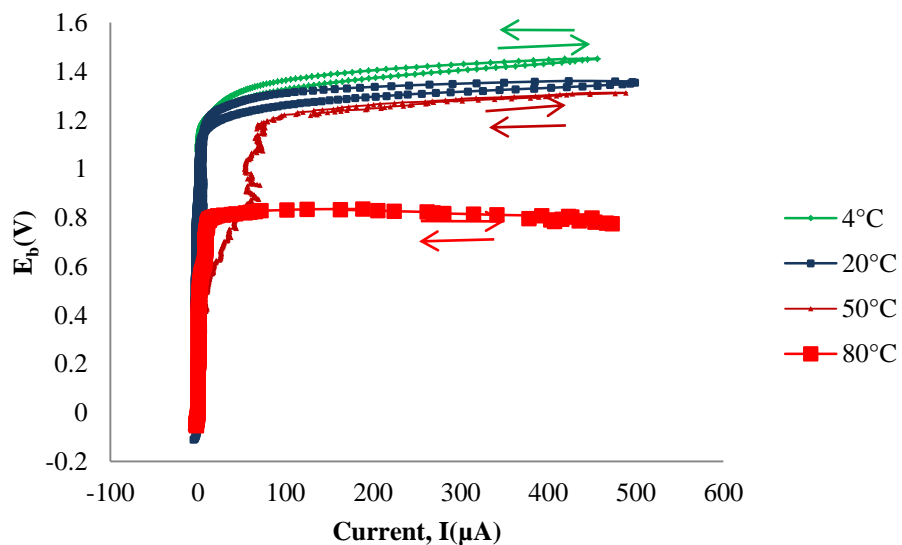
Figure 6.6 shows the anodic polarisation of 316L in seawater (solution 1) at different temperatures: 4°C, 20°C, 50°C and 80°C. It shows clearly that the breakdown potential ( $E_b$ ) decreased as the temperature increased. As expected, increasing the temperature decreased the passive region. At all temperatures, 316L shows a positive hysteresis in solution 1.

Figure 6.7 and 6.8 show the 25Cr duplex and Inconel 625 in seawater (solution 1) at different temperatures, respectively. Compared to 316L, the passivation and repassivation of 25Cr duplex is more stable compared to 316L according to their small gap in forward and reverse scan whereas Inconel 625 shows negative hysteresis at 4°C and 20°C, and stable hysteresis as well as positive hysteresis at 50°C and 80°C. There is only slight difference in the performance with increasing temperature, meaning that 25Cr duplex and Inconel 625 are stable at increasing temperature.



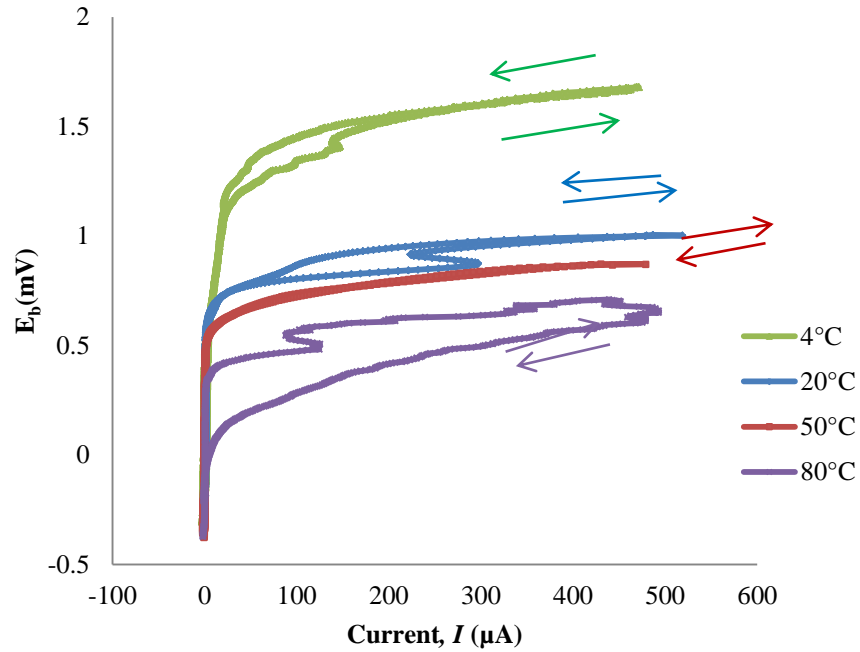
**Figure 6.6** Stainless steel 316L in solution 1 ( $\text{SO}_4^{2-}/\text{Cl}^-=0.14$ ) at different temperatures

For 25Cr duplex in seawater, the hysteresis at 4°C and 20°C presents as a negative while the plot changes to a positive hysteresis at increasing temperature, which means that pitting may occur since the passive film breakdown not repairs itself. The passive region also decreases as the temperature increases. As the applied anodic potential increases, the passive current is followed by a sharp increase due to the disruption of the passive layer formed on 25Cr duplex surface. The current increases after the breakdown of passive film, which might be associated with the transpassive dissolution of chromium and gas evolution [34].

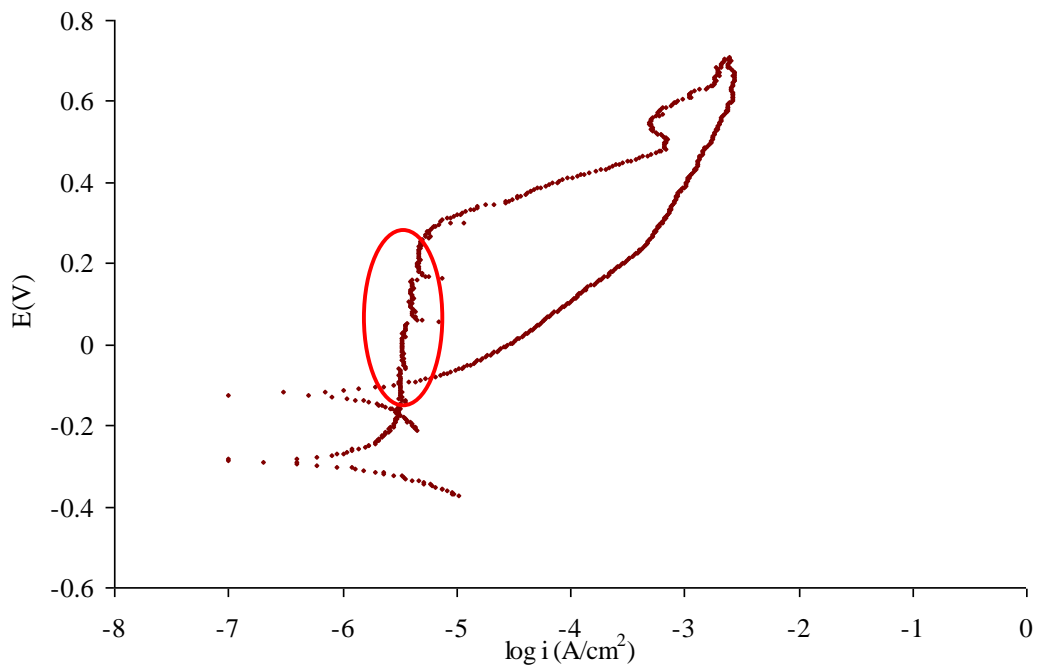


**Figure 6.7** 25Cr duplex in solution 1 ( $\text{SO}_4^{2-}/\text{Cl}^-=0.14$ ) at different temperatures

For Inconel 625 in seawater, despite of having small hysteresis (the forward and reverse scan) value which indicate the small disruption of surface passivity [26], Inconel 625 also present to have a metastable pitting before the passive film breaks at 80°C (Figure 6.8 (b)) as shown in red marked.



(a)



(b)

**Figure 6.8 Inconel 625 in solution 1 ( $\text{SO}_4^{2-}/\text{Cl}^- = 0.14$ ) (a) at different temperatures (b) having metastable pitting at 80°C**

According to breakdown potential, both 25Cr duplex and Inconel 625 show high in  $E_b$ . However, 25Cr duplex seems more corrosion resistance as breakdown potential is higher at every temperature. As tabulated in Table 4.2 (Chapter 4, section 4.1), chromium content is slightly higher in 25Cr duplex compared to chromium content in Inconel 625 (chromium content 22 wt%). Because of this, 25Cr duplex shows better performance compared to Inconel 625.

Figure 6.9 shows the effect of increased temperature on the  $E_b$  value for each material in seawater (solution 1) as compared to HW443 hydraulic fluid. 25Cr duplex and Inconel 625 proved to be the least affected by increased temperature compared to 316L. 316L shows a sudden drop in  $E_b$  from 4°C to 20°C. All the materials show the lowest  $E_b$  at 80°C and also active behaviour observed at higher temperature might be the result of insufficient oxygen available to aid complete repassivation [95]. This figure also presents the  $E_b$  value in HW443 at 20°C which has set before as the benchmark of acceptable corrosion attack. This indicates that the corrosion resistance has to improve more than 70% to switch the applications of commercial hydraulic fluid to seawater.

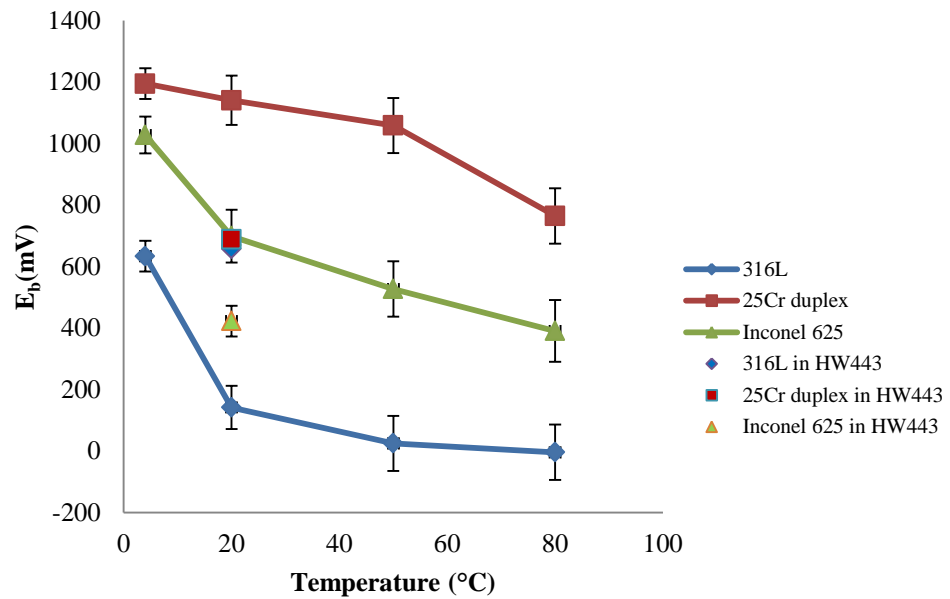


**Figure 6.9 The breakdown potential ( $E_b$ ) in S1 as a function of temperature with compared to  $E_b$  in HW443**



## 6.5 Materials in Different Sulphate-Chloride Ratios

This experiment was conducted to quantify the effect of sulphate and chloride anions in seawater. The composition of each solution which was synthesized in the laboratory is shown in Chapter 4. Figure 6.10 shows 316L in solution 2, which is higher in sulphate and lower in chloride compared to real seawater (S1). At all temperatures, there are oscillations at anodic polarisation. According to Indira and Doss (1967), the regular and persist oscillation at anodic polarization under controlled conditions is due to periodic change in the thickness of the film by alternate dissolution and deposition [191]. The increasing in thickness of the film will raise the pH which causes the leading to oxygen evolution and restores the original pH by agitation and facilitates solution of the film. Therefore, the process of oxygen evolution will disturbs the stationary film adjacent to the electrode on the solution side and thereby enhances dissolution. The breakdown potential at every temperature are higher compared to 316L in S1. This indicates that sulphate has an inhibiting effect on pitting corrosion [140,141], and the polarisation exhibits positive hysteresis at every temperature. The value of OCP and  $E_b$  are presented in appendix of this thesis.

Pistorius and Burstein (1992), in their study about the growth of corrosion pits on stainless steel in chloride solutions containing dilute sulphate on 304 stainless steels, found that the presence of sulphate causes the distribution of available pit sites to be shifted to a higher potential, which causes pit propagation in both metastable and stable states [142]. Figures 6.10 to 6.18 show the anodic polarisation curves of 316L, 25Cr duplex and Inconel 625 in S2, S3 and S4. Some materials such as Inconel 625 experience secondary breakdown potentials as shown in Figure 6.16 (Inconel 625 in solution 2 at 50°C and 80°C). The value of breakdown potentials at 4°C, 20°C, 50°C and 80°C for each material as compared to HW443 are shown in Figures 6.19, 6.20 and 6.21, respectively.

For passive alloys including austenitic stainless steels (316L), corrosion resistance is provided by a very thin surface film, known as passive film that is an invisible film of oxide, formed by the metal reacting with the ambient environment. Normally these films are free of pores, but their stability may be weakened locally in the environment contained aggressive anions. Figure 6.10, shows 316L in solution 2 (S2) which has higher sulphate and lower chloride ( $\text{SO}_4^{2-}/\text{Cl}^- = 19.15$ ) compared to seawater, S1 ( $\text{SO}_4^{2-}/\text{Cl}^- = 0.14$ ). The cyclic polarisation shows a positive hysteresis at all temperatures. The

differences of  $E_b$  values as compared to HW443 is shown in Figure 6.19 and indicates that the corrosion resistance of 316L in solution 2 has to be improved to almost 24% to an acceptable  $E_b$  as shown by 316L in HW443. The comparison of all solutions is shown in Figure 6.22 and 316L shows a increased  $E_b$  as the sulphate/chloride ratio is changed. However, the  $E_b$  values are not comparable to the  $E_b$  value of 316L in commercial inhibitor HW443. Nevertheless, this value is not significant to the amount of sulphate and chloride to affect corrosion attack on 316L and this is probably due to competition effect of anions on 316L and will be discussed later in Chapter 8.

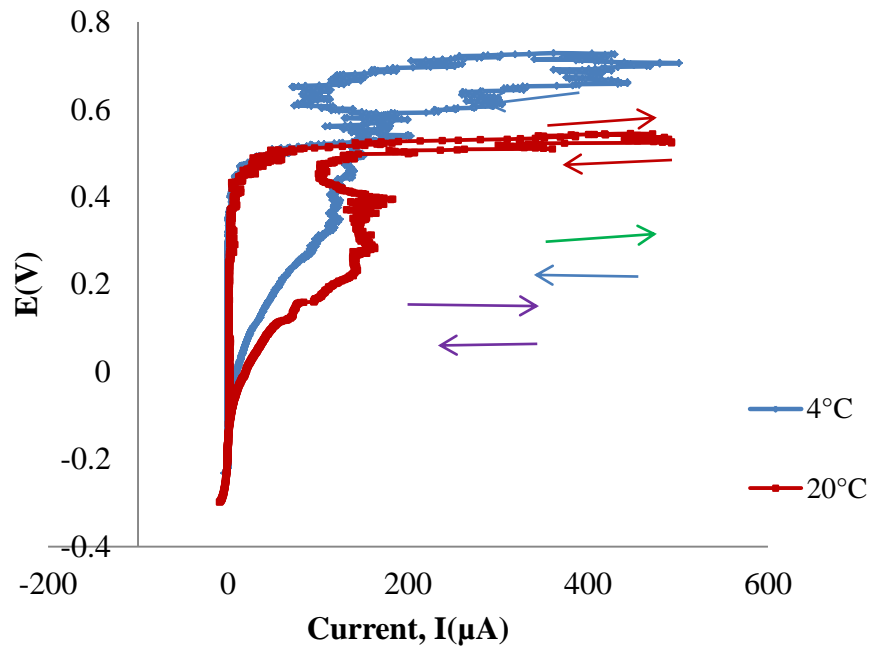


**Figure 6.10 Stainless steel 316L in S2 ( $\text{SO}_4^{2-}/\text{Cl}^- = 19.15$ ) at different temperatures**

Figure 6.11 and 6.12 presents the cyclic polarisation of 316L in solution 3 and 4. All the polarisations shows 316L in positive hysteresis at all temperatures. Solution 3 and 4 are having low sulphate composition compared to chloride. The ratio  $\text{SO}_4^{2-}/\text{Cl}^-$  of solution 3 is 0.75 whereas solution 4 contains  $\text{SO}_4^{2-}/\text{Cl}^-$  equal to 0.99. In both solutions, 316L exhibits a decrease in  $E_b$  as the temperature increases. For a better observation for  $E_b$  point due to anodic oscillation (oxygen evolution), some of the polarisation are presents in  $E$ - $\log i$  curve.

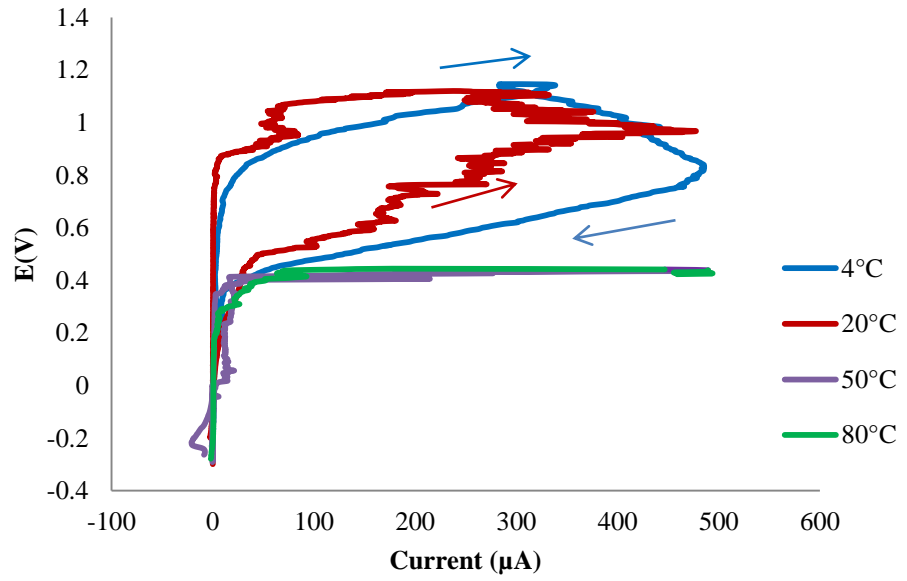


**Figure 6.11** Stainless steel 316L in S3 ( $\text{SO}_4^{2-}/\text{Cl}^- = 0.75$ ) at different temperatures

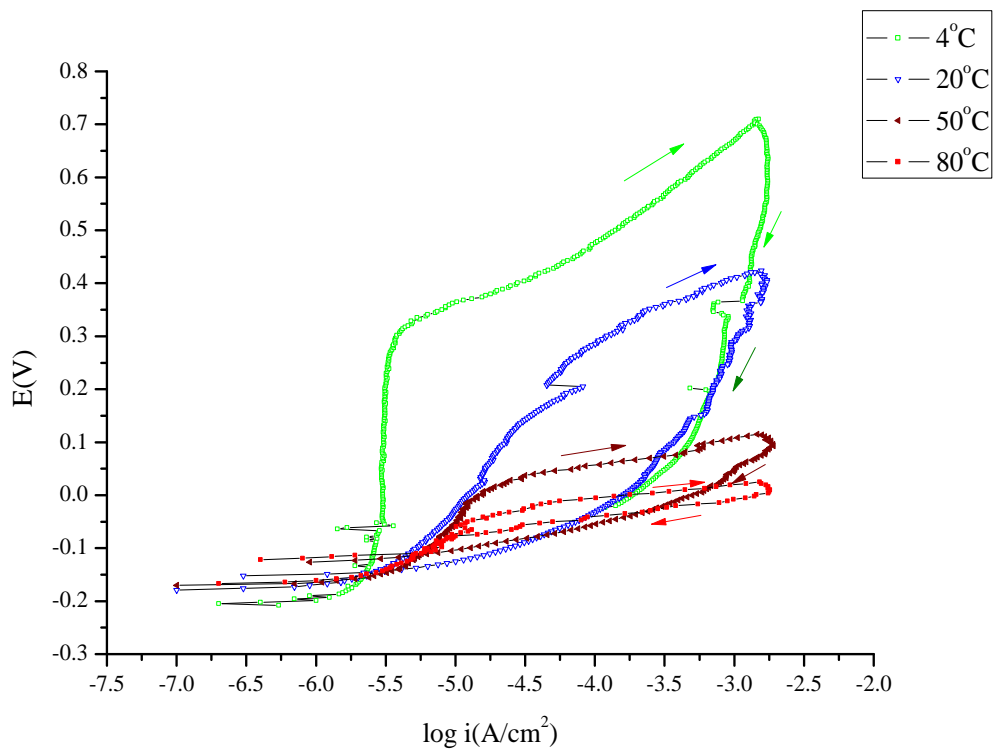


**Figure 6.12** Stainless steel 316L in S4 ( $\text{SO}_4^{2-}/\text{Cl}^- = 0.99$ ) at different temperatures

Figure 6.13 to 6.15 shows anodic polarisation for 25Cr duplex in solution 2 to 4 respectively. Almost all of the hysteresis shows positive directions and repassivation potential are close to anodic scan which indicate that the materials would be expected to

resist localised corrosion [26]. Some polarisations of 25Cr duplex in solution 2 and 4 perform to have secondary  $E_b$  in anodic polarisation.

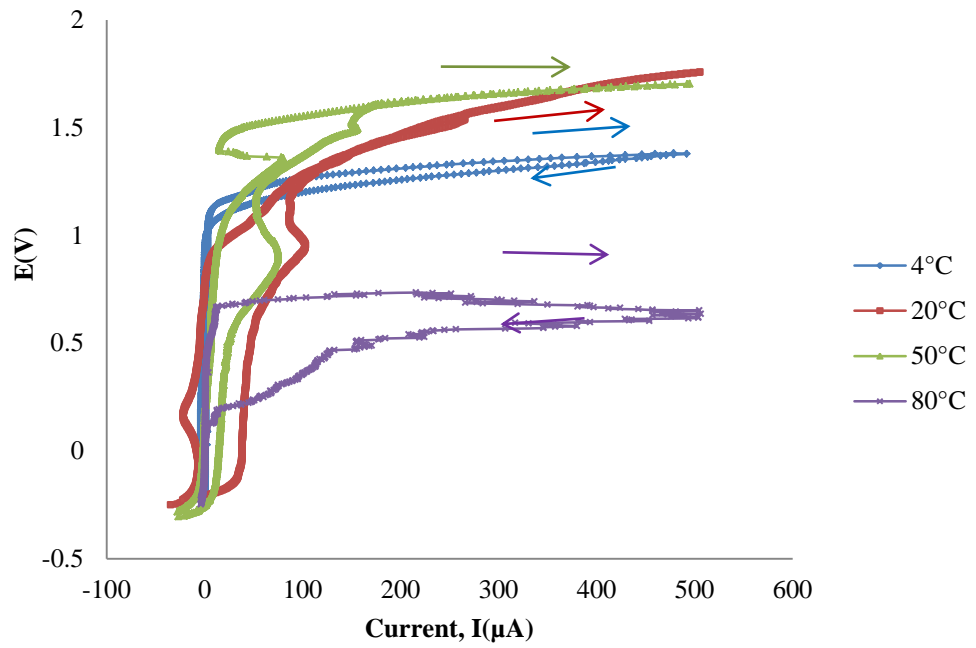


Figure 6.13 25Cr duplex in S2 ( $\text{SO}_4^{2-}/\text{Cl}^- = 19.15$ ) at different temperatures

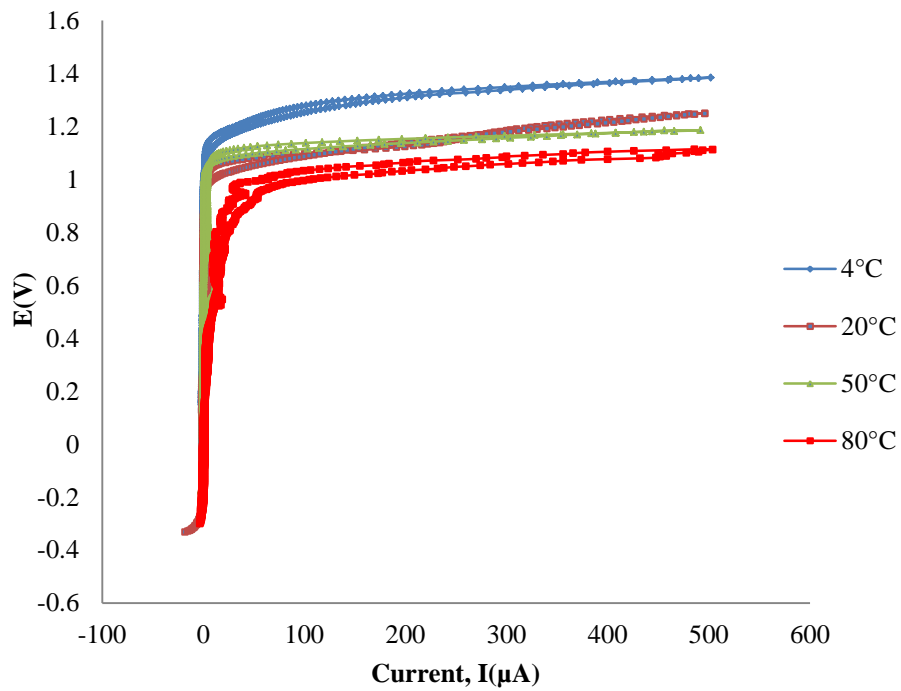
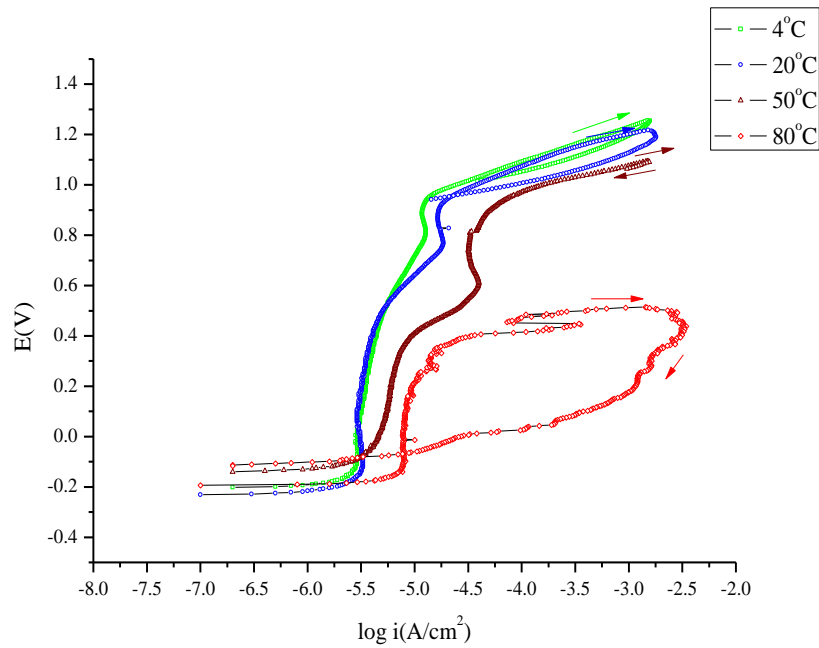
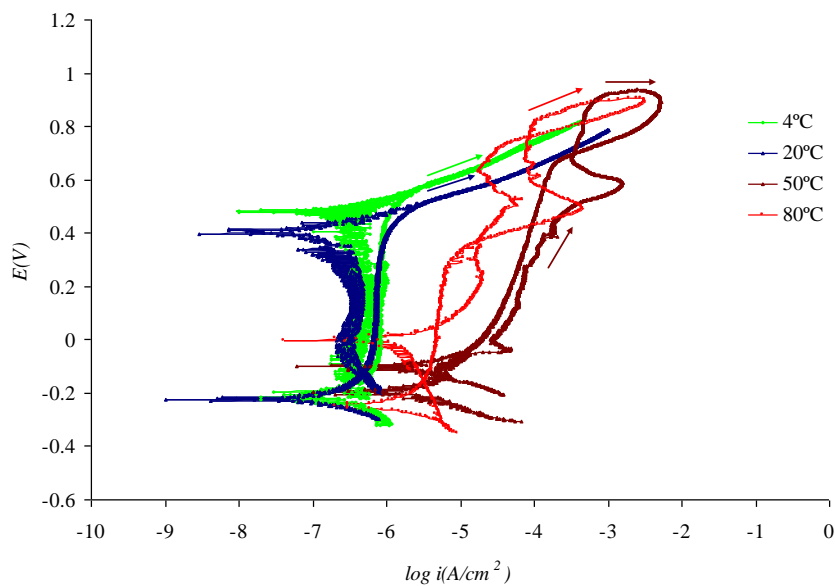


Figure 6.14 25Cr duplex in S3 ( $\text{SO}_4^{2-}/\text{Cl}^- = 0.75$ ) at different temperatures



**Figure 6.15 25Cr duplex in S4 ( $\text{SO}_4^{2-}/\text{Cl}^-=0.99$ ) at different temperatures**

Figure 6.16 to 6.18 presents the anodic polarisation of Inconel 625 in solution 2 to 4 respectively. At high temperature, Inconel 625 presents to have secondary  $E_b$  in solution 3 and 4. The comparison of  $E_b$  value to the acceptable  $E_b$  value in HW443 is presented in Figure 6.19 to 6.21. As predicted, the  $E_b$  value of Inconel 625 decrease as the temperature increase in both solutions. However, these values are not drastically reduced compared to 316L and this is indicating that Inconel 625 is stable in increasing temperature.



**Figure 6.16 Inconel 625 in S2( $\text{SO}_4^{2-}/\text{Cl}^-=19.15$ ) at different temperatures**

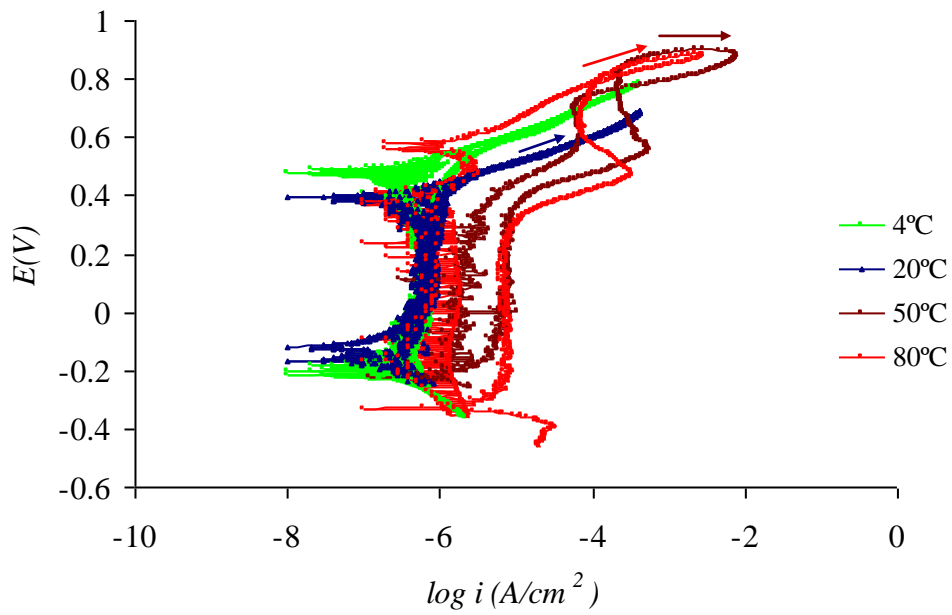


**Figure 6.17 Inconel 625 in S3( $SO_4^{2-}/Cl=0.75$ ) at different temperatures**

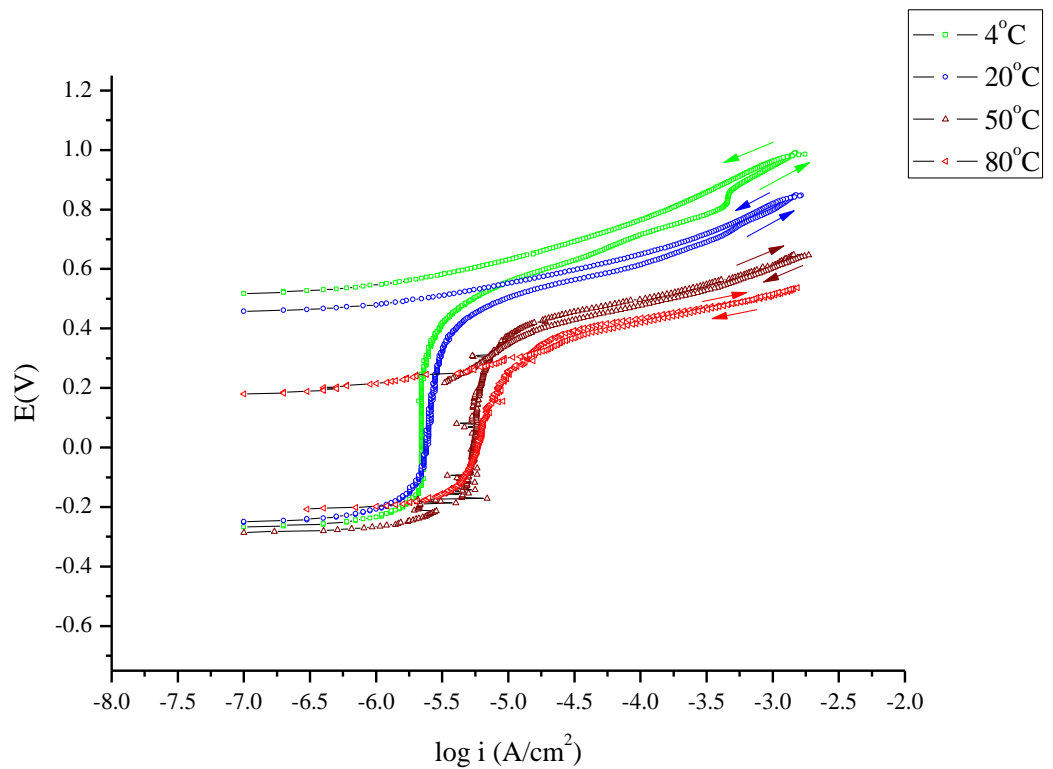


**Figure 6.18 Inconel 625 in S4 ( $SO_4^{2-}/Cl=0.99$ ) at different temperatures**

The full set of electrochemistry results are presented in the Appendix of this thesis. The breakdown potential for every material in every solution is presented in the

following figures. Figures 6.19, 6.20 and 6.21 present the breakdown potential values of 316L, 25Cr duplex and Inconel 625 in S2, S3 and S4, respectively. Figure 6.22 presents the breakdown potential of 316L, 25Cr duplex and Inconel 625 in every solution as compared to HW443 at 20°C. S2 has less  $\text{Cl}^-$  than  $\text{SO}_4^{2-}$  whereas S3 and S4 have more  $\text{Cl}^-$  than  $\text{SO}_4^{2-}$ . According to El-Naggar,  $\text{SO}_4^{2-}$  has an inhibiting affect on the surface of the metal whereas  $\text{Cl}^-$  is an aggressive ion that penetrates causing localised attack [49]. The  $E_b$  value for 316L increased drastically from solution 1 to solution 2 and 3 (sulphate higher than chloride) which indicate that resistance of material to passivity breakdown can be improved by changing the anions ratio ( $\text{SO}_4^{2-}/\text{Cl}^-$  ratio) of seawater. Other than that, the resistance to passivity breakdown could be improved by alternative way such as addition with chemical inhibitor or reducing the dissolve oxygen (DO) in seawater. 316L shows reducing in  $E_b$  value in S1 and sudden increased in S2 as compared to  $E_b$  of 316L in HW443. This explains the degradation effect of chloride (higher chloride content in S1) and inhibition effect by S2 (higher sulphate amount compare to chloride). If comparing the performance of these materials in seawater (solution 1) and chemical inhibitor (HW443), HW443 provide better inhibition effect on 316L and 25Cr duplex (16%-78%) than on Inconel 625 (only 3%).

316L and Inconel 625 shows decreasing in  $E_b$  in solution 3 and 4 compared to  $E_b$  in solution 2 whereas 25Cr duplex shows the opposite trend. The sulphate ratio in solution 3 and 4 is slightly lower than chloride which can explained that the inhibition effect of sulphate is not significant as both anions are comply to competition effect. However, in all solutions, the  $E_b$  values are lower than  $E_b$  value for the materials in HW443 which suggest that apart of changing the  $\text{SO}_4^{2-}/\text{Cl}^-$  ratio, the resistivity of materials to potential breakdown can be improve if use with inhibitor or reduced the oxygen content in seawater.

For 25Cr duplex, the lowest value of  $E_b$  is perform in solution 2 and the difference in  $E_b$  compared to HW443 is about 36%. Referring to Figure 6.22, 25Cr duplex is outstanding performance in  $E_b$  compared to 316L and Inconel 625 in all mediums. The difference of  $E_b$  in solution 3 and solution 4 are 23% and 27% respectively as compared to  $E_b$  value in HW443.

For Inconel 625, the difference of  $E_b$  value in solution 1 as compared to in HW443 is only 3%. Comparing the Inconel 625 to other materials explained that Inconel 625 is the least material that affected by different sulphate/chloride ratio and in HW443 inhibitor. Increasing the chloride content in solution 3 and 4 promotes chloride ions to dominating perforation of passive film on Inconel 625.

From the breakdown potential results, it can be concluded that 25Cr duplex and Inconel 625 will maintain the ability of having higher  $E_b$  to exist in higher or lower  $\text{SO}_4^{2-}/\text{Cl}^-$  ratios compared to 316L due to its composition.

From the breakdown potential results, it reveals that all of these passive materials especially 25Cr duplex and 316L needs additional corrosion protection such as addition with inhibitor to attain higher breakdown potential as performed by these materials in HW443. It also can be concluded that Inconel 625 react scantily with HW443 even it is very stable at different  $\text{SO}_4^{2-}/\text{Cl}^-$  ratio. The microscopic view of some of these pitting attacks can be seen in Figure 6.23 and Figure 6.24.

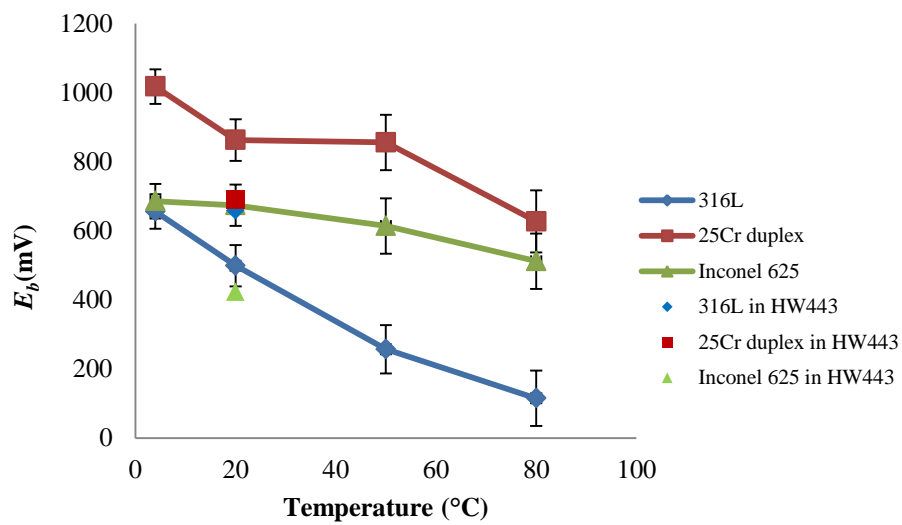


Figure 6.19 The breakdown potential in S2 as a function of temperature

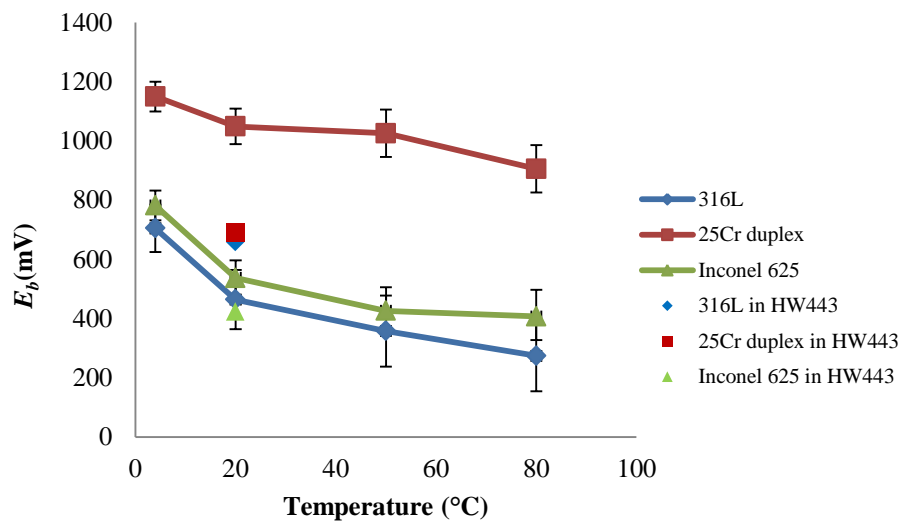


Figure 6.20 The breakdown potential in S3 as a function of temperature



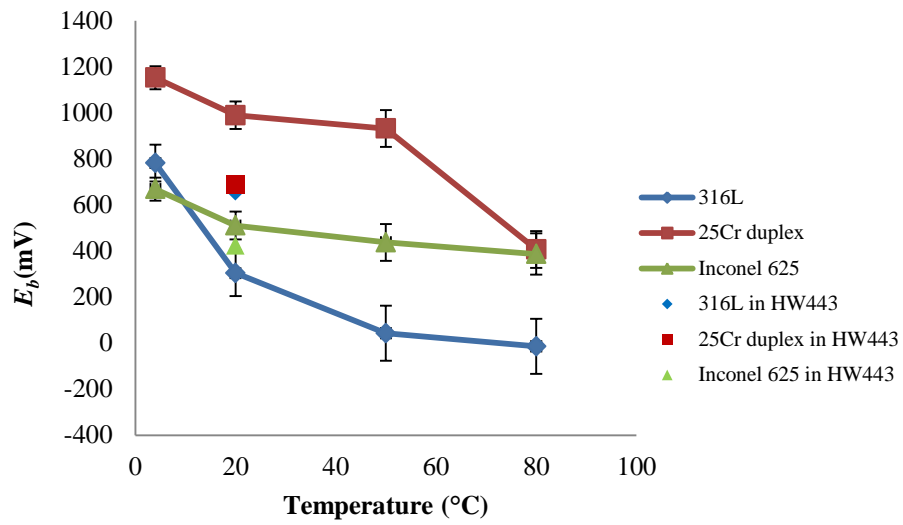


Figure 6.21 The breakdown potential in S4 as a function of temperature

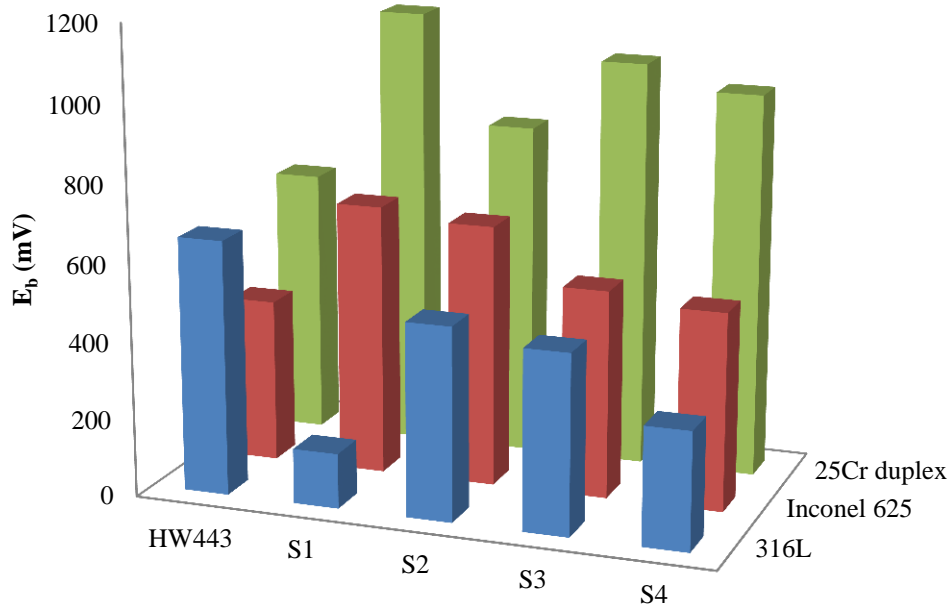


Figure 6.22 The breakdown potential value of every material in different  $\text{SO}_4^{2-}/\text{Cl}^-$  solutions as compared to HW443 at  $20^{\circ}\text{C}$

The microscopic view of some of the pitting attack can be seen in Figure 6.23 and Figure 6.24. Stainless steel 316L in most medium (solution 1-4) shows big surrounding area covered with metastable pitting before pitting propagate. The surface roughness also gives an effect to metastable pitting. This will be discussed further in Chapter 8.

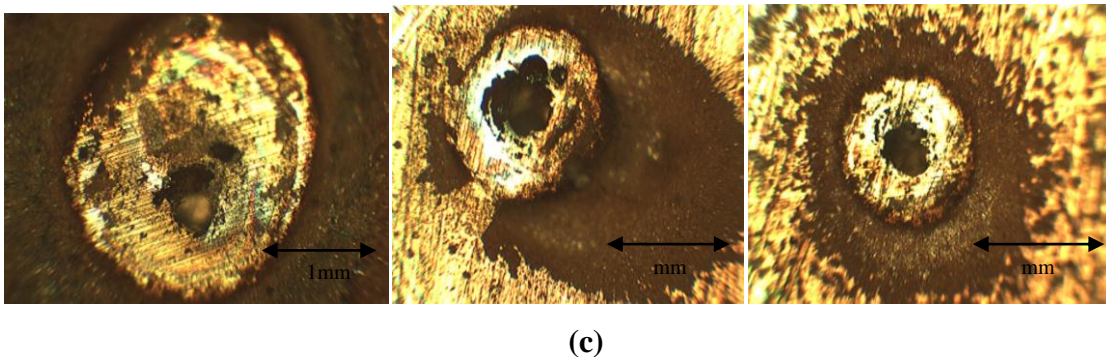
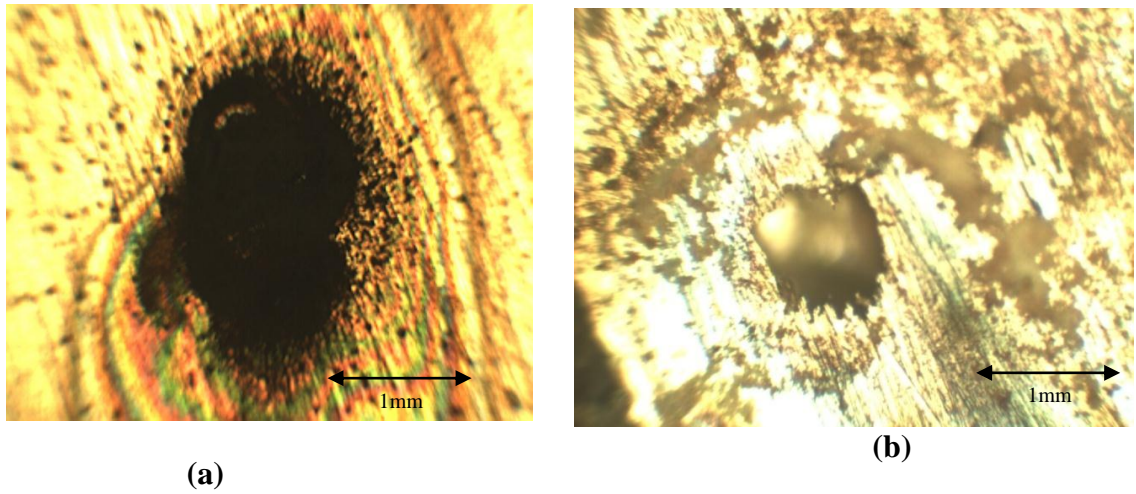
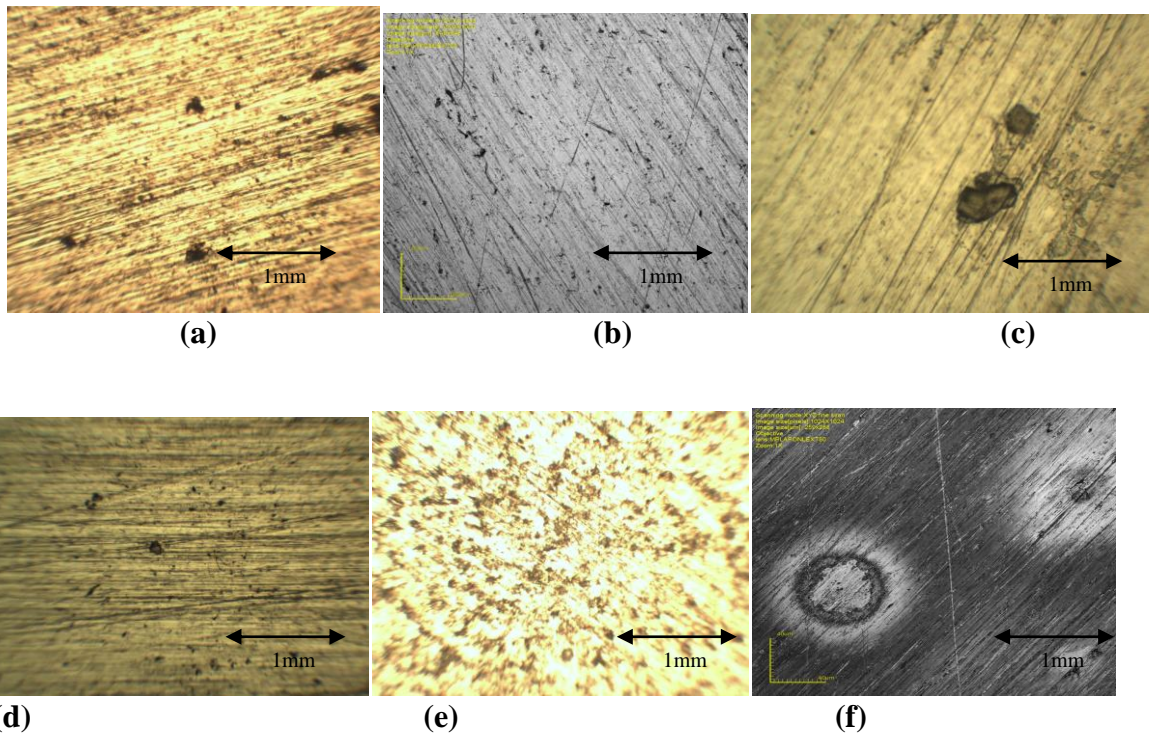
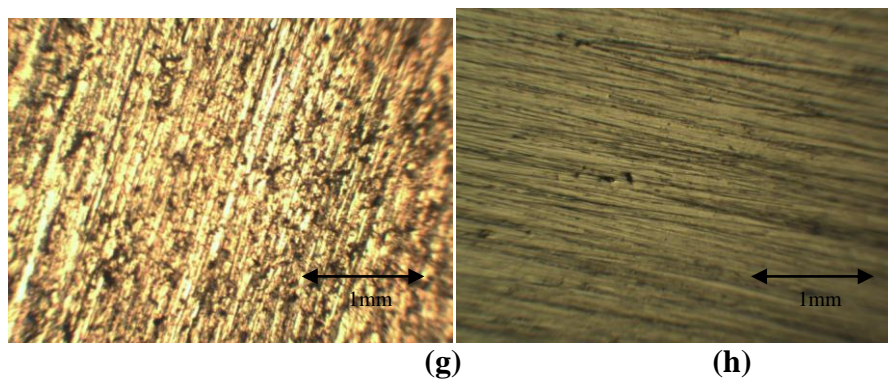


Figure 6.23 Microscopic image shows pitting of (a) 316L in solution 3 at 80°C, (b) 316L in solution 2 at 50°C and (c) 316L in solution 2 at 80°C





**Figure 6.24** Microscopic image shows pitting (a) 25Cr duplex in solution 3 at 80°C, (b) 316L in solution 2 at 80°C, (c) 25Cr duplex in solution 1 at 20°C, (d) 25Cr duplex in solution 1 at 50°C, (e) Inconel 625 in solution 3 at 80°C (f) 316L solution 3 at 20°C (g) Inconel 625 in solution 4 at 4°C (h) Inconel 625 in solution 3 at 4°C

## 6.6 Materials with Inhibition

As discussed in the previous chapter it is feasible that the corrosion rate of carbon steel can be controlled by addition of a green inhibitor. If this is added and there is other corrosion resistance alloys (CRAs) used, than until that present; it is important to understand the behaviour of the other alloys in particular their pitting behaviour. Figure 6.25 shows the comparison of breakdown potential,  $E_b$  of 316L, 25Cr duplex and Inconel 625 in solution 1 and solution 1 added with inhibitor CRW 89000. CRW 89000 is known a green inhibitor and used where oxygen exists in the corrosive environment. As stated previously, the nobility of the  $E_b$  gives an indication of the resistance of the material to passivity breakdown. This figure elucidate that, at 20°C the  $E_b$  value of materials are higher when S1 is added with 100 ppm CRW 89000. The  $E_b$  values are almost significant to  $E_b$  of materials in commercial hydraulic fluid, HW443. All passive alloys presents an increasing of  $E_b$  value if seawater (S1) is added with CRW89000 and the performance are better compared to materials in HW443 hydraulic fluid. 316L shows the highest increasing value of  $E_b$  when S1 is added with CRW89000 which is about 82% followed by Inconel (47%) and 25Cr duplex about 43%. The trend is similar to materials performances in solution 1 to 4 (25Cr duplex > Inconel 625 > 316L).

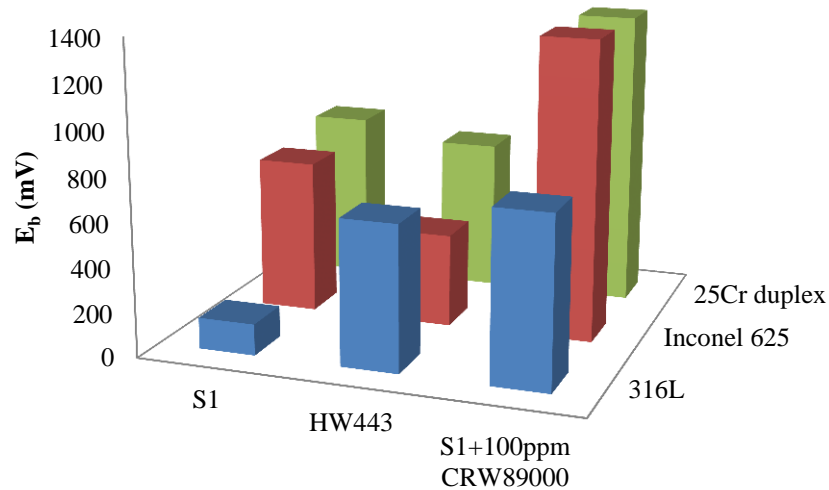


**Figure 6.25  $E_b$  of materials in S1 with and without CRW 89000 (100ppm) at 20°C**

### 6.7 Materials in a Reduced Oxygen Environment

The test continued exposing the materials to a reduced oxygen environment by purging with nitrogen to remove the oxygen. Accordingly, the nitrogen was still bubbled when the cyclic polarisation tests were running. For all the experiments, the bubbles are controlled with 1 bubble every 1 second and the oxygen reading was recorded using an oxygen concentration electrode. The oxygen was purging from solution until the measurement detected by oxygen meter at least 0.04ppb. The effect of oxygen was just considered at 4°C and 20°C with the assumption that higher temperatures will accelerate the corrosion rate.

Figure 6.26 and 6.27 presents the anodic polarisation of 316L in solution 1 with and without dissolved oxygen at 4°C and 20°C respectively. The polarisation of 316L in S1 at 4°C is presents in  $E-I$  plot for clear observation of  $E_b$  in a solution with no oxygen. Metastable pitting occurs on 316L in solution 1 without dissolved oxygen at 20°C (red marked). Figure 6.28 to 6.29 presents the anodic polarisation of 316L in solution 2. The material shows high  $E_b$  in S2 at 4°C when the dissolved oxygen is low. Figure 6.30 and 6.31 shows the anodic polarisation of 316L in solution 3 at 4°C and 20°C. With no oxygen in solution 3 at 20°C, 316L shows an increasing current at the repassivation curve. Figure 6.32 and 6.33 shows the anodic polarisation of 316L in solution 4 at 4°C and 20°C.

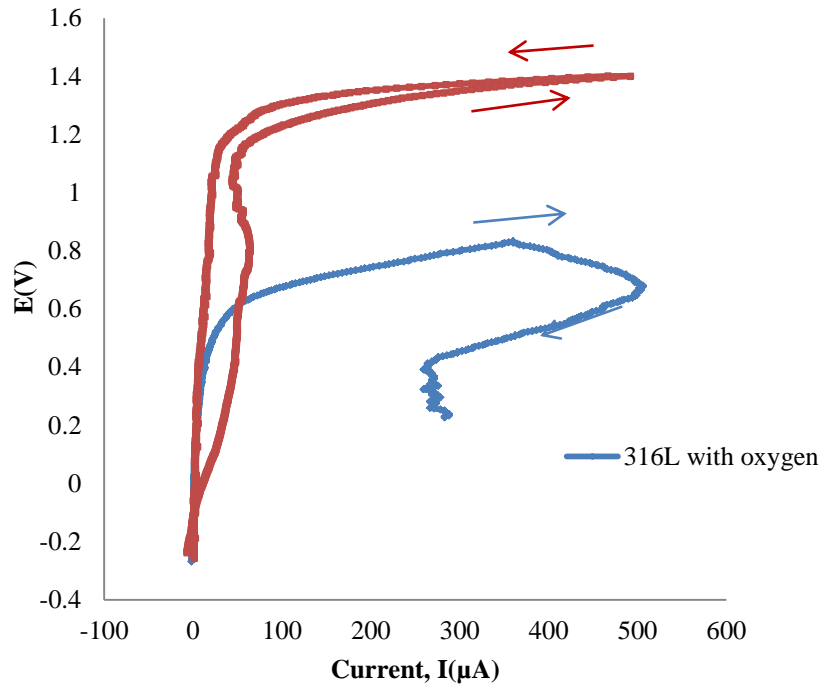


Figure 6.26 316L in S1 with and without oxygen at 4°C

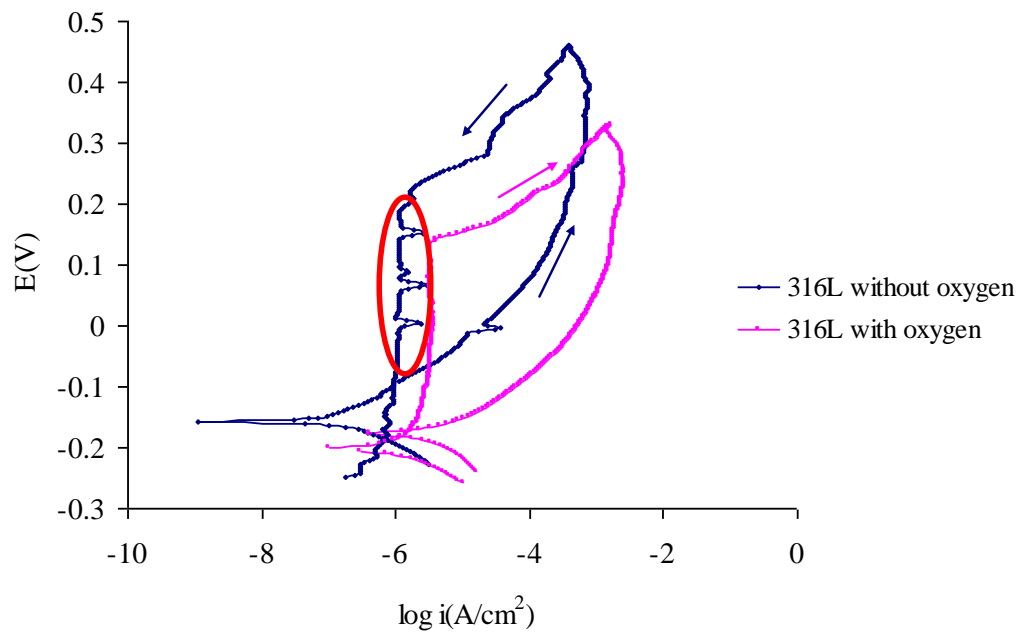


Figure 6.27 316L in S1 with and without oxygen at 20°C

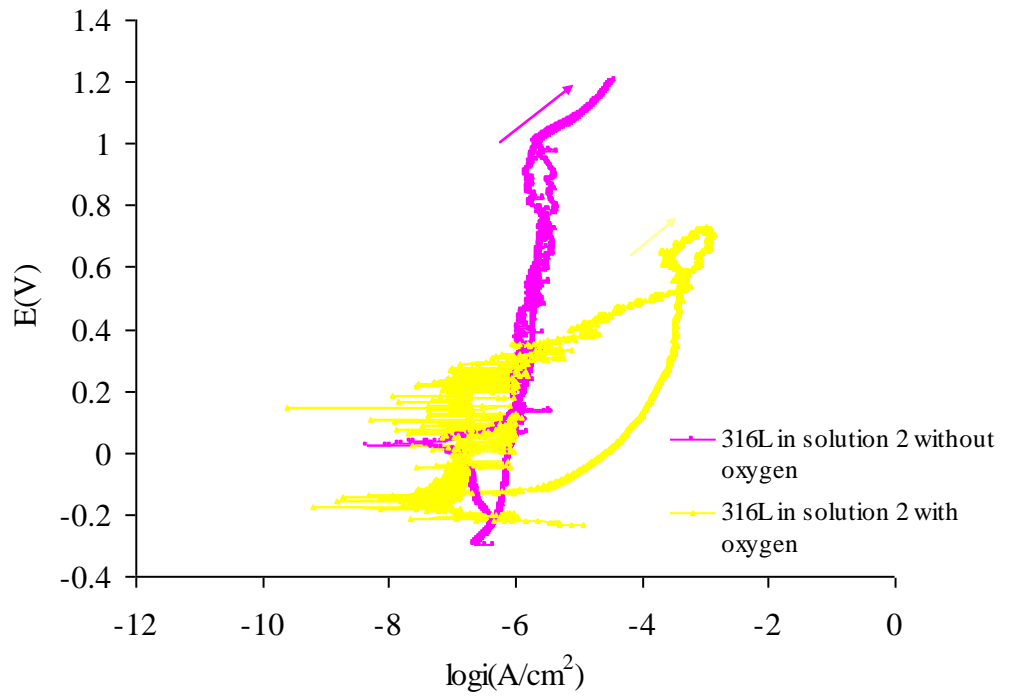


Figure 6.28 316L in S2 with and without oxygen at 4°C

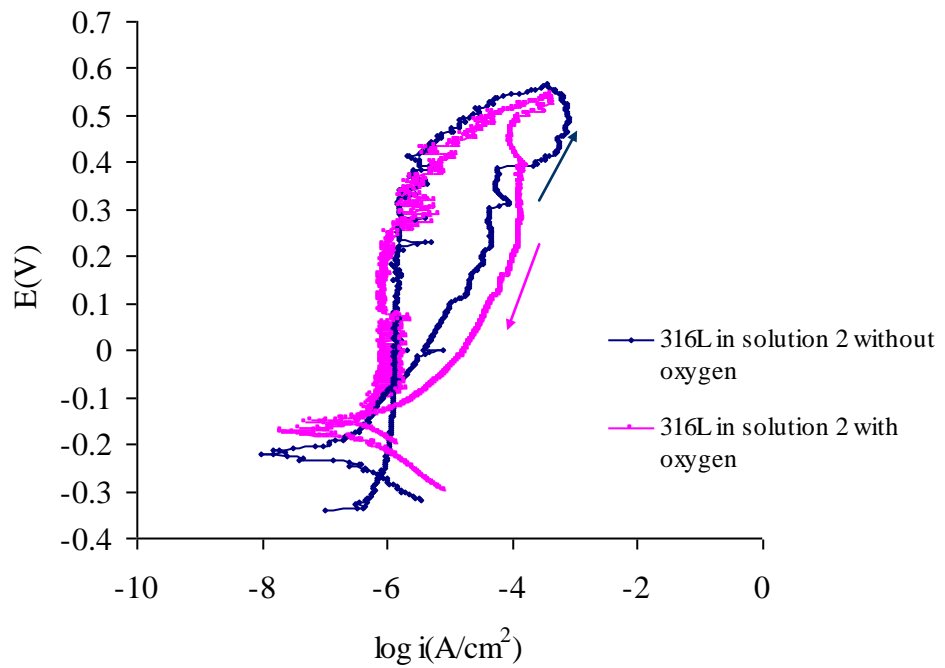


Figure 6.29 316L in S2 with and without oxygen at 20°C

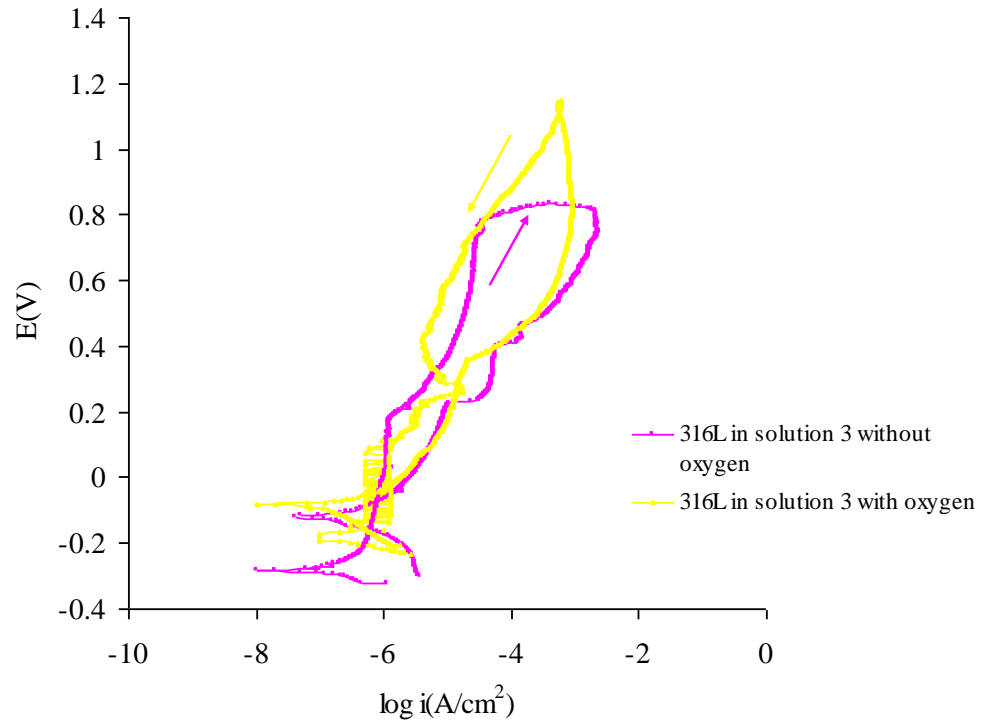


Figure 6.30 316L in S3 with and without oxygen at 4°C

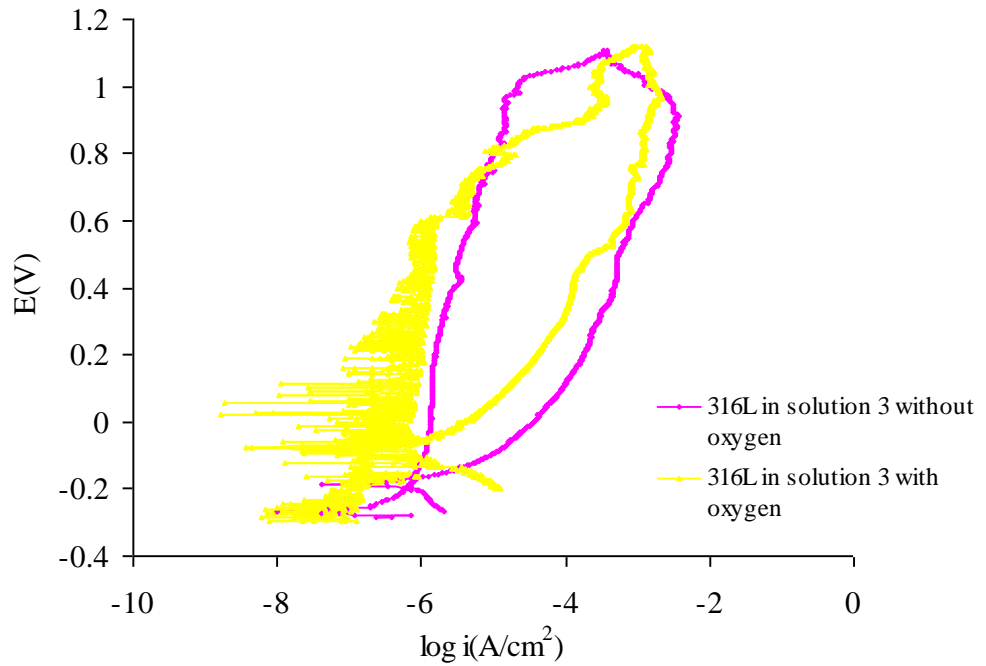
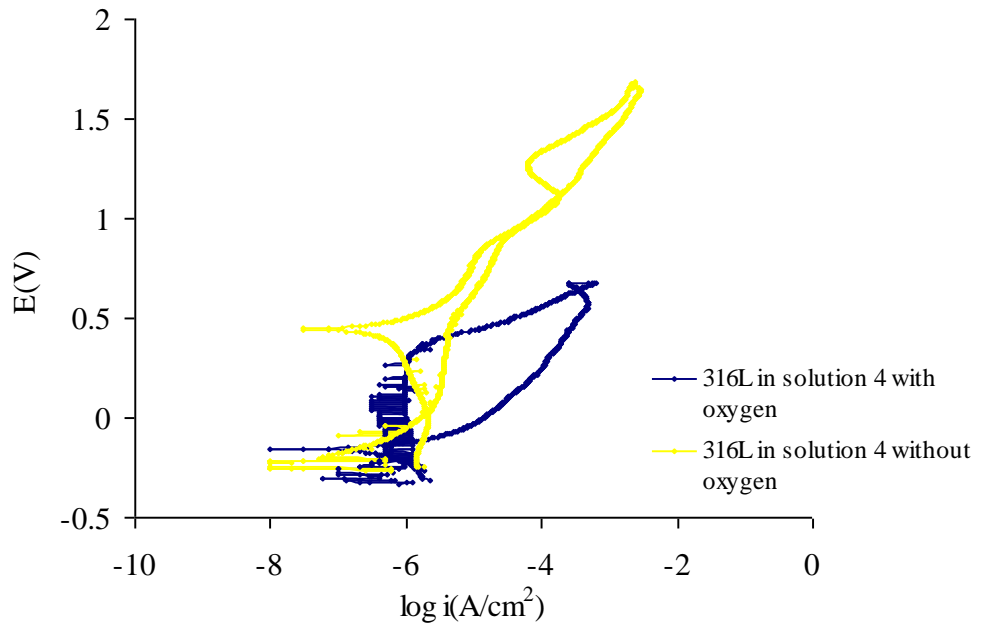
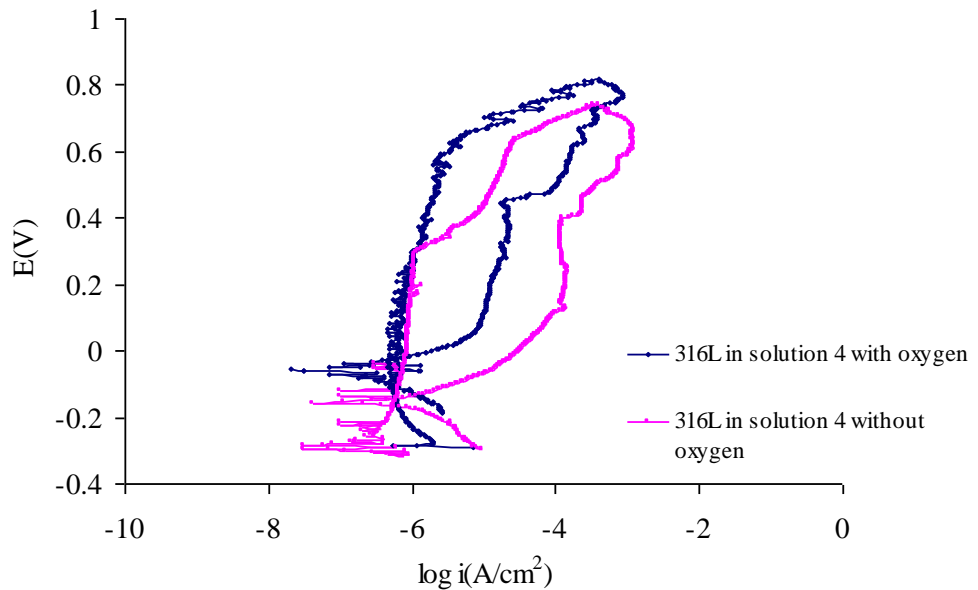


Figure 6.31 316L in S3 with and without oxygen at 20°C



**Figure 6.32 316L in S4 with and without oxygen at 4°C**



**Figure 6.33 316L in S4 with and without oxygen at 20°C**

Figure 6.34 to 6.41 presents the cyclic polarisation of 25Cr duplex in different  $\text{SO}_4^{2-}/\text{Cl}^-$  ratio with and without dissolved oxygen at 4°C and 20°C. The  $E_b$  value are summarised in Figure 6.50 and shows that 25Cr duplex are sustain at higher  $E_b$  value in every conditions which can be explained that 25Cr duplex is excel to resist corrosion attack in every environment conditions especially when there are no oxygen in solutions. However, the  $E_b$  value for 25Cr duplex is not really significant with and



without oxygen as compared to 316L which also explained that stability of 25Cr duplex in aggressive environment.

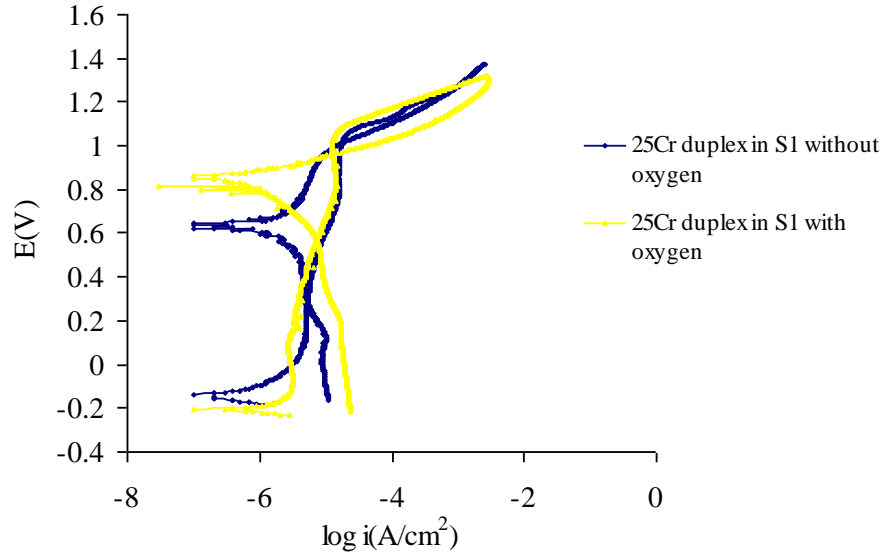


**Figure 6.34 25Cr duplex inS1 with and without oxygen at 4°C**

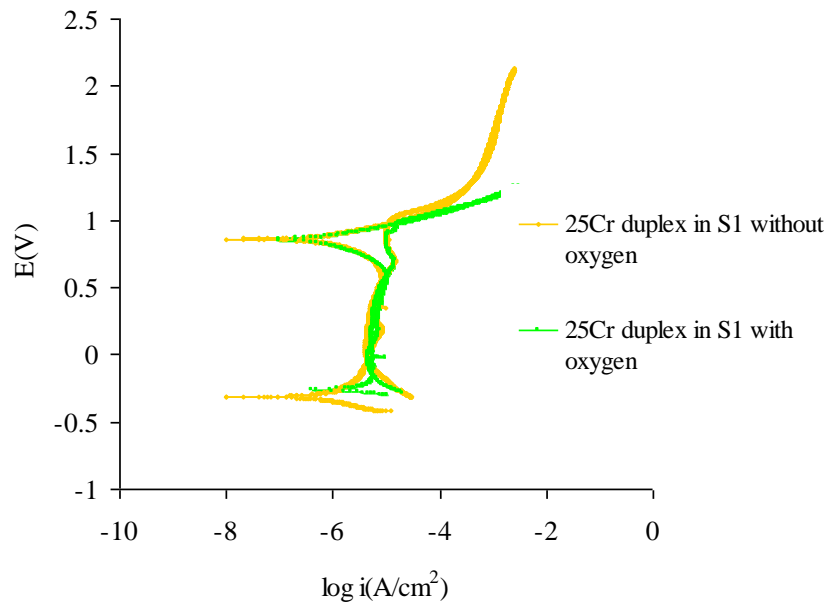


**Figure 6.35 25Cr duplex inS1 with and without oxygen at 20°C**

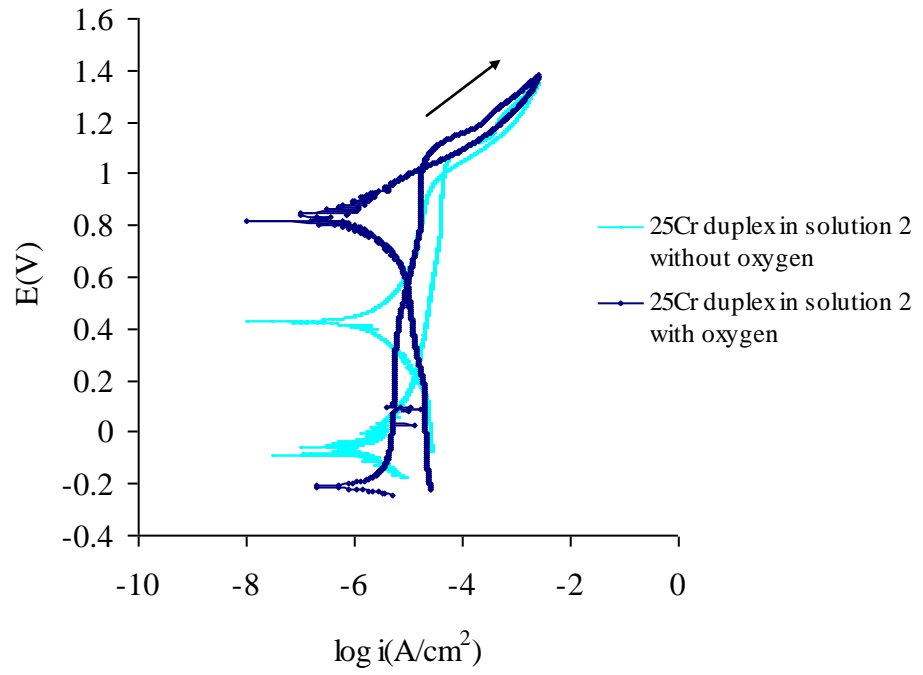


Figure 6.36 25Cr duplex inS2 with and without oxygen at 4°C

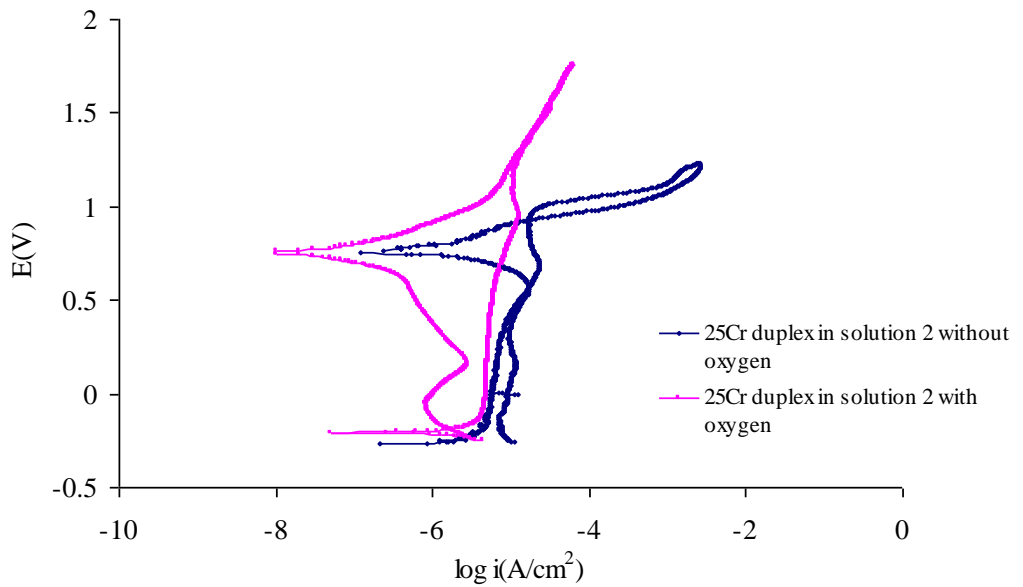


Figure 6.37 25Cr duplex inS2 with and without oxygen at 20°C

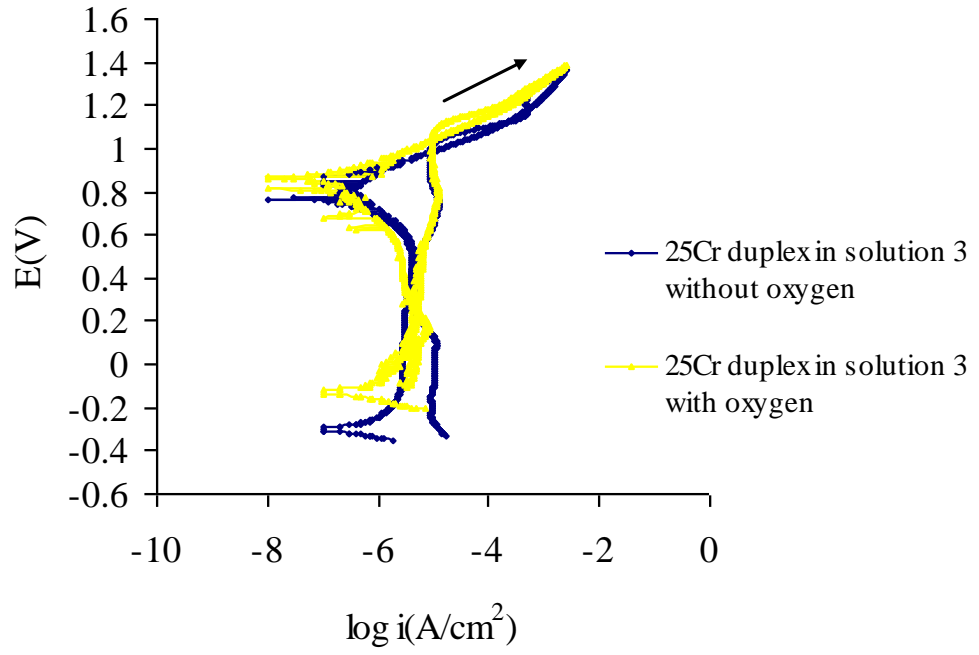


Figure 6.38 25Cr duplex inS3 with and without oxygen at 4°C

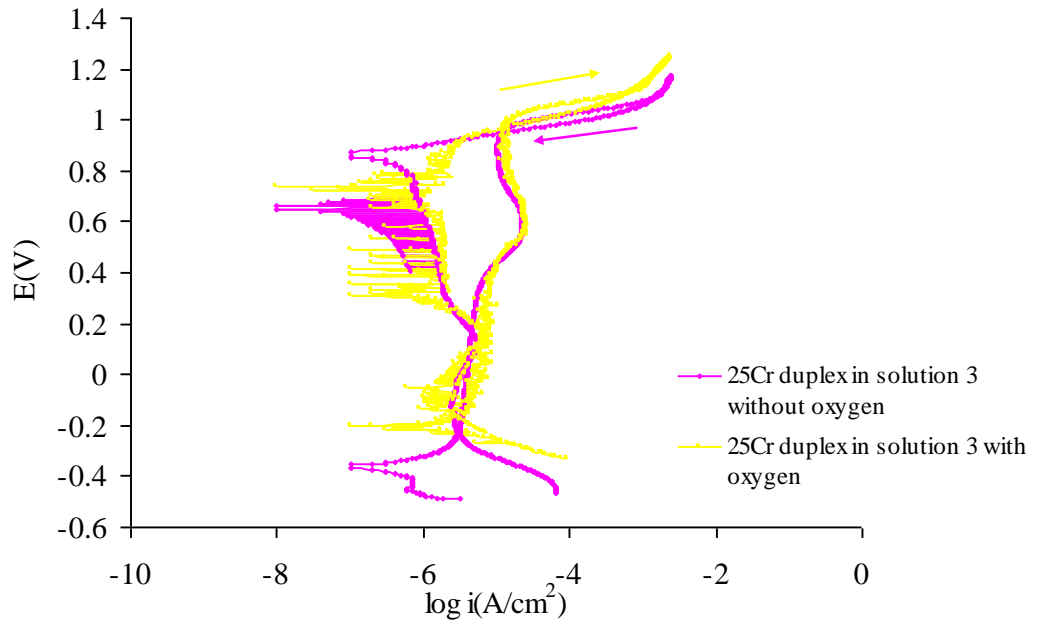
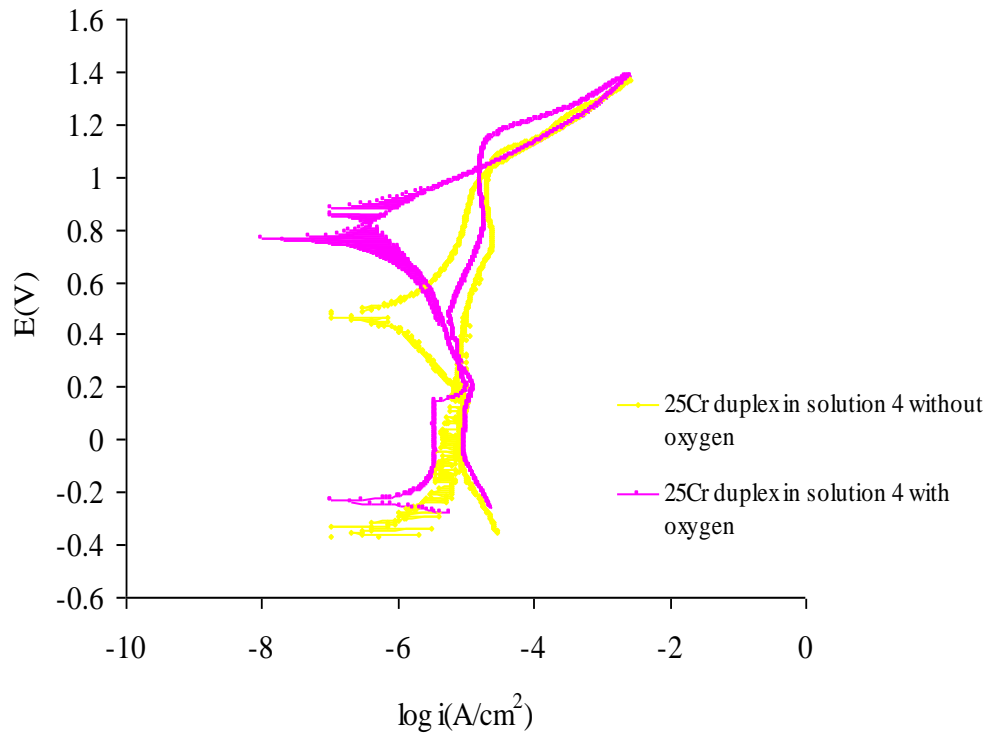
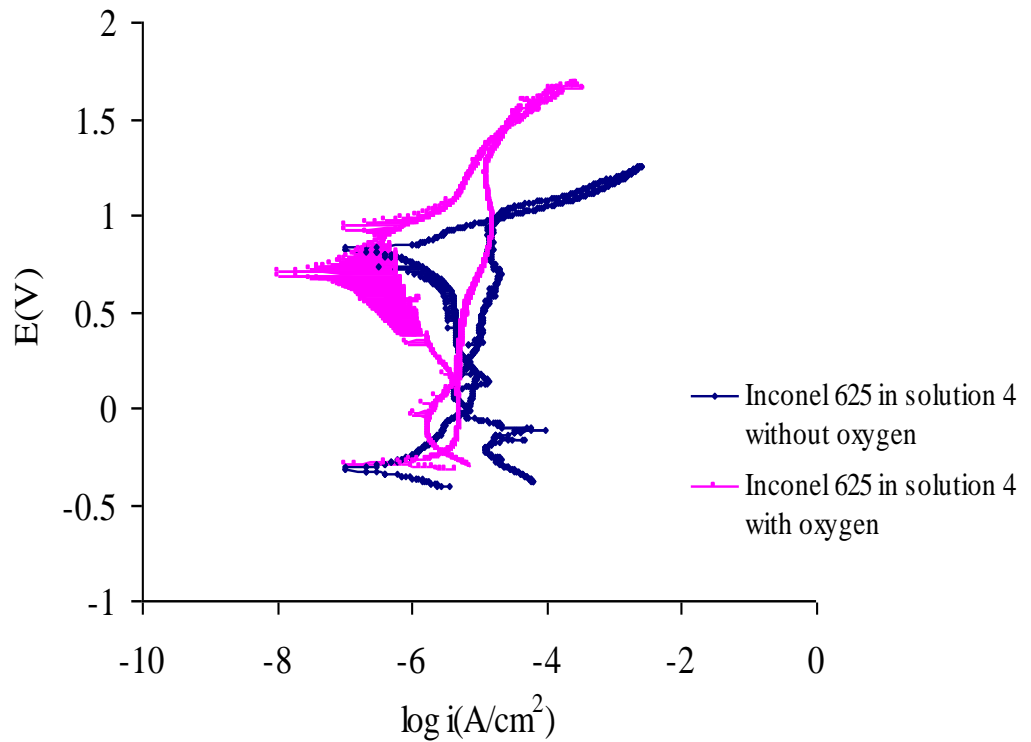


Figure 6.39 25Cr duplex inS3 with and without oxygen at 20°C



**Figure 6.40 25Cr duplex in S4 with and without oxygen at 4°C**



**Figure 6.41 25Cr duplex in S4 with and without oxygen at 20°C**

Figure 6.42 and 6.43 present cyclic polarisation curves of Inconel 625 in seawater (solution 1) at 4°C and 20°C respectively. Figure 6.44 to 6.51 presents the Inconel 625 in the changing  $\text{SO}_4^{2-}/\text{Cl}^-$  ratio conditions from seawater composition (solution 1) with and without dissolved oxygen at 4°C and 20°C. As stated previously, sulphate can behave as inhibiting effect to passive materials. However, the effectiveness depends on competitive reactions between sulphate and chloride [45]. Like the other materials, the  $E_b$  increased when the oxygen was purged from the solution. The value of  $E_b$  are quite complex to identified because sometimes the material presents to have secondary breakdown potential. According to Laycock (1999),  $E_b$  can be defined as a potential where the anodic *current* density first rise and *reached* a sustained level  $> 10 \mu\text{A}/\text{cm}^2$  [192]. In solution 2 and 3, the emergence of an active loop on the forward scan indicated that initial attempts to repassivate were not completely successful. The possibility that the observed active behaviour could be due to insufficient oxygen (it only happen in a solution without oxygen) to aid complete repassivation [193]. The value of  $E_b$  for 316L, 25Cr duplex and Inconel 625 in all solutions as compared to HW443 with and without oxygen content is summarised in Figure 6.50 and 6.50 at 4°C and 20°C respectively.

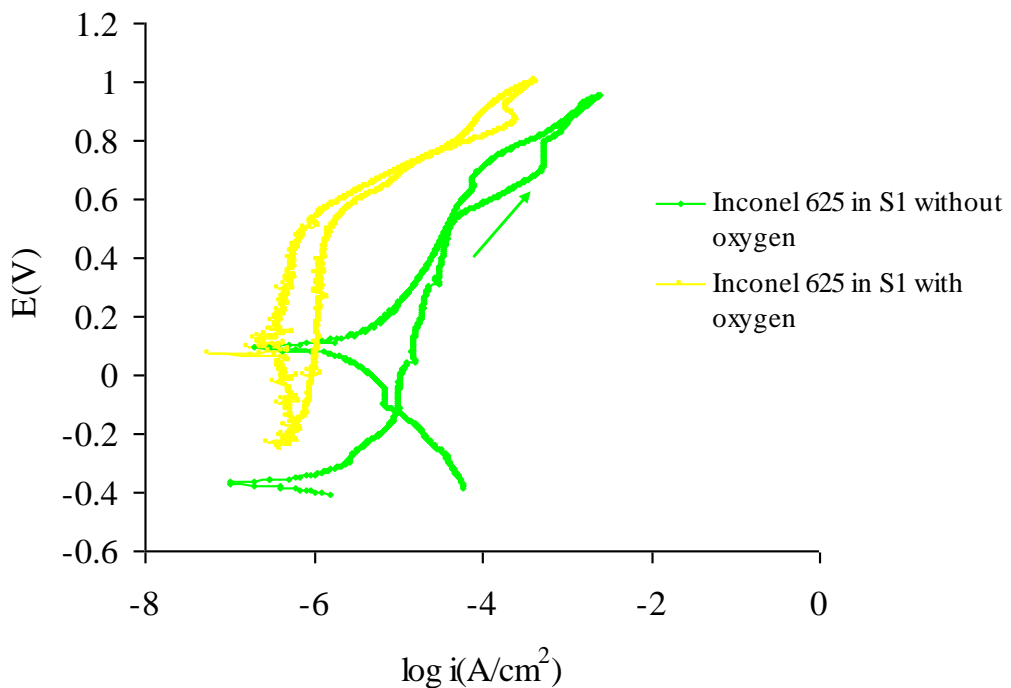


**Figure 6.42 Inconel 625 inS1 with and without oxygen at 4°C**

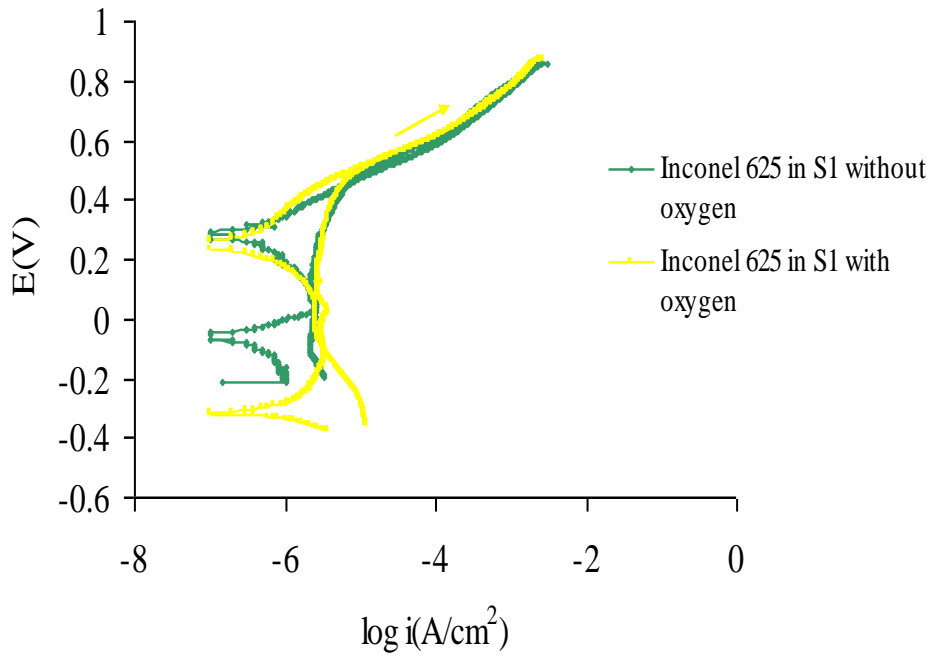


**Figure 6.43 Inconel 625 in S1 with and without oxygen at 20°C**

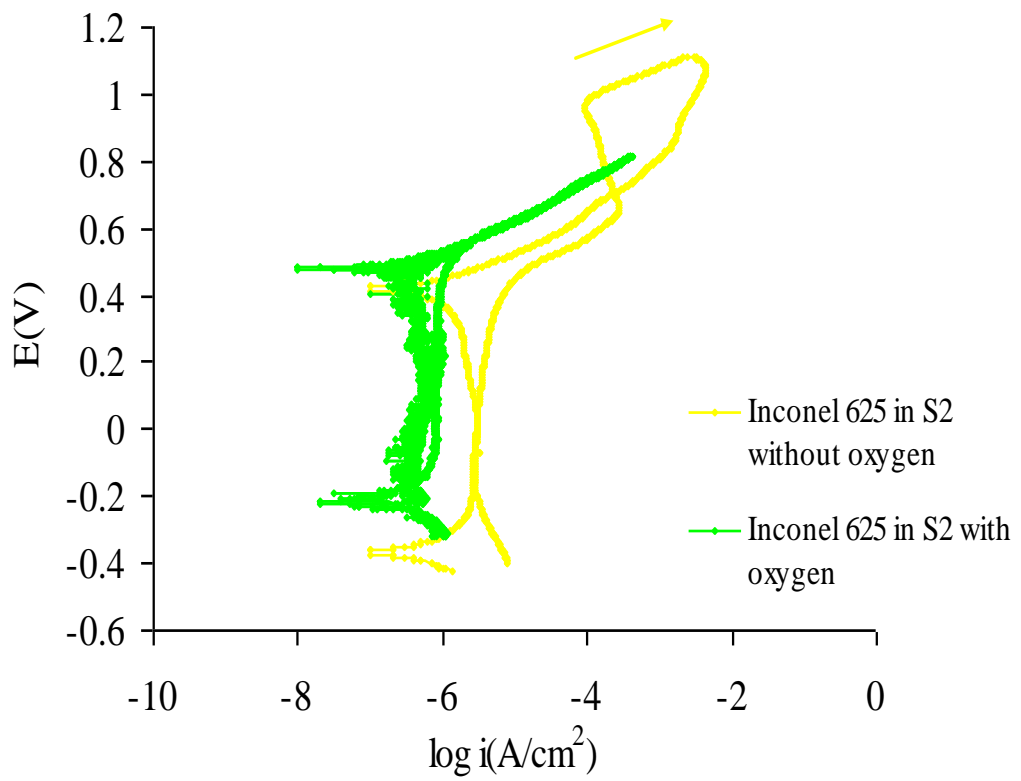


**Figure 6.44 Inconel 625 in S2 with and without oxygen at 4°C**

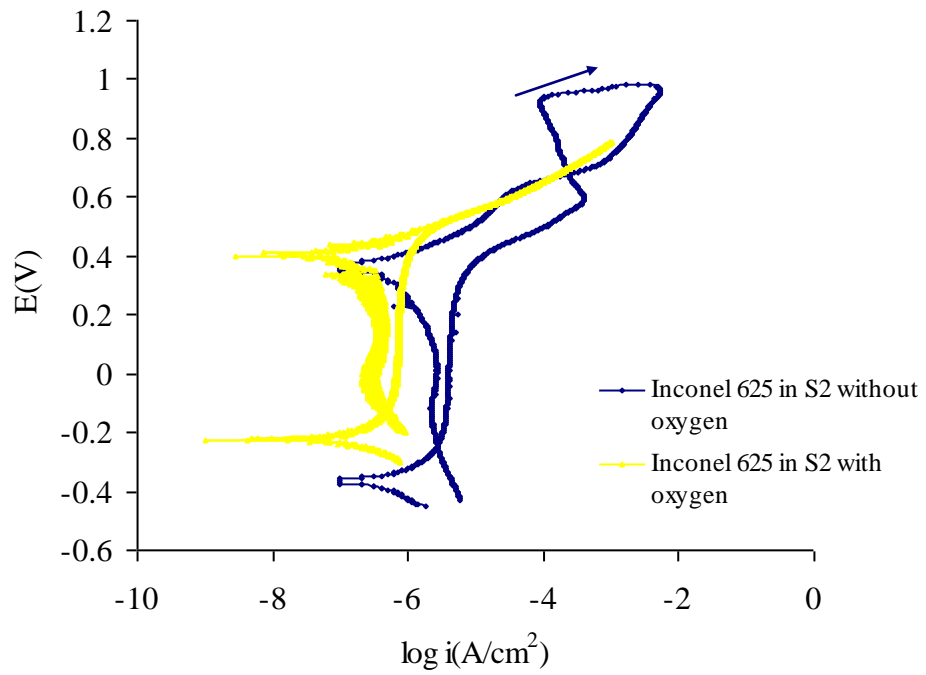


Figure 6.45 Inconel 625 in S2 with and without oxygen at 20°C

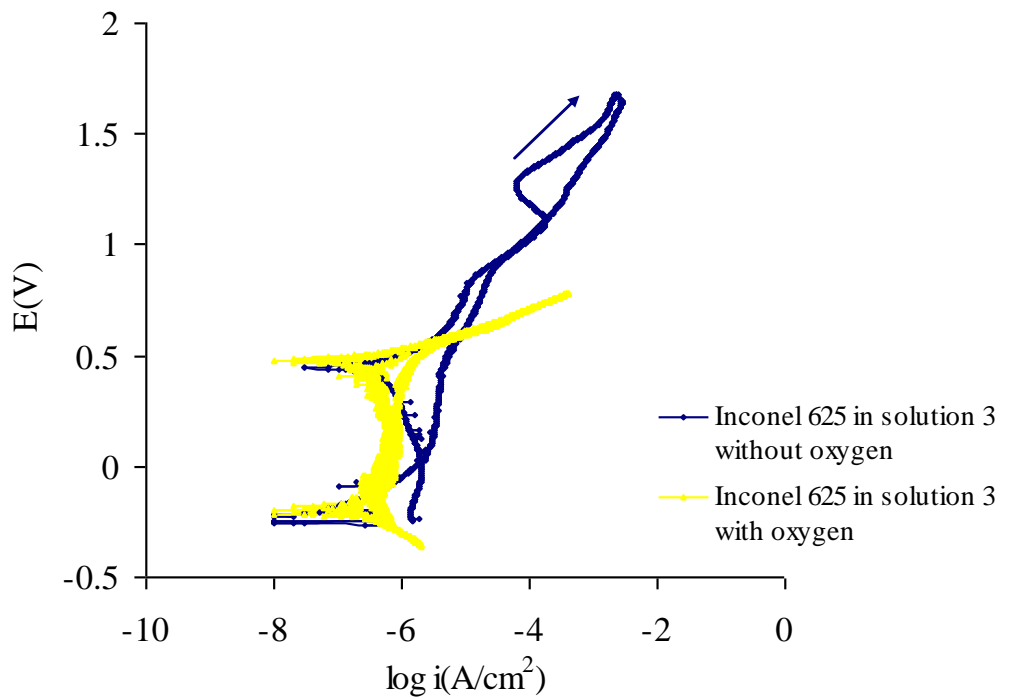


Figure 6.46 Inconel 625 in S3 with and without oxygen at 4°C

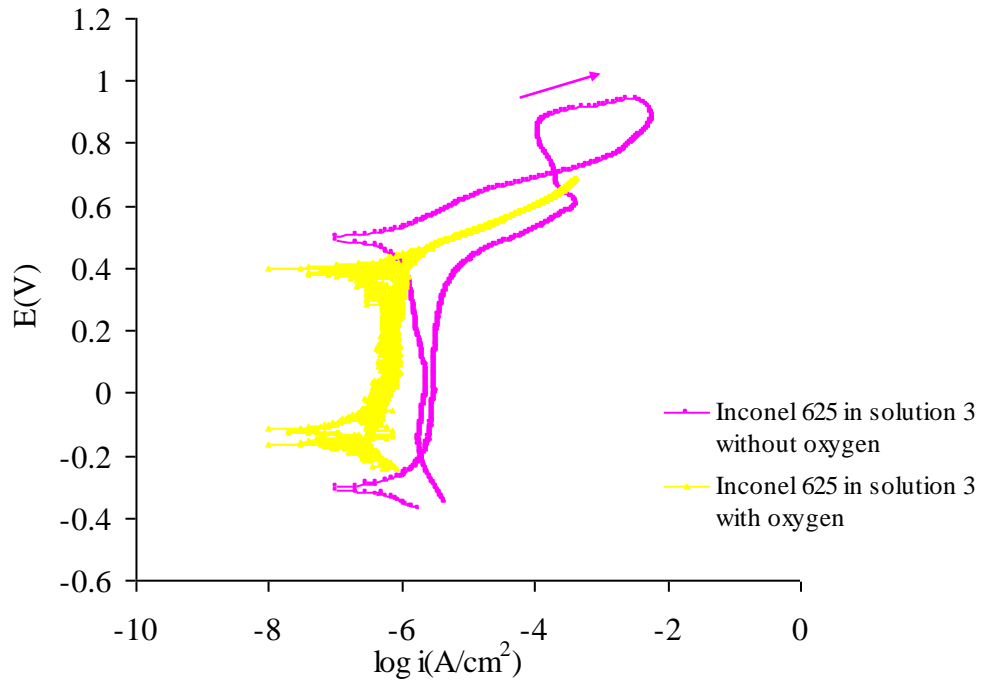


Figure 6.47 Inconel 625 in S3 with and without oxygen at 20°C

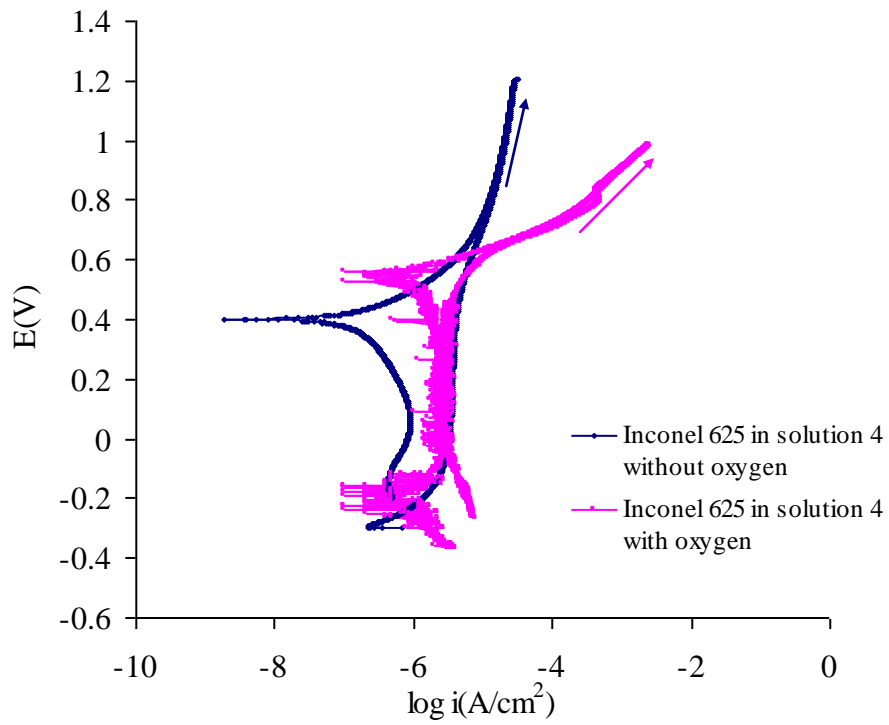
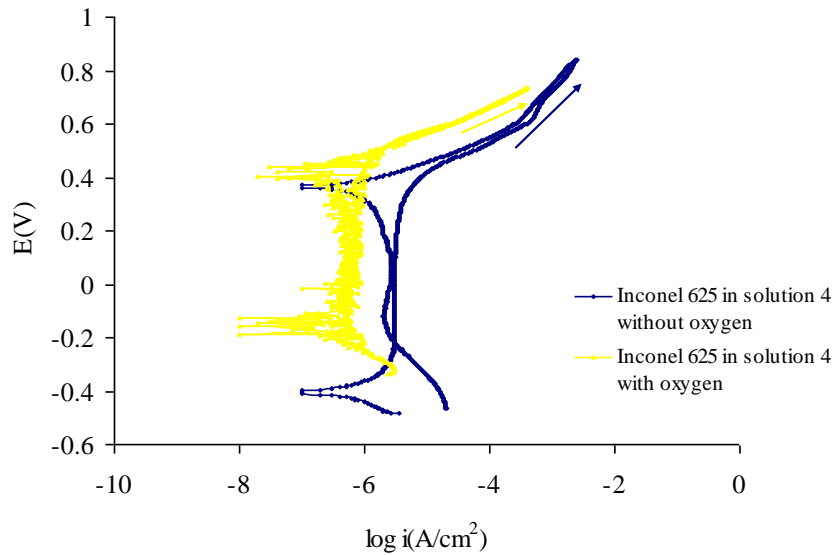


Figure 6.48 Inconel 625 in S4 with and without oxygen at 4°C





**Figure 6.49 Inconel 625 in S4 with and without oxygen at 20°C**

Figure 6.50 and 6.51 summarised the breakdown potential  $E_b$  value in all solutions with and without oxygen content at 4°C and 20°C. In both temperature, 316L presents to have the lowest  $E_b$  value compared to Inconel 625 and 25Cr duplex. The performance of Inconel 625 and 25Cr duplex more excel when oxygen was purged from solutions. However, the sulphate-chloride ratio is not significant in all solutions with or without oxygen. At 4°C, the highest  $E_b$  value was achieved by Inconel 625 in the solution 3 without oxygen content and 25Cr duplex perform to have high  $E_b$  in all solution at 20°C.

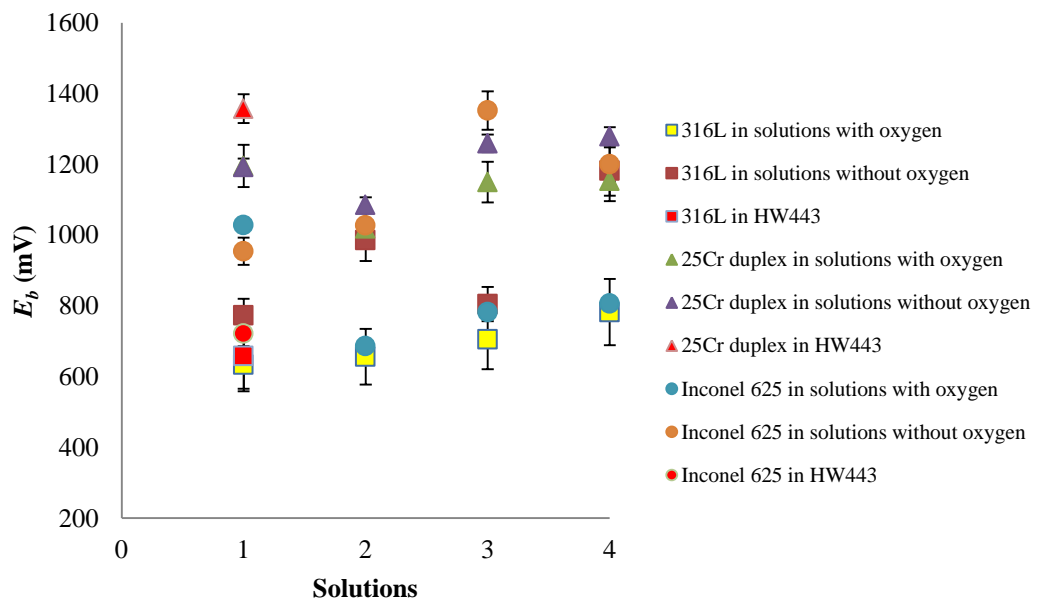


**Figure 6.50 Comparison of breakdown potential for passive alloys in every solution at 4°C**

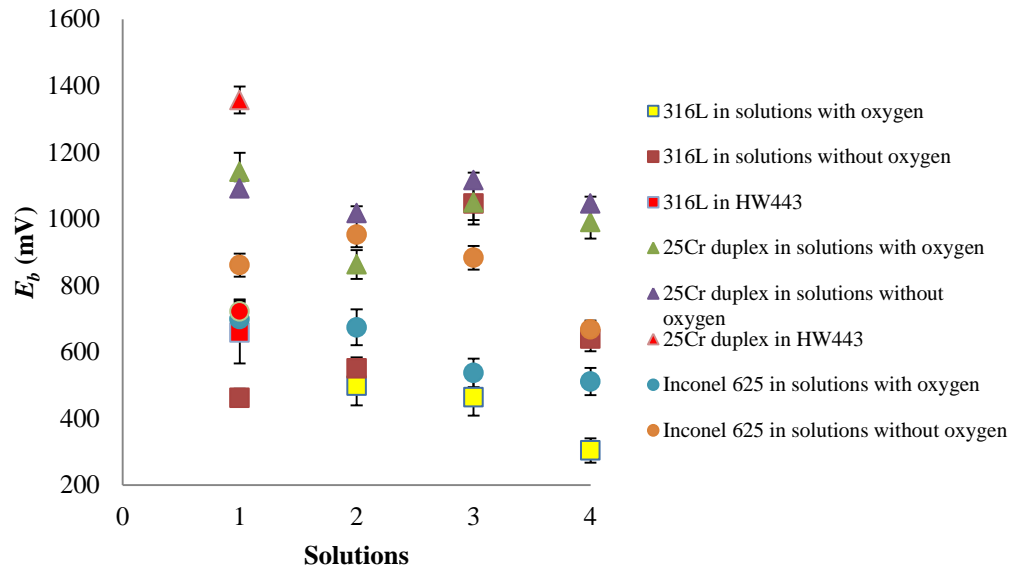



**Figure 6.51 Comparison of breakdown potential for passive alloys in every solution at 20°C**

## 6.8 Summary

This chapter presents all the data for CRAs alloy used in this research which are stainless steel 316L, 25Cr duplex and Inconel 625. The composition of these materials are presented in Chapter 4 section 4.1 and shows that 25Cr duplex has the highest chromium content followed by Inconel 625 and stainless steel 316L. The breakdown potential was used to study the aggressiveness of corrosion attack to different materials. The breakdown potential is an indication of the resistance to the initiation of corrosion [22]. A higher  $E_b$  signifies less corrosivity of material to localised attack and lower  $E_b$  signify easily attack by localised corrosion. Therefore, 25Cr duplex performs higher  $E_b$  in most of aggressive media. A ranking of fluid corrosivity from ‘best’ to worst’ at each temperature is prepared in Table 6.4 and Table 6.5 according to Figure 6.22. As temperature increased, the protective property of the oxide film degraded in every solution. Apart from varying the temperature, the composition of seawater was also varied according to different sulphate to chloride ratios. This table summarises that 25Cr duplex and Inconel 625 shows similar performance in corrosion resistance and 316L shows severe corrosion attack and is this proved by microscopy images. Table 6.5 was ranked according to Figure 6.6 to 6.8, 6.10 to 6.18 which presented the  $E_b$  of materials in different sulphate-chloride ratio at increasing temperatures. The value of  $E_b$  at 4°C in every solutions are considered the ‘Best’ and the difference of  $E_b$  from 0%-20% was labelled as 1 (best), 21%-40% labelled as 2, 41%-60% labelled as 3 (moderate), 61%

to 80% as 4 and 81% -100% is 5 (the 'Worst'). The performance of materials in solution 1 (seawater), solution 1 (S1) with inhibitor, S1 without oxygen at 4°C and 20°C and the highest  $E_b$  value (in S4 at 4°C) is presented in Figure 6.53 as compared to  $E_b$  value performed in commercial hydraulic fluid, HW443.

**Table 6.4** The performance of breakdown potential,  $E_b$  for passive alloys in different composition of sulphate/chloride ratio at increasing temperature.

Solutions	Best  Worst		
	Solution 1 ( $\text{SO}_4^{2-}=0.14$ )	25Cr duplex	Inconel 625
Solution 2 ( $\text{SO}_4^{2-}=19.15$ )	25Cr duplex	Inconel 625	316L
Solution 3 ( $\text{SO}_4^{2-}=0.75$ )	25Cr duplex	Inconel 625	316L
Solution 4 ( $\text{SO}_4^{2-}=0.99$ )	25Cr duplex	Inconel 625	316L

**Table 6.5** The rank of performance for passive alloys in different sulphate/chloride ratio (1-5 is Best to Worst)

Solutions	Material	Temperature			
		4°C	20°C	50°C	80°C
Solution 1 ( $\text{SO}_4^{2-}=0.14$ )	316L	1	4	5	5
	25Cr Duplex	1	1	1	2
	Inconel 625	1	3	3	4
Solution 2 ( $\text{SO}_4^{2-}=19.15$ )	316L	1	1	3	4
	25Cr Duplex	1	1	1	1
	Inconel 625	1	1	1	2
Solution 3 ( $\text{SO}_4^{2-}=0.75$ )	316L	1	2	3	5
	25Cr Duplex	1	1	1	2
	Inconel 625	1	2	3	3
Solution 4 ( $\text{SO}_4^{2-}=0.99$ )	316L	1	4	5	5
	25Cr Duplex	1	1	1	4
	Inconel 625	1	2	3	3

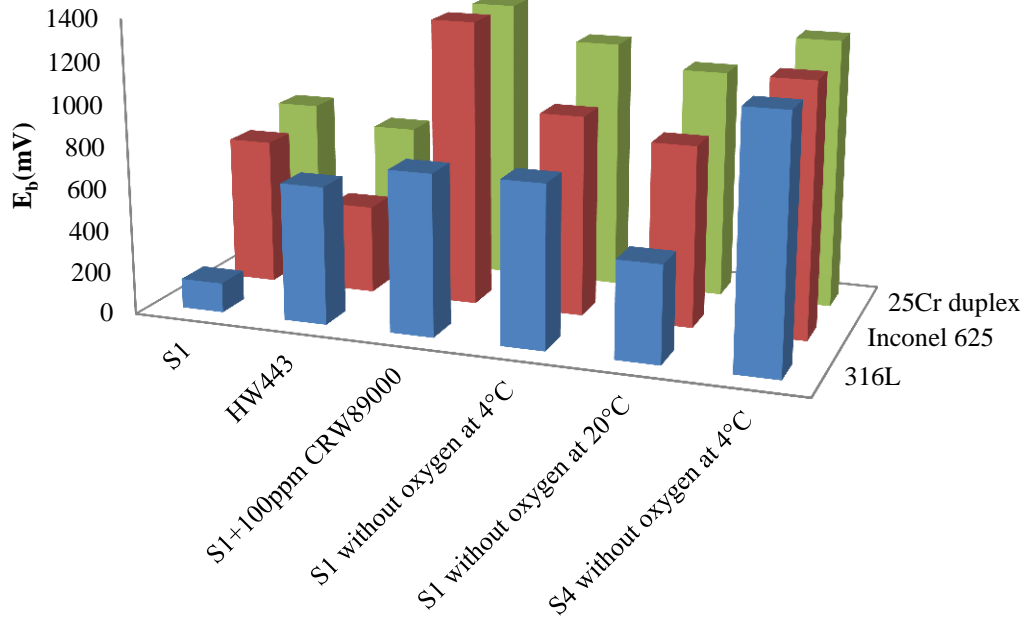


**Figure 6.52 Comparison of materials in different media as compared to HW443**

## Chapter 7

### CERMETS ALLOYS

#### 7.1 Introduction

Cermets have been used in some components in subsea valves and so this study assessed their corrosion behaviour in seawater and compared the rates and mechanisms with carbon steel and the passive alloys in chapter 6 using cyclic polarisation. Tungsten carbide (WC) or cemented carbides are composite materials consisting of tungsten carbide grains cemented together by a metallic binder, most probably cobalt (Co). They are known for their combined high hardness, due to the hard WC phase and working toughness due to the binder. Cemented carbides have applications spanning most engineering fields. However, applications in chemically aggressive environments are less successful because they are susceptible to corrosion [143]. For WC-Co, the corrosion properties in acidic and neutral electrolytes are controlled by the corrosion resistance of the Co binder [115,144]. WC dissolution becomes more significant at alkaline pH [39].

The Co binders are modified by dissolving tungsten (W) and carbon (C) during the sintering process [77]. This modification of composition slightly improves the corrosion resistance of cermets alloy. Since the corrosion behaviour of cermets alloy is governed by the galvanic coupling of the anodic metallic binder to the cathodic ceramic phase. Then, the only method that has been used to improve the corrosion resistance is the use of corrosion resistant binders such as Ni, Ni-Cr and Ni-Cr-Mo [144,145]. However, problems still exist in offshore oil industry field when using nickel tungsten carbide (WC-Ni) in the hydraulic system due to the complex factors relating to the corrosion process and how the environment parameters affect the corrosion mechanisms. A good understanding of the corrosion factors together with the critical point of environment parameters and cermets alloy is then necessary.

In this study, the cermet alloys – WC-6%Co and WC-9%Ni – are used to evaluate the corrosion performance in seawater and different  $\text{SO}_4^{2-}/\text{Cl}^-$  ratios of seawater at

different temperatures. The performance will then be compared to the performance of each material in HW443 hydraulic fluid.

The surface microstructure of WC-Co and WC-Ni are shown alongside the elemental composition respectively in Figure 7.1 and Figure 7.2 generated from SEM/EDX analysis.

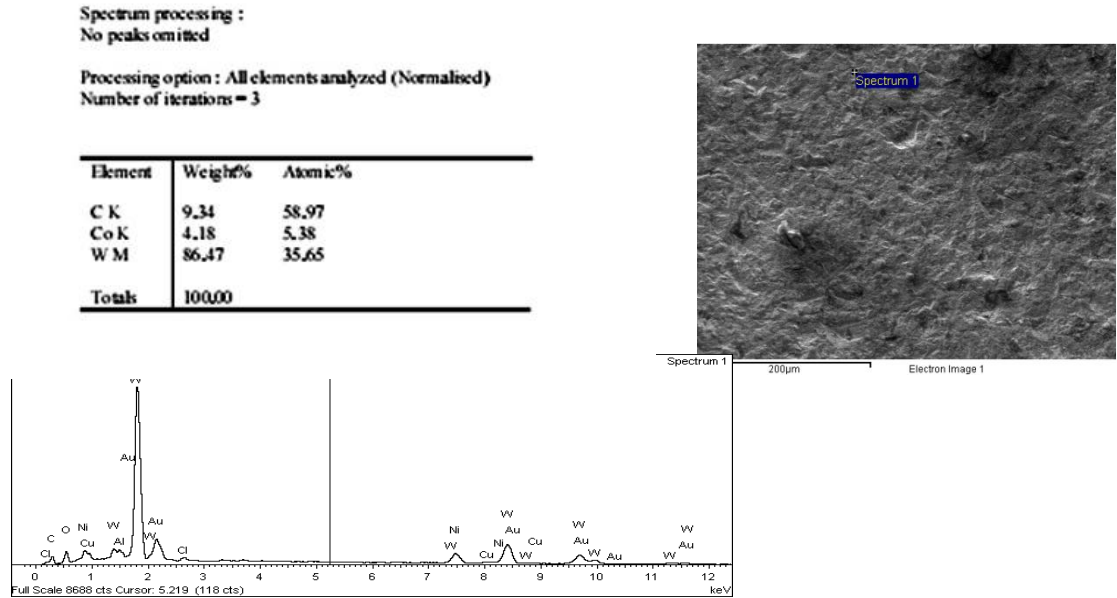


**Figure 7.1 SEM/EDX analysis of received cobalt tungsten carbide sample**

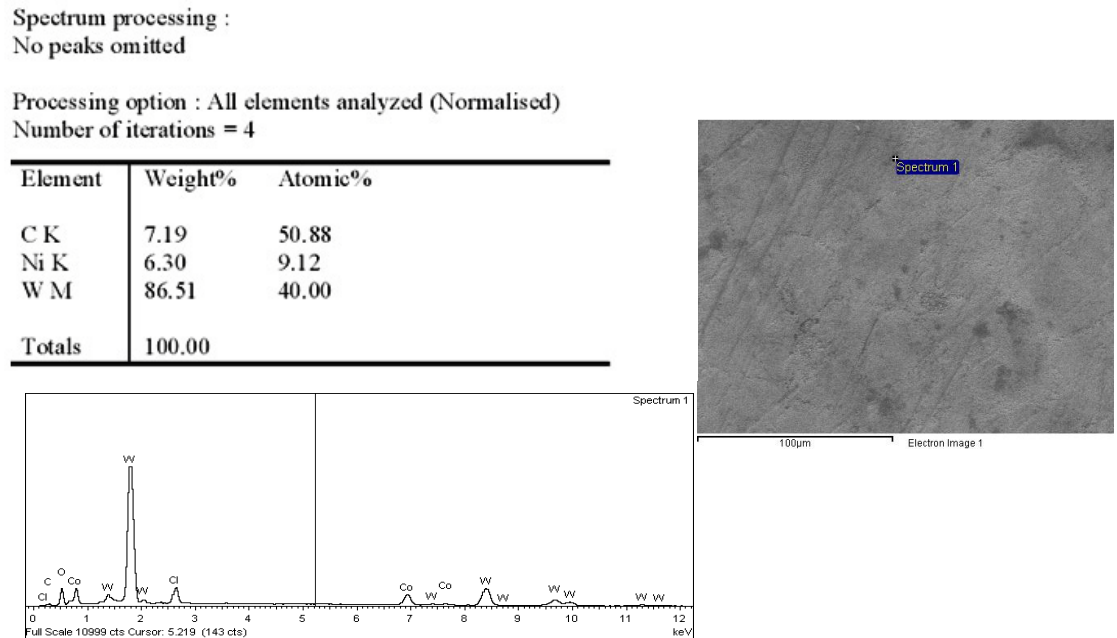


**Figure 7.2 SEM/EDX analysis of received nickel tungsten carbide sample**

## 7.2 Cermet Alloys in HW443

Figure 7.3 presents the anodic polarisation of WC-Co and WC-Ni in commercial hydraulic fluid HW443. The electrochemical response is totally different to passive materials, as they do not experience passive breakdown. These curves have negative hysteresis and do not have an obvious passive region on the forward scans. Both materials do not exhibit passivity but behave as active materials in HW443. In the forward scan, the current density increases consistently from the OCP as the potential progressively increases.

The corrosion current density,  $i_{corr}$  is determined by Tafel extrapolation, and the values are  $2.50 \mu\text{A}/\text{cm}^2$  for WC-Co and  $1.72 \mu\text{A}/\text{cm}^2$  for WC-Ni. The  $i_{corr}$  value for WC-Co is much higher than WC-Ni under the same condition, indicating that the corrosion resistance of WC-Ni is better than WC-Co in HW443. The forward scan becomes linear at around 20mV from OCP on E-log I relation allowing the  $i_{corr}$  to be determined.

The reverse potential,  $E_r$  is the potential at which the current density reaches the pre-set value of  $500 \mu\text{A}/\text{cm}^2$ . This could be an indication of the corrosion resistance of the active materials. A higher  $E_r$  demonstrates a larger over-potential required for corrosion to occur at the same rate. The  $E_r$  value for WC-Co and WC-Ni are 808 mV and 965 mV, respectively.

The protection potential,  $E_p$  reveals how efficiently the current density drops when the potential decreases. It is the point of intersection of anodic and cathodic branch on the reverse scan. The OCP is the potential of material under freely corroding conditions. The values of all electrochemistry in HW443 are presented in Table 7.2.

Although the corrosion rate is complex because of the nature of the material, but it is not negligible. With considering that the corrosion occurs generally on the entire surface, average corrosion rate of cermets alloy can be estimated by quoting  $i_{corr}$  value according to;

$$\text{Corrosion rate, } C_R \text{ (mpy)} = i_{corr} \times (\Lambda) \times (1/\rho) \times \varepsilon \text{ -----[23]}$$

Where  $\Lambda$  is a combination of several conversion terms and is  $1.2866 \times 10^5$  (equivalent  $\cdot$  sec  $\cdot$  mils)/(Coulombs  $\cdot$  cm  $\cdot$  years).  $\rho$  is the density of the cermets with a value of  $15\text{g}/\text{cm}^3$  and the value of  $\varepsilon$  of WC-Co cermets is 16.5 g/equivalent and  $\varepsilon$  of WC-Ni, the following equation is applied:

$$\varepsilon = \frac{1}{\sum_{i=1}^m \frac{x_i z_i}{M_i}} \text{-----[8]}$$

The weight percent, atomic weight and valence value for each element are listed below. The effective equivalent weight obtained is 18.40 g/equivalent. The corrosion rate obtained in Table 7.2 elucidate that corrosion rate of WC-Co is higher than WC-Ni in commercial hydraulic fluid HW443.

**Table 7.1 Element value**

Element	Weight% (x)	Atomic weight (M)	Valence (z)
C	7.2	12.01	4
W	86.5	183.85	6
Ni	6.3	58.70	2

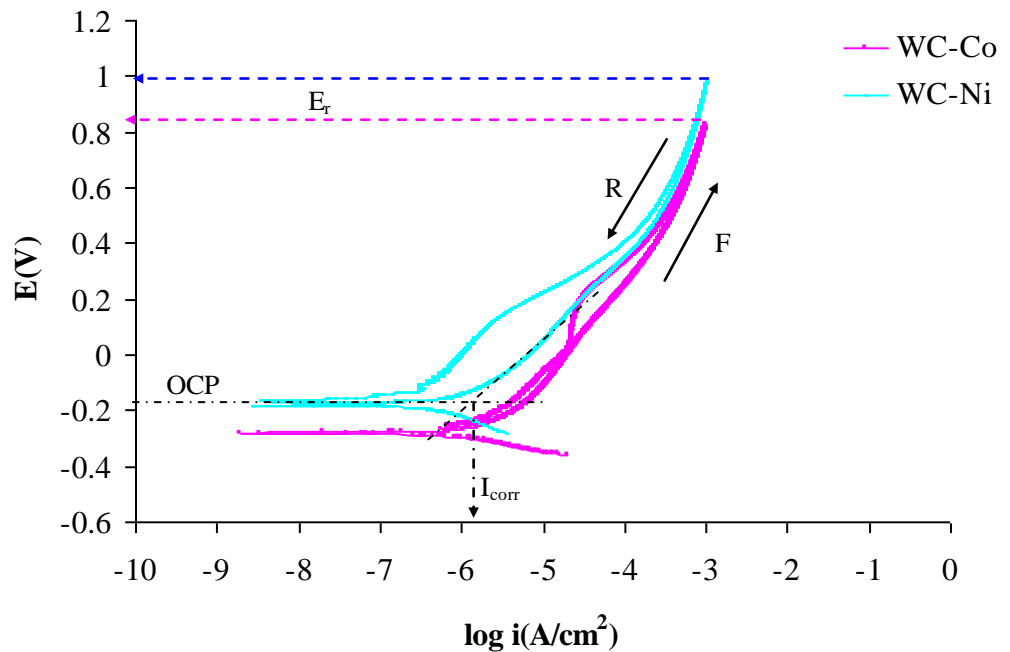


**Figure 7.3 Potential versus current density for WC-Co and WC-Ni in HW443 at 20°C**



**Table 7.2 Electrochemical parameters of materials in HW443 at 20°C**

Material	$E_r$ (mV)	OCP (mV)	$E_p$ (mV)	$i_{corr}$ ( $\mu\text{A}/\text{cm}^2$ )	$C_R$ (mpy)
WC-Co	965	-279	-286	2.50	0.35
WC-Ni	808	-182	-174	1.72	0.13

### 7.3 WC-Co in Seawater and Different $\text{SO}_4^{2-}/\text{Cl}^-$ Ratios

For passive alloys (Chapter 6), different  $\text{SO}_4^{2-}/\text{Cl}^-$  ratios do have some effect on the breakdown of the passive layer on the metal surface. The effect of the  $\text{SO}_4^{2-}/\text{Cl}^-$  ratio was also studied for cermets alloys. Figure 7.4 presents the cyclic polarisation of WC-Co in S1 (seawater) at different temperatures. Cyclic polarisation exhibits positive hysteresis (except at 20°C) as the reverse scan is below the forward scan. At the temperature, 4°C, 20°C and 80°C, there is no protection on the reverse scan until the potential drops to OCP. The temperature affects the corrosion behaviour in a same way as in HW443, which can be proved by the data supplied in Table 7.3. By using the same calculation as WC-Co in HW443, the value of corrosion rate (mpy) and other electrochemical parameters for WC-Co in different  $\text{SO}_4^{2-}/\text{Cl}^-$  ratio are presented in Table 7.3. CPP curves of WC-Co in other solutions are presented in the Appendix (Figure A.5 to Figure A.7).

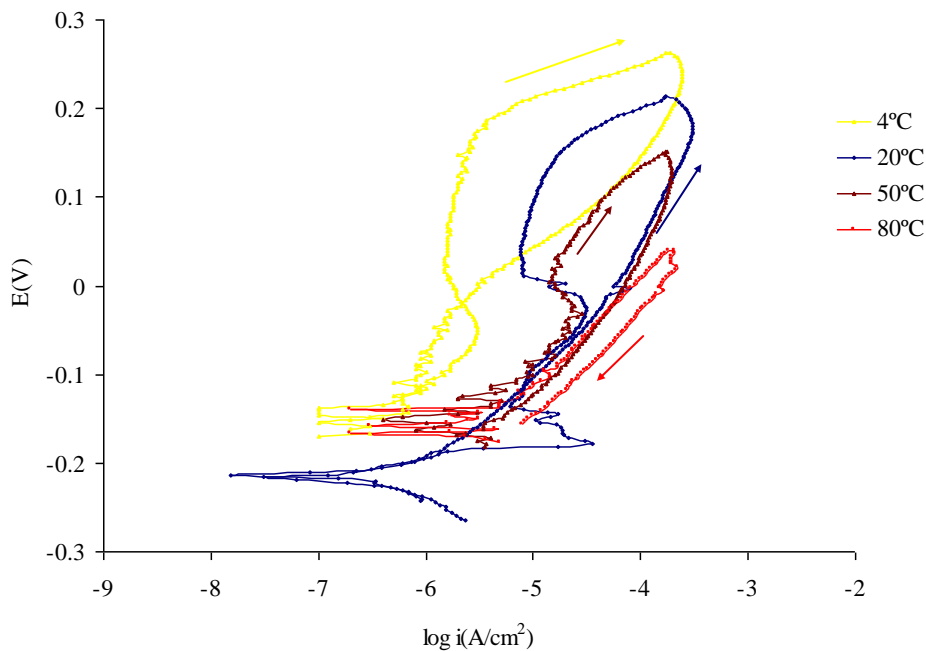


**Figure 7.4 Anodic polarisation of WC-Co in S1 at different temperatures**

The reverse potential,  $E_r$ , of WC-Co in all solutions as a criterion of corrosivity at elevated temperature are presented in Figure 7.5. This figure reveals that increasing the temperature gives an obvious effect of lowering the  $E_r$ . However, in solution 2 ( $\text{SO}_4^{2-}/\text{Cl}^-$  ratio is 0.75) WC-Co shows the value increase about 7% from 4°C to 20°C. WC-Co become least corrosive in solution 4 ( $\text{SO}_4^{2-}=10.95\text{mg/l}$  and the  $\text{Cl}^-=11\text{ mg/l}$ ) at 4°C and 20°C but become the most corrosion when the temperature increase to 50°C and 80°C. The amount of sulphate and chloride in solution 4 is almost equal. Therefore, the high value of  $E_r$  at low temperature might be inhibiting effect of sulphate whereas  $E_r$  value at high temperature are caused by competitive absorption between sulphate and chloride and left chloride to perforate corrosion attack. The  $E_r$  of WC-Co in solution 3 presents tremendous performance at elevated temperature regardless at 4°C and 20°C. Although the amount of sulphate is about half and chloride content is higher as compared to solution 2, this performance of  $E_r$  is better as compared to WC-Co in solution 2. WC-Co performs an outstanding performance in solution 4°C at 20°C when compared to commercial hydraulic fluid HW443. Clearly, the  $E_r$  value of WC-Co in solution 4 can compete the performance performed by HW443 at 20°C. However, at increasing temperature, the performance becomes the worse.

Figure 7.6 presents the corrosion rate of WC-Co in different  $\text{SO}_4^{2-}/\text{Cl}^-$  ratio as a function of temperature. Corrosion rate increased as the temperature increased as expected. The worse corrosion rate occur on WC-Co in solution 1 (seawater) and solution 2 performed the best result as compared to other solutions. The corrosion rate increased from 4°C to 20°C almost 83% and maintained until 80°C. Solution 2 has higher sulphate content compared to chloride ( $\text{SO}_4^{2-}=20.87\text{mg/l}$  and the  $\text{Cl}^-=1.09\text{ mg/l}$ ). At lower temperature, the sulphate content react as inhibiting agent while at higher temperature, the chloride dominate the competition and increased corrosion attack. By comparing the corrosion rate overall, all solutions are less corrosion attack compared to solution 1 (seawater). However, if compare to HW443 at 20°C, solution 3 and 4 has better corrosion rate. Solution 3 and 4 has higher chloride content than sulphate. This is contradict to explain that sulphate has inhibiting effect to WC-Co.

**Table 7.3 Electrochemical parameter for WC-Co in all solutions**

Solution	Temperature (°C)	$E_r$ (mV)	OCP (mV)	$E_p$ (mV)	$i_{corr}$ ( $\mu\text{A}/\text{cm}^2$ )	$C_R$ (mpy)
<b>S1</b> $\text{SO}_4^{2-}/\text{Cl}^-=0.14$	4	260	-170	N/A	1.60	0.23
	20	213	-214	N/A	5.01	0.71
	50	151	-151	149	7.92	1.12
	80	36	-140	N/A	15.03	2.13
<b>S2</b> $\text{SO}_4^{2-}/\text{Cl}^-=19.15$	4	337	-62	-56	0.5	0.07
	20	364	-96	N/A	3.0	0.42
	50	206	-163	N/A	3.1	0.44
	80	11.98	-256	-333	3.2	0.45
<b>S3</b> $\text{SO}_4^{2-}/\text{Cl}^-=0.75$	4	928	-117	-64	0.3	0.04
	20	770	-190	N/A	0.3	0.04
	50	530	-170	N/A	3.2	0.45
	80	394	-210	N/A	4.46	0.63
<b>S4</b> $\text{SO}_4^{2-}/\text{Cl}^-=0.99$	4	1127	-165	N/A	0.6	0.08
	20	1028	-152	N/A	1.9	0.27
	50	154	-224	N/A	5.6	0.79
	80	116	-175	-72	15.8	2.24

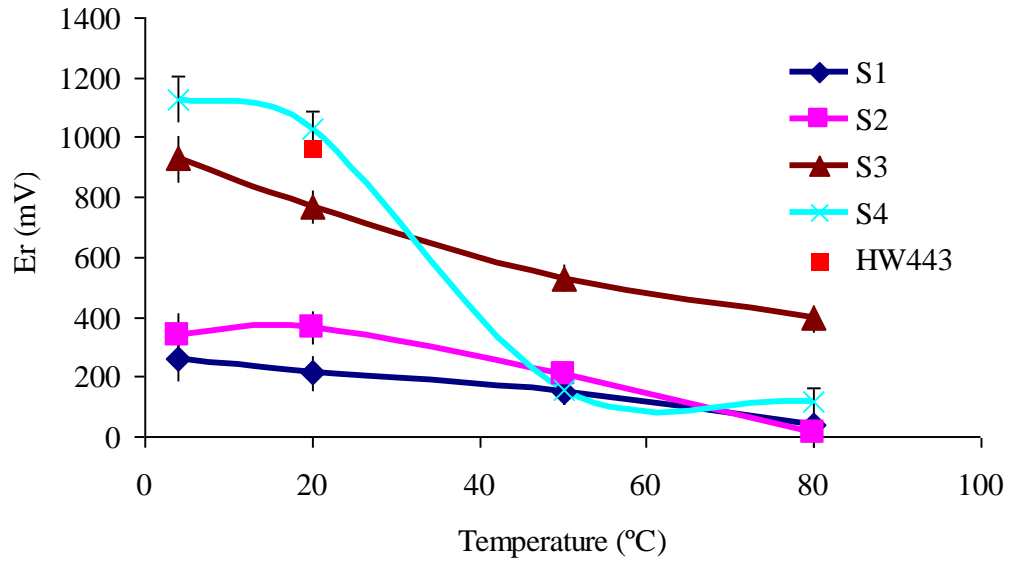


**Figure 7.5 Reverse potential of WC-Co as a function of temperature in every solution.**

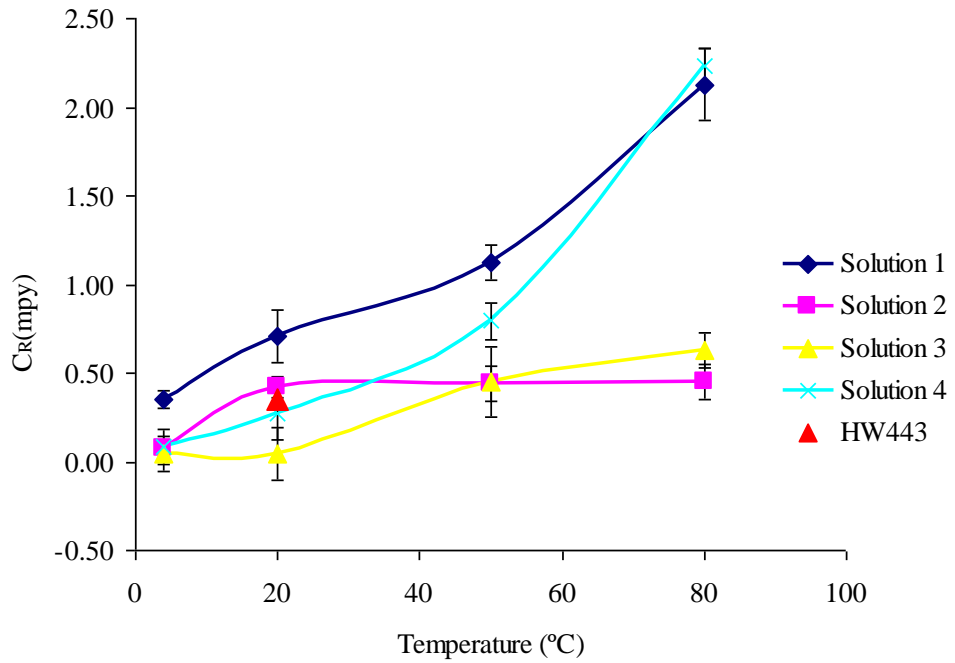


**Figure 7.6 Corrosion rate,  $C_R$  (mpy) of WC-Co in different sulphate/chloride ratios as a function of temperature**

## 7.4 WC-Ni in Seawater and Different $\text{SO}_4^{2-}/\text{Cl}^-$ Ratios

Because of the nature of cermets alloy, which consist of metal and ceramic composition, the corrosion rate is complex to identify. The corrosion attack could be assessed by calculating the corrosion rate or electrochemistry evaluation.

Figure 7.7 shows WC-9%Ni in S1 at 4°C, which has the same composition as real seawater. Like WC-Co, WC-Ni does not behave like passive material 316L. There is no breakdown potential as the potential increased. The temperature affects the corrosion behaviour in the same way as the other materials presented previously. The forward branch of the curve becomes linear after 50mV from OCP. Extrapolating this linear line and intersect with the current value will give  $i_{\text{corr}}$ . As WC-Ni behaves as an active material,  $i_{\text{corr}}$  is determined by Tafel extrapolation and the corrosion rate of WC-Ni in all solutions was calculated and presented in Table 7.4. WC-Ni in other solutions are presented in Appendix (Figure A.5 to Figure A.7).

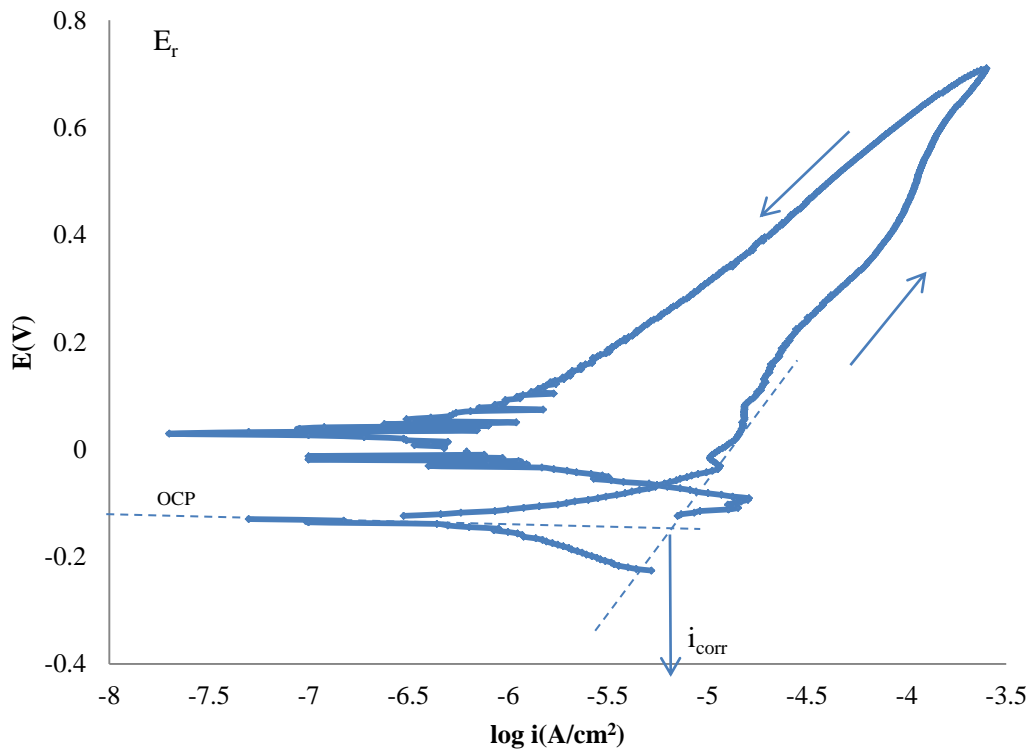


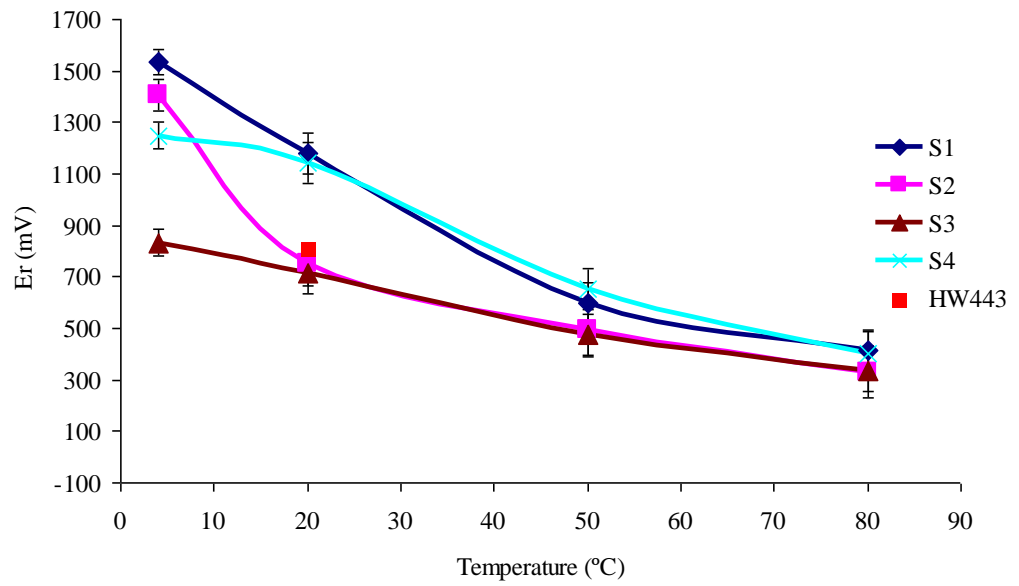
Figure 7.7 WC-Ni in solution 1 at 4°C

Figure 7.9 and 7.10 is generated from the list of electrochemistry data in Table 7.4, which shows the corrosion properties of WC-9%Ni for all solutions at increasing temperatures from 4°C to 80°C. Figure 7.9 presents the reverse potential of WC-Ni in every solution at increasing temperature. All the solutions show the same trend as increasing the temperature decreased the reverse potential. However, solution 1 shows mostly the highest  $E_r$  in every situation which explains that solution 1 is the least corrosive compared to other solutions while solution 3 is the most corrosive yet solution 3 presents constantly reduce as the temperature increased. WC-Ni shows drastically reduce in solution 2 from 4°C to 20°C about 18%. Comparing the corrosion rate with commercial hydraulic fluid HW443 at 20°C, present all solutions need to reduce 62% to 87% to reach acceptable corrosion rate. The open circuit potential is fluctuate in every solution.

The effect of temperature is different for the other solutions – S2, S3 and S4. S2 has the highest sulphate ( $\text{SO}_4^{2-}$ ) to chloride ( $\text{Cl}^-$ ) ratio, which is 19.15 mg/l and S3 and S4 are higher in  $\text{Cl}^-$  content compared to  $\text{SO}_4^{2-}$  while S3 has  $\text{SO}_4^{2-}/\text{Cl}^-$ , which is equal to 0.75 and S4 has a value for  $\text{SO}_4^{2-}/\text{Cl}^-$  of 0.99. The corrosion rate for WC-Ni in S2, S3 and S4 is lower than in S1, which is the real seawater composition. Although increasing the temperature affects the corrosion rate, different  $\text{SO}_4^{2-}/\text{Cl}^-$  does not have a significant effect on the corrosion rate. However, it shows that changing the  $\text{SO}_4^{2-}$  and  $\text{Cl}^-$  amount in seawater can decrease the corrosion rate. The effect of  $\text{SO}_4^{2-}$  in retarding the corrosion rate could not be seen in this result but, it is proved that by changing the amount of  $\text{SO}_4^{2-}$  and  $\text{Cl}^-$  ratio could decrease corrosion rate very close to hydraulic fluid HW443. Further electrochemistry for cermets in inhibitor was not evaluate as the aim for this research is to provide information for seawater to be used as hydraulic to replace chemical hydraulic fluid..

**Table 7.4 Electrochemical parameter for WC-Ni in all solutions**

Solution	Temperature (°C)	$E_r$ (mV)	OCP (mV)	$E_p$ (mV)	$i_{corr}$ ( $\mu\text{A}/\text{cm}^2$ )	$C_R$ (mpy)
<b>S1</b> $\text{SO}_4^{2-}/\text{Cl}^- = 0.14$	4	707	-127	29	1.99	0.31
	20	715	-161	98	6.31	1.00
	50	1156	-333	-239	7.94	1.25
	80	-61	-250	N/A	10	1.58
<b>S2</b> $\text{SO}_4^{2-}/\text{Cl}^- = 19.15$	4	705	-115	12	3.98	0.26
	20	576	-173	43.9	10	0.48
	50	1360	-330	-107	18	0.75
	80	139	-218	-255	31.6	0.87
<b>S3</b> $\text{SO}_4^{2-}/\text{Cl}^- = 0.75$	4	199	-152	N/a	1.99	0.27
	20	199	-130	-28.5	6.3	0.35
	50	235	-201	-149	6.3	0.64
	80	119	-385	N/a	10	0.70
<b>S4</b> $\text{SO}_4^{2-}/\text{Cl}^- = 0.99$	4	200	-145	-46	1	0.27
	20	698	-157	20.9	2.51	0.56
	50	172	-449	-119	7.9	0.60
	80	1004	-431	-181	10	0.97



**Figure 7.8 Reverse potential of WC-Ni as a function of temperature in every solution.**

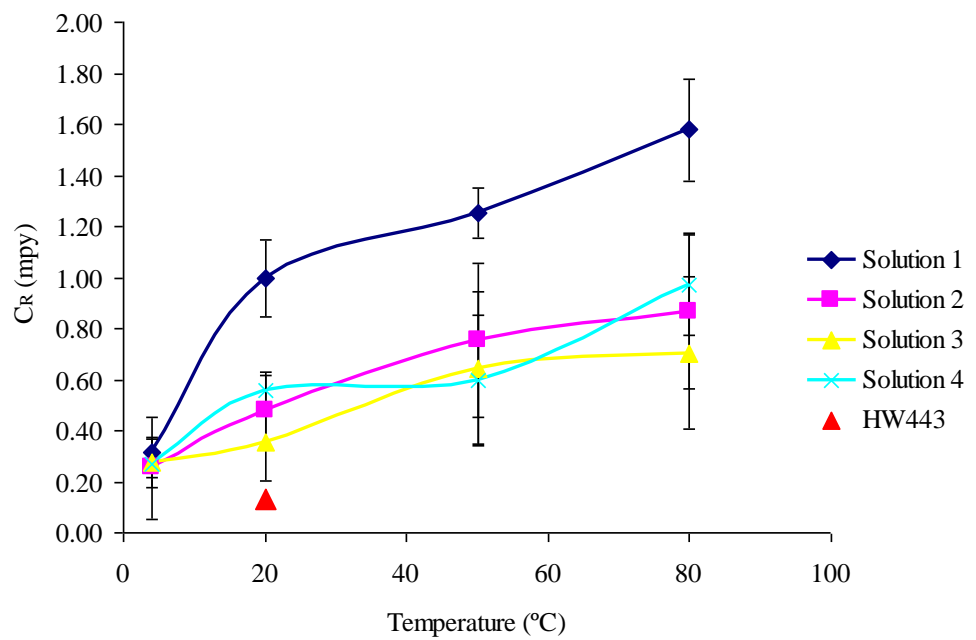


**Figure 7.9 Corrosion rate of WC-Ni in all solutions at increasing temperature.**



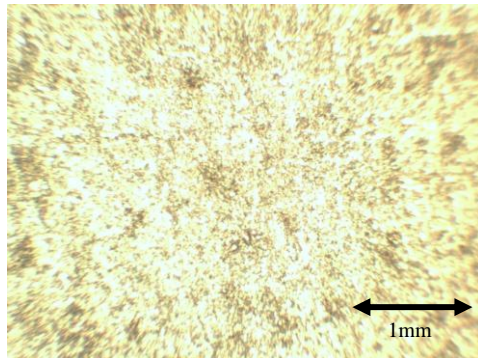
## 7.5 Summary

This chapter presents the electrochemistry results for cermets alloy which are WC-Co and WC-Ni. The sample composition is presented in Chapter 4 and WC-Ni was supplied by oil and gas company and the sample was cut from coupon into desired size. The EDX was taken to confirm the materials composition before the experiment. Both cermets alloys shows similar performance in Oceanic hydraulic fluid HW443 at room temperature (20°C). These alloys shows combination of active and passive behaviour however there are no breakdown potential to be observed. Therefore, the value of corrosion current density,  $i_{corr}$  was identified to obtain corrosion rate ( $C_R$ ) by calculation. An increase of temperature does not alter the trend of the curves, however the corrosion process is accelerated as expected. This is characterised by decreasing reverse potential and increasing free corrosion current density. Therefore, the protection potential reduces as well at higher temperature. Table 7.5 below presents the severity ranking of reverse potential and corrosion rate of solutions at different temperature. Solution 3 ( $SO_4^{2-}/Cl^-$  of 0.75) appears to be the best in terms of  $E_r$  for WC-Co whereas solution 1 ( $SO_4^{2-}/Cl^-$  of 0.14) appear to be the best solution in terms of  $E_r$  for WC-Ni. When comparing the corrosion rate calculated from current density, solution 3 becomes the best solution for both cermets. Nevertheless, solution 1 become the worst solution for both cermets.

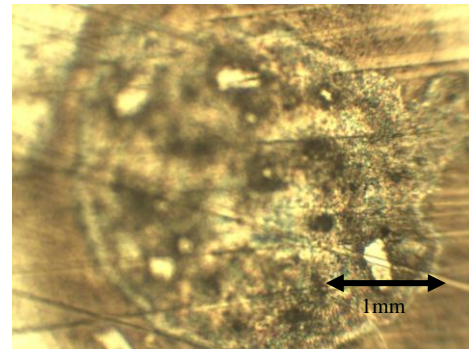
**Table 7.5 Ranking of cermets alloy in different solutions**

Temperature (°C)	$E_r$							
	High $\longrightarrow$				Low			
Cermets	WC-Co	WC-Ni	WC-Co	WC-Ni	WC-Co	WC-Ni	WC-Co	WC-Ni
4	S4	S1	S3	S2	S2	S4	S1	S3
20	S4	S1	S3	S4	S2	S2	S1	S3
50	S3	S2	S2	S1	S4	S3	S1	S4
80	S3	S4	S4	S2	S1	S3	S2	S1
Temperature (°C)	$C_R$ (mpy)							
	High $\longrightarrow$				Low			
Cermets	WC-Co	WC-Ni	WC-Co	WC-Ni	WC-Co	WC-Ni	WC-Co	WC-Ni
4	S1	S1	S4	S3	S2	S4	S3	S2
20	S1	S1	S2	S4	S4	S2	S3	S3
50	S1	S1	S4	S2	S3	S3	S2	S4
80	S4	S4	S1	S4	S3	S2	S2	S3

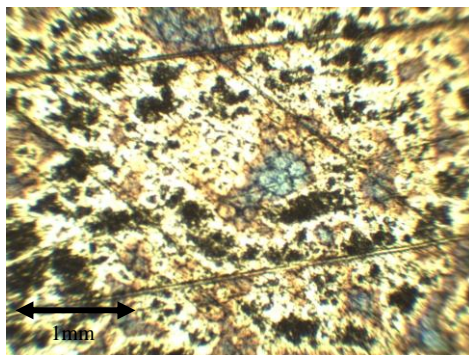
Figure 7.11 shows some microscopic view of cermets alloy. Figure 7.11 (a) show the WC-Ni in solution 4 at 4°C which showing no obviously of corrosion attack. However, at 50°C WC-Ni appear to have corrosion attack and from electrochemistry, the corrosion rate is 0.6 mpy at this environment. From Table 7.4, solution 2 could be classified as moderate solution will perforate corrosion. From microscopic view, WC-Ni in solution 2 at 50°C (Figure 7.11(c)) does not show any severe corrosion attack. WC-Co appears to have dark surface under microscope after electrochemistry and difficult to increased the picture contrast. Figure 7.11 (d) show WC-Co in solution 1 at 80°C and observed likely a pitting appear on WC-Co surface even though WC-Co in solution 1 do not show breakdown potential.



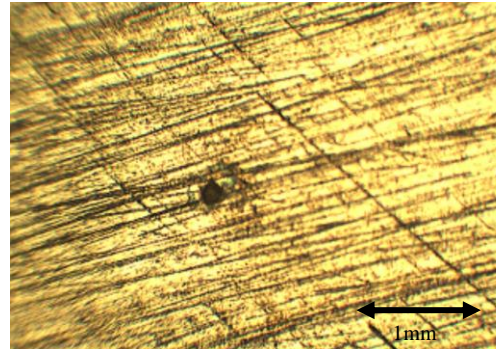
(a)



(b)



(c)



(d)

**Figure 7.10 Cermets alloy under microscopic observation (a) WC-Ni in solution 4 at 4°C, (b) WC-Ni in solution 4 at 50°C, (c) WC-Ni in solution 2 at 50°C and (d) WC-Co in solution 1 at 80°C.**

## Chapter 8

### DISCUSSION

#### 8.1 Introduction

It has been proven by several authors that pitting corrosion can be avoided by using oil-based hydraulic fluids. However the demand by environmental policies insist that all oil and gas activities especially when discharging to environment must be non-toxic, must not bio accumulate and be biodegradable. This request a cleaning process before discharging to the environment and such cleaning under marine conditions is complicated and the oil-water mixtures are needed to be transported along pipelines to onshore separation units. This task could be minimised if hydraulic fluids are being replaced by seawater. In addition to the potential cost benefits, seawater could also be easily discharged into the sea.

The corrosion behaviour of carbon steel was evaluated and presented in Chapter 5 and considered as an active material. In contrast to active material, passive materials show a different kind of corrosion attack and mechanism. Evaluations of passive materials – 316L, 25Cr duplex and Inconel 625 – were provided in Chapter 6, whereas cermet alloys, which consist of a combination of metal and ceramic can show active and passive behaviour, were presented in Chapter 7. The objective of this research is to study the corrosion attack of Directional Control Valve (DCVs) material for use in seawater by applying seawater as a hydraulic fluid. As such all classes of construction materials are considered and corrosion mechanism and rates were identified to provide some data for corrosion control. All the acceptable corrosion rates and passive film breakdowns were compared to commercial hydraulic fluid HW443, which has been used by previous researchers. All the electrochemistry was evaluated either at different temperatures and sulphate/chloride ratios, oxygen and inhibitor. Contradict approach to corrosion was examined and evaluated where it was presented that carbon steel experiences general corrosion, passive alloys experience localised corrosion and cermets alloys experience as general corrosion.

## **8.2 The Demand for Green Hydraulic Fluid**

Generally, successful and economical exploration and exploitation is heavily dependent on material performance and the need for protection against corrosion of equipment. Materials could degrade due to corrosion caused by the aggressiveness of seawater. However, the technology advances on many fronts are increasing the productivity and efficiency of oil and gas production. Applying new technologies in every stage of oil and gas production will simultaneously increase productivity. In addition, manufacturers keep identifying solutions that balance the benefits of production with the ongoing drive for environmental protection. Where companies once focused solely on complying with regulations, many now view environmental performance more broadly as a core business value. This research is part of an attempt to find an alternative for hydraulic fluid to replace oil-based hydraulic fluid which is not harmful when discharged to the environment. It would be easier if seawater is treated with inhibitors or deionised in some way that could be used as a hydraulic fluid; however, this presents many challenges associated with the corrosion of the materials of construction, the environment and the material's lifetime. The health and safety practices for subsea activities, means that oil-based hydraulic fluid is no longer suitable for use in oil and gas operations. However, water-based hydraulic fluid may cause several disadvantages such as leakage due to low viscosity, instability at higher temperature and may need coolant. The process of discharging the waste hydraulic fluid is very costly, which has led to the suggestion to use seawater as the hydraulic fluid. Not only the seawater is readily available in subsea, but, also, by using the seawater as a hydraulic fluid, no further waste water treatment is needed when discharging. This also will contribute to reducing the cost of the operation for subsea activities. Nevertheless, the most crucial problem of using seawater as a hydraulic fluid is the risk of corrosion attack on material involved.

The main objective of this research is to identify the critical parameters in the aqueous environment, which accelerates the corrosion rate and find a means of reducing the corrosion attack to something comparable to the behaviour of hydraulic fluid when using in subsea operations. The best hydraulic fluid as the benchmark to determine an acceptable corrosion rate and the hydraulic fluid chosen is HW443.

### 8.3 The Corrosion Mechanism on Carbon Steel

Carbon steel can be attacked either by uniform or pitting corrosion in seawater. Uniform or general corrosion can be classified as corrosive attack proceeding evenly over the entire exposed surface area. It is probably the most common form of corrosion for carbon steel and is relatively easily measured and predicted. Figure 5.3 in Chapter 5 presents the corrosion rate of carbon steel in distilled water as compared to commercial hydraulic fluid HW443. It reveals that when there are no halide anions in a solution (distilled water) except oxygen, the corrosion rate can be reduced beyond the commercial hydraulic fluid. The figure reveals that the corrosion rate of carbon steel in distilled water is much lower compared to the corrosion rate in HW443 and increasing the temperature has low significant effect to corrosion rate. This elucidates that by removing salt content in seawater would reduce corrosion rate on carbon steel.

According to Ying and Haichao (2001), the general corrosion rate of low alloy steels in seawater is approximately equal to 0.1 mm/year for local corrosion of low alloy steel in 3.5% NaCl [151] and referring to Figure 5.4(a), the corrosion rate for AISI 1040 in 3.5% NaCl for this research is around 0.32 mm/year at 20°C. However, AISI 1040 can be categorised as medium carbon steel and this reason contributes to higher corrosion rate. Increasing the temperature has an effect on the electrochemical kinetics, which relates to the electron flow to or from the metal-electrolyte interface. The rate of any transformation is controlled by the magnitude of one or more energy barriers that every particulate entity must surmount to transform or could be simplified as the minimum energy required to start a chemical reaction. The activation energy of a reaction is usually denoted by  $-\Delta G^\#$ . The reaction rate,  $r$  can be expressed as below for the reaction rate, which applies to many reactions over moderate temperature range, using Arrhenius' equation [104].

$$r = A \frac{\exp(-E_a)}{RT} \quad 8.1$$

where  $A$  is the pre-exponential factor, there is an empirical relationship between temperature and rate coefficient. This equation can be applied by replacing the reaction rate,  $r$  by current,  $I$  and the energy of the process is the product of the charge and the potential drop,  $E$ , through which it is carried. Thus, the activation energy is the change in free energy ( $\Delta G = -nFE$ ) during the process and the relation is;

$$i = k \exp \frac{-\Delta G^*}{RT} = k \exp \frac{nFE^*}{RT} \quad 8.2$$

Where  $k$  is a constant depending on the process and on the ion activity.

Figure 8.1 shows the Arrhenius relationship for AISI 1040 in 3.5% NaCl. The negative slope of Arrhenius plot indicates the activation energy was positive value. Therefore, the metal atom must overcome the activation energy peak which indicates that only a part of metal with higher energy can be corroded (Figure 8.2).

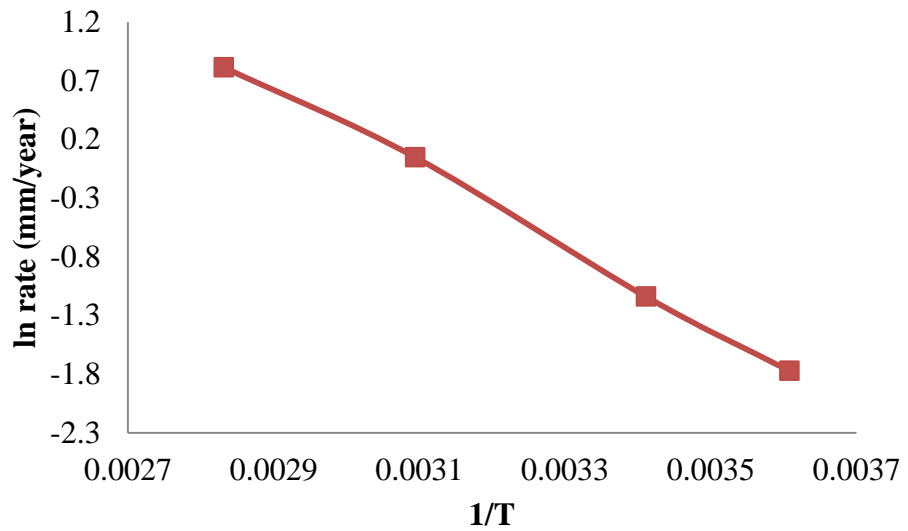


Figure 8.1 Arrhenius relations in 3.5% NaCl

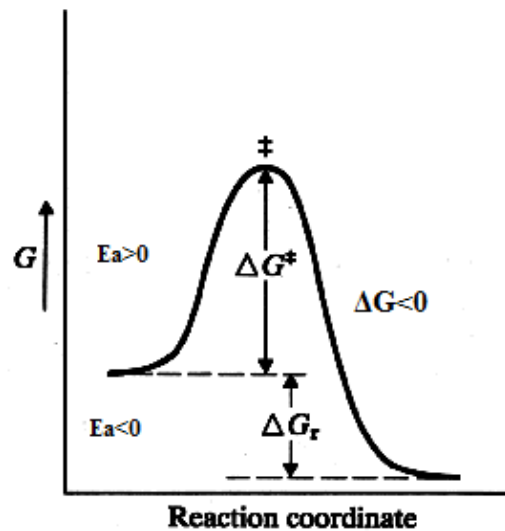
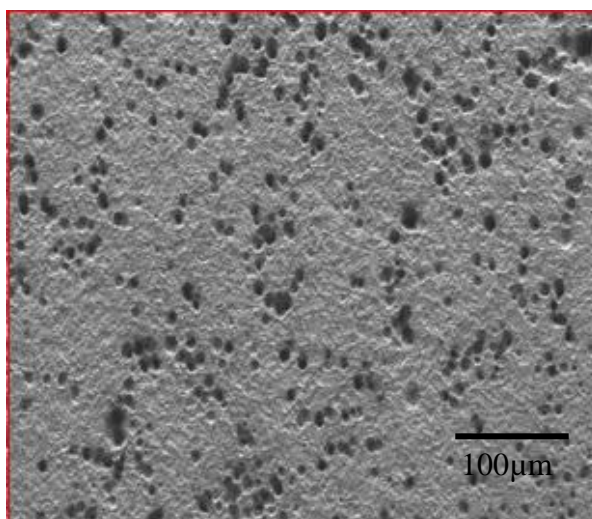


Figure 8.2 Schematic of the activation energy peaks for nucleation

The immersion test had done to three types of carbon steels namely AISI 1040, AISI 8260 and AISI 4140. The carbon steels was immersed in 3.5% NaCl for various periods and the corrosion rate was calculated. The effect of corrosion product to corrosion rate can be seen in Figure 5.5 in Chapter 5 where all the carbon steels are behave as same trend. Apart of comparing different compositions of carbon steels (low–medium-high carbon steel) on corrosion attack, the trends of corrosion attack also can be studied by using more than one carbon steel. The corrosion rate for all carbon steels decreased as the exposure time increased. This is due to the property of corrosion products which are porous and soluble as shown in Figure 8.3 below. However, for AISI 8620 and AISI 4140, the corrosion rate slightly increased at 24 hours immersion. According to Li *et al.*(2013), corrosion product may retard the corrosion uniform corrosion attack, but if it is not fully covered the steel surface, it may lead to initiation of localised corrosion due to galvanic effect [195].



**Figure 8.3**Microscopy view of AISI 1040 in 3.5% after corrosion attack at 20°C

According to Rosales *etal.*(2003) the increasing protective rust thickness increased with increasing time and resulted in a decrease in the corrosion rate for carbon steel [146]. However, after several periods, the thickness reaches a limit and falls. The results are consistent with Zhu *etal.* (2002) who studied the characterisation of corrosion products on carbon steel. They found that with an increase in the immersion time in NaCl solution, the polarisation resistance of the recrystallized alloy steadily increases, which reflects an increase in the protective characteristics of the corrosion product film[147]and in the NaCl concentration between 0.5-1M.The rate of carbon steel corrosion continuously drops with time and this behaviour is influenced by the

formation of an oxide layer, which reduces the limiting current density for oxygen reduction[148].

There are several factors that affect corrosion attack on carbon steel including pH, anions, oxygen and temperature. An increase in temperature affects the chemical composition and physical properties of water, the nature and properties of deposits and the actual behaviour of the metal exposed. The water composition is affected by changes in the stability and solubility of the dissolved solids. The study by Takasaki and Yamada (2007), revealed that corrosion of carbon steel increased in proportion to the concentration of aggressive anions and with increasing temperature [45]. The underlying concept is a mechanism of chemical reactions involving the passage of reaction species through an intermediate activated complex, subsequently dissociating into reaction products. This activated complex is known at an energy level exceeding the energy of the reactants by the activation energy.

Anions were identified by several authors as the main attack by corrosion in a seawater environment [149]. Figure 5.6 reveals that other anions also contribute to corrosion for carbon steels. According to Wren *et al.*,(2010) the corrosion rate to carbon steel does not depend on halide anion type or concentration. However, it will accelerate breakdown and inhibit the repassivation process [150]. For passive alloy, El Wanees *et al.*(2010)reported that the breakdown potential of stainless steel in 3.5% NaCl is lower compared to real seawater because non aggressive anions exist in real seawater, which can resist corrosion [47]. However, this behaviour could be different to carbon steel, which behaves as an active material and was attacked by general corrosion.

To get an acceptable corrosion rate, the carbon steel was tested in commercial hydraulic fluid HW443 and compared to S1 (Solution 1), which was synthesised with the same compositions as real seawater. Figure 5.6 shows that the corrosion rate of AISI 1040 in solution 1 at 20°C is 93% higher compared to corrosion rate of AISI 1040 in commercial hydraulic fluid HW443. The corrosion rate of AISI 1040 in HW443 was used as a benchmark to identify the critical environment parameter (pH, oxygen and anion) to obtain 'acceptable' or 'unacceptable' corrosion rate. Other approach such as either using green chemical inhibitor or deaerated dissolved oxygen was used to obtain the corrosion rate as closed to commercial hydraulic fluid (HW443).

As it is known that chloride can accelerate corrosion and that other anions, such as  $\text{SO}_4^{2-}$ , can resist corrosion, the  $\text{SO}_4^{2-}/\text{Cl}^-$  ratio was identified to study the anion effect to corrosion rate of carbon steel. The composition of  $\text{SO}_4^{2-}$  and  $\text{Cl}^-$  are listed in Table 5.1,



which shows that Solution 2 has the highest  $\text{SO}_4^{2-}$  compared to  $\text{Cl}^-$ . As Figure 5.4 reveals that all carbon steels used are showing a same trend to corrosion attack, therefore, the following experimental was only run for AISI 1040. This was chosen because AISI 1040 is plain medium carbon steel. Four different solutions of  $\text{SO}_4^{2-}/\text{Cl}^-$  ratio were prepared and corrosion rate of AISI 1040 was identified. Figure 5.7 presents the corrosion rate of carbon steel for every solution compared to 3.5% NaCl at increasing temperature (4°C, 20°C, 50°C and 80°C). At 4°C to 20°C, the corrosion rate of carbon steel in 3.5% NaCl is the lowest as compared to corrosion rate of AISI 1040 in different  $\text{SO}_4^{2-}/\text{Cl}^-$  ratio content. However, increasing the temperature to 50°C and above increased the corrosion rate of AISI 1040 in 3.5% NaCl tremendously higher than AISI 1040 in different  $\text{SO}_4^{2-}/\text{Cl}^-$  ratio. Apart of that, AISI 1040 in S2 ( $\text{SO}_4^{2-}/\text{Cl}^- = 19.15$ ), which has the highest  $\text{SO}_4^{2-}$  to  $\text{Cl}^-$  ratio, is more stable at increasing temperature. Even at 80°C, the corrosion rate of carbon steel in S2 is the lowest. This shows that the role of sulphate ( $\text{SO}_4^{2-}$ ) in chloride environments is complex to understand either it can speed or inhibit corrosion attack on carbon steel.

The corrosion rate of carbon steel was also studied using an inhibitor. CRW85155 was chosen as this has been used by other researchers with carbon steel in erosion corrosion. However, the corrosion rate only reduced to 71% after CRW 85155 was added and there was no significant difference when the concentration was increased up to 100ppm, as shown in Figure 5.11. The trend is also the same at increasing temperature when the concentration of CRW 85155 is increased, as shown in Figure 5.12. In addition to using CRW 85155, another inhibitor was chosen as used by several oil and gas companies in an oxygen environment. This inhibitor – CRW 89000 – consists of  $2\text{mg}/\text{m}^3$  sodium hydroxide and sodium nitrate. Figure 5.15 shows that at 20°C, with the addition of 400 ppm of CRW 89000 to S1, the corrosion rate can be reduced as close to the corrosion rate of carbon steel in HW443; however, the corrosion rate increased as the temperature increased. Nevertheless, when using this inhibitor at 100ppm, the corrosion rate was still higher compared to carbon steel in HW443 and carbon steel in S1 with CRW 85155 added (Figure 5.16). This reveals that apart from changing the  $\text{SO}_4^{2-}/\text{Cl}^-$  ratio, the corrosion rate of carbon steel can be reduced by increasing the inhibitor concentrations up to 400 ppm to control the corrosion of carbon steel in a static and oxygen environment. Figure 5.17 concludes the corrosion rate of AISI 1040 in seawater (S1) with different concentrations of green inhibitor (CRW 89000) and AISI 1040 in 3.5% NaCl compared to the bench mark of corrosion rate (the corrosion rate in HW443). The graph presents that the corrosion rate of carbon steel

is reduced when 400 ppm CRW 89000 was added to S1 and the corrosion rate is closed to HW443 when the carbon steel with this electrolyte composition in a temperature 20°C and below.

### 8.3.1 Protective film on passive alloys

As revealed by several authors, chloride accelerates corrosion and penetrates the protective film [92, 122, 150]. The critical chloride concentration can be identified by increasing the chloride concentrations from 0g/L in an oxygen environment. The corrosion rate for carbon steel drastically increases at chloride concentrations around 0.05 g/L as shown in Figure 5.9 (a) and (b). This value is then used to get critical oxygen concentrations by increasing the oxygen content from 0ppm (Figure 5.10 (a) and (b)). According to Jordan and Williams (1996), the corrosion rate of carbon steel in corrosive agents and without oxygen is 0.02 mpy [152]. For this research, the critical oxygen content was evaluated by purging nitrogen gas to the solution overnight. The reading of oxygen content was then read using a Dissolved Oxygen (DO) probe. Linear polarisation was taken from time to time until 35ppb at 4°C and 20°C considering that it is difficult to control the oxygen level at higher temperatures (50°C and 80°C). This is because during the electrochemical process, oxygen is produced and this process rapidly increases as the temperature increases.

Figure 8.4 below shows oxygen transport mechanism entering the mild steel through seawater and corrosion product (rust layer).

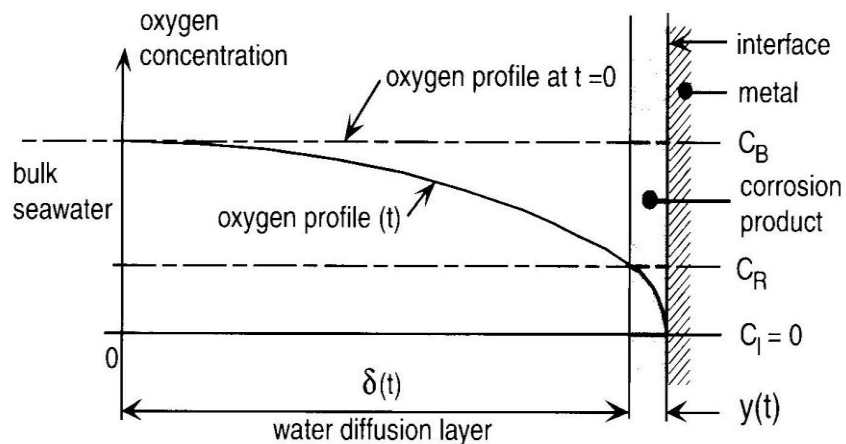


**Figure 8.4 Oxygen concentration profiles through seawater and corrosion product (rust) layer [224].**

Even corrosion rates increased as the oxygen concentration increased, but at a certain limit, once water diffusion layer increased, the oxygen concentration decreased. As a result, the corrosion rate will decreased. This study was presented by Melchers and Jeffrey (2005) to describe the rate of material loss (corrosion rate) with time [153].

Figure 8.5 below shows a schemetic of oxygen diffusion from bulk water to the corrosion surface through the waters surrounding the corroding surface and through the corrosion product (rust) layer.



**Figure 8.5 Current (oxygen) transfer through water and rust layer [154].**

Even though the corrosion rate for carbon steel strongly depends on oxygen concentrations, some modifications of seawater are able to control the corrosion attack. Figure 5.17 reveals that at 20°C, the corrosion rate of AISI 1040 can be reduced to 'acceptable' corrosion rate (AISI 1040 in HW443) either the carbon steel is in seawater with 400ppm CRW 89000 or reduced the chloride content to 0.05 g/L with lowering the oxygen content to approximately 16 ppb (Figure 5.9 in Chapter 5).

## 8.4 The Role of Metastable Pitting

Metastable pitting of metals and alloys has been studied by many authors in order to understand the early mechanism of localised corrosion, and to find a potential method to predict the pitting tendency of metals, as there is a close relationship between metastable and stable pitting behaviours [111-114]. Figure 6.23 (Chapter 6 section 6.5) shows that metastable pitting occurs at surrounded pit and becomes the point from which pitting propagates. It can be said that for 316L at higher concentrations, there also occurs corrosion of the remaining part of the metal surface, which refers to metastable pitting. Metastable pitting is nucleated at some electrochemically active site, probably a sulphide inclusion, although other sites, such as iron-rich clusters in the

metal matrix have also been proposed [115]. The transition to stable pit growth occurs when the pit has grown sufficiently for its own depth to act as a diffusion barrier. Then the pit propagates without its cover and is thus stable. The early metastable pits are controlled by the diffusion of metal cations away from the nucleation pit. Some authors have focused on the current oscillations and transients, which reflect the influence of chloride concentrations on the potential of metastable pitting on polarization curves. These current fluctuations before pitting are the results of nucleation, growth and repassivation of metastable pits on the metal surface [116].

Y. Zuo *etal.* (2002) studies the nucleation number of metastable pits at time different according to different surface roughness. They reveal a graph as shown in Figure 8.6 below as the number of metastable pits decreased as the surface roughness of sample increased (900 grit paper). It can be conclude that the smoother the surface, the more corrosion resistance. This is also affect pitting corrosion attack as the pitting decreased as the metastable pits decreased. However, the effect of surface roughness cannot be seen in this research because the entire samples are polished at the same grit. Nevertheless, metastable pits can be identified from anodic polarisation in cyclic polarisation potential. Figure 6.27 and Figure 6.8 in Chapter 6 reveals the metastable pitting developed on 316L at 20°C and Inconel 625 in S1 at 80°C respectively.

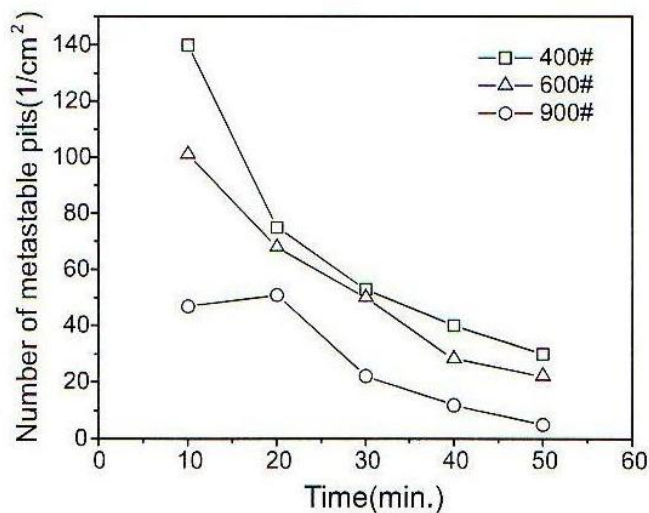


**Figure 8.6** Changes of number of metastable pits with time on different paper finished surfaces.

The way by which the solution composition affects the occurrence of metastable pitting remains to be described. Pistorius (1992) in his paper described that the role of

dilute sulphate concentration in the chloride solution (where the sulphate concentration is significantly less than the chloride concentration) is to shift the distribution of metastable pit sites to a higher potential at which they are activated [117]. However, the number of sites activated is barely discernible and it is only marginally affected. Thus, the pitting potential, which is considered as the potential below which no stable pits could be observed, is unchanged. He also determined that pit propagation in metastable and stable states are inhibited by sulphate ion and that the growth is also independent of the electrode potential [117]. From observation of contrasting measurements of the pitting potential in chloride solutions containing higher concentrations of sulphate with sulphate-to-chloride ratio  $>1$ , Uhlig (1979) found that an increase in pitting potential is observed [118]. Subsequently, he explored the extended effect of some important features of the solution composition on the frequency of occurrence of metastable pits, the pH, the chloride concentration and the effects of dissolved oxygen. Because metastable pitting causes pitting growth, previous research can be used as a reference to this study.

It is well known that chloride ions,  $\text{Cl}^-$  cause pitting corrosion in aqueous solutions by aggravating the protective property of the surface oxide film. Many researchers [115, 119, 120] have studied metastable pitting to understand the pitting corrosion mechanism of metals. Laycock *et al.* (1998) reported that the metastable pitting activity of 304 stainless steel reached a peak of around  $0.3 V_{\text{SCE}}$  and then decreased with increasing applied potential below the pitting potential (breakdown potential,  $E_b$ ) [155]. They attributed the decrease in metastable pitting activity after it reached a peak to the exhaustion of active sites. The total number of available sites for metastable pitting was observed to be smaller for the smoother surface in comparison with the rougher finish.

While Pistorius (1992) and Uhlig (1979) studied the solution composition effect of electrode potential and the direct effect of pitting corrosion, C.J. Semino (1979) elucidated that the corrosion resistance of high alloy steels in many environments is due to their ability to produce an oxide film, which keeps the alloy in a metastable state of passivity [120]. He also concluded that the increase of chloride concentration shifts the pitting potential to become more negative and that the value of pitting potential is not affected by oxygen content in solution. Figure 8.7 below shows a schematic model of how metastable pits are induced by a stable pit, where the growing stable pit produces  $\text{Fe}^{2+}$  ions, and the hydrolysis of  $\text{Fe}^{2+}$  ions will attract more anions, such as  $\text{Cl}^-$ , into the pit cavity. Generally,  $\text{Cl}^-$  ions have stronger mobility and can diffuse readily into the

cavity to acidize the local chemistry, resulting in accelerating growth of the pit [122]. El-Sayed *etal.* (2009) in their research presented that increasing the chloride concentration shifts the pitting potential in the active direction until at about 5%, when it stays constant indicating complete depassivation [156]. However, it is difficult to conceive that such large ions like  $\text{ClO}_4^-$  and  $\text{SO}_4^{2-}$ , which can also provoke pitting, should travel through the passive film lattice [124] whereas chloride ( $\text{Cl}^-$ ) can interfere at a higher driving force to form the passivation oxide film [125].

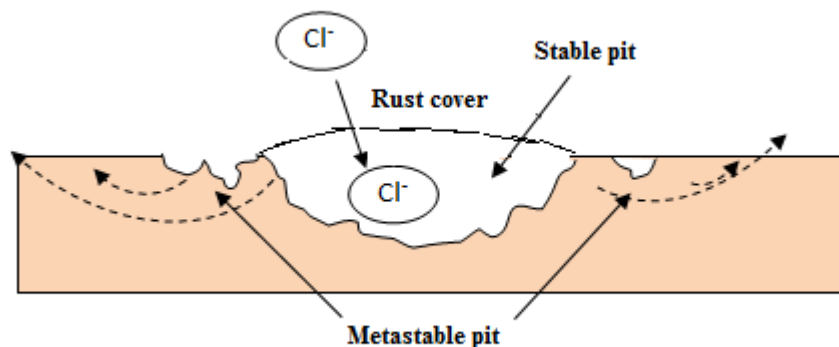


**Figure 8.7 Schematic model of metastable pits [93].**

## 8.5 Pitting Corrosion on Passive Alloys

As mentioned before, the corrosion resistance of high alloy steels in many environments is due to their ability to produce an oxide film that keeps the alloy in a metastable state of passivity. The stability of this passive state is damaged when these alloys are polarised above some electrode potential in environments containing aggressive ions, such as chloride ( $\text{Cl}^-$ ) ions, causing pitting to appear. Pitting corrosion can be described as the destructive failure through perforations by a single pit, which can cause complete equipment failure. It occurs when discrete areas of a material undergo rapid attack, although the vast majority of the surface remains virtually unaffected. Mankowski and Szklarska-Smialowska (1975) observed that the higher accumulation of  $\text{Cl}^-$  content within pits indirectly decreases the pH value and slows pit development [157]. However, Jingyi *etal.* (1989) stated that changes of passivating behaviour indicate that the corrosivity of occluded solutions increased as the pH decreased and they found that  $\text{Cl}^-$  concentration in occluded solutions increased with decreasing pH. However, the effect of  $\text{Cl}^-$  concentration is less pronounced than the pH value [158]. In another research, Mankowski and Szklarska-Smialowska (1975) found

that the concentration of  $\text{Cl}^-$  ions in the pits is higher than that in the bulk solution. This affects the pH of the solution inside the pits, which results from the hydrolysis of corrosion products and high concentrations of chloride ions [159]. Apart from environmental factors including composition of the solutions that affect the corrosion, pitting and crevices can only be distinguished according to the mechanism of corrosion attack. Green and Fontana (1958) differentiated between pitting and crevice corrosion. They suggested that crevice corrosion is an attack that is limited to surface areas shielded from direct exposure to the electrolyte, regardless of the surface structure produced by the attack [129].

The pitting tendency of a metal or alloy is governed by many factors. From the perspective of controlling pitting corrosion, it is essential to highlight the factors that influence pitting corrosion. As of now, no quantitative relation exists that can predict a pitting failure. Qualitative understanding exists between various parameters that affect the pitting tendency of an alloy, which, in fact, forms the basis for material selection and environmental control for preventing pitting failures.

For pitting to occur, the most basic requirement is the existence of a passive state for the material in the environment of interest. Pitting occurs when portions of the metal surface lose their passivity and dissolve rapidly. Thus, in this research, the corrosion attack for passive materials was identified by their breakdown potential (also known as pitting potential, where the bare surface fails to repassivate and the occurrence of an abrupt permanent increase in current) at each temperature, which can be seen in Chapter 6. The favourable aspect of pitting is that only certain types of anions are responsible for pitting in certain environments with sufficiently oxidizing potential. In many situations, pitting can severely limit the performance of material including DCV materials.

## **8.6 Passivation**

Passivation of metals results from the formation of a condensed phase of continuous oxide layer on the metal surface. According to Wagner (1965), a metal or alloy is passive when the amount of at least one of the metallic components consumed by a chemical or electrochemical reaction in a given time is significantly lower at a higher affinity than at a lower affinity [160]. The phenomenon of metal passivation was discovered by Keir as far back as 1790, when it was observed that metallic iron in concentrated nitric acid suddenly became in an altered state (the passive state) after

violent metal dissolution had occurred in the fresh state (the active state) [131]. The passivation mechanism has been explained in Chapter 6 and this chapter presents all the results for passive materials of DCV materials, which are 316L, 25Cr duplex and Inconel 625.

Figure 6.2 in Chapter 6 shows 316L in HW443 at 20°C. The close curve of forward and reverse scan of potential dynamic shows that 316L behaves as stable repassivation in HW443. Figure 6.3 shows the anodic polarisation for all materials- 316L, 25Cr duplex and Inconel 625 in HW443 hydraulic fluid. The figure shows that Inconel 625 has the lowest breakdown potential and 25Cr duplex has the highest. Table 6.1 presents the electrochemistry data for these materials in HW443 at 20°C. By comparing the breakdown potential at 20°C, the best performance materials in HW443 can be ranked as 25Cr duplex >316L > Inconel 625. By referring to this figure, 316L performs better than Inconel 625, which has a higher nickel and chromium content compared to 316L. The chromium content hinders the pit growth and thereby should increase the breakdown potential and extend the passive region of Inconel 625. The results of  $I_{max}$  shows that the ranking is 25Cr duplex >Inconel 625>316L in which  $I_{max}$  represents the maximum current attained should the current not begin to fall immediately after scan reversal. It also represents the stability of materials after the repassivation process, which is supported by Yin *etal.*(2009) who studied Ni-based alloys exposed in oil/gas field environments. They elucidated that Inconel 625 has a stable passivation region compared to other Ni-based alloys due to its higher nickel content [161].

To study the environmental effect, which accelerates corrosion, the materials were tested in 3.5% NaCl and compared to the performance in HW443. Figure 6.4 shows 316L in 3.5% NaCl, and, as expected, the breakdown potential decreased as the temperature increased. The hysteresis also changed from negative hysteresis at 4°C to positive hysteresis at 20°C, 50°C and 80°C. Negative hysteresis indicates that the materials of the damaged passive film repair itself and pits do not initiate whereas positive hysteresis occurs when the passive film damage is not repaired and pits might initiate. The electrochemical data of 316L in 3.5% NaCl are presented in Table 6.2 and show that the OCP shifted to a positive value and breakdown potentials decreased as the temperature increased. At 80°C, 316L in 3.5% NaCl changed from passive to active reaction as there is no breakdown potential in anodic polarisation. Figure 6.5 shows the anodic polarisation for passive materials in 3.5% NaCl at 20°C and electrochemical data



are presented in Table 6.3. Similar to anodic polarisation in HW443, the ranking based on breakdown potential,  $E_b$ , is 25Cr duplex >Inconel 625>316L.

## 8.7 Role of Anion on Corrosion Attack

Chloride ions are one of the most significant natural contaminants in the marine environment, and play a major role in the corrosion process of structural steel. Many researchers agree that increasing  $\text{Cl}^-$  concentrations will decrease resistance to pitting corrosion, especially for stainless steel [133-139]. Corvo *et al.* (2007) proposed a mathematical model and suggested that the chloride ions deposited accelerate the corrosion rate on mild steel caused by chloride ions [162]. He also suggested that the rust layer becomes porous and induces chloride ions from outside easily, which promotes corrosion. However, chloride ions only play a key role during the initial stages of atmospheric corrosion, as the rust layer grows in thickness, the supply of fresh chloride ions may gradually diminish, and, as a result, the formation of chlorides would be slower. According to Hoar (1967), the method of passive breakdown by anions is due to the small size, which could easily penetrate the pores in the passivating oxide film [163].

To date, there is no research studying the effect of sulphate/chloride ratio using the same composition of real seawater, as they used sulphuric acid or hydrochloric acid instead of synthesised seawater based on the same salinity as real seawater. Szklarska-Smialowska (1972) studied the pitting kinetics of nickel in solutions containing different ratios of  $\text{SO}_4^{2-}$  and  $\text{Cl}^-$ . He found that the pitting perforation depends on the  $\text{Cl}^-$  concentration added to the  $\text{SO}_4^{2-}$  solutions. An excess of  $\text{Cl}^-$  causes general corrosion whereas excess  $\text{SO}_4^{2-}$  in solution inhibits pitting [168]. Figure 6.9 reveals the breakdown potential of passive alloys in seawater (S1) and HW443 as a function of temperature. All the materials show the same trend of a decrease in  $E_b$  as the temperature increases. 25Cr duplex and Inconel 625 has higher breakdown potential in S1 than in HW443. This presents that 25Cr duplex and Inconel 625 may corrode in seawater and HW443 is not well protected for these alloys from chloride environment. Conversely, the HW443 is able to protect 316L in S1 (seawater). This could be considered as 316L reacts actively with HW443 to perform an oxide layer on the surface of the metals to form a protective film and 25Cr duplex and Inconel 625 do not actively react with HW443. Furthermore, the decision to use HW443 as comparative performance is based on previous research [5] who studied the performance of Oceanic HW443 hydraulic fluid which is low in

toxicity. However, the study was not include Inconel and 25Cr duplex in their study. By comparing the anodic polarisation for 316L, 25Cr duplex and Inconel 625 in S1 according to temperature, 316L shows the lowest in breakdown potential compared to 25Cr duplex and Inconel 625. From  $E_b$  performance, the ranking of the best materials is; 25Cr duplex > Inconel 625 > 316L for every temperature. However, Inconel 625 had a negative hysteresis more than 25Cr duplex at increasing temperature, which shows that Inconel 625 is able to self-repair damaged passive film compared to others.

Apart from the study of electrochemical performance in S1, which has the same elements as seawater, the solutions also varied in  $\text{SO}_4^{2-}/\text{Cl}^-$ . Table 4.7 (Chapter 4 section 4.2) shows the composition for the elements. S4 has the highest ratio and S2 the least ratio. The study is based on the effect of sulphate ( $\text{SO}_4^{2-}$ ) and chloride ( $\text{Cl}^-$ ) on pitting corrosion where S2 has the highest sulphate and lowest chloride content and S1 has lowest sulphate and highest chloride content. Unlike to the anodic polarisation performance shown for 316L, the 25Cr duplex shows more stable forward and reverse scan for all temperatures. Figures 6.16 show the anodic polarisation of Inconel 625 in S2 at increasing temperature. The difference can be seen in Inconel 625 for anodic polarisation, as it shows primary and secondary breakdown potential, as shown in solution 2 at 50°C and 80°C. This shows that there is a sudden increase in current at potentials around 400-500 mV and then the potential increased at 200  $\mu\text{A}/\text{cm}^2$ . At the potential around 700-800 mV, the current increased and the breakdown potential can be detected. At increasing temperature from 50°C to 80°C, Inconel 625 presents to have secondary breakdown potential with increasing current in S2 and S3. This reveals that even at higher temperatures, Inconel 625 manages to self-repair the damaged passive film.

The compilation of breakdown potential of S2, S3 and S4 with the function of temperature is presented in Figures 6.19, 6.20 and 6.21, respectively. By comparing the  $E_b$  of materials in all solutions to  $E_b$  obtained from the anodic polarisation of materials in HW443, 25Cr duplex and Inconel 625 show the same performance as they show in S1. The value of  $E_b$  were not increased for 25Cr duplex and Inconel 625 in hydraulic fluid HW443. For stainless steel 316L, the  $E_b$  in HW443 is higher than  $E_b$  in solution 2 and solution 4. In solution 3, which has  $\text{SO}_4^{2-}/\text{Cl}^- = 0.75$  g/L, the  $E_b$  shows a decrease in performance in HW443 at 20°C. Microscope images in Figure 6.23 show that the large area of metastable pitting could result in a higher  $E_b$  for 316L in solution 3. The study by L. Tarja (2000) regarding localised corrosion of UNS S30403 in chloride, sulphate

and thiosulphate containing environments reveal that thiosulphate has a synergistic effect with chloride in inducing localized corrosion where thiosulphate prepares the surface while chloride weakens the passive surface, and, furthermore, initiates the pits [169]. This study also elucidates that sulphate has an inhibiting effect on pitting corrosion on UNS S30403 steel when the molar ratio  $\text{Cl}^-/\text{SO}_4^{2-} \leq 0.5$ .

In considering that a material's composition has an effect on the breakdown potential, 316L has the least chromium content compared to 25Cr duplex and Inconel 625. Chromium will react with oxygen to form chromium-rich oxide at the metal surface, which retards the corrosion by passive film formation, and the solutions composition and surface condition also affects the repassivation potential ( $E_r$ ) of materials [147]. However, the addition of other elements to 316L could increase the corrosion performance. The study by K. Hashimoto (1979) revealed that the addition of molybdenum to the stainless steel reduces the passive current density and enhances the rate of passivation [170]. In this work, the Mo usage is 2.0% in 316L, 3.0% in 25Cr duplex and 9.0% in Inconel 625. This reveals how Inconel 625 has a higher passive range and manages to self-repair the passive film.

Ann and Song (2007) in their study of assessing the chloride threshold level (CTL) ions of steel concrete in corrosive medium, found that at lower CTL, the corrosion of steel was initiated at defects at the steel-concrete interface, commonly at entrapped air voids [141]. CTL can be defined as the content of chloride at the steel depth that is necessary to sustain local passive film breakdown, and, hence, initiate the corrosion process. The assessment of CTL is a key element predicting the service life of concrete structures exposed to chlorides.

Although most researchers agree with the contribution that  $\text{Cl}^-$  could accelerate pitting in stainless steel, the effect of nonaggressive anions in aqueous solutions play an important role in the passivation process not only in stainless steel, but also in low alloy steel [142, 143]. For stainless steel, the risk of pitting decreased with increasing sulphate concentration. Pohjanne *etal.* (2007) found that increasing the sulphate concentration decreased pitting corrosion and a higher sulphate/chloride ionic ratio was needed to inhibit the pitting corrosion of stainless steels at higher chloride concentrations [122]. In another study by Pyun *etal.*, (1999) it was found that in addition to the anionic ratio, the anions competition also has an effect on corrosion attack. In their study, they also found that the addition of  $\text{Cl}^-$  and  $\text{SO}_4^{2-}$  reduces the anodic dissolution rate and the additional  $\text{SO}_4^{2-}$  was accounted for by the reduced

reacting surface area caused by competitive adsorption of  $\text{SO}_4^{2-}$  ions and  $\text{OH}^-$  ions. The pitting was only observed in the presence of  $\text{Cl}^-$  and was not caused by the adsorption of  $\text{SO}_4^{2-}$  ions [123]. Figure 6.19 presents the breakdown potentials of passive alloys in S2 ( $\text{SO}_4^{2-}/\text{Cl}^- = 19.15$ ) which has higher sulphate compared to chloride ratio. The same results present as these alloys in S1. 25Cr duplex and Inconel 625 used to have better corrosion protection in S2 compared to these alloys in HW443. However, the breakdown potential of 316L is lower in S2 compared to 316L in HW443 which elucidate that HW443 gives better protection on 316L in higher sulphate content. S3 and S4 have slightly lower sulphate content compared to chloride. However, the trends are still the same; changing the  $\text{SO}_4^{2-}/\text{Cl}^-$  ratio does not gives a significant effect to  $E_b$  of 316L and HW443 does not significant for 25Cr duplex and Inconel 625.

Generally, the initiation of pitting attack can be ascribed to the halide ion, such as  $\text{Cl}^-$  ion. Firstly, they adsorb on the passive film, especially on the weak sites [225]. Secondly, they penetrate the passive film with the assistance of a high electric field across the passive film and attack the base metal until stable pitting occurs by the quick dissolution of metal without the protection of the passive film. As the ratio increased, it is effect the adsorption of  $\text{Cl}^-$  ion on the passive film.

When the concentration of  $\text{SO}_4^{2-}$  is much lower,  $\text{Cl}^-$  ion were the main ions adsorbed on the surface. Since there was competitive adsorption between  $\text{SO}_4^{2-}$  and  $\text{Cl}^-$  ion,  $\text{Cl}^-$  ion would arouse the convergence of the  $\text{Cl}^-$  ion at certain local sites and increase the concentration of  $\text{Cl}^-$  ion at such locations indicated in Figure 8.8(b). One would expect that with increasing the number of  $\text{Cl}^-$  ion adsorbed on certain sites, more  $\text{Cl}^-$  ion would penetrate the passive film and attack the base metal. Since the ability of  $\text{Cl}^-$  ion to attack the passive film became lower because of the lower density of  $\text{Cl}^-$  ions as shown in Figure 8.5 (c), the inhibited effect of  $\text{SO}_4^{2-}$  ion on pit initiation. When the concentration of the  $\text{SO}_4^{2-}$  ion rose considerably high, the surface was completely covered with  $\text{SO}_4^{2-}$  ion, attributed to its easier ability to absorb on the surface than  $\text{Cl}^-$  ion. Now  $\text{Cl}^-$  ion was unable to be close to the surface, the 316L was protected in such solution. Zuo *et al.* (2002) also found that the competitive adsorption between  $\text{SO}_4^{2-}$  and  $\text{Cl}^-$  ions at active surface sites is the reason for inhibition [165-167]. The ratio of  $\text{Cl}^-$  to  $\text{SO}_4^{2-}$  ratio influences the pits nucleation and growth.

The competitive adsorption process between those two kinds of anions occurred in a dynamic way. The whole process could be characterized by the following course: the anions adsorbed on the metal surface while they left off at the same time when they

both adsorbed on the same location.  $\text{Cl}^-$  ion would be usually edged out of the location and move over the passive film because of the repulsive force between them and the lower weight of  $\text{Cl}^-$  ion. This process may lead to the convergence of  $\text{Cl}^-$  ion at certain sites. With this knowledge about the convergence of  $\text{Cl}^-$  ion at certain sites caused by the competitive adsorption between  $\text{Cl}^-$  and  $\text{SO}_4^{2-}$  ions as shown in Figure 8.8 below, elucidate the effect of sulphate chloride ratio to corrosion attack. It can be described as,  $\text{Cl}^-$  ion evenly adsorbed on the metal surface without the  $\text{SO}_4^{2-}$  ion presented.

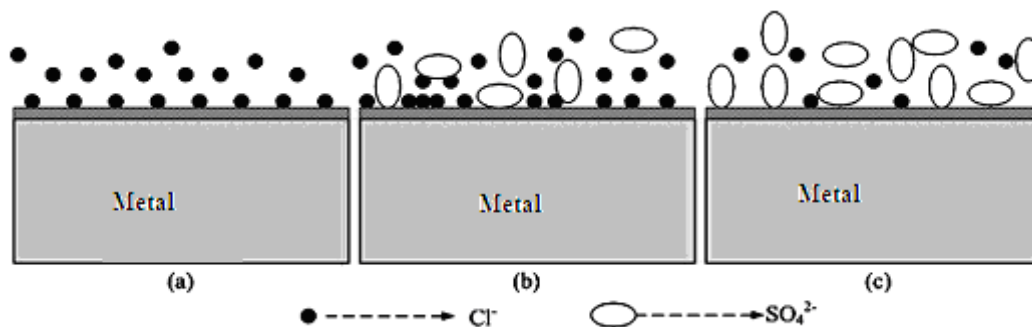


**Figure 8.8 Schematic drawing showing an adsorption of two kinds of anions at different concentration.**

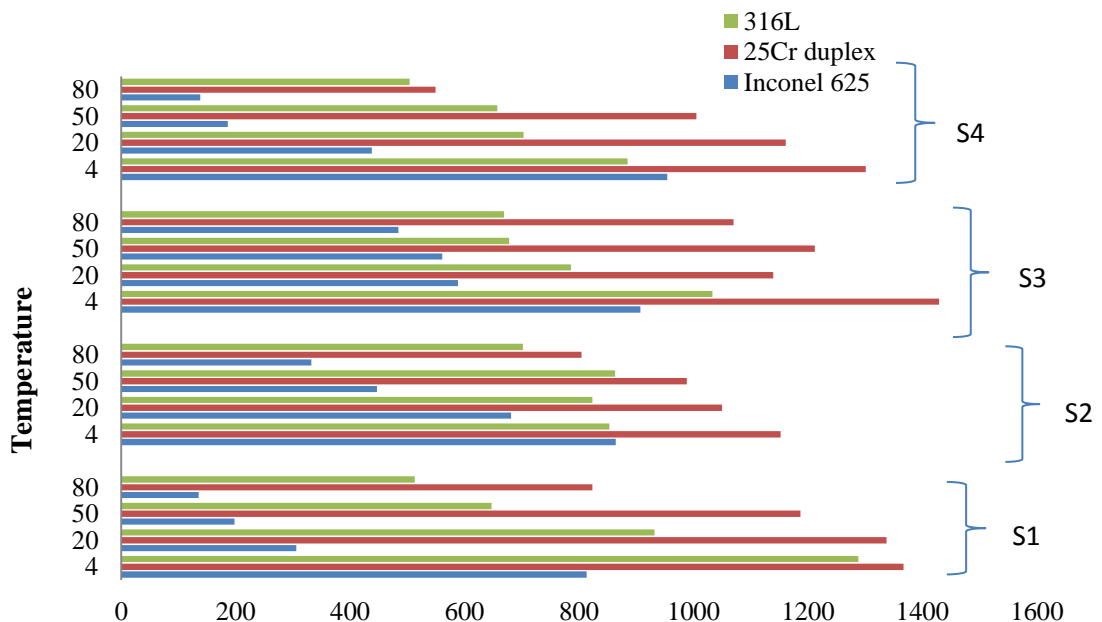
## 8.8 Passive Potential Range

The passive potential range of materials can be determined between primary passivation potential  $E_{pp}$  and  $E_b$  which also known as passive range or passivity region. The  $E_{pp}$  is the potential after the current decreases or becomes essentially constant over a finite potential region. The range of passive region can be used to characterise the corrosion behaviour and evaluate how the effectiveness of a passive film protects the metals from corrosion. Figure 8.9 below shows the passive range for 316L, 25Cr duplex and Inconel 625 in all solutions. In all solutions, it can be seen that the passive range increased as the temperature decreased from 80°C to 4°C for all materials. For 316L, the passive range decreased about 83% from 4°C to 80°C in S1 whereas 25Cr duplex decreased 40% and Inconel decreased 60% for the same range of temperatures. This shows that temperature drastically affects the corrosion attack for 316L compared to 25Cr duplex and Inconel 625.

The same figure also shows the passive range in S2 which has the highest sulphate compared to chloride content. 316L shows a decrease in the passive range of about 62% compared to 25Cr duplex and Inconel 625, which decreased 30% and 17%,

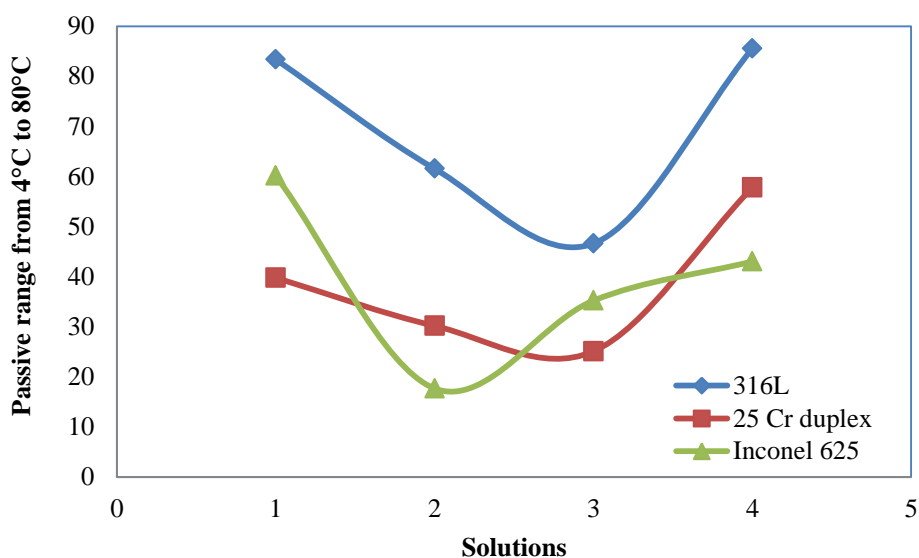
respectively. The same trend is shown for S3, which decreased 47%, 25% and 35% presents by 316L, 25Cr duplex and Inconel 625 respectively. However, all these passive alloys show the highest passive range in S3. The solution 3 has almost equal  $\text{SO}_4^{2-}/\text{Cl}^-$  ratio. The highest passive range might be due to competition effect between anions on metal surface. Increasing the temperature does not give a significant effect to passive region change for Inconel 625 and 25Cr duplex, in fact, the passive range of 25Cr duplex was decreased from 50°C to 20°C in solution 3. In S4, the passive range decreased for 85%, 58% and 43% by 316L, 25Cr duplex and Inconel 625 respectively.

Figure 8.10 reveals that Inconel 625 has the shortest passive range in S2 ( $\text{SO}_4^{2-}:\text{Cl}^-$  is 20.87:1.09) whereas 316L and 25Cr duplex has the shortest passive range in S3 ( $\text{SO}_4^{2-}:\text{Cl}^-$  is 9.41:12.54). A small difference in passive range can be concluded that the temperature does not have a significant effect on corrosion attack from 4°C to 80°C, especially for 316L, which has a massive difference in every solution at every temperature. This indicates that sulphate can inhibit materials from corrosion attack especially from localised corrosion attack. This is supported by Hong and Nagumo (1997) who studied the effect of  $\text{SO}_4^{2-}$  concentration in NaCl solution on the early stages of pitting corrosion on stainless steel. By using the AC impedance method, they found that the Warburg impedance coefficient,  $\omega$  (calculated from Nyquist impedance plots) decreases with increasing  $\text{Na}_2\text{SO}_4$  in the solution [171].



**Figure 8.9** Passive range for 316L, 25Cr duplex and Inconel 625 in all solutions as a function of temperature

This is because increasing the concentration of  $\text{SO}_4^{2-}$  in NaCl solution decreases the total number of surface sites available for metastable pits. Thus, increasing  $\text{SO}_4^{2-}$  concentration in NaCl solution causes the shift of not only pitting potential but also the metastable potential to more positive potentials. They also studied the effect of chloride concentration for the same criteria on type 304 stainless steel. They found that the impedance coefficient increases with increasing chloride concentration at low potentials in the passive region when the diffusion process begins to occur at the surface. The chloride concentrations also have an effect when metastable pitting starts to grow [172].



**Figure 8.10 The difference in passive range from 4°C to 80°C for passive alloys in different sulphate-chloride ratio solutions**

While Naggar (2006) elucidated that  $\text{SO}_4^{2-}$  ion retards the localised penetration in the pitting area [49], Alhajji and Reda (1996) found that increasing  $\text{SO}_4^{2-}$  ion from 15 ppm to 150 ppm in tap water increases the corrosion rate due to uniform corrosion for long-term experiments conducted over an eight month period under stagnant conditions [173]. The study by Newman and Moayed (2006) on adding sulphate at critical pitting potential (CPT-the first temperature when stable pitting occurs at intermediate potentials) on 904L shows that sulphate increases the critical concentration of metal salt in the pit, expressed as a fraction of the saturation concentration, which is required to sustain pit dissolution [174].

From the kinetic point of view, a compact non-porous film is produced from the formation of film growth by the transfer of the metal into the film by ionic conduction

within the film and by ion transfer between the film and electrolyte. Porous films may form by precipitation from a supersaturated electrolyte, which allows direct contact between the metal and the electrolyte and are not passivating in the sense that the mean corrosion rate drops at positive electrode potentials. The true current density in the pores continues to grow with the electrode potential at the interface between the metal and the electrolyte. Porous films are sometimes formed by precipitation from the electrolyte on top of a compact passivating film [154].

## 8.9 Effect of Temperature on Pitting Corrosion

Temperature gives has a great effect to corrosion attack not only on active materials (carbon steel) but also on corrosion resistant alloys (CRAs) such as 316L, 25Cr duplex and Inconel 625. While the active materials built rust as a protective layer, passive materials built a passive film to protect them from corrosion attack. However, in highly aggressive environment, the passive film will destroy and exposed the base metal for further corrosion attack, which is called breakdown potential,  $E_b$ . To carbon steel, temperature may accelerate the corrosion attack by losing their weight, while temperature may give an effect to passive alloys by destroying the passive film. According to Laycock and Newman (1998), at higher temperatures, the passive film became thicker, but more porous, and, therefore, less protective [155]. Until now, no theory has satisfactorily explained the effect of temperature on breakdown potential,  $E_b$ . This effect is probably related to changes concerning the kinetics of passivation and repassivation, diffusion rate, hydrolysis kinetics, properties of passivating films and dissolution rate of the alloy in its passive state. All of them change with increasing temperature.

For stainless steel, increasing the temperature not only decreases the breakdown potential to more negative values, but also increases the kinetics of the pitting corrosion. According to Szklarska-Smialowska and Mankowski (1975), increasing the temperature also increases the number of pits formed at the same potential as a higher temperature provides more sites susceptible to the nucleation of pits [157]. Increasing the temperature also accelerates the reagent transport and reaction products to or from the electrode. Thus, it affects chloride ions adsorption in the pits as well as an increase in the initial current density in the pits. As the concentrations change, it leads to an increasing concentration polarization, which affects ohmic polarisation when the salt layers or other solid corrosion products appear in the pits. However, the mechanism of



pitting corrosion in stainless steel not only depends on temperature, as the oxidation process also strongly depends on oxygen at the metal interface. According to Resenfeld and Danilov (1967), the strength of the oxygen-metal bond cannot be considered the same at all parts of the surface [175]. Therefore, the dissolution passive film in aggressive environment sometimes is not significant to increasing the temperature as other factors may also contribute to corrosion attack on metal surface.

Figure 6.9, 6.19-6.21 in Chapter 6 shows the breakdown potential,  $E_b$  of 316L, 25Cr duplex and Inconel 625 as a function of temperature. The effect of temperature to corrosion attack on carbon steel has been explained in section 8.3 and the Arrhenius relations to activation energy at increasing temperature was presented in Figure 8.2. the temperature also gives an impact to breakdown potential,  $E_b$  of passive alloys. Increasing the temperature in solutions was reduced the  $E_b$  value for every materials. The  $E_b$  was also compared to  $E_b$  of materials in HW443 at 20°C. According to Piantini *etal.*(1997), temperature has a significant influence on the passivity behaviour for duplex stainless steel. They determined that temperatures between 23°C and 60°C improve the stability of passive films [176]. This is explained by the constant breakdown (small significant change) of passive film at increasing temperatures, due to changes in the composition and structure of the passive film as well as the increasing velocity of the phenomena involved. In this research 25Cr duplex was the most stable in corrosive environment even at increasing temperature followed by Inconel 625 and 316L.

## **8.10 Effect of Oxygen on Corrosion Attack**

Since seawater is a complex, delicately balanced solution of many salts containing living matter, suspended silt, dissolved gases, and decaying material, the individual effect of each of the factors affecting corrosion behaviour is not readily distinguishable. Because of the interrelation between the effects of many variables in the seawater environment, an alteration in one may affect or depend on the relative magnitude of others.

The reaction of oxygen with a clean metal surface follows the sequence: 1) adsorption, 2) formation of oxide nuclei, and 3) growth of continuous oxide. The adsorption of oxygen forms a stable structure that remains on the metal surface and is considered to make up a passive film. Continuous exposure to low oxygen pressure,

oxide nuclei will grow rapidly to a thickness limited by the electro tunnelling distance and growth of the continuous film following logarithmic oxidation kinetics [159].

It has been observed in a number of cases that the corrosion rate of carbon steel should be linearly dependent on the oxygen concentration. Schumacher (1979) reported the effect of dissolved oxygen on the corrosion of carbon steels from laboratory experiments and concluded that the corrosion rate of steel is linearly proportional to the dissolved oxygen [177]. For stainless steel, the specific function of oxygen in the passivation process is still not clearly understood. Three mechanisms are postulated to describe the reaction of oxygen with stainless steels to produce passivity – adsorbed gas, oxide film and passivating inhibitor [118, 159, 161-163]. However, under practical conditions the formation of layers or films often interferes with the exception of alloys, which tend to require oxygen to function in the passive state with low corrosion rate. Furthermore, alloys that have rather active corrosion potentials may cause corrosion with a cathodic reaction involving the reduction of hydrogen ions and/or water itself [164]. Covino *et al.* (1986) used the OCP technique to measure the quantity of oxygen consumed during the passivation process showed that alloys with lower amounts of chromium consumed less oxygen [178]. They found that 1.7 ppm oxygen is required to stabilise the passivity of Fe-Cr alloys containing >12.5% wt Cr.

The strength of the oxygen-metal bond is not the same at all parts of the surface. In the zones where this bond is less strong, adsorption displacement or substitution of the oxygen by the chloride ions is possible [157]. The chloride ions displacing the oxygen from the surface penetrate under the oxide film and the process develops in a relatively enclosed zone where the diffusion of oxidizers is hampered.

## **8.11 The Role of Inhibitor to Corrosion Protection**

The corrosion behaviour for 316L, 25Cr duplex and Inconel 625 was also studied in CRW 89000 inhibitor. This is the inhibitor used in oxygen environments by oil and gas companies. Figures 6.25 in Chapter 6 compares the breakdown potential of 316L, 25Cr duplex and Inconel 625 in solution added with 100 ppm inhibitor CRW 89000 at 20°C. All passive alloys show higher  $E_b$  when solution 1 (seawater) added with inhibitor. This shows that the inhibitor chemically modifies the surface of these materials to mitigate or prevent the corrosion process. While numerous corrosion inhibitors have been suggested, the detrimental effect of many of them in the oil and gas process limit their commercial use, for example, the presence of chloride in marine

environments can penetrate the porous structure of passive film [166]. However, the presence of non-aggressive anions could inhibit corrosion naturally apart from using inhibitors to increase the corrosion resistance.

## **8.12 The 25Cr Duplex Stainless Steel**

As described in Chapter 3, duplex stainless steels exist in a two-phase microstructure, austenite-ferrite. Chromium (Cr) and molybdenum (Mo) enrich in ferrite, while nitrogen (N) and nickel (Ni) are mainly found in austenite [71]. Because of the high content of alloying elements, the duplex stainless steels show complex phase transformation and precipitation behaviour [167]. The best general properties are obtained with approximately equal amounts of austenite and ferrite and the absence of third phases such as  $\sigma$  and  $\chi$  [168, 169]. However, due to high chromium and molybdenum contents and their high diffusion rate in ferrite, duplex stainless steel are prone to form some unwanted secondary phases during exposure to elevated temperatures between 400 and 1000°C. The study by Ezuber *et al.* (2007) found that sigma phase precipitation, which is produced during the pre-quenched heat treatment of duplex stainless steel was immune to pitting corrosion in seawater at ambient temperature but susceptible to pitting at 50°C and above [179]. The results also clearly indicated that the presence of nitrogen and relatively higher chromium content duplex stainless steel is an advantage for seawater pitting corrosion resistance. This shows that apart from composition, heat treatment during the duplex process contributes to the higher resistance of this material to corrosion attack. In this research, 25Cr duplex presents to have the highest  $E_b$  value in all solution at increasing temperature compared to other passive alloys (316L and Inconel 625).

## **8.13 Cermet Alloys**

### **8.13.1 Introduction**

WC-Co hardmetals are composed of hard WC particles in a tough metallic matrix produced during a liquid phase sintering process. Due to strength, cemented carbides have applications spanning most engineering fields. However, application in chemically aggressive environments is less successful because they are susceptible to corrosion. However, there is little research on cermet alloys for material degradation due to corrosion. Various efforts have been made to reduce the corrosion susceptibility of WC-Co. It was found that using Ni instead of Co as the binder material or alloying element

into the binder phase leads to higher corrosion resistance [39]. However, in terms of wear, cemented carbides bonded with nickel show lower toughness than that of cobalt-bonded carbides [78]. Other carbides are also introduced during sintering to improve processibility, mechanical and corrosion properties and prevent grain growth during sintering. It has been shown that the addition of tungsten (W) and molybdenum (Mo) in cobalt-base alloys influences the corrosion behaviour by stabilising the face centred cubic (fcc) phase [171]. In WC WC-based cermets, both the corrosion protection efficiency afforded to the substrate (which is usually anodic to the carbide) and the corrosion of the coating constituents themselves have been investigated [172, 173]. Studies concerning the corrosion process of carbon steel coated with WC-Co cermets in 3.5% NaCl [174] show that increasing the cobalt content from 12% to 17% provides more protection by changing the pore morphology from interconnecting the isolated pores.

Due to the heterogeneous microstructure and binder phase composition, the corrosion mechanisms of WC-Co are very complex, and only very little is known about the exact corrosion processes taking place. This is in respect of the relationship behaviour between the electromechanical and in-service corrosion performance. Some researchers claim that the whole WC-Co surface does not behave equally active, and that the corrosion attack proceeds predominantly at locations where the WC phase has fallen out after localized initiation of corrosion has taken place. Bozzini *et al.* (2009) reported that the corrosion of WC-Co is controlled by the galvanic coupling of the anodic metallic binder to the cathodic ceramic phase, which exhibits electronic conductivity [180]. Aristizabelet *al.* (2011) revealed that the oxidation resistance of WC-Co increases with metallic content [181]. This is observed by materials containing higher fractions of tungstates. However, Lekatou *et al.* (2008) claim that the corrosion resistance of cermet alloys strongly depends on the binder composition [182]. They also found that corrosion of WC-Co begins with active dissolution of Co in preferential sites, such as intersections of adjacent WC particles [178]. They also explained that pseudopassivity proceeds via a passive process (oxide formation), pseudopassive (limitation of  $\text{Co}^{2+}$  diffusion), binder dissolution (active process), and, lastly, followed by localised corrosion. However, the reactions taking place on the hardmetal surface are strongly dependent on the potential of the system. At open-circuit conditions or at small applied potentials, the binder phase undergoes selective dissolution, while it is only in the higher potential range that the dissolution of the WC phase takes place. At intermediate potentials (i.e., below the dissolution of the WC phase), the observations of

different researchers diverge. Some authors report a passive behaviour of the composite, others claim a kind of pseudo-passive state, where the presence of non-adherent, but diffusion-inhibiting corrosion products leads to a limitation of current density.

Figure 8.11 below gives a schematic description of the reaction taking place on the hardmetal surface. Because the WC are more noble in oxidation potential compared to Co, a galvanic coupling between the two phases will force the anodic part of the overall corrosion reaction to proceed on the Co phase. Thus, Co dissolution occurs due to the unfavourable surface ratio of anodic compared to cathodic sites. In parallel, cathodic reaction occurs in oxygen or hydrogen reduction will take place on the WC phase, and, consequently, protect the hardmetals against corrosion.

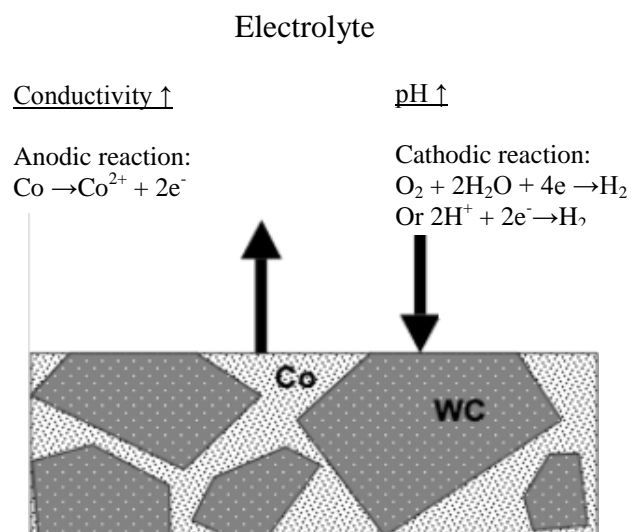


**Figure 8.11 Schematic presentation of the reactions taking place on the WC-Co surface [39].**

## 8.14 Pseudo-passivation

Pure cobalt does not passivate and remains active with increasing potential. A film forms on Co(W,C) alloys causing the current to become relatively independent of potential but remaining very high. This behaviour is termed here 'pseudo-passivation'. According to Machio *etal.* (2010) the behaviour happens when the current density decreases minimally as the potential is increased [183]. With increasing carbon and tungsten additions, the corrosion current density and critical current density are reduced. The corrosion potential shifts to more positive values with increasing additions. It is shown that carbon and tungsten additions influence the corrosion behaviour by a stabilisation of the fcc phase. Empirical equations are derived, which quantitatively

relate the volume fraction of the fcc phase to the composition of the alloy, i.e., the carbon and tungsten content in the binary and ternary alloys.

Investigations performed in aqueous solution, containing chloride ions, revealed that the whole WC-Co surface does not behave equally active, as the corrosion attack proceeds predominately at locations where the WC phase has fallen after localised initiation of corrosion has taken place.

### **8.15 Active Corrosion of Cermet Alloys**

The corrosion behaviour of cermet alloys should be affected by:

- a) the corrosion behaviour of its components
- b) the galvanic effect of the WC-Co and WC-Ni couple
- c) the galvanic effect between matrix regions of higher W concentration

In spite of intensive research, the mechanism of the active dissolution of Co and Ni, is not completely understood. Anions and also the structure of the surface, affect the anodic current-density potential curves in oxide-free dissolution, as in acid solutions [180]. Ebersbach *etal.* (1967) in their research about kinetics of the anodic passivation of cobalt and nickel found that active corrosion is pH dependent, which suggests OH<sup>-</sup> contribution [184].

### **8.16 Effect of Binder**

As explained before, cemented alloys consist of hard WC particles in a tough metallic matrix produced during a liquid phase sintering process. For WC-Co and WC-Ni, corrosion attack will depend on the matrix – Co and Ni – and the corrosion attacks are mainly between the WC-Co interfaces. The corrosion attack at the interface will produce an oxide layer. The study by Aristizabel *etal.* (2008) concerning oxidation behaviour of WC-Co found that Co content has an effect on the oxidation layer, thus, affecting the oxidation behaviour. Co content increases the oxide layers and exhibits a more compact structure [181], however, Co binder has low corrosion resistance [185].

In terms of grain size, according to Virtanen *etal.* (2009), the smaller the grain size, the higher the corrosion resistance because the corrosion behaviour is strongly influenced by the WC dissolved in the Co binder [185].

Human and Exner (1997) in their research concerning the relationship between electromechanical behaviour and in-service corrosion found that electromechanical behaviour of WC-Co composites can be modelled using the linear rule of mixture [187]

$$i^{WC-Co} = A_A^{WC} \cdot i^{WC} + A_A^{Co} \cdot i^{Co} \dots\dots\dots 8.1[187]$$

Where  $i^{WC-Co}$ ,  $i^{WC}$ ,  $i^{Co}$  is current density for WC-Co, WC and Co, respectively, and  $A_A^{WC}$ ,  $A_A^{Co}$  are the cross-sectional area fractions of the WC and Co phase respectively. Human also added that at increasing polarisation, the corrosion current is due to oxidation of the binder. This agrees with other authors who claimed that corrosion resistance only depends on the cermet binder. Figure 8.12 below shows WC-Ni in seawater at 20°C. The partial current due to binder phase oxidation initially increases exponentially with increasing potential. A maximum is reached after which the current abruptly decreases. Thereafter, the current density appears to remain relatively independent of the applied potential, as shown in Figure 8.13, as distinct potentials but remaining very high. This behaviour is termed ‘pseudo-passive’. Although this phenomenologically looks similar to passive behaviour, the form of the polarisation curve is due to an ohmic drop at the specimen surface, caused by a thick surface deposit [185].

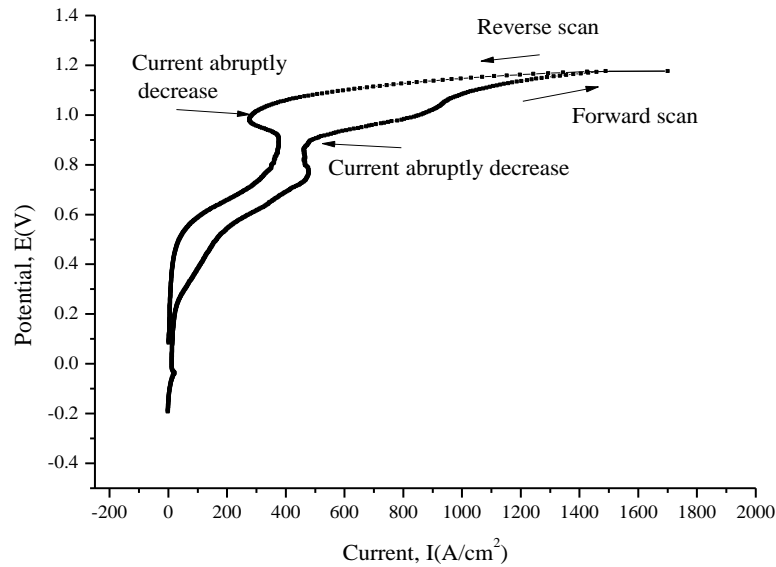


**Figure 8.12 WC-Ni in S1 at 20°C**

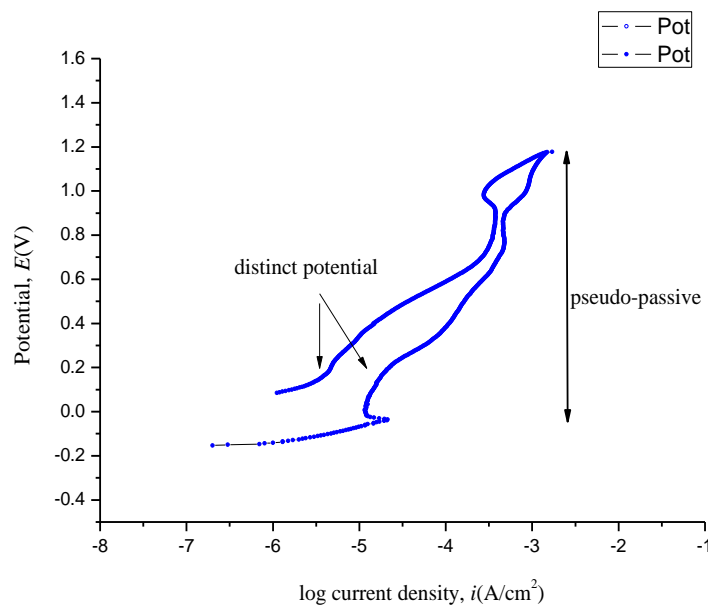


**Figure 8.13 Current density appear as independent applied potential**

The rise of current density is similar to transpassive behaviour, however, according to Human and Exner (1997), by comparing with the individual phases of cermet compositions, it is apparent that the current increase is due to WC oxidation and not to a surface film breakdown like passive materials.

### 8.17 The Effect of pH to Corrosion Attack

Concerning the corrosion susceptibility, the solution pH dominates the effect of specific ions. In neutral and acidic solutions, the corrosion process of WC-Co consists mainly of Co dissolution. WC dissolution becomes more significant at alkaline pH. Degradation is mainly the result of selective uniform dissolution of the phases (Co or WC) not of localised corrosion because of the poor passivating ability of Co [101]. Synergistic effects due to galvanic coupling between the Co binder and WC accelerate Co dissolution and hinder WC dissolution in the hardmetals compared to the pure compounds. However, the Co binder phase contains W and C, which make it more corrosion resistant than pure Co.

The presence of aggressive chloride ions in the electrolyte solution causes increasing corrosion rates, whereby the effect was found to be dependent on the solution pH [102], which agrees with Ghandehari *etal.*(1976) who said that hydrogen (which contributes to pH value) has no significant effect on the oxygen reduction of copper [115].



According to Schmutz *et al.*, (2007) the corrosion process of WC-Co in neutral and acidic solutions mainly consists of Co dissolution whereas WC dissolution is more significant in alkaline solutions [144]. The study by Gilli *et al.* (1969) on the passivation of Ni caused by salt layers in concentrated H<sub>2</sub>SO<sub>4</sub>, found that as the concentration of H<sub>2</sub>SO<sub>4</sub> increases (acidic), the solubility of Ni sulphate decreases gradually and results in precipitation as a layer on the electrode [188].

Figure 7.3 and 7.4 in Chapter 7 shows an anodic polarisation of WC-Co and WC-Ni in commercial hydraulic fluid HW443 at 20°C. Both materials show similar polarisation and both have a negative hysteresis. Figures 7.5 and 7.6 show the reverse potential,  $E_r$  and corrosion rate of WC-Co as a function of temperature in S1, S2, S3 and S4, respectively. All the polarisations exhibit positive hysteresis and there is no obvious in passive range at increasing current density. Lekatou *et al.* (2010) reported that almost 80% appear to have a positive hysteresis and 20% appear as a negative hysteresis during potentiodynamic polarisation of WC-Co [189]. However, changing the SO<sub>4</sub><sup>2-</sup>/Cl<sup>-</sup> to higher SO<sub>4</sub><sup>2-</sup> shows that the polarisation mostly changed from positive to negative hysteresis. The rest of cyclic polarisation for WC-Co were compiled in Appendix and some of WC-Co hysteresis presents to have secondary  $E_b$ . WC-Co in S4 having secondary breakdown potential  $E_b$  at 4°C and 20°C. This is similar to  $E_b$  but in the WC-Co system, this emerging can be related to a pseudo-passivation peak. This is typical of the corrosion behaviour of this material, due to precipitation of corrosion products [187].

The anodic polarisation of WC-Ni in S1, S2, S3 and S4 are shown in Figures 7.9-7.10. In contrast to WC-Co, WC-Ni has a more negative hysteresis than positive hysteresis in every solution. WC-Ni in S1 behaves as pseudo-passive at 20°C, which also happens for WC-Ni in S2 at 4°C and in S4 at 20°C. It has been assumed thus far that the passivation can be produced only by oxygen layers. "Passivation", however, can also be obtained by a salt layer. Ghandehari *et al.* (1976) in their study about oxygen reduction of copper in dilute sulphuric acid solutions report that sulphate ions caused decreased solubility of oxygen and inhibited oxygen reduction by adsorption and blocking the surface as well as decreasing the oxygen solubility [115].

The current maximum (the hump as shown in Figure 7.11) is due to cathodic film formation, which inhibits the rate of oxygen reduction. The reduction process may also contain adsorbed sulphate ions. Ghandehari *et al.* (1976) also added that hydrogen ions have no significant effect at this region [115]. Figures 7.10 and 7.11 also show that WC-

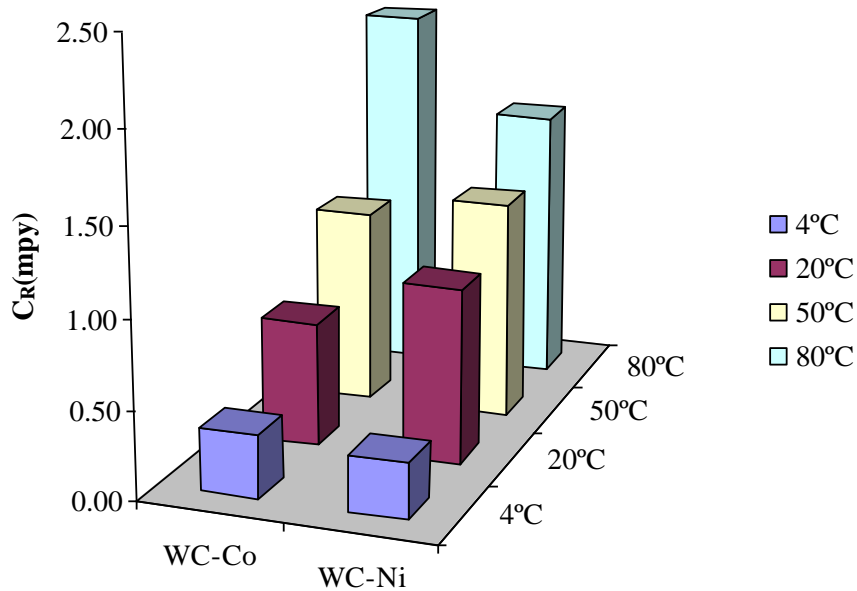
based cemented carbides oxidate at all temperature ranges. This finding is supported by the research of R.B. Perez-Saez *etal.*(2009)who studied the kinetics inversion of WC-based carbides [190].

As explained in Chapter 3, WC-Ni perform as active corrosion and corrosion rate can be determined using the formulae

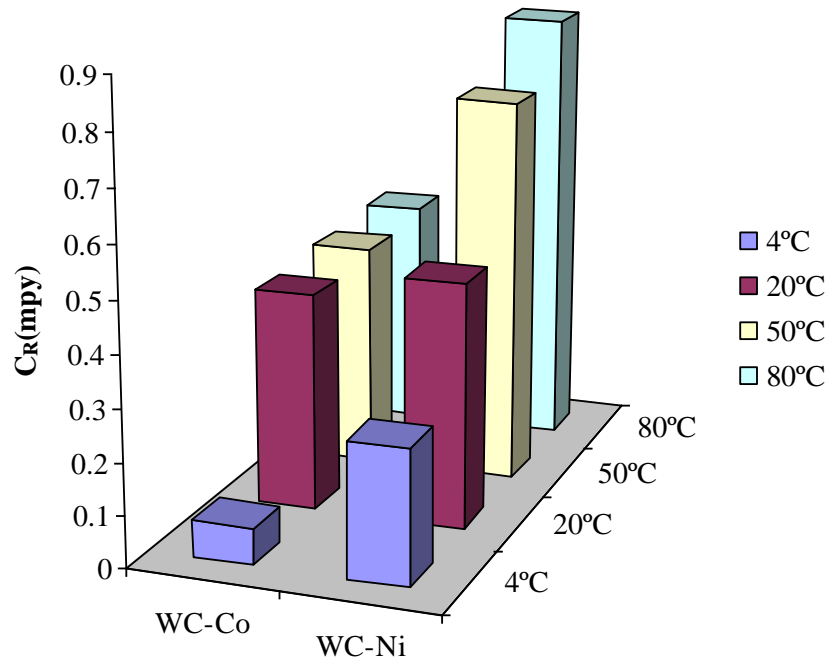
$$\text{Corrosion rate, } C_R \text{ (MPY)}= i_{\text{corr}} \times (\Lambda) \times (1/\rho) \times \varepsilon$$

The corrosion rates for WC-Ni in all solutions are presented in Table 7.4. The highest corrosion rates are obtained in S1. Figure 7.8 and 7.9 shows the corrosion rate and reverse potential for WC-Ni for all solutions as a function of temperature. As expected, the corrosion rate increased linearly to the increasing temperature of S1, S2, S3 and S4. At 20°C, the WC-Ni has higher value in corrosion rate in all solutions compared to corrosion rate of WC-Ni in HW443.

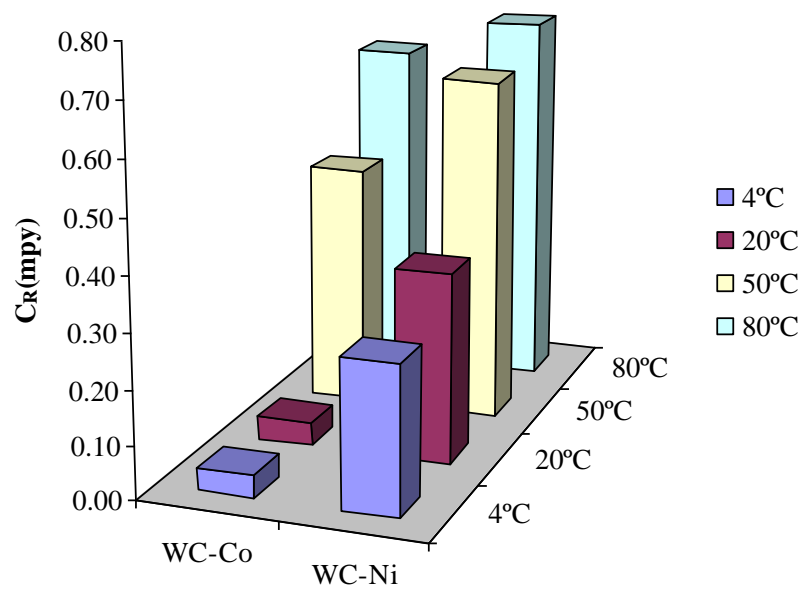
Figure 8.14 below presents the comparison of WC-Co and WC-Ni at increasing temperature in S1, S2, S3 and S4 respectively. Both materials present increase in corrosion rate at the temperature increased. In all solutions WC-Ni shows increased steadily as the temperature increased.



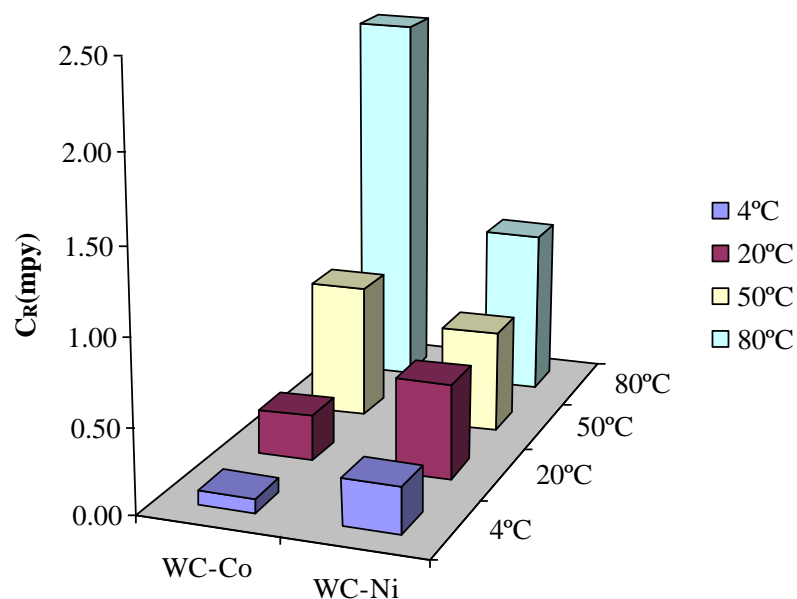
(a)



(b)



(c)



(d)

**Figure 8.14 Corrosion rate for cermets alloy in different sulphate/chloride ratio at increasing temperature. (a) Solution 1( $\text{SO}_4^{2-}/\text{Cl}^- = 0.14$  g/L), (b) Solution 2( $\text{SO}_4^{2-}/\text{Cl}^- = 19.15$  g/L), (c) Solution 3( $\text{SO}_4^{2-}/\text{Cl}^- = 0.75$  g/L) and (d) Solution 3( $\text{SO}_4^{2-}/\text{Cl}^- = 0.99$ )**

The corrosion rate of WC-Co increased drastically from 4°C to 20°C in solution 2 (b) and the rate stable from 20°C to 80°C which explain that at high sulphate content WC-Co in stable at high temperature. However, in solution 3 and 4 which contain almost equal content of sulphate and chloride, the corrosion rate increased drastically from 20°C to 50°C which explained that reducing of sulphate content contribute to reducing of inhibition effect for WC-Co at high temperature. Conversely, WC-Ni presents to have stable corrosion rate in different sulphate/chloride ratio.

## Chapter 9

### CONCLUSIONS AND FUTURE WORK

#### 9.1 Conclusions

- The corrosion products produced on the carbon steel surface can slow the corrosion attack, however, after sometime the protective product collapses and the carbon steel surface is exposed to corrosion again.
- The corrosion rate of carbon steel can be reduced by using CRW 85155 added to seawater. However, increasing the inhibitor concentrations from 20ppm to 100ppm at 20°C does not reduce the corrosion rate for the carbon steel in static conditions.
- Changing the inhibitor to CRW 89000 could obtain a corrosion rate close to the corrosion rate in HW443 by using seawater added with 400 ppm CRW 89000 at 20°C.
- Another alternative to control the corrosion rate of carbon steel in seawater is by controlling the chloride content at 0.05 g/L and oxygen content about 16 ppb.
- For passive materials, increasing the temperature reduces the breakdown potential for all materials and solutions.
- 25Cr duplex and Inconel 625 show higher breakdown potential in seawater (S1) compared to HW443, but 316L shows lower breakdown potential in S1.
- Overall, the experiment shows that 25Cr duplex shows better performance compared to Inconel 625 and 316L when comparing the breakdown potential. However, Inconel 625 is able to self-repair for the second time after the first time breakdown in potential. Furthermore, Inconel 625 shows the most stable breakdown for all solutions and temperatures. The passive range difference shows that Inconel 625 is the most stable for all solutions and temperatures.
- For cermet alloys, WC-Co has a more positive hysteresis compared to WC-Ni, which has a more negative hysteresis, especially at higher temperature.
- WC-Co presents as pseudo-passive at low temperature.

- The corrosion rate of WC-Ni is determined by calculation as WC-Ni is considered to perform as an active material.
- Changing the composition of the sulphate-to-chloride ratio of seawater reduces the corrosion rate of WC-Ni.
- It should be noted that some inconsistency in the results might be due to the non-homogeneous composition of the materials. Thus, there is often no local uniformity of the current distribution on the entire surface and this affects the electrochemistry results.
- Apart from having a smaller size compared to  $\text{Cl}^-$ ,  $\text{SO}_4^{2-}$  anions also increase the pH value of solutions, thus, it helps in decreasing corrosion attacks.

## 9.2 Suggestions for Future Work

- i. The oxygen content is very difficult to control at increasing temperature plus the electrochemical reaction also contributes to the oxygen content. Future experimental work should only concentrate on active materials to study the oxygen parameters that affect corrosion attack.
- ii. As the heat treatment process affects the stainless steel composition and cermet binder, the materials used in the experimental work should only be purchased from the same supplier.
- iii. To study the corrosion behaviour of cermet alloys, the cyclic polarisation curve should be compared to other percentages of WC-Co alloys as increasing the current density and constant potential might not be due to surface film breakdown, but to WC oxidation.
- iv. There should be different approaches to studying the corrosion behaviour of cermet alloys because cermets consist of ceramic and metal compositions. The corrosion behaviour is in between active and passive corrosion mechanism.
- v. Induction time is the time spent between the injection of the aggressive anion into solution and the start of pitting
- vi. The effect of velocity should be studied in the future.

## References

1. Fontana M.G. *Corrosion Engineering*, McGraw-Hill, 1987, pp. 3-13.
2. Koch, G.H., Michiel P.H. and Thompson N.G., Corrosion costs and preventive strategies in the United States, *Federal Highway Administration (FHWA). FHWA-RD-01-156*[online], 2001, [Accessed Jan 2011]. Available from: <http://www.corrosioncost.com/summary.htm>
3. GuoB., Chacko J., Ghalambor A., Offshore pipelines. *Gulf Professional Publishing*[online], 2005, p.302. [Accessed October 2008]. Available from: [http://books.google.com.my/books/about/Offshore\\_Pipelines](http://books.google.com.my/books/about/Offshore_Pipelines).
4. Chen, M.A., Influence of hydrolysis time on the structure and corrosion protective performance of (3-mercaptopropyl)triethoxysilane film on copper. *Corrosion Science. In Press*, 2001
5. Mary Tiemann the Specialist in Environmental Policy and Adam Vann, the Legislative Attorney, *Hydraulic Fracturing and Safe Drinking Water Act Issues* 2 Congressional Research Service, July 12, 201, p.1-42
6. Group, N.E.P.D., *Sustainable Development of North America's Oil and Natural Gas Ensuring Plentiful Energy and a Clean Environment*, 2001, Department of Energy: United States of America. p. 3.
7. Azeri, Chirag and Gunashli, *Subsea Water Injection Development*, 2004, Environmental & Socio Economic Impact Assesment Phase 3
8. Daniel R.S and Newell K.D, *Fracturing of Oil and Gas Wells in Kansas*, December 2011, Kansas Geological Survey Hydraulic, pp.1-6
9. Knight G.C. 1977, Water hydraulics: Application of water-based fluids to hydraulic systems. *Tribology International*, **10**(2): pp. 105-108.
10. Rushau G..R., *Oil and gas exploration and production*, 1997.
11. McManus., W.M. Canning Ltd, 1996, Presentations hydraulic fluids for Angola.
12. Zheng, L., Corrosion in hydraulic fluids for subsea applications, in *School of Mechanical Engineering* 2009, University of Leeds: United Kingdom. p. 219.
13. Roberg P.R., *Corrosion engineering: Principles and practice*: McGraw-Hill, 2008, pp 5, 169-177.
14. Kamachi I U. M., *Corrosion Science and Technology: Mechanism, Mitigation and Monitoring* 2009, Mumbai: narosa publishing house.
15. Denis B., Randy E., Andrew H., Donald H., Shreekant M., and Tony M., Corrosion in the oil industry, *Schlumberger Oilfield review*[online], 1994, [Accessed 2010]. pp. 1-15. Available from: [http://www.slb.com/~media/Files/resources/oilfield\\_review/ors94/0494/p04\\_18.pdf](http://www.slb.com/~media/Files/resources/oilfield_review/ors94/0494/p04_18.pdf)
16. Butler G., H.C.K.I., *Corrosion and Its Prevention in Waters* 1966: A Leonard Hill Book. 281.
17. ToolBox, T.E. *Oxygen solubility in fresh and sea water*. 2011; Available from: [http://www.engineeringtoolbox.com/oxygen-solubility-water-d\\_841.html](http://www.engineeringtoolbox.com/oxygen-solubility-water-d_841.html).

18. Stansbury E.E. and Buchanan R.A., *Fundamental of electrochemical corrosion*, The University of Tennessee, ASM International, 2000. pp 172-197.
19. Shinagawa K, Anti-corrosion Measures for Cable Bearers and Other Iron Fittings in Manholes. *NTT Technical Review* [online], 2008. **6**(11). [Assessed April 2011]. Available from: <https://www.ntt-review.jp/archive>.
20. Davis J.R., *Corrosion: understanding the basics*, Ohio, ASM International, 2000, pp
21. Dawson J.L., *Corrosion monitoring of steel in concrete in crane*. A.P. (ed) corrosion of reinforcement in concrete construction, 1983: p. 175-92.
22. Ahmad Z., *Principles of Corrosion Engineering and Corrosion Control*. 2006: p. 90-109.
23. Tait W.S., *An introduction to electrochemistry corrosion testing for practicing engineers and scientist*, 1994, PairODocs Publications. p. 119.
24. Revie R.W., *Uhlig's Corrosion Handbook*. John Wiley & Sons, 2nd ed, 2000
25. LiI J. et al., *Critical pitting and repassivation temperatures for duplex stainless steel in chloride solutions*. *Electrochimica Acta*, 2008. **53**(16): p. 5220-5225.
26. Roberge P.R. *Handbook of Corrosion Engineering*, United States, McGraw Hill, 2008,
27. Malik A.U., Ahmad S., Andijani I., Corrosion behavior of steels in Gulf seawater environment., *Saline Water Conversion Corporation*, [online], 1999. **123**: pp. 205-213. [Accessed March 2011]. Available from : <http://www.swcc.gov>
28. Roberge P.R. [online]. 2000. [Accessed 19 May 2011]. Available from : <http://www.corrosion-doctors.org/Forms-crevice/crevice1.htm>.
29. Frankel G.S., Sridhar N., *Understanding localized corrosion*. [online], *Materials Today*, 2008. **11**(10): p. 38-44. [Accessed 2011]. Available from: <http://www.matsceng.ohio-state.edu/~frankel/fcc/pubs/data/102.pdf>
30. Leckie H.P., Uhlig H.H., Environmental factor affecting the critical potential for pitting in 18-8 stainless steel. *J. Electrochemical Society*, 1966. **113**(12): p. 1262-1267.
31. Galvele J.R., Transport processes in passivity breakdown-II. Full hydrolysis of the metal ions. *Corrosion Science*, 1981. **21**(8): p. 551-579.
32. Schwenk W, Electrochemical investigations of pitting corrosion. *Corrosion Science*, 1973. **13**(10): pp. 739-746.
33. Sastri V.S, Edward G. and Mimoun E., *Corrosion: Prevention and protection. Practical solutions* 2007: John Wiley & Sons, Ltd.
34. Watkins J.W. and Kincheloe W., *Corrosion of steel in water by varied ratios of dissolved gasses*. *Corrosion*, 1958. **14**: p. 341-344.
35. Sridhar N., Brossia C.S, Dunn D.S. and Anderko A., *Predicting localized corrosion in seawater*. *Corrosion*, 2004. **60**(10): p. 915-936.
36. Uhlig H. H. , Triadis D.N., and Stern M., *Effect of oxygen, chlorides and calcium ion on corrosion inhibition of iron by polyphosphates*. *J. Electrochemical Society*, 1955. **102**(2): p. 59-66.



37. Caceras L., Vargas T. and Parra M., *Study of the variational patterns for corrosion kinetics of carbon steel as a function of dissolved oxygen and NaCl concentration*. *Electrochimica Acta*, 2009. **54**: p. 7435-7443.
38. Allen J.B., and Larry R.F., *Electrochemical methods, Fundamentals and applications*. 2nd ed 2001: John Wiley & Sons, Inc.
39. Hochstrasser(-Kurz) S., Mueller Y., Latkoczy C. and Virtanen S., *Analytical characterization of the corrosion mechanisms of WC-Co by electrochemical methods and inductively coupled plasma mass spectroscopy* *Corrosion Science*, 2007. **49**(4): p. 2002-2020.
40. Kirkwood D., *Microbial corrosion of metals in seawater*. proceeding of a meeting organised by the Scottish Marine Biological Association, 1982: p. 16-19.
41. Grobe H. and Majewsky S., Proportion of salt to sea water and chemical composition of sea salt, *Institute for Polar and Marine Research, Bremerhaven, Germany* [online], 2008. [Assessed 2009]. Available from: <https://www.walfredwegener.de>
42. Mauchline J., *Fouling and corrosion of metals in seawater*. Science direct, 1982. : p. 281-292.
43. Todd B., *Materials Selection for High Reliability Seawater Systems*, *Nickel Development Institute* [online], 2007. [Assessed 2008]. Available from: [http://www.copper.org/applications/cuni/txt\\_materials\\_selection.html](http://www.copper.org/applications/cuni/txt_materials_selection.html)
44. Brown E., *Seawater: its composition, properties and behaviour*. England, Butterworth Heinemann in association with The Open University, 1999. **2**: p. 14-17.
45. Takasaki S. and Yamada Y., *Effects of temperature and aggressive anions on corrosion of carbon steel in potable water*. *Corrosion Science*, 2007. **49**(1): p. 240-247.
46. Duthil, J.P., Mankowski, G. and Giusti A., *The synergetic effect of chloride and sulphate on pitting corrosion of copper*. *Corrosion Science*, 1996. **38**(10): p. 1839-1849.
47. Abd El Wanees, Abd El Haleem, S.M., S., Abd El Aal, E.E. and Diab, E., Environmental factors affecting the corrosion behavior of reinforcing steel. IV. Variation in the pitting corrosion current in relation to the concentration of the aggressive and the inhibitive anions, *Corrosion Science*, 2010. **52**(5): pp. 1675-1683.
48. Strehblow H.H. and Titze B., Pitting potentials and inhibition potentials of iron and nickel for different aggressive and inhibiting anions. *Corrosion Science*, 1977. **17**(6).
49. El-Naggar M.M., Effects of Cl<sup>-</sup>, NO<sub>3</sub><sup>-</sup> and SO<sub>4</sub><sup>2-</sup> anions on the anodic behavior of carbon steel in deaerated 0.50 M NaHCO<sub>3</sub> solutions, *Applied Surface Science*, 2006. **252**(18).
50. The Hendrix Group Reporter, *Hydrogen Embrittlement of High Strength Fasteners!* [online]. 1997. **7**(1), [Accessed 2011], Available from: <http://hghouston.com/resources/technical-newsletters/he-of-high-strength-fasteners.aspx>

51. Lim, G.H., Chua P.S.K., and He Y.B., Modern water hydraulics--the new energy-transmission technology in fluid power, *Applied Energy*. **76**(1-3): pp. 239-246.
52. Foszcz and Joseph L., "Hydraulic fluid choices." *Plant Engineering*, 1996. **50**(4): p. 68-72. 53. Agency, U.S.E.P., *Exemption of oil and gas exploration and production wastes from federal hazardous waste regulations*.
53. Knight G.C., *Water Hydraulics. Application of water-based fluids to hydraulic systems*, Tribology International, April 1977:pp. 105-107.
54. Naylor J. and McManus S., *Hydraulic fluids and their future in a more environemntally conscious industry*, Martson Bentley report, .: p.1-9
55. Zelman et al., *Pipeline and Gas Technology* [magazine], November/December 2008, Hart Energy Publishing, LP, p.50
56. Anon, The Centre for Environment, Fisheries & Aquaculture Science (Cefas), [online], 2008, [Assessed June 2011], Available from: <http://www.cefas.co.uk/about-us.aspx>.
57. Ernest W. K., *Use of Corrosion Inhibitors on the Trans Alaska Pipeline*, VCI Corrosion Control Supplement to Materials Performance, January 2001 ORTEC CORP, pp 1-3
58. Ramesh S. and Rajeswari S., *Evaluation of inhibitors and biocide on the corrosion control of copper in neutral aqueous environment*. *Corrosion Science*, 2005. **47**(1): pp. 151-169.
59. Alentejano C.R. and Aoki I.V., *Localized corrosion inhibition of 304 stainless steel in pure water by oxyanions tungstate and molybdate*. *Electrochimica Acta*, 2004. **49**(17-18): p. 2779-2785.
60. Uhlig H.H., *Structure and growth of thin films on metals exposed to oxygen* *Corrosion Science*, 1967. **7**(6): pp. 325-339.
61. Gregory R. R and Mohammed A. Al-Anezi., *Oil and gas exploration and production*. 2000.
62. Dudukcu M., Yazici B. and Erbil M., *The effect of indole on the corrosion behaviour of stainless steel*. *Materials Chemistry and Physics*, 2004. **87**(1): p. 138-141.
63. Arshadi M.R., Parsafar Gh.A. and Sastri V.S., *Cluster/polarized continuum models for density functional theory investigations of benzimidazole corrosion inhibitors at metal/solution interface*. *NACE International*, 2006. **62**(3): p. 199-206.
64. Delgado A. V., Gonzalez-Caballero F., R., Hunter J., Koopal L.K. and. Yklema J., *Measurement and Interpretation of Electrokinetic Phenomena*, International Union of Pure and Applied Chemistry Physical Biophysical Chemistry Division, 2005 **77**(10), pp. 1753–1805
65. Osman M.M., *Corrosion inhibition of aluminium-brass in 3.5% NaCl solution and sea water*. *Materials Chemistry and Physics*, 2001. **71**(1): pp. 12-16.
66. Hosseini S.M.A., Salari M. and Motlagh M.G., *Thioamide compounds as corrosion inhibitors for stainless steel in H<sub>2</sub>SO<sub>4</sub> solution*. *NACE International*, 2010. **66**(11): pp. 115003:1-115003:12.

67. YurtA., Balaban A., Kandemir S.U., Bereket G. and Erk B., *Investigation on some Schiff bases as HCl corrosion inhibitors for carbon steel*. Materials Chemistry and Physics, 2004. **85**(2-3): pp. 420-426.
68. Omanovic S. and Ggreba S., *Interaction of 12-aminododecanoic acid with a carbon steel surface: Towards the development of 'green' corrosion inhibitors*. Corrosion Science, 2010. **52**(6): p. 2104-2113.
69. Sethuraman M.G and Kamal C., *Spirulina platensis-A novel green inhibitor for acid corrosion of mild steel*. Arabian Journal of Chemistry, 2010: pp. 1-7.
70. Khaled K.F., *Experimental and theoretical study for corrosion inhibitor of mild steel in hydrochloric acid solution by some new hydrazine carbodithioic acid derivatives*. Applied Surface Science, 2006. **252**(12): p. 4120-4128.
71. Hosseini M.G., Ehteshamzadeh M. and Shahrabi T., *Protection of mild steel corrosion with Schiff bases in 0.5 M H<sub>2</sub>SO<sub>4</sub> solution*. Electrochimica Acta, 2007. **52**(11): p. 3680-3685.
72. Lalitha A., Ramesh S. and Rajeswari S., *Surface protection of copper in acid medium by azoles and surfactants*. Electrochimica Acta, 2005. **51**(1): p. 47-55.
73. Saracoglu, M., Zor S., Kandemirli F. and Arslan T., *Inhibition effects of amides on the corrosion of copper in 1.0 M HCl : Theoretical and experimental studies*. NACE International, 2011. **67**(12): p. 125003:1-11.
74. Myles M., Jordan N.F., David C.J., Morag and Morag E., *Biodegradable scale inhibitors. Laboratory and field evaluation of "Green" carbonate and sulphate scale inhibitors with deployment histories in the north sea*. Chemistry in the oil industry X. Oilfield Chemistry: REACHing the Solution, 2007. **1**: pp. 286-308.
75. Division, P.A., *The Harmonised Offshore Chemical Notifications Format (HOCNF) Scheme 2006*.
76. Wm Canning Ltd, Marston Bentley Division, Cale Lane, Wigan, UK, *Technical Manual: OCEANIC HW 600 series: Oceanic HW625, HW 640, HW660: Water based production control fluids for operation of high temperature, high pressure conventional oil and gas wells*, 1998, :. 1-58.
77. Manganon P.L., *The Principles of Materials Selection for Engineering Design*, Prentice Hall, 1999, pp.512-535.
78. Ueda M., *Development of corrosion resistance alloys for the oil and gas industry-based on spontaneous passivity mechanism*. NACE International, Corrosion conference, 2006. **62** (10): pp. 856-867.
79. Yang S., Guo J., Shang C. Wang Y. and He X., *Influence of carbon content and microstructure on corrosion behaviour of low alloy steels in a Cl<sup>-</sup> containing environment*, Corrosion Science, 2008. **51** : pp. 242-251.
80. Xu J., Bright M. A., Liu X. and Barbero E., *Liquid metal corrosion of 316L stainless steel, 410 stainless steel and 1015 carbon steel in a molten zinc bath*, Metallurgical and Materials Transactions A, 2007. **38A**: pp.2727-2736.
81. Andijani I. and Turgoose S., *Studies on corrosion of carbon steel in deaerated saline solutions in presence of scale inhibitor*, Gulf Conference, 1999.: pp. 2231-2246.
82. Lee J. S., Ray R.I., Lemieux E.J., Falster A. U., and Little B. J., *An evaluation of carbon steel corrosion under stagnant seawater conditions*, Biofouling, 2004. **20** (4/5):. pp. 237-247.

83. Nesmeyanoka, K.A., *Effect of oxygen on steel corrosion in steam-water flows at a temperature of 280°C*, Atomnaya Energiya, 1969. **29** (2) :. pp. 781-785.
84. Kamachi U.M., and Pujar M.G., *Pitting Corrosion of Austenitic Stainless Steels and Their Wekdmnt*. 2002, Narosa Publishing House, pp. 89-91.
85. Smith W.F., *Principles of materials science and engineering* 1996: McGraw Hill.
86. Strafford K.N., Venkatesan K., Subramaniam C. and Green L.K., *Influence of chromium content on corrosion of plasma-nitrided steel*, NACE International. 1997, **53** (7) :. pp. 507-515.
87. Nascimento D., Ierardi M.C.F, Kina A.Y. and Tavares S.S.M., *Pitting corrosion resistance of cast duplex stainless steels in 3.5%NaCl solution*. Materials Characterization, 2008. In Press, Corrected Proof: pp. 1-5.
88. Marcus P., Maurice V. and Strehblow H.H., *Localised corrosion (pitting): A model of passivity breakdown including the role of oxide layer nanostructure*. Corrosion Science. 2008, **50**:. pp. 2698-2704.
89. Cunha Belo M.D., Rondot B., Compere C., Montemor M.F., Simões A.M.P., Ferreira M.G.S., *Chemical composition and semiconducting behaviour of stainless steel passive films in contact with artificial seawater*. Corrosion Science, 1998. **40**(2-3): pp. 481-494.
90. Qvarfort R. and Olsson J., *Transpassive corrosion of high alloy stainless steels and bickel base alloys*, NACE International. 2002. **02133**:.pp. 1-17.
91. Fredriksson W., Malmgren S., Gustafsson T., Gorgoi M. and Edstroma K., *Full depth profile of passive films on 316L stainless steel based on high resolution HAXPES in combination with ARXPS*, Applied Surface Science, 2012. **258**:. pp. 5790-5797.
92. Souza E.C., Sergio M., Rossiti and Rollo J.M.D. *A Influence of chloride ion concentration and temperature on the electrochemical properties of passive films formed on a superduplex stainless steel*. Science Direct, 2010: .pp. 240-244.
93. Magellan Metals, *Inconel 625* [online]. 2004. [Accessed 7 April 2011], Available from: [http://www.magellanmetals.com/inconel\\_625.html?gclid=CNi1v7LJiqgCFUdP4QodrXs6Cw](http://www.magellanmetals.com/inconel_625.html?gclid=CNi1v7LJiqgCFUdP4QodrXs6Cw).
94. Cunha Belo D., Hakiki M., Ferreira N.E., Belo M.G.S., M. C. D and N.E. Hakiki, *Semiconducting properties of passive films formed on nickel-base alloys type Alloy 600: influence of the alloying elements*. Electrochimica Acta , 1999, **44** :. pp. 2473-2481.
95. Wu X. , Huang J. and Han E.H., *Influence of pH on electrochemical properties of passive films formed on Alloy 690 in high temperature aqueous environments*. Corrosion Science, 2009 (**51**):. pp. 2976-2982.
96. Kawashima A., Asami K. and Hashimoto K., *An XPS study of passive films on nickel and alloy 600 in acids*. Corrosion Science. 1985, **25**(12):.pp. 1103-1114.
97. Yin Z.F., Zhao W.Z., Lai W.Y. and Zhao X.H., *Electrochemical behaviour of Ni-base alloys exposed under oi/gas field environments*, Corrosion Science. 2009, **51** :.p. 1702-1706

98. Chen C. F., Jiang J., Zheng S.Q., and Cui L.S., *The non-linear fitting method to study the semiconductor properties of passive films of Inconel alloy G*, Journal of Electroanalytical Chemistry, 2011, **658** :. p.52–56.
99. Marcus, P., Machet A., Galtayries A., Zanna S., Klein L., Maurice V., Jolivet P, M. Foucault P., Combrade and Scott P., *XPS and STM study of the growth and structure of passive films in high temperature water on a nickel-base alloy*, Electrochimica Acta 2004. **49** (4):. pp. 3957–3964.
100. Yih S.W.H and Wang C.T., *Tungsten: sources, metallurgy, properties, and applications* 1979: Plenum press, New York and London. 358-359.
101. Lekatou A., Zois D., Karantzalis A.E., and Griminelis D., *Electrochemical behaviour of cermet coatings with a bond coat on Al7075: Pseudopassivity, localized corrosion and galvanic effect considerations in a saline environment*, Corrosion Science, 2010, 52, pp. 2616-2635.
102. Viljus M., Klaasena H., Kubarseppa J., Roosaara T., and Traksmäa R., *Adhesive wear performance of hardmetals and cermets*, Wear, 2010. **268**: p. 1122-1128.
103. Lackner A. and Filzwieser A., *Gas carburizing of tungsten carbide (WC) powder*. U.S Patent 6447742, 2002.
104. Wells, Alexander F., *Structural inorganic chemistry*. **5** 1945: Clarendon Press. p. 590.
105. Scholl H., Hofman B. and Rauscher A., *Anodic polarization of cemented carbides of the type [(WC,M): M = Fe, Ni or Co] in sulphuric acid solution*. Electrochimica Acta, 1992. **37**(3): pp. 447-452.
106. Batchelor A.W., Loh N.L. and Chandrasekaran M., *Materials: Degradation and its control by surface engineering*, 2002(**2**), Singapore: Imperial College Press. p. 412.
107. Upadhyaya G.S., *Cemented Tungsten Carbides: Production, Properties, and Testing* 1998: Noyes Publications. p.403.
108. Potgieter J.H., Thanjekwayo N., Olubambi P., Maledi N. and Potgieter-Vermaak S.S., *Influence of Ru additions on the corrosion behaviour of WC-Co cemented carbide alloys in sulfuric acid*. Int. Journal of Refractory Metals and Hard Materials, 2011. 29:.. pp. 478-487.
109. Buss K. *Thesis: High temperature deformation mechanisms of cemented carbides and cermets*. Institute of Complex Matter. France, 2004, p 8.
110. Tomlinson W.J. and Linzell C.R., *Anodic polarization and corrosion of cemented carbides with cobalt and nickel binders*. Journal of Materials Science, 1988. **23**(3): p. 914-918.
111. Human A.M., Roebuch B. and Exner H.E., *Electrochemical polarization and corrosion behaviour of cobalt and Co (W,C) alloys in 1 N sulphuric acid*. Materials Science and Engineering , 1998. **241**: p. 202-210.
112. Anik M., *Effect of concentration gradient on the anodic behavior of tungsten*, Science Direct. 2006. 48, pp. 4158-4173.
113. Suleiman A., Skeldon P., Thompson G.E., Echeverria F., Graham M.J., Sproule G.I., Moisa S., Quance T. and Habazaki H., *Anodic oxides on InAlP formed in sodium tungstate electrolyte*, Corrosion Science. 2010, 52, pp. 595-601.

114. Lekatou A., Regoutas E., Karantzalis A.E., *Corrosion behaviour of cermet-based coatings with a bond coat in 0.5 M H<sub>2</sub>SO<sub>4</sub>*, Corrosion Science. 2008. 50, pp. 3389-3400.
115. Ghandehari M.H., Andersen T.N. and Eyring H., *The electrochemical reduction of oxygen on copper in dilute sulphuric acid solutions*. Corrosion Science, 1976. **16**(3): p. 123-135.
116. Sutthiruangwong S. and Mori G., *Corrosion properties of Co-based cemented carbides in acidic solutions*. International Journals of Refractory Metals & Hard Materials, 2003. 21. pp. 135-145.
117. Warren A., Nylund A and Olefjord I., *Oxidation of tungsten and tungsten carbide in dry and humid atmospheres*. International Journals of Refractory Metals & Hard Materials, 1996. 14. pp. 345-353
118. Andersson K.M. and Bergstrom L., *Oxidation and dissolution of tungsten carbide powder in water*, International Journals of Refractory Metals & Hard Materials, 2000. 18. pp. 121-129.
119. Trueman A.R., Schweinsberg D.P. and Hope G.A., *A study of the effect of cobalt additions on the corrosion of tungsten carbide/carbon steel metal matrix composites*, Corrosion Science, 1999, 41, pp. 1377-1389.
120. Trueman A.R., Schweinsberg D.P., and Hope G.A., *The effect of chromium additions on the corrosion behaviour of tungsten carbide/carbon steel metal matrix composites*, Corrosion Science, 1998, 40 (**10**), pp. 1685-1696.
121. Kirkov P., *The influence of halide ion concentration on the effects of surface active inhibitors in strong electrolytes*. Corrosion Science, 1973. **13**(10): p. 697-706.
122. Pohjanne P., Carpen L., Kinnunen P., Ramo J., Sarpola A., Riihimaki M., and Hakkarainen T., *Stainless steel pitting in chloride-sulfate solutions-the role of cations*, 2007, NACE International, Corrosion conference and expo: USA.
123. Pyun P.I, Moon S., Ahn S.H. and Kim S.S., *Effects of Cl<sup>-</sup>, NO<sub>3</sub><sup>-</sup> and SO<sub>4</sub><sup>2-</sup> ions on anodic dissolution of pure aluminium in alkaline solution*. Corrosion Science, 1999. **41**(4): p. 653-667.
124. Smialowska Z., *Effect of the ratio of Cl<sup>-</sup>/SO<sub>4</sub><sup>2-</sup> in solution on the pitting corrosion of Ni*. Corrosion Science, 1971. **11**(4): p. 209-221.
125. Dechema Handbook of Corrosion, **11**, Weinheim, NY: VCH Publishers, 1992: p.66.
126. Hinds G., *The electrochemistry of corrosion*, [online]. 2006. [Accessed 2012], Available from: [http://www.npl.co.uk/upload/pdf/the\\_electrochemistry](http://www.npl.co.uk/upload/pdf/the_electrochemistry)
127. Melcher R.E., *Effect on marine immersion corrosion of carbon content of low alloy steels*. Science direct, 2003. **45**(11): p. 2609-2625.
128. Adhikari A.V. and Saliyan V.R., *Quinoline-5-ylmethylene-3-[[8-(trifluoromethyl)quinolin-4-yl]thio] propanohydrazide as an effective inhibitor of mild steel corrosion in HCl solution*. Science direct, 2008. **50**. pp.55-61.
129. Christov M. and Popova A., *Adsorption characteristics of corrosion inhibitors from corrosion rate measurements*. Corrosion Science, 2004. **46**. pp.1613-1620.
130. Szklarska-Smialowska Z., *The kinetics of pit growth on Ni in solutions with different Cl<sup>-</sup>/SO<sub>4</sub><sup>2-</sup> ratios*. Corrosion Science, 1972. **12**(6): pp. 527-536.

131. Thompson N. G. and Payer J.H., *DC electrochemical test methods*. Vol. 6. 1998. 98.
132. Sedriks A.J., *Corrosion stainless steel* 1979: John Wiley & Sons, New York. 282.
133. Scully J.C., *The fundamentals of corrosion* 1966: Pergamon press. 192.
134. Ziemniak S.E. and Hanson M., *Corrosion behavior of 304 stainless steel in high temperature, hydrogenated water*. Corrosion Science, 2002. **44**(10): p. 2209-2230.
135. Oguzie E.E., *Corrosion inhibition of aluminium in acidic and alkaline media by Sansevieria trifasciata extract*. Corrosion Science, 2007. **49**(3): p. 1527-1539.
136. Stellwag B., *The mechanism of oxide film formation on austenitic stainless steels in high temperature water*. Corrosion Science, 1998. **40**(2/3): p. 337-370.
137. Garfias-Mesias L. F., Sykes J.M., *Metastable pitting in 25 Cr duplex stainless steel*. Corrosion Science, 1999. **41**(5): p. 959-987.
138. Fischer K. P., Steensland O., Steinsmo U. and Wallen, B., *Comparison of seawater corrosivity in Europe*, in *EFC* 1996: UK.
139. Bardal E., Drugli J.M. and Gartland P. O., *The behaviour of corrosion-resistant steels in seawater: A review* Corrosion Science, 1993. **35**(1-4): p. 257-267.
140. Dexter S. C. and Gao G.Y., *Corrosion*, 1988. **44**: p. 717.
141. Laitinen T., *Localized corrosion of stainless steel in chloride, sulfate and thiosulfate containing environments*. Corrosion Science, 2000. **42**(3): p. 421-441.
142. Pistorius P.C. and Burstein G.T., *Growth of corrosion pits on stainless steel in chloride solution containing dilute sulphate*. Corrosion science, 1992. **33**(12): p. 1885-1897.
143. Engqvist H., Beste U. and Axén, N., *International Journal of Refractory Metals and Hard Materials*. 2000. **18**, 103-109.
144. Hochstrasser(-Kurz) S., Mueller Y., Latkoczy C., Virtanen S. and Schmutz P., *Analytical characterization of the corrosion mechanisms of WC-Co by electrochemical methods and inductively coupled plasma mass spectroscopy*. Corrosion Science, 2007. **49**(4): p. 2002-2020.
145. Benedetto, B., Fanigliulo A. and Mele C., *Electrochemical oxidation of WC in acidic sulphate solution* Corrosion Science, 2004. **46**(2): p. 453-469.
146. Rosales, B.M. Vera, R., and Tapia, C., *Effect of the exposure angle in the corrosion rate of plain carbon steel in a marine atmosphere* Corrosion Science, 2003. **45**(2): p. 321-337.
147. Zhu, X., Lei, T., *Characteristics and formation of corrosion product films of 70Cu-30Ni alloy in seawater*. Corrosion Science, 2002. **44**(1): p. 67-79.
148. Cáceres, L., Vargas, T. and Herrera, L., *Determination of electrochemical parameters and corrosion rate for carbon steel in un-buffered sodium chloride solutions using a superposition model*. Corrosion Science, 2007. **49**(8): p. 3168-3184.
149. Larson, D.T., *Surface analytic techniques in corrosion science*. Corrosion Science, 1979. **19**(10): p. 657-673.

150. Wren, Yazdanfar, K., Zhang, X., Keech, P.G., Shoesmith, D.W., *Film conversion and breakdown process on carbon steel in the presence of halides*. Corrosion Science, 2010. **52**(4): p. 1297-1304.
151. Yang, G., Ying, L., and Haichao, L., *Experimental studies on the local corrosion of low alloy steels in 3.5% NaCl*. Corrosion Science, 2001. **43**(3): p. 397-411.
152. Jordan, K.G., and Williams V.T., *Popeye project: Hydraulic Umbilical*, in *Offshore Technology Conference*, S.O.P. Company, Editor 1996, OTC: Texas. p. 113-120.
153. Melchers, R.E., and Jeffrey, R., *Early corrosion of mild steel in seawater*, Corrosion Science, 2005, **47**, pp. 1678-1693.
154. Machio, C.N., D.S.KONADU., J. van der Merwe, J.H. Potgieter, S. Potgieter-Vermaak, *The corrosion behaviour of WC-VC-Co hardmetals in acidic media*. Corrosion Science, 2010. **52**(9): pp. 3118-3125.
155. N.J. Laycock, S.E.W., C.A. Johnson, P.T. Wilson, B.J. Webster, *Pitting of Type 304 stainless steel in the presence of a biofilm containing sulphate reducing bacteria*. Corrosion Science, 1998. **40**(2-3): p. 465-480.
156. El-Sayed, A.-R., H.S. Mohran, and H.M. Abd El-Lateef, *Potentiodynamic studies on anodic dissolution and passivation of tin, indium and tin-indium alloys in some fruit acids solutions*. Corrosion Science, 2009. **51**(11): p. 2675-2684.
157. J. Mankowski and Z.Szklarska-Smialowska., *Studies on accumulation of chloride ions in pits growing during anodic polarization*. Corrosion Science, 1975. **15**(6-12): p. 493-501.
158. Jingyi, Z.P.M., Chunchun Xu Youping Liu, *Kinetic and thermodynamic behaviour inside occluded corrosion cells interpreted by potential/pH diagrams* Corrosion Science, 1989. **29**(5): p. 557-566.
159. J.Mankowski, Z.S.-S., *Studies on accumulation of chloride ions in pits growing during anodic polarization*. Corrosion Science, 1975. **15**(6-12): p. 493-501.
160. Wagner, C., *Passivity and inhibition during the oxidation of metals at elevated temperatures*. Corrosion Science, 1965. **5**(11): p. 751-764.
161. Z.F. Yin, W.Z.Z., W.Y. Lai, X.H. Zhao, *Electrochemical behaviour of Ni-base alloys exposed under oil/gas field environments*. Corrosion Science, 2009. **51**(8): p. 1702-1706.
162. Corvo, F., et al., *Indoor atmospheric corrosion in Cuba. A report about indoor localized corrosion*. Corrosion Science, 2007. **49**(2): p. 418-435.
163. T.P. Hoar, D.C.M.a.G.P.R., *The production and breakdown of the passivity of metals*. Corrosion Science, 1967. **7**(6): p. 341-355.
164. K.Y. Ann and H.W.Song., *Chloride threshold level for corrosion of steel in concrete* Corrosion Science, 2007. **49**(11): p. 4113-4133.
165. Y.Zuo, H.W.a.J.X., *The aspect ratio of surface grooves and metastable pitting of stainless steel*. Corrosion Science, 2002. **44**(1): p. 25-35.
166. Y.Zuo, H.W., J. Zhao and J. Xiong, *The effects of some anions on metastable pitting of 316L stainless steel* Corrosion Science, 2002. **44**(1): p. 13-24.
167. M. Duan, H.W., J. Xie, K.P. Yan and Y. Zuo, *The nucleation and growth of metastable pitting on pure iron*. Corrosion Science, 2009. **51**(1): p. 181-185.



168. Z. Szklarska-Smialowska, J.M., *Effect of temperature on the kinetics of development of pits in stainless steel in 0.5N NaCl + 0.1N H<sub>2</sub>SO<sub>4</sub> solution.* Corrosion Science, 1972. **12**(12): p. 925-934.
169. L. Tarja, *Localized corrosion of stainless steel in chloride, sulfate and thiosulfate containing environments* Corrosion Science, 2000. **42**(3): p. 421-441
170. K. Hashimoto, K.A., K. Teramoto, *An X-ray photo-electron spectroscopic study on the role of molybdenum in increasing the corrosion resistance of ferritic stainless steels in HCl.* science direct, 1979. **19**(1): p. 3-14.
171. T. Hong, M. Nagumo., *The effect of SO<sub>4</sub><sup>2-</sup> concentration in NaCl solution on the early stages of pitting corrosion of type 430 stainless steel* Corrosion Science, 1997. **39**(5): p. 961-967.
172. T. Hong, M. Nagumo., *The effect of chloride concentration on early stages of pitting for type 304 stainless steel revealed by the AC impedance method.* Corrosion Science, 1997. **39**(2): p. 285-293.
173. J.N. Alhajji and M.R. Reda, *Role of solution chemistry on corrosion of copper in tap water : Effect of sulfate ion concentration on uniform and localized attack.* NACE, 1996. **52**(2): p. 232-238.
174. M.H. Moayed, R.C. Newman, *Deterioration in critical pitting temperature of 904L stainless steel by addition of sulfate ions.* Corrosion Science, 2006. **48**(11): p. 3513-3530.
175. I.L. Rosenfeld, I.S.D., *Electrochemical aspects of pitting corrosion.* Corrosion Science, 1967. **7**(3): p. 129-142.
176. M. Piantini, N.D.C., N. Zacchetti, *The influence of temperature on the passivation behaviour of a super duplex stainless steel in a boric-borate buffer solution.* Corrosion Science, 1997. **39**(12): p. 2181-2191.
177. Schumacher, M., *Sea water corrosion handbook* 1979: Noyes Data, New Jersey.
178. B.S. Covino Jr., M.R., T.J. Driscoll, T.C. Murphy, C.R. Molock, *The effect of oxygen on the open-circuit passivity of Fe-18Cr* Corrosion Science, 1986. **26**(2): p. 95-107.
179. H. M. Ezuber, A.E.-H., F. El-Shawesh, *Effects of sigma phase precipitation on seawater pitting of duplex stainless steel.* science direct, 2007. **207**(1-3): p. 268-275.
180. B. Bozzini, M.D., G. P. De Gaudenzi, L. D'Urzo and L. Gregoratti, *An investigation of the corrosion of WC-Co cermets in CN--containing aqueous solutions. Part II: Synchrotron-based high lateral-resolution XPS study* Corrosion Science, 2009. **51**(8): p. 1675-1678.
181. M. Aristizabal, J.M. Sanchez, N. Rodriguez, F. Ibarreta, R. Martinez *Comparison of the oxidation behaviour of WC-Co and WC-Ni-Co-Cr cemented carbides* Corrosion Science, 2011. **53**(9): p. 2754-2760.
182. A. Lekatou, E.R., A.E. Karantzalis, *Corrosion behaviour of cermet-based coatings with a bond coat in 0.5 M H<sub>2</sub>SO<sub>4</sub>.* Corrosion Science, 2008. **50**(12): p. 3389-3400.
183. C.N. Machio, D.S. KONADU., J. van der Merwe, J.H. Potgieter, S. Potgieter-Vermaak, *The corrosion behaviour of WC-VC-Co hardmetals in acidic media.* Corrosion Science, 2010. **52**(9): pp. 3118-3125.

184. U.Ebersbach, K.S., K. Ritter, *On the kinetics of the anodic passivation of iron, cobalt and nickel*. *Electrochimica Acta*, 1967. **12**(8): p. 927-938.
185. E.J. Wentzel, C.A., *The erosion-corrosion resistance of tungsten-carbide hard metals*. *International Journal of Refractory Metals & Hard Materials*, 1997. **15**(1-3): p. 81-87.
186. S.Virtanen, f.J.J.K., H. Hildebrand, *Effect of WC grain size on the corrosion behavior of WC-Co based hardmetals in alkaline solutions*. *International Journal of Refractory Metals & Hard Materials*, 2009. **27**: p. 806-812.
187. A.M. Human, H.E.E., *The relationship between electrochemical behaviour and in-service corrosion of WC-based cemented carbides*. *International Journal of Refractory Metals & Hard Materials*, 1997. **15**(1-3): p. 65-71.
188. G.Gilli, P.B., F.Zucchi, G. TrabANELLI, *Passivation of Ni caused by layers of salts in concentrated H<sub>2</sub>SO<sub>4</sub>*. *Corrosion Science*, 1969. **9**(9): p. 673-681.
189. A.Lekatou, D.Z., A.E. Karantzalis, D. Grimanelis, *Electrochemical behaviour of cermet coatings with a bond coat on Al7075: Pseudopassivity, localised corrosion and galvanic effect considerations in a saline environment*. *Corrosion Science*, 2010. **52**(8): p. 2616-2635.
190. R.B. Perez-Saez, L.d.C., L. Gonzalez-Fernandez, M.J. Tello, *Kinetics inversion in isothermal oxidation of uncoated WC-based carbides between 450 and 800 °C*. *Corrosion Science*, 2009. **51**(4): p. 707-712.
191. K.S. Indra and K.S.G. Doss. *A new approach to explain the anodic passivation and periodic phenomena: The PN junction and SR mechanisms*, Central Electrochemical Research Institute, June 3 1967
192. N. J. Laycock. *Effects of Temperature and Thiosulfate on Chloride Pitting of Austenitic Stainless Steels*, *Corrosion* June 1999, 55 (6), p. 590-595
193. A. Neville and T. Hodgkiess, *An Assessment of the Corrosion Behaviour of High-Grade Alloys in Seawater at Elevated Temperature and Under a High Velocity Impinging Flow*, *Corrosion Science* 1996, 38 (6), p. 927-956
194. M.A. Deyab, *Adsorption and inhibition effect of Ascorbyl palmitate on corrosion of carbon steel in ethanol blended gasoline containing water as a contaminant*, *Corrosion Science* 2014, 80, p.359-365
195. W. Li, B. Brown, D. Young and S. Nestic, *Investigation of Pseudo-Passivation on mild steel in CO<sub>2</sub> corrosion*, *NACE Corrosion* 2013, Paper No. 2149
196. M. Hoseinpoor, M. Momeni, M.H. Moayed and A. Davoodi, *EIS assessment of critical pitting temperature of 2205 duplex stainless steel in acidified ferric chloride solution*, *Corrosion Science* 2014, 80, p. 197-204

## Appendices

- The reaction of  $KCl$ :

Because of 0.39g of  $K^+$  needed, thus, the amount of  $KCl$  needed is:

$$\text{Mass of } KCl = \frac{\text{Mass of } K^+}{\text{Molecular weight of } K^+} \times \text{Molecular weight of } KCl \dots \dots \dots (1)$$

$$\text{Mass of } KCl = \frac{0.39}{39.098} (39.098 + 35.45) = 0.743g$$

$$\text{Mass of } Cl^- = \frac{0.39}{39.098} (35.45) = 0.3536g$$

- The reaction of  $CaCl_2$ :

Referring to equation 1, the mass of  $CaCl_{2.6H_2O}$  is obtained

$$\text{Mass of } CaCl_{2.6H_2O} = \frac{0.42}{40.078} \times (218.978) = 2.29g$$

$$\text{Mass of } Cl^- = \frac{0.42}{40.078} 2(35.45) = 0.743g$$

\* The total amount of Mg = 1.30g, which is separated into 0.68g in  $MgSO_{4.7H_2O}$  and 0.62g in  $MgCl_{2.6H_2O}$

- The reaction of  $MgSO_4$ :  $MgSO_4 \longrightarrow Mg^{2+} + SO_4^{2-}$

$$\text{Mass of } MgSO_{4.7H_2O} = \frac{0.68}{24.305} \times (246.97) = 6.89g$$

$$\text{Mass of } SO_4^{2-} = \frac{0.68}{24.305} (96.062) = 2.69g$$

- The reaction of  $MgCl_2$ :  $MgCl_2 \longrightarrow Mg^{2+} + 2Cl^-$

$$\text{Mass of } MgCl_{2.6H_2O} = \frac{0.62}{24.305} \times (203.205) = 5.18g$$

$$\text{Mass of } Cl^- = \frac{0.62}{24.305} 2(35.45) = 1.81g$$

\* The total amount of sodium = 10.71g, which is separated into 9.72g in NaCl and 0.98g in  $NaHCO_3$

- The reaction of  $\text{NaHCO}_3$ :  $\text{NaHCO}_3 \longrightarrow \text{Na}^+ + \text{HCO}_3^-$

$$\text{Mass of NaHCO}_3 = \frac{0.98}{23.0} \times (84.016) = 3.58g$$

- The reaction of  $\text{NaCl}$ :  $\text{NaCl} \longrightarrow \text{Na}^+ + \text{Cl}^-$

$$\text{Mass of NaCl} = \frac{9.72}{23.0} \times (58.45) = 24.70g$$

$$\text{Mass of Cl}^- = \frac{9.72}{24.305} (35.45) = 14.98g$$

The remaining  $\text{Cl}^-$  is, Total  $\text{Cl}^- = 19.25 - (0.3536 + 0.743 + 1.81 + 14.98) = 1.3634g$ .  
Thus,  $\text{HCl}$  is added to cover the remaining total of  $\text{Cl}^-$  needed.

- The reaction of  $\text{NaCl}$ :  $\text{HCl} \longrightarrow \text{H}^+ + \text{Cl}^-$

$$\text{Mass of HCl} = \frac{1.3634}{35.45} \times (36.45) = 1.40 \text{ ml}$$

- Considering the ratio,  $\text{SO}_4^{2-} / \text{Cl}^-$  for this solution is 0.14 and this is labelled as solution 1 (S1).

### Calculation for Solution 2 ( $\text{SO}_4^{2-} = 20.87g$ and $\text{Cl}^- = 1.09g$ )

- The reaction of  $\text{KCl}$ :

Because of 0.39g of  $\text{K}^+$  needed, thus the amount of  $\text{KCl}$  needed is:

$$\text{Mass of KCl} = \frac{\text{Mass of K}^+}{\text{Molecular weight of K}^+} \times \text{Molecular weight of KCl} \dots \dots \dots (1)$$

$$\text{Mass of KCl} = \frac{0.39}{39.098} (39.098 + 35.45) = 0.74g$$

$$\text{Mass of Cl}^- = \frac{0.39}{39.098} (35.45) = 0.3536g$$

- The reaction of  $\text{CaCl}_2$ :  $\text{Ca}^{2+} \longrightarrow \text{Ca}^{2+} + 2\text{Cl}^-$

Referring to equation 1, mass of  $CaCl_{2.6H_2O}$  is obtained

$$\text{Mass of } CaCl_{2.6H_2O} = \frac{0.42}{40.078} \times (218.978) = 2.29g$$

$$\text{Mass of } Cl^- = \frac{0.42}{40.078} \times 2(35.45) = 0.743g$$

- The reaction of  $MgSO_4$ :  $MgSO_4 \longrightarrow Mg^{2+} + SO_4^{2-}$

$$\text{Mass of } MgSO_{4.7H_2O} = \frac{1.27}{24.305} \times (246.97) = 12.87g$$

$$\text{Mass of } SO_4^{2-} = \frac{1.27}{24.305} (96.062) = 5.0196g$$

- The reaction of  $NaHCO_3$ :  $NaHCO_3 \longrightarrow Na^+ + HCO_3^-$

$$\text{Mass of } NaHCO_3 = \frac{10.50}{23.0} \times (84.016) = 38.35g$$

- The reaction of  $H_2SO_4$ :  $H_2SO_4 \longrightarrow H^+ + SO_4^{2-}$

The remaining  $SO_4^{2-}$  is; Total  $SO_4^{2-} = 20.87 - 5.0196 = 15.89g$ . Thus,  $H_2SO_4$  is added

$$\text{Mass of } H_2SO_4 = \frac{15.89}{98.062} \times 96.062 = 15.57 \text{ ml}$$

- Considering the ratio,  $SO_4^{2-} / Cl^-$  for this solution is 19.15 and this is labelled as Solution 2 (S2).

**Calculation for Solution 3 ( $SO_4^{2-} = 9.41 \text{ g}$  and  $Cl^- = 12.54g$  :  $SO_4^{2-}/Cl^-=0.75$  )**

- The reaction of  $KCl$  :

Because of 0.39g of  $K^+$  needed, thus, the amount of  $KCl$  needed is:

$$\text{Mass of } KCl = \frac{\text{Mass of } K^+}{\text{Molecular weight of } K^+} \times \text{Molecular weight of } KCl \dots \dots \dots (1)$$

$$\text{Mass of } KCl = \frac{0.39}{39.098} (39.098 + 35.45) = 0.743g$$

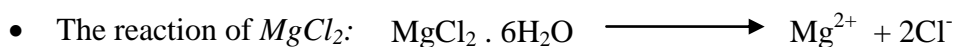
$$\text{Mass of } Cl^- = \frac{0.39}{39.098}(35.45) = 0.3536g$$



Referring to equation 1, the mass of  $CaCl_2$  is obtained

$$\text{Mass of } CaCl_{2.6H_2O} = \frac{0.42}{40.078} \times (218.978) = 1.16g$$

$$\text{Mass of } Cl^- = \frac{0.42}{40.078} \times 2(35.45) = 0.743g$$



$$\text{Mass of } MgCl_{2.6H_2O} = \frac{1.30}{24.305} \times (203.205) = 10.87g$$

$$\text{Mass of } Cl^- = \frac{1.30}{24.305} \times 2(35.45) = 3.79g$$



$$\text{Mass of } H_2SO_4 = \frac{9.41}{98.062} \times 98.062 = 9.41ml$$



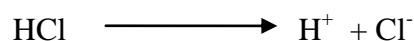
$$\text{Mass of } NaHCO_3 = \frac{8.70}{23.0} \times (84.016) = 31.77g$$



$$\text{Mass of } NaCl = \frac{1.998}{23.0} \times (58.45) = 5.08g$$

$$\text{Mass of } Cl^- = \frac{1.998}{24.305} (35.45) = 3.08g$$

The remaining  $Cl^-$  is, Total  $Cl^- = 12.54 - (0.743+0.3536 + +3.79+3.08)= 4.57g$ .  
Thus,  $HCl$  is added to cover the remaining total of  $Cl^-$  needed.



- The reaction of NaCl:

$$\text{Mass of HCl} = \frac{4.57}{35.45} \times (36.45) = 4.70 \text{ml}$$

- Considering the ratio,  $\text{SO}_4^{2-} / \text{Cl}^-$  for this solution is 0.99 and this is labelled as solution 4 (S4).

**Calculation for Solution 4 ( $\text{SO}_4^{2-} = 10.95 \text{ g}$  and  $\text{Cl}^- = 11 \text{ g}$  :  $\text{SO}_4^{2-}/\text{Cl}^- = 0.99$  )**

- The reaction of KCl:

Because of 0.39g of  $\text{K}^+$  needed, thus, the amount of KCl needed is:

$$\text{Mass of KCl} = \frac{\text{Mass of K}^+}{\text{Molecular weight of K}^+} \times \text{Molecular weight of KCl} \dots \dots \dots (1)$$

$$\text{Mass of KCl} = \frac{0.39}{39.098} (39.098 + 35.45) = 0.743 \text{g}$$

$$\text{Mass of Cl}^- = \frac{0.39}{39.098} (35.45) = 0.3536 \text{g}$$

- The reaction of  $\text{CaCl}_2$ :  $\text{Ca}^{2+} \longrightarrow \text{Ca}^{2+} + 2\text{Cl}^-$

Referring to equation 1, the mass of  $\text{CaCl}_2$  is obtained

$$\text{Mass of CaCl}_{2.6\text{H}_2\text{O}} = \frac{0.42}{40.078} \times (218.978) = 1.16 \text{g}$$

$$\text{Mass of Cl}^- = \frac{0.42}{40.078} \times 2(35.45) = 0.743 \text{g}$$

- The reaction of  $\text{NaHCO}_3$ :  $\text{NaHCO}_3 \longrightarrow \text{Na}^+ + \text{HCO}_3^-$

$$\text{Mass of NaHCO}_3 = \frac{4.69}{23.0} \times (84.016) = 17.16 \text{g}$$

- The reaction of NaCl:  $\text{NaCl} \longrightarrow \text{Na}^+ + \text{Cl}^-$

$$\text{Mass of NaCl} = \frac{6.02}{23.0} \times (58.45) = 15.29 \text{g}$$

$$\text{Mass of Cl}^- = \frac{6.02}{23.0} (35.45) = 9.27 \text{g}$$



$$Mass\ of\ MgSO_{4.7H_2O} = \frac{1.30}{24.305} \times (246.97) = 13.21g$$

$$Mass\ of\ SO_4^{2-} = \frac{1.30}{24.305} (96.062) = 5.138g$$

The remaining  $SO_4^{2-}$  is; Total  $SO_4^{2-} = 10.95 - 5.138 = 5.812$  g. Thus, HCl is added to cover the remaining total of  $Cl^-$  needed.



$$Mass\ of\ H_2SO_4 = \frac{5.812}{96.062} \times 98.062 = 5.93\ ml$$

The remaining  $Cl^-$  is, Total  $Cl^- = 11.0 - (0.3536 + 0.743 + 9.27) = 0.6334$  g. Thus, HCl is added to cover the remaining total of  $Cl^-$  needed.



$$Mass\ of\ HCl = \frac{0.6334}{35.45} \times (36.45) = 0.65\ ml$$

- Considering the ratio,  $SO_4^{2-} / Cl^-$  for this solution is 0.99 and this is labelled as solution 4 (S4).



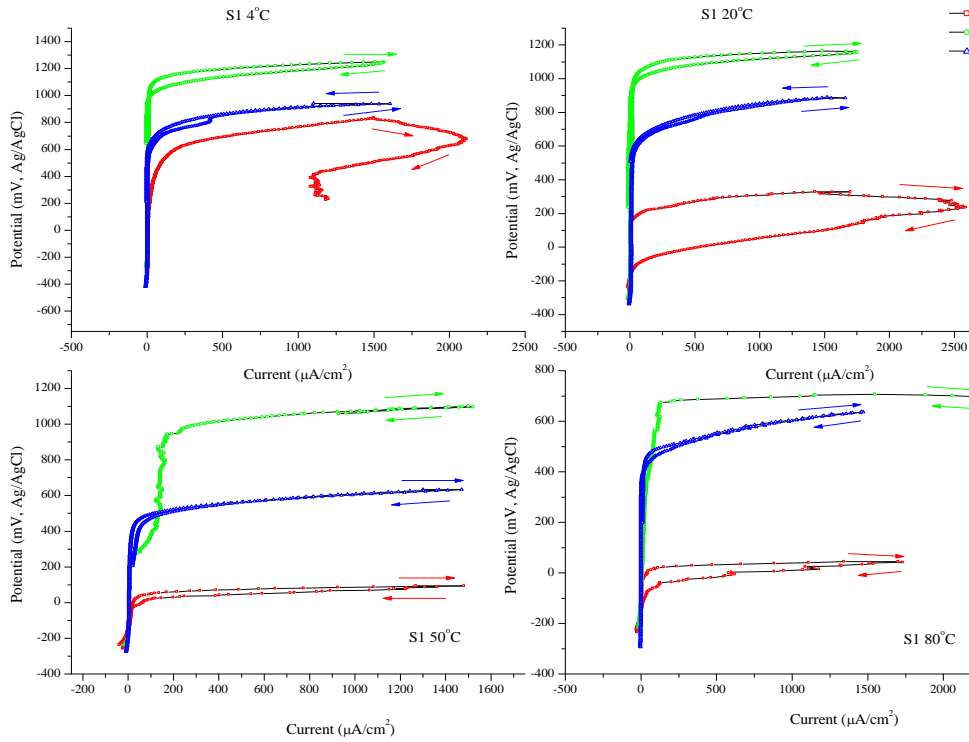


**Figure A.1: Anodic polarisation for passive materials in S1 at different temperatures**

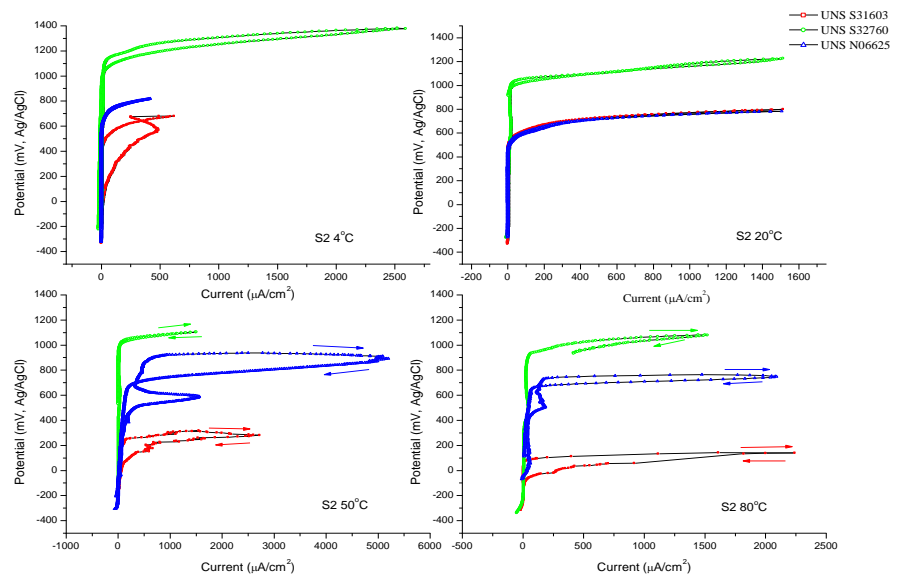


**Figure A.2: Anodic polarisation for passive materials in S2 at different temperatures**

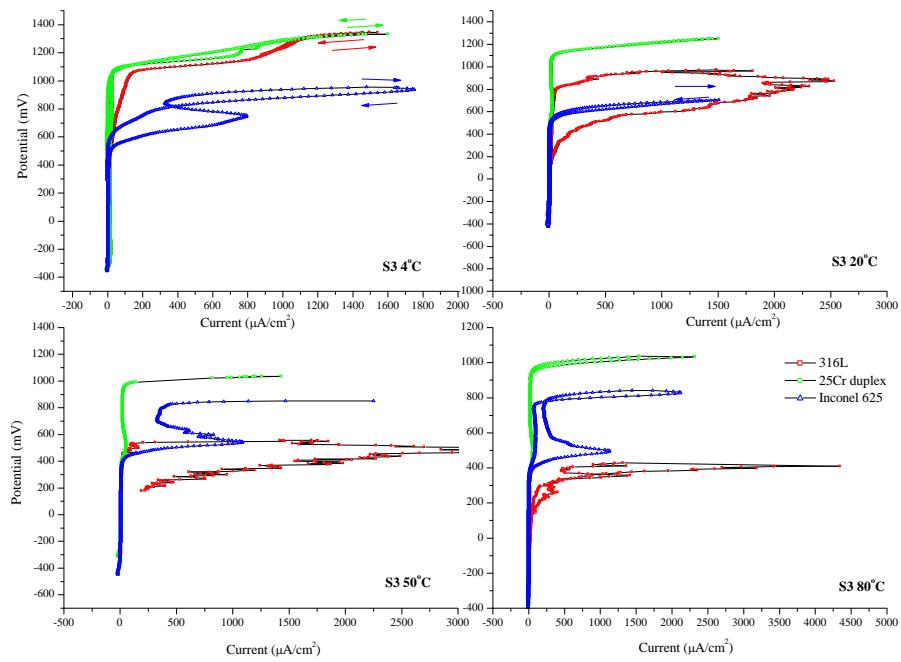


**Figure A.3: Anodic polarisation for passive materials in S3 at different temperatures**

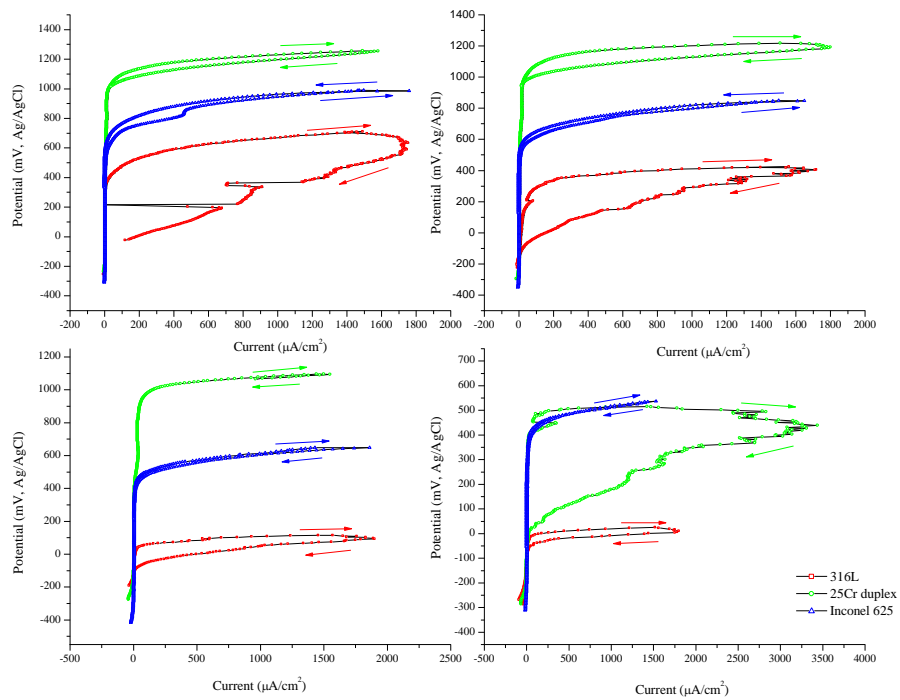


**Figure A.4: Anodic polarisation for passive materials in S4 at different temperatures**

**Table A1: Electrochemical data of 316L**

Solution	Temp	OCP (mV)	$E_{pp}$ (mV)	$E_b$ (mV)	$i_p$ ( $\mu\text{A}/\text{cm}^2$ )	$i_{cc}$ ( $\mu\text{A}/\text{cm}^2$ )	$I_{max}$ ( $\mu\text{A}$ )
1	4°C	-224	-179	634 1185	2.06	-5.66	2110
	20°C	-203	-164	142 200	-5.47	-5.72	2583
	50°C	-188	-173	25	-4.46	-5.48	1494
	80°C	-163	-139	-3.99	-4.35	-5.51	1737
2	4°C	-268	-208	656 986	1.49	1.14	586
	20°C	-230	-182	499 551	1.02	0.39	1512
	50°C	-250	-190	257	46.2	12.7	2720
	80°C	-256	-217	115	8.9	4.1	2239
3	4°C	-253	-202	705 805	133.8	1.6	1540
	20°C	-193	-124	464 1046	65	3.3	2530
	50°C	-254	-203	358	111	5.9	3510
	80°C	-255	-210	274	1314	6.2	4337
4	4°C	-211	-172	782 1182	4.8	1.7	1752
	20°C	-182	-134	304 640	130.5	3.3	1718
	50°C	-167	-143	43	73.2	4.8	1555
	80°C	-167	-152	-14	47.3	2.1	1800

\* the value in red colour is  $E_b$  of metal in the solutions without oxygen

**Table A2: Electrochemical data of 25Cr duplex**

Solution	Temp	OCP (mV)	$E_{pp}$ (mV)	$E_b$ (mV)	$i_p$ ( $\mu\text{A}/\text{cm}^2$ )	$i_{cc}$ ( $\mu\text{A}/\text{cm}^2$ )	$I_{max}$ ( $\mu\text{A}$ )
<b>1</b>	4°C	-238	-172	1195 1080	-4.70	-5.37	1560
	20°C	-250	-196	1141 1091	-4.58	-5.36	1750
	50°C	-191	-128	1059	-5.00	-5.33	1520
	80°C	-127	-58	765	-3.88	-5.21	2300
<b>2</b>	4°C	-205	-134	1018 1085	0.11	-0.24	2595
	20°C	-235	-187	863 1017	-4.61	-5.431	1513
	50°C	-174	-132	856	-4.31	-5.21	1500
	80°C	-231	-177	627	-4.21	-5.30	1520
<b>3</b>	4°C	-336	-279	1150 1259	-4.43	-4.85	1600
	20°C	-162	-90	1049 1116	-4.71	-5.49	1504
	50°C	-258	-186	1026	-4.45	-5.17	1430
	80°C	-228	-164	906	1.44	1.042	3.37
<b>4</b>	4°C	-205	-148	1153 1279	-4.58	-5.60	1580
	20°C	-234	-171	990 1046	-4.47	-5.57	1800
	50°C	-142	-73	932	-4.19	-5.47	1550
	80°C	-193	-142	407	-4.38	-5.15	3440

\* the value in red colour is  $E_b$  of metal in the solutions without oxygen

**Table A 3: Electrochemical data of Inconel 625**

Solution	Temp	OCP (mV)	$E_{pp}$ (mV)	$E_b$ (mV)	$i_p$ ( $\mu\text{A}/\text{cm}^2$ )	$i_{cc}$ ( $\mu\text{A}/\text{cm}^2$ )	$I_{max}$ ( $\mu\text{A}$ )
1	4°C	-323	-260	1028 954	-4.69	-5.57	1608
	20°C	-296	-233	699 701	-4.54	-5.19	1660
	50°C	-192	-120	527	-4.63	-5.48	1470
	80°C	-182	-122	391	-4.94	-6.12	1470
2	4°C	-239	-167	686 466	-4.62	-5.83	1516
	20°C	-209	-149	674 395	-4.89	-6.35	1506
	50°C	-300	-249	614	-4.52	-5.67	1574
	80°C	-229	-190	512	-4.94	-6.14	2250
3	4°C	-302	-251	782 847	-3.48	-5.82	1730
	20°C	-297	-249	537 417	-4.06	-5.74	1484
	50°C	-300	-252	426	-4.36	-5.69	2242
	80°C	-316	-262	407	-4.08	-5.52	2120
4	4°C	-270	-216	669 558	-4.64	-5.88	1760
	20°C	-258	-192	511 414	-4.67	-5.92	1650
	50°C	-288	-219	438	-4.67	-5.57	1860
	80°C	-210	-117	387	-4.60	-5.37	1528

\* the value in red colour is  $E_b$  of metal in the solutions without oxygen

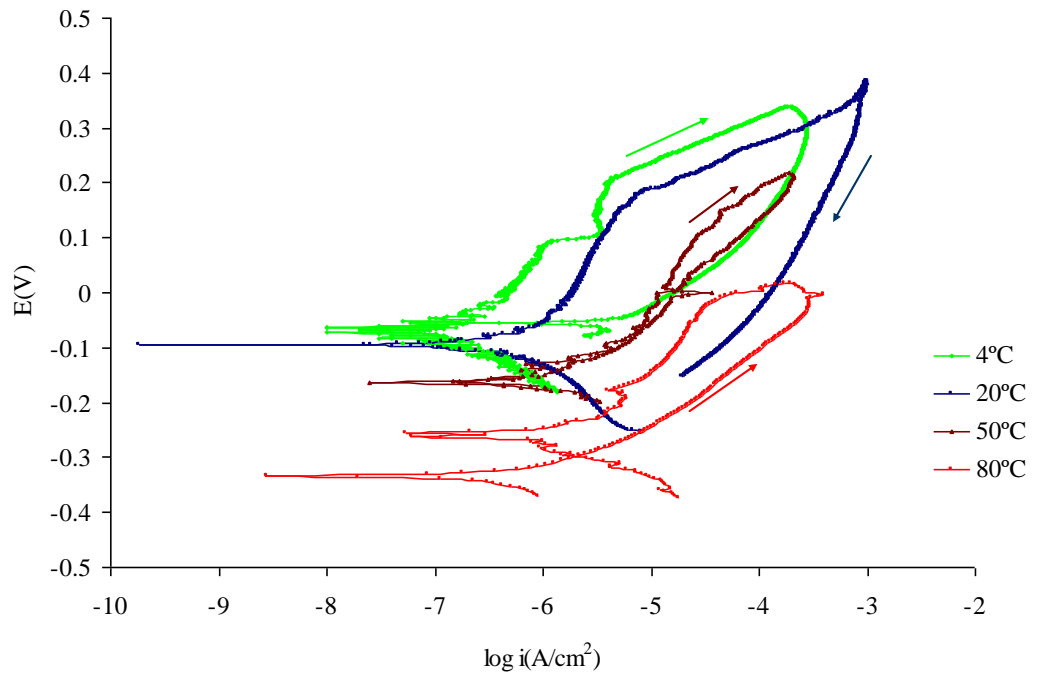


**Figure A.5: Cyclic polarisation of WC-Co in solution 2 ( $SO_4^{2-}/Cl^- = 19.15$ ) at different temperatures.**

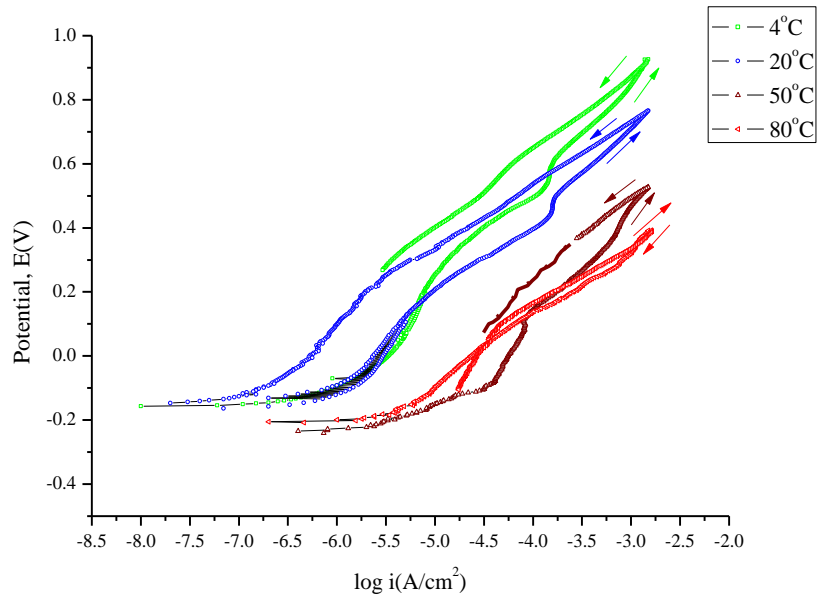


**Figure A.6: Cyclic polarisation of WC-Co in solution 3 ( $SO_4^{2-}/Cl^- = 0.75$ ) at different temperatures**

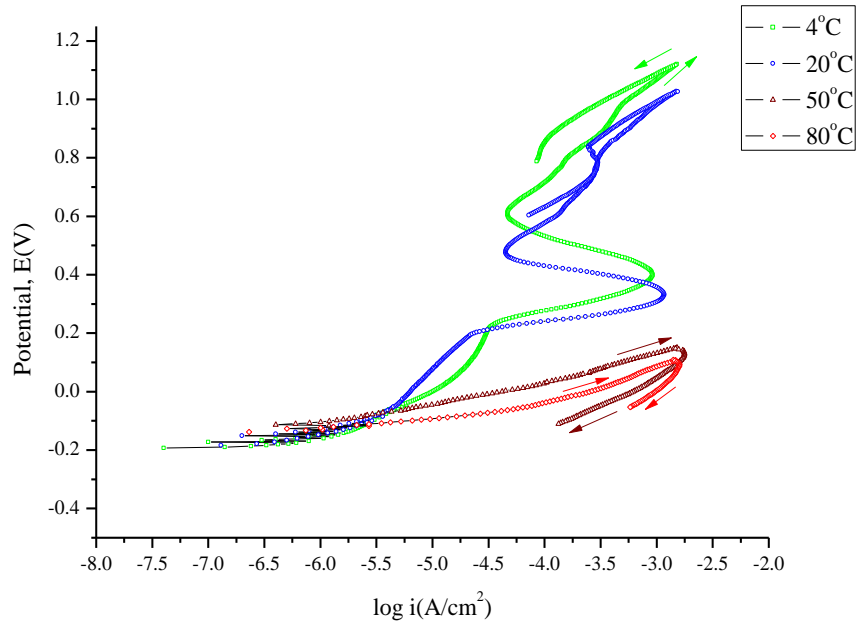


**Figure A.7: Cyclic polarisation of WC-Co in solution 4 ( $SO_4^{2-}/Cl^- = 0.99$ ) at different temperatures**

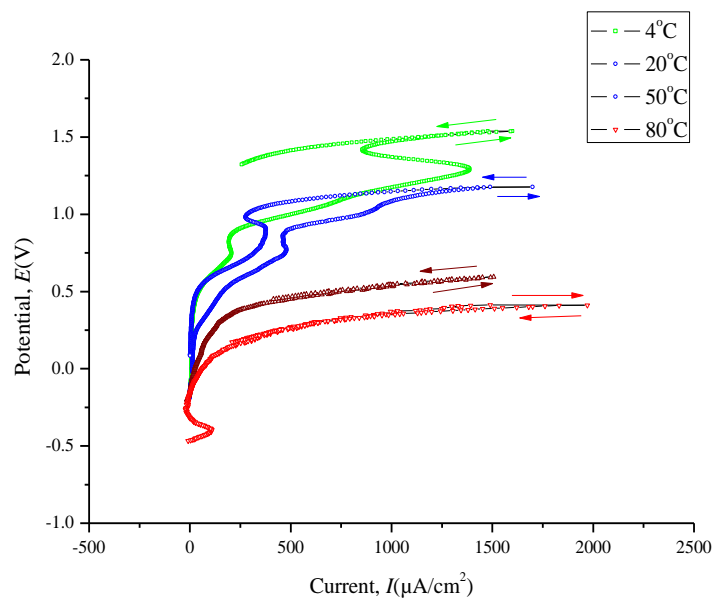


**Figure A.8: WC-Ni in S1 at different temperatures**

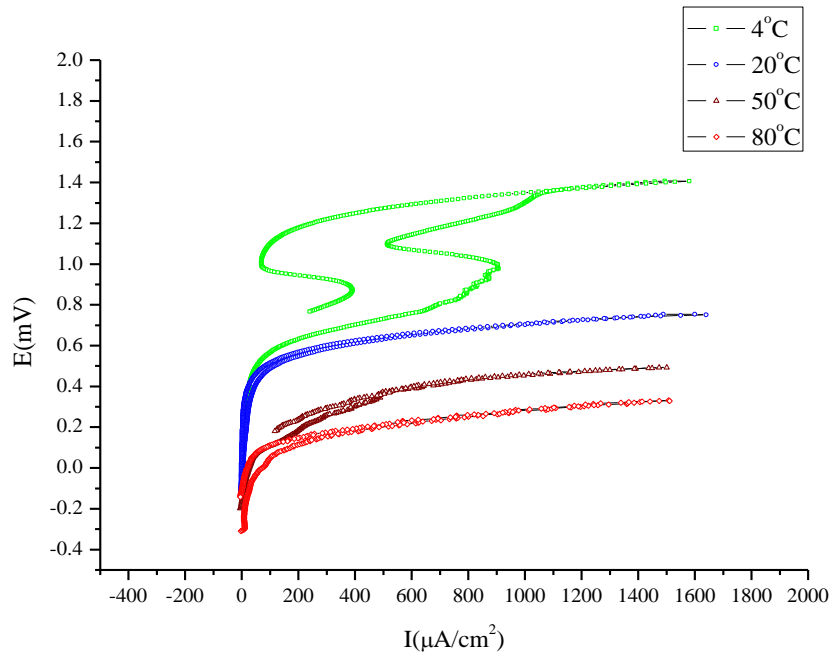


Figure A.9: WC-Ni in S2 at different temperatures

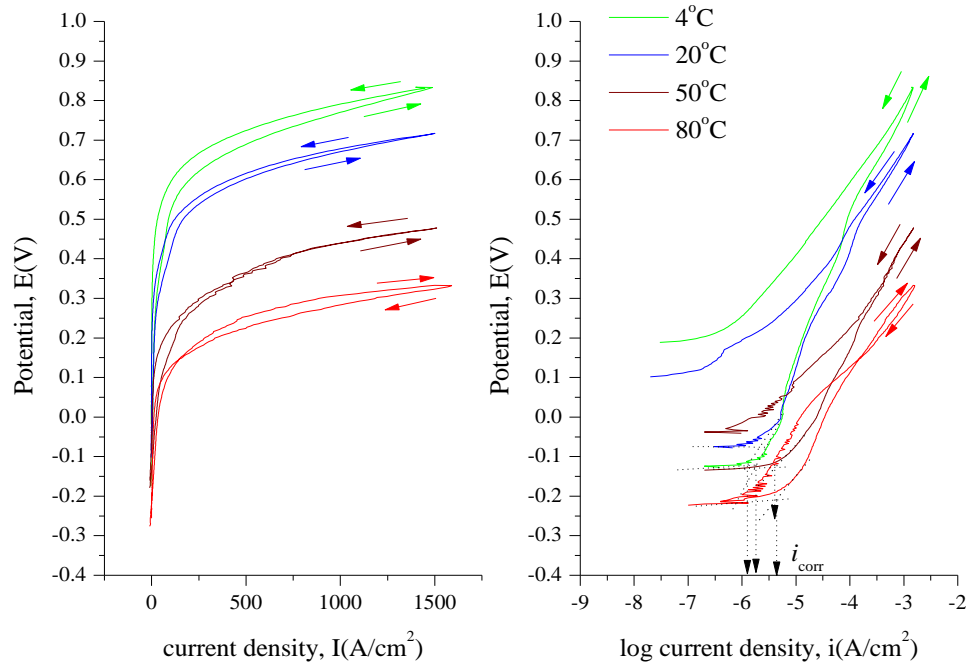
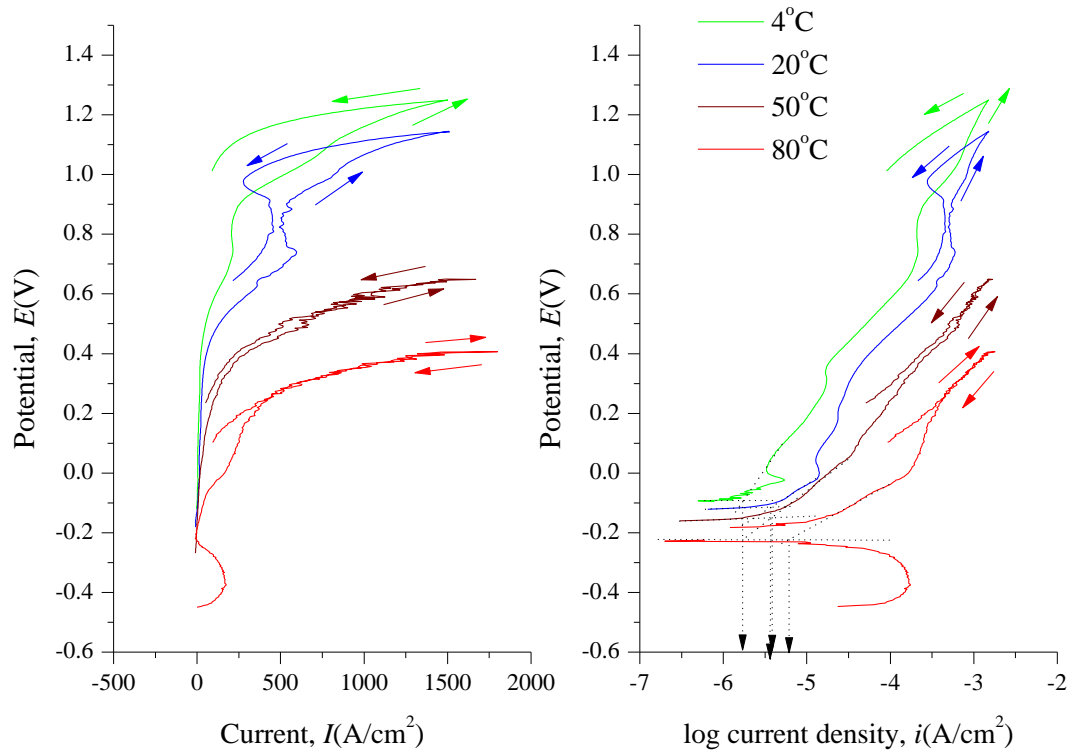
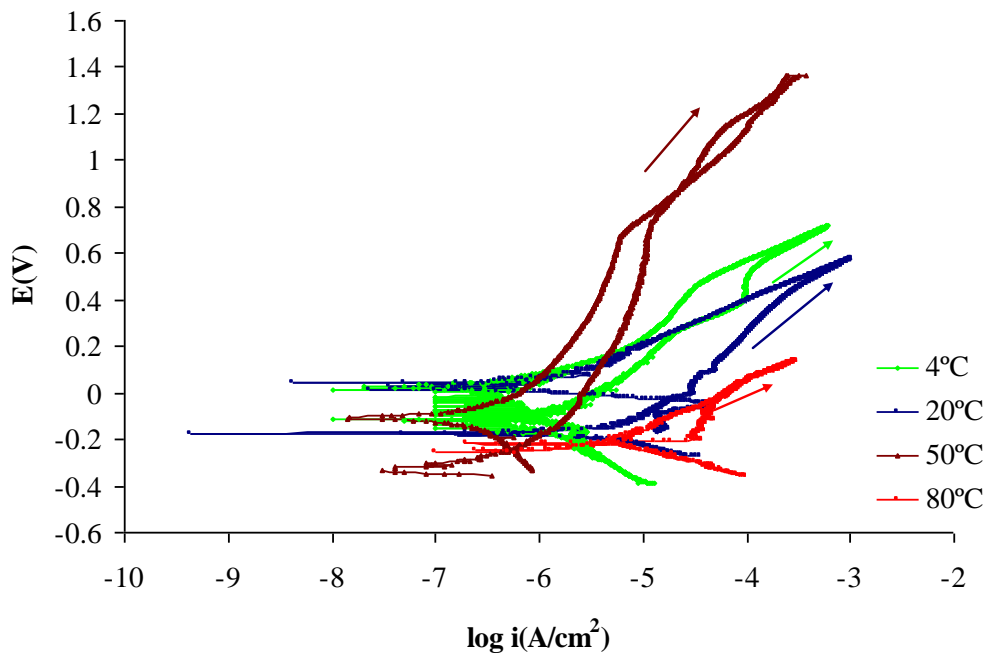


Figure A.10: WC-Ni in S3 at different temperatures





**Figure A.11: WC-Ni in S4 at different temperature**



**Figure A.12: Cyclic polarisation of WC-Ni in solution 2 ( $SO_4^{2-}/Cl^- = 19.15$ ) at different temperatures**

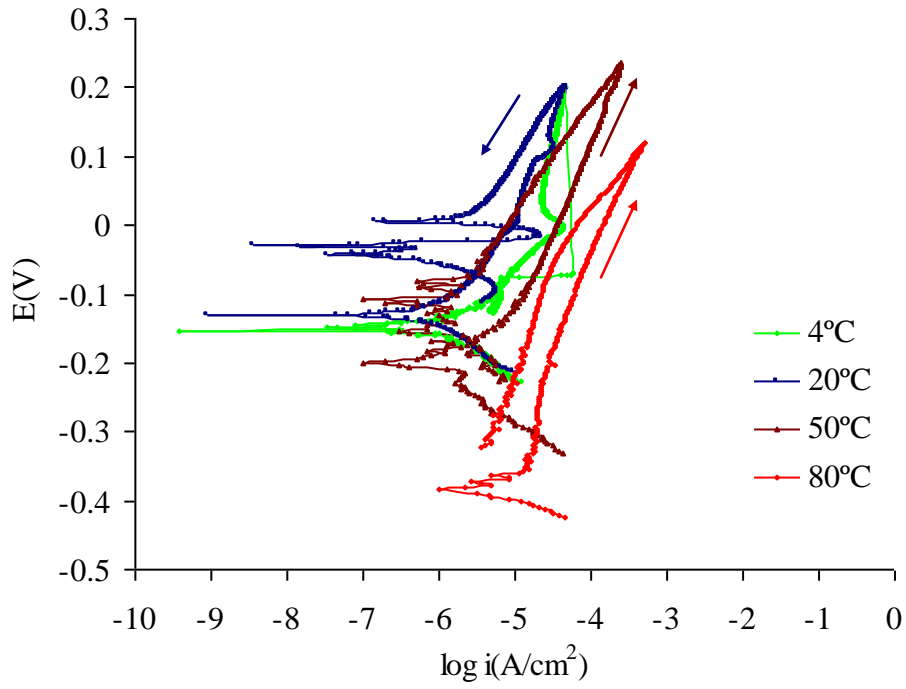


**Figure A.13: Cyclic polarisation of WC-Ni in solution 3 ( $SO_4^{2-}/Cl^- = 0.75$ ) at different temperatures**

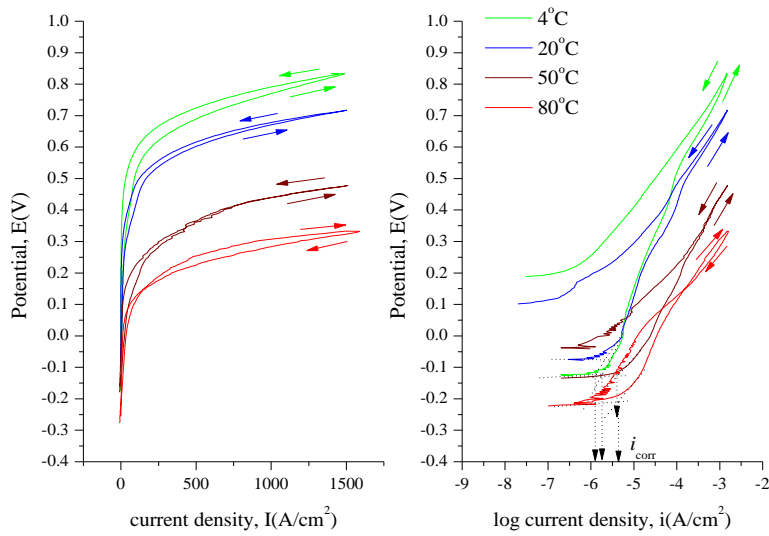


**Figure A.14: Cyclic polarisation of WC-Ni in solution 3 ( $SO_4^{2-}/Cl^- = 0.75$ ) at different temperatures**

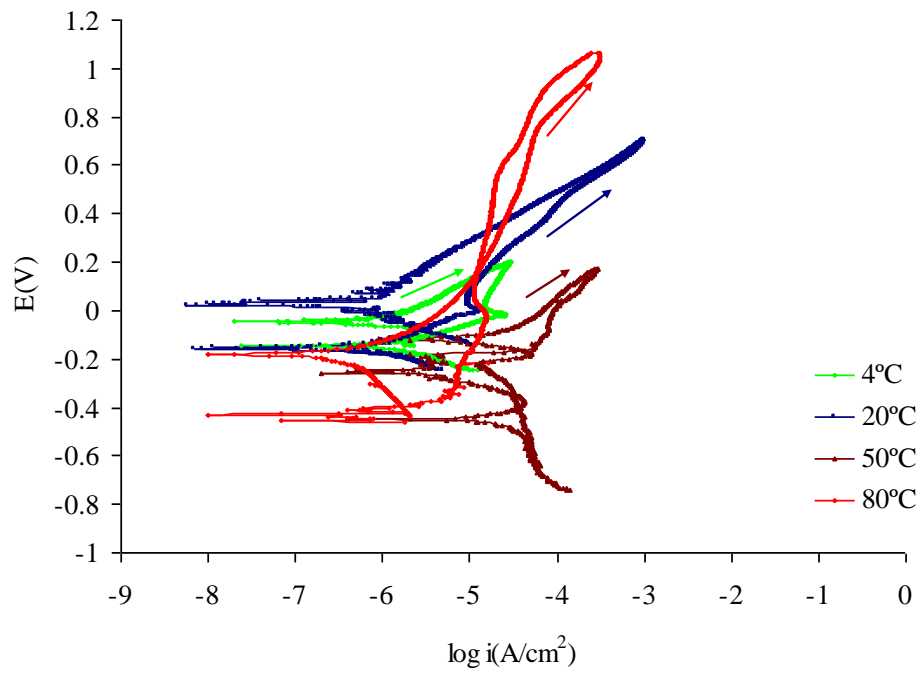


**Figure A.15: Cyclic polarisation of WC-Ni in solution 4 ( $\text{SO}_4^{2-}/\text{Cl}^- = 0.99$ ) at different temperatures**